Journal of Duhok University

Journal of Duhok University

Pure and Engineering Sciences
Published biannual by Duhok University

Address:
Zakho Street 38
1006AJ
Kurdistan Region-Iraq
The Secretariat, JDU Editorial Board,

Mobile.: 00964 (0) 07508504928
www.jdu.uod.ac E-mail: jdu@uod.ac

UoD Printing Press

JOURNAL **O**F **D**UHOK **U**NIVERSITY

(Pure and **E**ngineering **S**ciences**)**

VOLUME 17 **DECEMBER**

NUMBER 1 2014

JOURNAL PAPER INSTRUCTIONS TO AUTHORS

General

The paper should be valuable and should not have been published or submitted for publication in any other Journals. The text should be complete with abstract, introduction, material and methods, results, discussion and reference. The text must not exceed 15 pages for sciences papers and 25 for the humanities

Content Text

The content text must be Normal, 10 pt., Times New Roman, at least 12 lines spaced, and justified. Each paragraph should be spaced after 6 pt. The first line of the paragraphs should not be indented.

Footnotes

Footnotes should not be used.

Page Margins

The paper size should be A-4 size and page margins must be 2.5 cm top and bottom, 3 cm left and 2 cm right.

Page Numbers

Include page numbers. The page numbers should be placed in the lower right hand corner.

Titles

The paper title must be capitalized, bold, centered, 11 pt., and spaced after 18 pt. Main titles and abstract title should be capitalized 9 pt., aligned left, bold, spaced before 12 pt., and after 6 pt., and numbered as (1., 2.,3.). Principle subtitles must be written in 10 pt, bold, aligned left.

Author(s)

The name(s) of the author(s) should be written only in the first page, capitalized, 8 pt, normal, centered, and spaced after 18 pt.
(See below).

ALI MUHAMMED1, JALAL AMEEN 2 and DLOVAN ASSAD 2

The authors' names should not cover all line and if there are more than, 3 or 4 writers the rest should be spaced to the line below, and writers also should be single spaced. The writers from the same department or the institution should be numbered by different numbers and indicated in the line below in 8 pt, as the following:

1 Department of Geography, College of Arts, University of Duhok, Kurdistan Region, Iraq
2 Department of Soil & Water Science, College of Agriculture, University of Duhok, Kurdistan Region, Iraq

Abstract

Abstract body should be 8 pt., bold, aligned left, and single spaced. The abstract must not exceed 300 words. (4-6) keywords must be provided at the end of abstract. The keywords title must be capitalized, 8 pt., aligned left, and Italic. The keywords should be written in 8 pt., Italic, and their initials should be capitalized. Paragraphs in the abstract should be spaced after 6. (See below)

KEYWORDS: *Erosivity factor, Rainfall, Fournier index, Water Quality*

Summary should be provided also in Kurdish and Arabic at the end of the paper.

Figures and Tables

Except the tables, all the graphs, maps and photographs must be named as figures. Tables and Figures should be numbered consecutively by Arabic numerals. The tables and figures must not exceed the page margins and must be on one page. All Table outline border should be (1 ½ pt.), inside border should be (½ pt.); table details should be Arial font and written with 7 pt. the figure and table names must be written with 8 pt. style. Names must be written in the middle on top for the tables with space 4 after and for the diagrams/figures, underneath on the bottom with space 4 before and 12 after. If the figure and table names have to be more than one line, the line spacing should be single spaced, and the terms of "Figures" and "Tables" must be bold. (See below)

Table (1): The effect of pepper shoot & root aqueous extract on the growth of different other plants:

	Shoot Extract					Root Extract				
Plant type	Conc. %	Root length (cm)	Shoot length (cm)	Intact plant length (cm)	Inhibition %	Conc. %	Root length (cm)	Shoot length (cm)	Intact plant length (cm)	Inhibition %
Okra	0	*25.7 a**	27.8 a	53.5a	-	0	25.7a	27.8a	53.5a	-
	5	25.00a	26.77a	51.77a	3.23	1	24.50a	27.00a	51.50a	3.73
	10	24.50a	25.95a	50.45a	5.70	2	23.87a	25.65a	49.52a	7.43
Sorghum	0	21.6a	27.2a	48.8a	-	0	21.7a	27.2a	48.9a	-
	5	13.00b	17.25b	30.25b	38.03	1	9.8b	25.5ab	35.3b	27.6
	10	6.00c	5.50c	11.50c	76.44	2	9.4b	22.6b	31.9 b	34.6

Figure (1): xxxxxxxxxxxxx

Bullets and Numbering

Bullets and numbers should be indented 1 cm from the left margin and hanging indent should be 0.5 cm. Each line of bullets and numbers should be single spaced.

References

References should be indicated in the typescript by giving the author's name, with the year of publication in parentheses, as detailed in the APA style guide. All lines after the first line of each entry in your reference list should be indented one cm from the left margin (hanging indentation). If several papers by the same author(s) and from the same year are cited, a, b, c, etc. should be put after the year of publication. The references should be listed in full at the end of the paper in standard APA format. For example:

For Books:

Ritter, D. F., Kochel, R. C., and Miller, J. R. (2002). Process Geomorphology (4th ed.). New York: McGraw-Hill.

Massey, W. R., and Jameson, W. M., Jr. (2001). Organizational behavior and the new internet logic (3rd ed.). New York: McGraw-Hill.

For articles:

- Harlow, H. F. (1983). Fundamentals for preparing psychology journal articles. *Journal of Comparative and Physiological Psychology*, 55, 893-896.
- Loughran, J., and Corrigan, D. (1995). Teaching portfolios: A strategy for developing learning and teaching in preservice education. *Teaching and Teacher Education*, 11, 565-577.

For chapters within books:

- Smith, N. (1997). Challenges and choices facing social studies teachers. In R. Case & P. Clark (Eds.), The Canadian anthology of social studies (pp. 3-9). Burnaby, BC: Simon Fraser University Field Relations.

For conference proceedings:

- Demirci, A., McAdams, M. A., Alagha, O., and Karakuyu, M. (2006). The relationship between land use change and water quality in Küçükçekmece Lake watershed. In A. Demirci, M. Karakuyu, and M. A. McAdams (Eds.). *Proceedings of 4th gis days in Türkiye* (pp. 27-35). Đstanbul, 13-16 September.
- Healey, M., Foote, K., and Hay, I. (2000). Developing the International Network for Learning and Teaching (INLT) *Geography in Higher Education. In: International Geographical Union Commission on Geographical Education* (Eds.). Geographical Education at the Cross-roads: Directions for the Next Millennium, Proceedings of the Kyongju Symposium (pp. 203-207), Korea.

For online documents:

- Standler, R. (2000). Plagiarism in colleges in the USA. Retrieved August 6, 2004, from www.rbs2.com/plag.htm
- Bernstein, M. (2002). 10 tips on writing the living Web. A List Apart: For People Who Make Websites, 149. Retrieved May 2, 2006, from http://www.alistapart.com/articles/writeliving
- Titles of journals and names of publishers, etc. should not be abbreviated. Acronyms for the names of organisations, examinations, etc. should be preceded by the title in full.

Note: Referred scientific materials such as: e-journals, e-books, etc. can be used as reference by authors.

For further information about APA reference style please visit http://owl.english.purdue.edu/owl/resource/560/01/

Submission

Four copies of the research paper with CD containing the paper in one file (Microsoft word 2003) should be submitted to the following address:

The Secretariat,
JDU Editorial Board,
Presidency of Dohuk University, Dohuk Governorate,
Kurdistan Region, Iraq.
Tel: 062-7225259
E-mail: jdu@uod.ac

CONTENTS

EFFECT OF THE TRANSVERSE MAGNETIC FIELD ON MERCURY DISCHARGE PARAMETERS

MAHMOOD **E**. **A**L- **H**AKARY and **J**UNDI **K**H. **Y**OUSIF
Dept. of Physics, Faculty of Science, University of Zakho, Kurdistan region-Iraq

(Received: October 4, 2012; Accepted for publication: November 25, 2013)

ABSTRACT

The current –voltage characteristics of Glow discharge has been measured experimentally, from these characteristics the electrical conductivity was calculated at different currents values (0, 30, and 60mA) or from (0-45.4μT) of transverse magnetic field. Also we studied the effect of transverse magnetic field on (I-V) characteristics, the electrical conductivity, and the resistance of the mercury discharge at constant gas pressure (0.75torr.). The results show that the magnetic field effect on the (I-V) characteristic for glow discharge is analogous completely to Abnormal Glow Discharge., the average voltage increases while the current decreases with transverse magnetic field and this lead to decrease the electrical conductivity. And the resistance glow discharge is increases with the electric current magnetic field.

KAY *WORDS:* Glow discharge, electrical conductivity, current voltage, transverse magnetic field

1. INTRODUCTION

Many theoretical and experimental works have dealt with the characteristic of the discharge current as a function of the applied voltage (Qais , 2007, Ahmad, 2010, Escho, 2009, Akbar, 1996, Hippler, et al. 2008, Chen, 1984). The changes that take place in the gas as a function of the applied voltage are described by the typical dependence of the discharge current (I) on the applied voltage (V) is called (I-V) characteristic of the discharge. The main characteristics of the discharge such as the breakdown voltage, the voltage current characteristic and the structure of the discharge depend on the geometry of the electrodes, the gas used, the pressure and the electrode material.

The production of plasma in rectangular tubes (Qais , 2007) has been carried out and reported by various authors .They were concerned mainly with the study of the characteristics of the positive column. When a magnetic field act upon a glow discharge, various changes such as increase of equivalent pressure take place. If a D.C. transverse magnetic field is applied to the positive column, the electron density distribution is deflected to the wall by the influence of the magnetic field. The aim of the present work is to study the effect of a D.C. transverse magnetic field on the I-V characteristic curve and electric field gradient in discharge tube.

When a magnetic field is applied to plasma glow discharge will occur many changes on plasma parameters. Allen (Allen, 2007) noted that the current decreases while the voltage increases with transverse magnetic field.

Many theoretical and experimental researches are studied results for the electrical conductivity of noble gas plasmas are presented in comparison with experiment (Ahmad, 2010, Akbar, 1996, Adams, et al, 2007). The composition is determined within a partially ionized plasma model. The conductivity is then calculated using linear response theory, in which the relevant scattering mechanisms of electrons from ions, electrons, and neutral species are taken into account. In particular, the Ramsauer-Townsend effect in electron-neutral scattering is discussed and the importance of a correct description of the Coulomb logarithm in electron scattering by charged particles. And the effect of the magnetic field on plasma parameters were studied previously, Kameda (Kameda , 1979) studied the effect transverse magnetic field (0-50G) on plasma parameters for plasma Argon gas. Teruo et al (Teruo Kaneda, 1979) studied the influence of a transverse magnetic field on a glow discharge tube.

Selvarajen and Natarjan (Selvarajen and Natarjan,1982) studied the effect axial magnetic field (0-2050G) on breakdown voltage for dry air. Hosouba (Hassouba, 2001) studied the effect axial magnetic field for (DC) negative glow discharge for Argon gas at pressure range (0.4-

0.5Torr.). Kanedn and Antoni (Kanedn, Antoni, 2000) studied the transverse magnetic on plasma parameters of Positive Column. Al-Badrani (Al-Badrani, 2005) studied the effect of Axial Magnetic Field on DC Glow Discharge Plasma parameters.

In this work a magnetic field perpendicular on the plasma was applied on the plasma properties (electron conductivity) at gas pressure (0.75torr) and different magnetic field strength studied. Also studied some other properties such as; the relation between volt and current of discharge, these studies were done on normal glow state.

The plasma parameters such as electrical conductivity were founded from the (I-V) characteristics at pressure (0.75torr), and calculated from the current density relation. The electrical conductivity as a function of magnetic field (0mA, 10mA, 30mA and 60mA), or from (0-45.4μT) as well as, we study the effect of transverse magnetic field on these parameters .Also we found the effect of the magnetic field on the resistance discharge. Finally we calculate the magnetic field (B) theoretically from Biot-Savart law, the value of the magnetic field at a point is directly proportional to the both value of the current (I) in the conductor and the number of turns per unit length (N) of the current-carrying segment, and depend on the permeability (μ)

$$B = «NI \ \ watt/m^2 (Tesla)$$

2. DISCHARGE ELECTRIC CIRCUIT AND EXPERIMENTAL PROCEDURE

The experimental system employed is shown in Diagram (1),the discharge tube is made of Pyrex of radius (2cm) and length (20cm).The discharge contain a mercury gas evacuated to a pressure (0.75torr), high power supply used to give a required electric field, and a digital ammeter is used, a transverse magnetic field of magnetic current (0,10,30,60mA) or from (0-45.4μT).

The type of plasma formed by applying of a voltage at (100 V to several kV) through a gas, usually argon or another noble gas. The glow discharge owes its name to the fact that plasma is luminous; the luminosity is produced because the electrons gain sufficient energy to generate visible light by excitation collisions which generate photons.

A simple electric circuit used high power supply voltage for generating glow discharge through the confined gas between the two electrodes, also a high resistance connected in this circuit for discharge stability and to protect the power supply from the higher currents during suddenly higher conductivity of the gas.

For studying the properties under the effect transverse magnetic field, we applied two coils of (600turn) on the two opposite side on the middle discharge tube, an electric current from power supply supplied to the coils for generating the required transverse magnetic field,

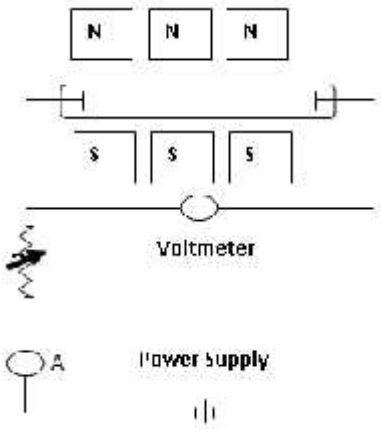

Diagram (1): Electrical circuit for glow discharge

3. CALCULATION OF PLASMA PARAMETERS

The very important process to measure the plasma parameters is the electric probe method:

The three processes to measure the plasma parameters are:

1. Studding Emission 2. Microwave Process 3. Langmuir Probe

There has been much recent interest in the investigation of the plasma parameters we report on the technique of using the electrical probes, double and single Langmuir probes. The Electrostatic Probes (Langmuir Probes) Simple diagnostic tools techniques, electrical probes can give valuable information on the plasma properties, and very important to measure the parameter in cold plasma, such as electron density n_e, electron temperature (T_e), electrical conductivity (σ), and electron energy distribution (EED).

Conductivity is the ability of the material to conduct electric current, we create a cylindrical glow discharge by applying a high voltage between the electrode that is sufficient to make the break down of a gas and convert the insulator to conductor (abnormal glow discharge)

The conduction is well described by Ohm's law which state that:

The current density (J) is proportional to the applied electric field (E)

$$J = \sigma E$$

Where: $J = \frac{I}{A}$ where (J) is the current per unit area, $A = \pi r^2 = \frac{(\pi D^2)}{2}$ where, D is the diameter of the tube (1.98cm), and (d) is the distance between the two electrodes (16.8cm).And $E = \frac{V}{d}$ is potential gradient.

4. RESULT AND DISCUSSIONS

The plasma parameters such as electrical conductivity were founded from the (I-V) characteristics at pressure (0.75torr) as shown in fig.(1), and calculated from the current density relation.

Fig. (2) Represents the electrical conductivity as a function of magnetic field (0mA, 10mA, 30mA and 60mA),as well as, we study the effect of transverse magnetic field on these parameters are shown in figs.(3) and (4), fig. (5) Discharge resistance versus magnetic field.

A metals has high conductivity (σ) and low resistivity (ρ) , while an insulator has low conductivity but high resistivity.

Table (1): I-V Characteristic without transverse Magnetic field (B= 0 μTesla)

Vd(volt)	Id(mA)	J= I/A	E=V/d	±=J/E
2000	0.01	3.247	11904.8	0.000272727
2400	0.03	4.221	14285.7	0.000295455
2600	0.04	5.195	15476.2	0.000335664
2800	0.06	6.169	16666.7	0.00037013
3000	0.1	7.468	17857.1	0.000418182

Table (2): I-V Characteristic with transverse Magnetic field (B= 7.53μTesla)

Vd(volt)	Id(mA)	J= I/A	E=V/d	±=J/E
2000	0.01	0.325	11904.8	2.72727E-05
2400	0.03	0.974	14285.7	6.81818E-05
2600	0.04	1.299	15476.2	8.39161E-05
2800	0.06	1.948	16666.7	0.000116883
3000	0.1	3.247	17857.1	0.000181818

Table (3): I-V Characteristic with transverse magnetic field (B=22.6μTesla)

Vd(volt)	Id(mA)	J= I/A	E=V/d	±=J/E
2400	0.01	0.325	11904.8	2.72727E-05
2600	0.02	0.649	14285.7	4.54545E-05
2800	0.05	1.299	15476.2	8.39161E-05
3000	0.08	1.948	16666.7	0.000116883
3200	1.00	2.597	17857.1	0.000145455

Table (4): I-V Characteristic with transverse magnetic field (B= 45.2μTesla)

Vd(volt)	Id(mA)	J= I/A	E=V/d	±=J/E
2400	0.01	0.325	14285.7	2.27273E-05
2600	0.02	0.649	15476.2	4.1958E-05
2800	0.05	1.623	16666.7	9.74026E-05
3000	0.08	2.597	17857.1	0.000145455

Table (5): Average voltage as a function of average discharge current

Vd(volt)	Id(mA)	J= I/A	E=V/d	±=J/E
2500	0.15	16667	0	0
2500	0.04	62500	10	7.536
2545	0.036	70694	30	22.61
2700	0.038	80130	60	45.21

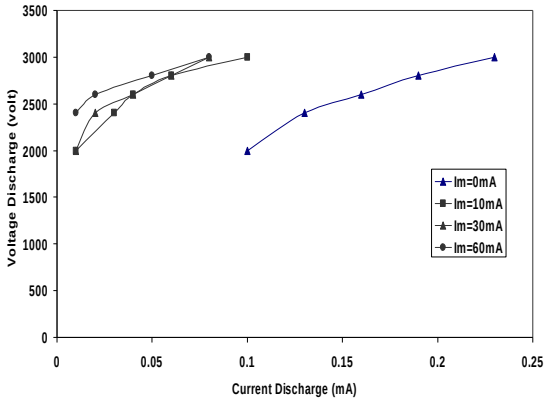

Fig.(1): I-V characteristic at Glow discharge mercury at pressure 0.025 torr

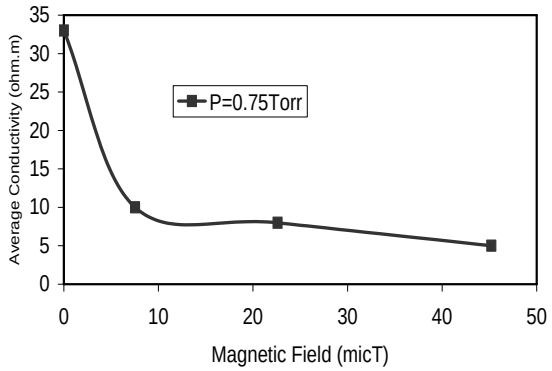

Fig.(2) Average conductivity versus magnetic field

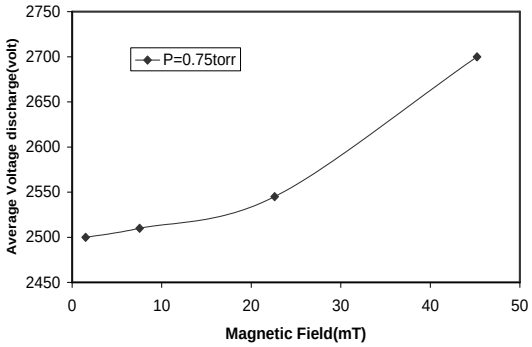

Fig.(3) Average discharge voltage versus magnetic field

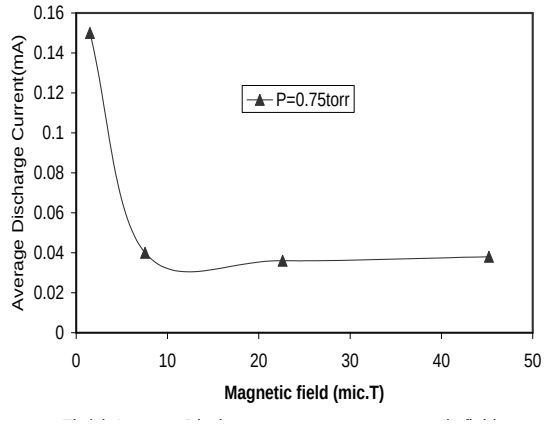

Fig.(4) Average discharge current versus magnetic field

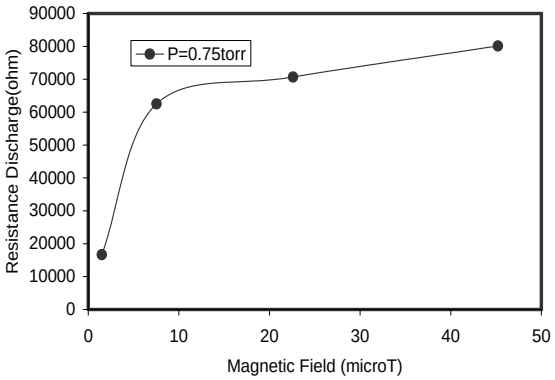

Fig.(5) Resistance discharge versus magnetic Field

5. CONCLUSIONS

1. The (I-V) characteristic for glow discharge is analogous completely to Abnormal Glow Discharge.
2. The average voltage increases while the current decreases with transverse magnetic field and this lead to decrease the electrical conductivity.
3. The resistance glow discharge is increases with the electrical conductivity.
4. Excellent agreement between theory and experiment is observed, showing considerable improvement upon previous calculations.

REFERENCES

- Qais**,** T. Algwari, Mosul University, Raf. Jour. Sci., Vol. **18**, No.2, pp.91-97, (2007)
- Ahmad, F. Abdulraman, Experimental Investigation of Hollow Cathode at Glow
- Discharge, M.Sc Thesis, Duhok University, College of Education,(2010)
- Escho, K. Yohana, Plasma Parameters of Hot Cathode Discharge, M.Sc. Thesis, Duhok University, College of Education, (2009)
- Akbar, DS, Experimental study of plasma parameters in air and N2 glow discharge. M.Sc. Thesis, College of Science, Mosul University, (1996)
- Hippler, R., Kersten, H., Schmidt, M., Schoenbach, K.M., ed. "Plasma Sources". Low Temperature Plasmas: Fundamentals, Technologies, and Techniques (2 ed.). Wiley-VCH. ISBN3-527-40673-5. 27, (2008)
- Chen, Francis F. Plasma Physics and Controlled Fusion. Plenum Press. ISBN 0-306-41332-9. 28, (1984).
- Allen J. E. Phys. Plasmas **14**, 024701, (2007).
- Adams J. R. etal, Electrical conductivity of noble gases at high pressures, Phys.RevE, Statistical, non linear, and soft matter physics,**76,**(2007)
- Kameda, studied the effect transverse magnetic field (0-50G) on plasma parameters for plasma Argon gas.(1979)

- Kanedn, Antoni, The plasma parameters of Positive Column in a transverse magnetic field, J. Physics, D, Appl, Phys. **12**,PP 61-69,(2000)
- Al-Badrani, F. Mohmammed, Effect of Axial Magnetic Field on DC Glow Discharge Plasma parameters, M.Sc. Thesis Collage of Education, University of Mosul,(2005)
- Teruo Kaneda, The influence of a transverse magnetic field on a glow discharge tube, J. Light & Vis. Env., **2**, No. 1, pp.45, (1979).
- Selvarajen and Natarjan., studied the effect axial magnetic field (0-2050G) on breakdown voltage for dry air (DC) negative glow discharge for Argon gas at pressure range, (0.4-0.5Torr.), (1982).
- Hassouba, M. A, The effect of magnetic field on the Plasma parameters .J. Applied Physics, **14**, pp131-135,(2001).

الخلاصة

لقد تم في هذا البحث قياس خواص (الفولطية– التيار) عملياً .ومن هذه الخواص تم حساب التوصيلية الكهربائية عند مختلف التيارات تتروح قيمتها (0,30,60mA) لتوليد المجال المغناطيسي المستعرض.

وقمنا ايضاً بدراسة تأثير المجال المغناطيسي المستعرض على كلاً من خواص (الفولطية– التيار) و التوصيلية الكهربائية و مقاومة التفريغ التوهجي عند ضغط (0.75torr) لغاز الزئبق .وقد لوحظ ان الخواص مشابهة تماماً لخواص تحت التفريغ التوهجي ومعدل الفولطية يزداد والتيار يقل كلما زاد المجال المغناطيسي المستعرض ويؤدي بدوره الى نقصان التوصيلية الكهربائية . ولوحظ ايضاً ان مقاومة التفريغ التوهجي تزداد بزيادة تيار المجال المغناطيسي المستعرض.

پوختە

دڤێ ڤەکولینێ دا ساخلەتێن (ڤولت_تەزوو) هاتنە پێڤان بریکا پراکتیکی. و ژڤان ساخلەتان گەیاندنا کارەبێ بو چەند تەزوویان دناڤبەرا (0.30,60 mA)هاتنە هژمارتن بو پەیدابوونا بواریّ موگناتیسی یێ پانراو و هێشتا ئەم رابوین ب خاندنا کارتێکرنا بواریّ موگناتیسی یێ پانرەو ل سەر هەردوو تایبەت مەندیێن (ڤولتیە–تەزوو) و گەهاندنا کارەبای و بەرگریا خالیکرنا ئاراستەی ل پەستانا(0.7تور)بو گازا جیوە. ودیار بو کو تایبەتمەندی وەکی تایبەت مەندیێن بەرگریا خالیکرنا ئاراستەینە و ریژا ڤولتی زیدە دبیت و تەزوو کێم دبیت هەرگاڤا بواریّ موگناتیسی یێ پانرەو زێدە ببیت د بیتە ئەگەریّ کێم بونا گەهاندنا کارەبایی. و هاتە تێبینی کرن کو بەرگریا خالیکرنا ئاراستەی زێدە ببیت بزێدەبو نا بواریّ موگناتیسی یێ پانرەو.

IMMUNOHISTOCHEMICAL MARKERS FOR RECOGNITION TISSUE OF ORIGIN IN METASTATIC CANCERS

MAYADA **I**. **Y**ALDA,**M**ELAD **A**. **Y**ALDA and **B**ASHAR **A**. **H**ASSAWI
School of Medicine, University of DuhoK, Kurdistan Region-Iraq

(Received: March 28, 2013; Accepted for publication: June 4, 2014)

ABSTRACT

Metastatic cancer can be the first manifestation in patient with malignancy, where the primary cancer's source is undetermined. The immunohistochemistry (IHC) is required in such cases, by using certain panels of immune-stains, to identify the cancer type or tissue of origin to determine the specific therapy in the oncology unit. The aim of the study is to apply different IHC panels to tissue sections of cases suspected to be metastatic cancers of undetermined origin by histopathological examination (H.P) to predict different tissue of origin and to clarify certain criteria of metastatic cancers including the type and main primary and secondary sites. After reviewing 1316 cancer cases diagnosed by H.P from August 2009 to December 2012, a total of 175 cases were diagnosed as metastatic cancers of undetermined origin. Panels of IHC markers were used to identify the type and tissue of origin. Among the 1,316 reviewed malignant cases, 175 cases were diagnosed as secondary by histology. The IHC analysis showed that only 162 of them were secondary cancers (12.3%). The commonest site of secondary at time of diagnosis was the abdominal cavity followed by the bone, lymph nodes, liver, lung, pleura and ovary. The IHC revealed that carcinoma (62%) was the commonest type of metastasis followed by undifferentiated malignancy (16%), lymphoma, sarcoma, and neuroendocrine tumors. The commonest primary malignant site was the GIT (37%), metastasized to the abdomen cavity, bone, lymph nodes, liver and ovary. In conclusion the use of IHC is an important ancillary test to approach the diagnosis of secondary tumors and to identify their type and tissue of origin.

***KEY WORDS*:** immunohistochemistry, metastasis, primary site, CUPs.

INTRODUCTION

Metastasis is an important hallmark of malignancy (Kumar et al, 2005). It is theorized that metastasis always coincides with a primary cancer. However, 4-10% of patients presenting to oncology units have metastatic cancer of unknown primary site (also called CUP). CUPs are heterogeneous groups of metastatic cancer for which the site of origin cannot be identified at the time of diagnosis (Pavlidis et al, 2010). However most studies involve minimum investigations before the term is used. The patient should have a biopsy-proven malignancy, a detailed history, physical examination, lab and radiological studies (Briasoulis and Pavlidis, 1997, abdArmstrong and Blackhall, 2007). Other studies have shown that, if simple questioning does not reveal the cancer's source (coughing up blood—"probably lung", urinating blood—"probably bladder"), complex imaging will not either. In some of these cases a primary tumor may appears later. In rare cases (e.g., of melanoma), no primary tumor is found, even on autopsy. It is therefore thought that some primary tumors can regress completely, but leave their metastases behind (Briasoulis and Pavlidis, 1997, and American Cancer Society, 2007).

In order to permit an easier way to give identity to many of these metastases, one may recall the theory of "the organ-specific targets" which stated that there is a propensity for certain tumors to seed in particular organs. This was first discussed as the "seed and soil" theory. For example, stomach cancer often metastasizes to the ovary in women, causing Krukenberg tumor (Robert Weinberg, 2007).

In many cases the cells in a metastatic tumor resemble those in the primary tumor and a pathologist can tell whether that type of cell is normally found in the part from which the tissue sample was taken. Still, the determination of the primary tumor can sometimes be very difficult, and pathologist has to use several adjuvant techniques, such as immunohistochemistry (IHC). Some studies have demonstrated that IHC can identify unique subsets of CUPs, and that organ-specific chemotherapy for these subsets may have benefit (Varadhachary, et al, 2008, Horlings HM, et al, 2008.). Approach to these lesions begins with the use of certain select

panels of immune-stains, based on the site and the histopathology impression of the tumor, both are extremely useful to narrow the diagnostic considerations, if not definitively identify the tumor. For example: in lymph nodes, epithelioid neoplasm most commonly represents large cell lymphomas or metastases of visceral carcinomas and malignant melanomas. The separation of these differential diagnostic possibilities principally involves the use of antibodies to CD45 (for lymphomas), Cytokeratin (for carcinomas), and S100 (for melanomas) (Lotan et al, 2009).Then further markers should be use to classify the carcinoma and other cancers (Tot T, 2002).

PATIENTS AND METHODS

This study was conducted from August 2009 to December 2012, by reviewing 1316 (irrespective to the age and sex of the patients) cancer cases diagnosed in the central lab of Duhok/ Iraq. From these cancers 175 were diagnosed as cancers of undetermined origin histologically by using the conventional histopathology stain.

The paraffin embedded blocks (PEBs) of those patients containing the cancer tissues were selected to perform the immune-histochemical staining protocol according to the Avidin Biotin Complex (ABC) detection system (Mangham et al 2000).

Sections from the PEBs where obtained in a 4 microns thickness and placed on positively charged slides together with adjacent parallel control sections which were processed with each set of staining for the IHC. Primary and secondary antibody kits were used, provided by the DAKO (an American company for Technologies), detected with the Envision+ system that employs peroxidase-labeled polymer conjugated to anti-mouse immunoglobulin antibodies. Immune complexes were identified by using peroxidase reaction with DAB+ as chromogen (Envision+ detection system, K4006, Dako Corp, Carpinteria, CA). The markers were used in panels, as shown in text table, according to the distinguishing microscopic characteristics, whether the malignant cells are large, small, spindle or forming glands, but in general the first panel consists mainly of the combination of four markers:

- Cytokeratin (for epithelial cells) as carcinoma marker
- CD45 as lymphoid marker
- S100 as melanoma marker
- Vimentin as mesenchymal marker

A second and a third panel of IHC carried out according to the results of the previous panel. Other markers used in IHC panels are all listed in the text table (Miettinen, 1993, and Bahrami et al, 2008).

RESULTS

This is a descriptive study of the undetermined (175) cases (13.3%). They were analysis and investigated by The IHC. The secondary tumors were proven in (162) cases 12.3%. The other (13) cases 1% were primary undifferentiated cancers and they were excluded from the study.

The age ranged from 1 to 92 years, with a mean age on presentation of 51 years. The youngest patient (1 year old boy) presented with sarcoma and the oldest patient (92 years old female) with lymphoma. The male to female ratio was 1.3:1 (92 males 70 females). The commonest sites of secondary in descending order were the abdominal cavity (peritoneum) (37) cases, 23% followed by the bone (28) 17%, lymph nodes (24) 15%, liver (14) 9%, lung (13) 8%, pleura and ovary (11) 7% for each. Other, less common areas are skin and subcutaneous tissues, colon, soft tissue, stomach, esophagus, testis, brain and breast as shown in figure 1.

After applying different IHC markers, that are available in the central lab, the 162 cancers were classified according to the tissue of origin and the types of their putative malignant cells. Carcinoma was the commonest type included (100) case 62% followed by undifferentiated malignancy in (26) 16%, lymphoma (19) 12%, sarcoma (8) 5%, neuroendocrine tumors (5) 3%, Melanoma and malignant germ cell tumors (2) 1% for each one of them (figure 2). The relation of these types to the metastatic site at time of diagnosis is shown in table 1. The commonest primary origin (when detected) was the GIT which metastasized to the abdomen cavity (peritoneum, as shown in figure 3), bone, lymph nodes, liver and ovary. The 100 cases of carcinoma were further divided by IHC analysis into: adeno-carcinoma (66) cases 40.1%, poorly differentiated carcinoma in (28) 17.3%, squamous cell carcinoma (4) 2.5%, transitional cell carcinoma (2) 1.2% (Figure 2). No clue could be given on the primary site in cases of the undifferentiated cancer and the poorly differentiated carcinoma (54) cases for each of them and this represents 3.5% out of total (1316) malignant cases included in this study.

Text Table:- Panels of IHC markers used for different types of tissue.

First panel	Types (Histogenesis)	Second panel	Organ (Histogenesis)	Third panel*
Cytokeratin	Carcinoma (epithelial cells)	CK20+ CK7-	Colorectal	CEA EMA Thyroglobulin PSA GCDFP-15 TTF-1 Uroplakin ER CA-125
		CK20- CK7+	Adenocarcinoma lung, breast, ovary (non-mucinous), endometrium, thyroid	
		CK20+ CK7+	Adenocarcinoma stomach, biliary tract, pancreas, ovary (mucinous), transitional caecinoma	
		CK20- CK7-	Carcinoma prostate, renal, adrenal cortex, hepatocellular, squamous carcinoma.	
**CD45	Lymphoma	B cell marker+	B cell lymphoma	Bcl6, **CD3, CD5, CD10, CD20,..
		T cell marker+	T cell lymphoma	
S100	Melanoma and some others	HMB45+, melanA+	Melanoma	
		**CD99+	Ewing's sarcoma/PNET	
Vimentin	Mesenchymaltumor	Myoglobin	Skeletal muscle	Put in mind the Co-expression of vimentinwith carcinoma (carry out other markers)
		Sooth muscle actin+ Desmin+	Leiomyosarcoma	
		**CD117+	Gastrointestinal stromal tumor	
		**CD34+	Vascular tumors	
Others Neuroendocrine and germ cell tumor		A-PLAP+	Germ Cell Tumor Markers	Markers to exclude certain primary tumors e.g. To excluded Mesothelioma(Calretinin CK5/6WT1) all negative
		OCT3/4+		
		Alpha-fetoprotein+		
		b-HCG+		
		Chromogranin	Neuroendocrine tumor	
		Synaptophysin		
		NSE		

* The results of panel 3 depend on the positive and negative combination.
** CD stands for cluster of differentiation

CK7: Cytokeratin 7, CK20: Cytokeratin 20, CEA: Carcinoemberionicantigene, EMA: Epithelial membrane antigen, PSA: Prostate-specific antigen, GCDFP-15: Gross cystic disease fluid protein-15, TTF-1: Thyroid transcription factor-1,ER: Estrogens receptors, CA-125:Cancer antigen 125, Bcl-6: B-cell lymphoma 6, HMB45: Human melanoma black 45,PNET: Primitive neuroectodermaltumor,PLAP:Anti-Placental alkaline phosphatase,OCT3/4: octamer-binding transcription factor3/4, b-HCG: beta- Human chorionic gonadotropin, NSE: Neuron-Specific Enolase, CK5/6: Cytokeratin 5/6, WT-1: Wilms tumor protein1

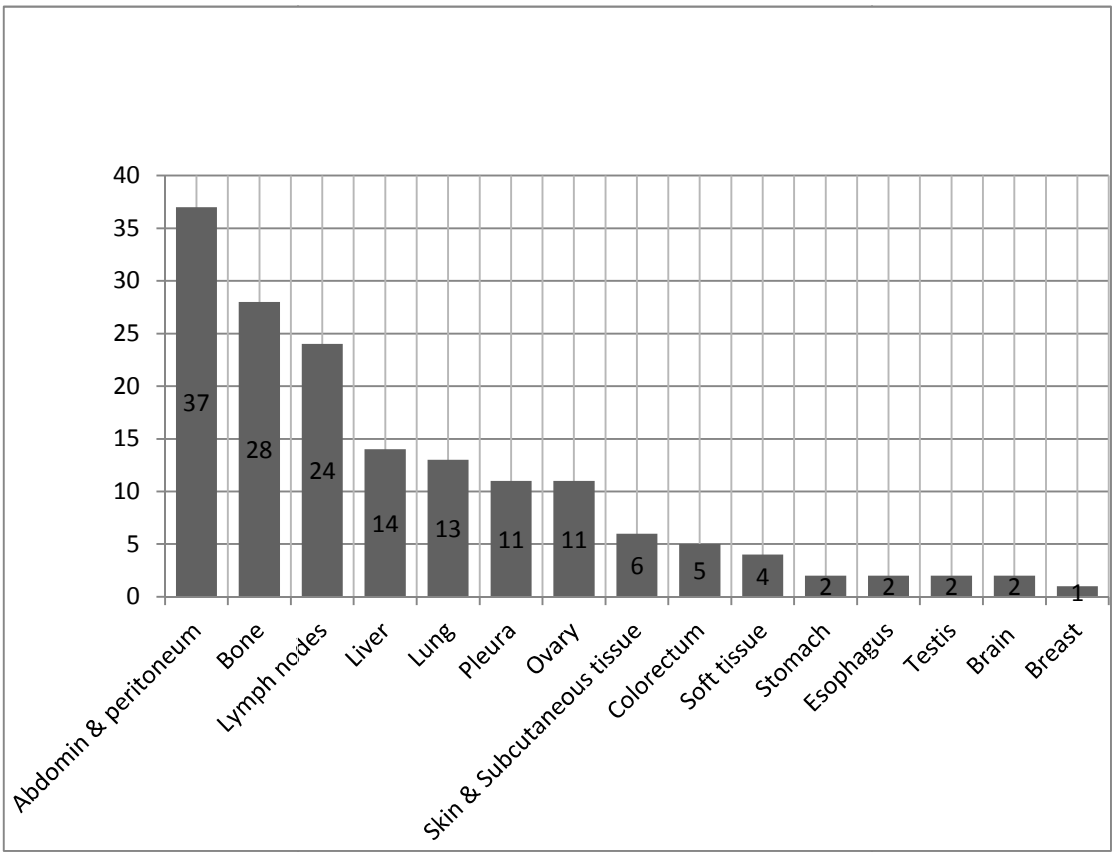

Fig.(1):- Metastatic sites at time of diagnosis

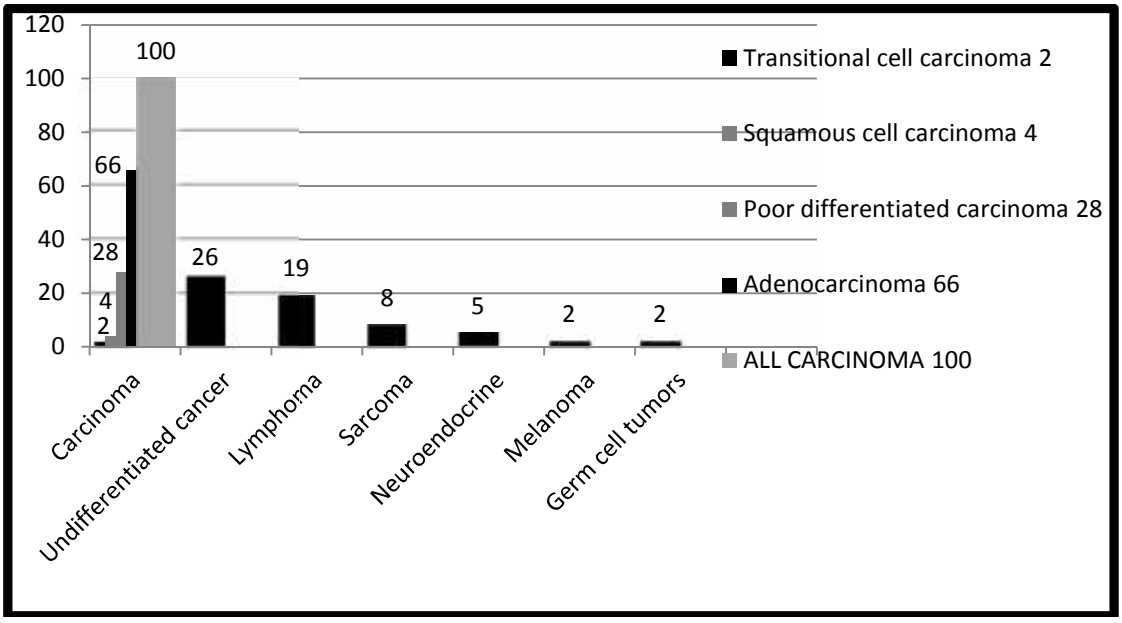

Fig.(2): -Types of malignancy accurding to the histogenesis.

Table(1):- Metastatic site at time of diagnosis versus IHC diagnosis of tissue of origin

Metastatic site at time of diagnosis	IHC diagnosis of tissue of origin							Total	
	Carcinoma	Undifferen-tiated	Lymphoma	Sarcoma	Neuro-endocrine	Melanoma	Germ cell tumor	No	%
abdomen cavity & peritoneum	22	3	6	3	1	0	2	37	23%
Bone	19	5	3	0	1	0	0	28	17%
Lymph nodes	14	5	0	1	2	2	0	24	15%
Liver	10	4	0	0	0	0	0	14	9%
Lung	7	4	0	2	0	0	0	13	8%
Pleura	8	3	0	0	0	0	0	11	7%
Ovary	10	0	1	0	0	0	0	11	7%
Skin & subcutaneous	3	1	1	1	0	0	0	6	4%
Colorectal	3	0	2	0	0	0	0	5	3%
Soft tissue	1	0	1	1	1	0	0	4	2%
Stomach	0	0	2	0	0	0	0	2	1%
Esophagus	2	0	0	0	0	0	0	2	1%
Testis	0	0	2	0	0	0	0	2	1%
Brain	1	1	0	0	0	0	0	2	1%
Breast	0	0	1	0	0	0	0	1	1%
Total	100	26	19	8	5	2	2	162	100%

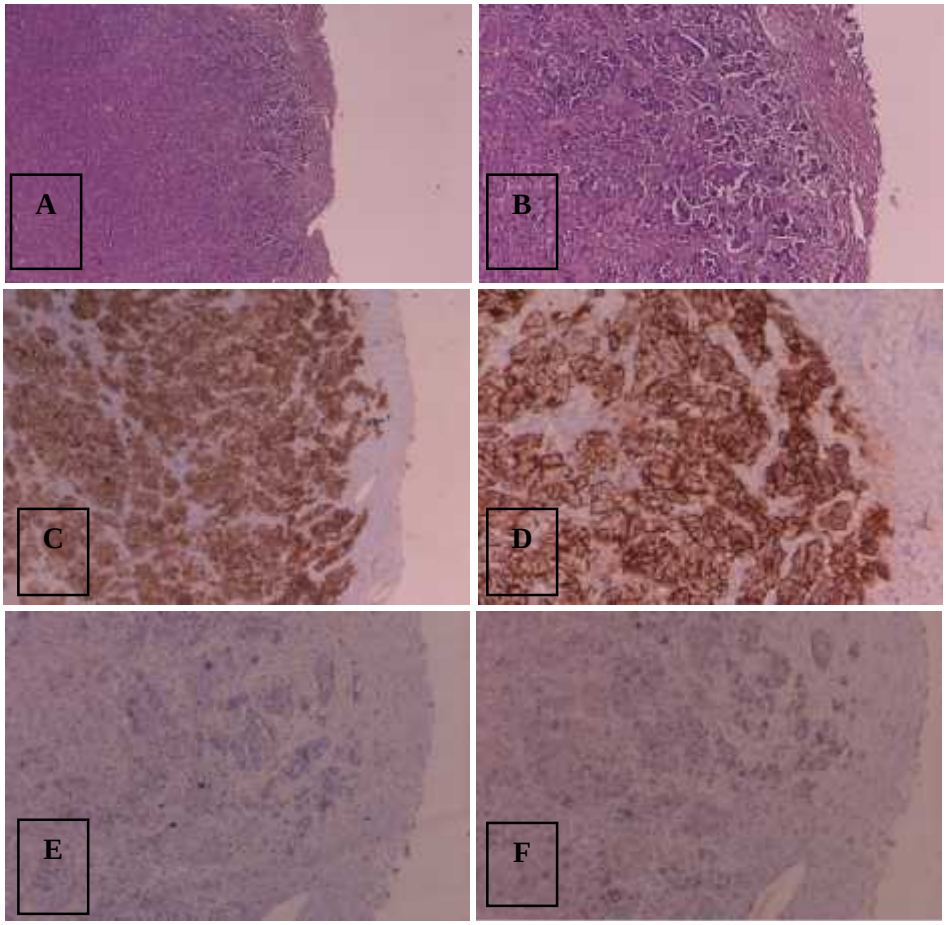

Fig.(3):- A-F Mass in the peritoneum of female patient, metastasized from the colon. A, H&E stain X 4 HPF. B, H&E stain X 10HPF. C, IHC positive stain for CEA. D, IHC positive stain for CK20. E, IHC negative stain for CA125. F, IHC negative stain for CK7.

DISCUSSION

The definition of cancer of unknown primary site (CUP) varies greatly from a study to another. Consensus has not been reached on whether CUP is simply a malignancy of undefined origin (MUO) or a distinct entity with specific genetic characteristics. It is possible that both subsets coexist (Armstrong and Blackhall, 2007). CUPs accounts for 4-10% of malignancy (Armstrong and Blackhall, 2007, and American Cancer Society, 2007).

Improvement in radiological investigations decreased the percentage to 3-7% (American Cancer Society, 2013). The relatively high percentage of malignancy of unknown origin seen in this study could be attributed and related to the improper evaluation of the cases and the shortage (lack) of important advanced radiological diagnostic techniques. The application of IHC decreased our percentage of CUP from 12.3 to 3.5%. The main reason to look for the primary site is to guide treatment, especially for cancers that respond well to specific chemotherapy or hormone drugs and to expect the outcome and prognosis (Jerusalem et al, 2006). Regarding the age and sex in this study was in agreement with other studies. Most series reviewing CUP patient groups gave an approximate equal incidence for men and women and a median age on presentation for both sex ranged 59-66 years (Glover et al, 2008, and Greco and Hainsworth, 2008).

The site of metastases on presentation also varies in different studies. Briasoulis E. (1997) reported the liver and bone then the lung and lymph nodes as the commonest metastases sites (Briasoulis and Pavlidis, 1997).

Rades D, et al (2001) found that commonest presenting metastatic sites were lymph nodes and visceral organs. The National Cancer Institute (2008) declared that lungs, liver, brain, and bones are the most common metastasis sites seen in solid tumors. In the current study the peritoneum was the commonest site of metastases, this was in agreement with the results of other series (Agarwal et al, 2004 and Shaw and Sobin, 2006). LevyAD et al (2008) also found that the peritoneal cavity is the most common side for secondary cancers and consider it as a merrier for carcinomas of gastrointestinal tract and ovary (LevyAD et al, 2008).

In the past, peritoneal metastases were considered as a final stage of cancer, and patients were offered a palliative chemotherapy. In 2003 and the following years, prolonged survival of patients was reported in randomized trials, after recognition and treating primary site and treating the peritoneal metastases with a preoperative hyper-thermic intra-peritoneal chemotherapy (Verwaal et al, 2003,Sugarbaker, 2009, and Yonemura et al, 2010).

In the current study as in the majority of other studies (American Cancer Society, 2013) CUPs were mainly adenocarcinomas and undifferentiated tumors; less commonly, squamous cell carcinoma, melanoma and sarcoma.

Secondary metastasis is the main presentation of about 2-6% of cancer's patients in which investigations fail to find the primary site lesion. (Sendler A, et. 2008)

The development and application of more sophisticated diagnostic tests will decrease the incidence and prevalence of CUP. However, CUP follows an aggressive biological and clinical behavior, with a median survival ranging from only 2 to 10 months (Pavlidis and Fizazi, 2009). Nevertheless, it can be hypothesized that detection of a primary tumor may optimize treatment planning, which, in turn, may improve patient outcome. Indeed, some studies have shown that the survival of patients in whom a primary tumor was eventually detected was higher than in patients in whom the primary tumor remained undetected (Raber et al, 1991 and Haas et al, 2002).Sometimes the primary site cannot be determined even at postmortem examination (Neumann and Nystrom 1982).

CONCLUSION

The appropriate use and interpretation of IHC is necessary to differentiate primary from secondary tumor and to minimize the list of possible origin in CUP. The lack of a generally agreed definition of CUP has limited the ability to obtain accurate data about incidence and outcome for this group of patients. In the near future, an advanced multi-parametric approach, including the use of CT scan or whole-body MRI techniques, IHC and molecular technology is expected to decrease the incidence of CUP and improve the therapeutic management and survival in patients diagnosed with primary of unknown primary origin.

REFERENCES

- Agarwal A, Yeh BM, Breiman RS et-al. (2004).Peritoneal calcification: causes and distinguishing features on CT. AJR Am J Roentgenol.182 (2): 441-5.
- American Cancer Society.(2013). Cancer Facts and Figures. Atlanta, Ga: American Cancer Society 2013.
- American Cancer Society. Statistics for 2007. American Cancer Society Statistics. Available at http://www. cancer.org/ Research/CancerFactsFigures/index.Accessed July 11, 2007.
- Armstrong AC, Blackhall FH (2007). Management of cancer from an unknown primary. Expert Opin Pharmacother; 8:445-55.
- Bahrami A., Truong L. D., Ro J. Y.(2008). Undifferentiated tumor: True identity by immune-histochemistry. Arch Pathol Lab Med 132, 326–48.
- Briasoulis E, Pavlidis N (1997). "Cancer of Unknown Primary Origin". Oncologist 2 (3): 142–52.
- Glover KY, Varadhachary GR, Lenzi R, et al. (2008). Unknown primary cancer. In: Abeloff MD, Armitage JO, Lichter AS, Niederhuber JE. Kastan MB, McKenna WG.eds.Clinical Oncology. 4th ed. Philadelphia, Pa; Elsevier;: 2057-74.
- Greco FA, Hainsworth JD. (2008). Cancer of unknown primary site. In: DeVita VT, Lawrence TS, Rosenberg SA, eds. DeVita, Hellman, and Rosenberg's Cancer: Principles and Practice of Oncology. 8th ed. Philadelphia, Pa: Lippincott Williams & Wilkins; 2363-87.
- Haas I, Hoffmann TK, Engers R, Ganzer U. (2002).Diagnostic strategies in cervical carcinoma of an unknown primary (CUP) Eur Arch Otorhinolaryngol. 9:323–25.
- Horlings HM, van Laar RK, Kerst JM, et (2008) Gene expression profiling to identify the histo-genetic origin of metastatic adeno-carcinomas of unknown primary. J Clin Oncol 26:4435–4441.
- Jerusalem G, Rorive A, Ancion G, et al. (2006).Diagnostic and therapeutic management of carcinoma of unknown primary: radio-imaging investigations. Ann Oncol. Sep;17Suppl 10:x168-176
- Kumar, Vinay; Abbas, Abul K; Fausto, Nelson; Robbins, Stanley L; Cotran, Ramzi S (2005). Robbins and Cotran pathologic basis of disease (7th Ed.). Philadelphia: Elsevier Saunders. 978-187-8.
- LevyAD, Arnáiz J, Shaw JC, Sobin LH. (2008). Primary peritoneal tumors: imaging features with pathologic correlation. *RadioGraphics*; 28: 583–607.
- Lotan TL, Ye H, Melamed J, Wu XR, Shih Ie M, et al. (2009). Immunohistochemical panel to identify the primary site of invasive micropapillarycarcinoma.Am J SurgPathol 33: 1037–41.
- Mangham DC, Bradwell AR, Isaacson PG.(2000). MICA-a highly sensitive and avidin-free immune-histochemical detection system. dv AnatPathol. Nov; 7 (6):360-4.
- Miettinen M. Keratin (1993).Immunohistochemistry: update of applications and pitfalls. *PatholAnnu* ; 28: 113–43
- National Cancer Institute: Metastatic Cancer: Retrieved on 2008-11-01
- Pavlidis N, Briasoulis E, Pentheroudakis G (2010). Cancers of unknown primary site: ESMO Clinical Practice Guidelines for diagnosis, treatment and follow-up. Ann Oncol 21: Suppl 5v228–31.
- Pavlidis N, Fizazi K. (2009). Carcinoma of unknown primary (CUP) Crit Rev OncolHematol. ; 69:271–278.
- Raber MN, Faintuch J, Abbruzzese JL, Sumrall C, Frost P. (1991).Continuous infusion 5-fluorouracil, etoposide and cis-diamminedichloroplatinum in patients with metastatic carcinoma of unknown primary origin. Ann Oncol. 2:519–20.
- Rades D, Kühnel G, Wildfang I, Börner AR, Schmoll HJ, Knapp W. (2001). Localised disease in cancer of unknown primary (CUP): the value of positron emission tomography (PET) for individual therapeutic management. Germany Ann Oncol. Nov;12(11):1605-9.
- Ringenberg QS (1985).Tumors of unknown origin. Med PediatrOncol 13 (5): 301-6.
- Robert Weinberg, (2007). The Biology of Cancer, cited in Basics: A mutinous group of cells on a greedy, destructive task, by Natalie Angier, New York Times, 3 April
- Sendler A, et. Carcinoma of unknown primary site (CUP syndrome). Chirurg. 2008 Jul;79(7):689-95
- Shaw JC, Sobin LH. (2006). Secondary tumors and tumorlike lesions of the peritoneal cavity: imaging features with pathologic correlation. Radiographics. 29 (2): 347-73.
- Sugarbaker P. H., (2009). "Epithelial appendiceal neoplasms," Cancer Journal, vol. 15, no. 3, pp. 225–35.
- Tot T (2002).Cytokeratins 20 and 7 as biomarkers: usefulness in discriminating primary from metastatic adenocarcinoma. Eur J Cancer 38: 758–63.
- V. J. Verwaal, S. Van Ruth, E. De Bree et al., (2003). "Randomized trial of cytoreduction and hyperthermicintraperitoneal chemotherapy versus systemic chemotherapy and palliative surgery in patients with peritoneal carcinomatosis of colorectal cancer," Journal of Clinical Oncology, vol. 21, no. 20, pp. 3737–43.
- Varadhachary GR, Raber MN, Matamoros A, Abbruzzese JL (2008).Carcinoma of unknown primary with a colon-cancer profile-changing paradigm and emerging definitions. Lancet Oncol 9: 596–99.
- Y. Yonemura, A. Elnemr, Y. Endou, et al., (2012)."Effects of neoadjuvantintraperitoneal/systemic chemotherapy (bidirectional chemotherapy) for the treatment of patients with peritoneal metastasis from gastric cancer," International Journal of Surgical Oncology, vol. 2012, Article ID 148420, p. 8.

ماركەرێن بویاغێن كیمیایی یێن شانەیی یێن بەرگریێ بۆ دیاركرنا شانەیێن دەستپێكی یێن نەخوشیا پەنجەشێرا ڤەگوهێزەر پوختە

باكگراوەند :

پەنجەشێرا ڤەگوهێزەر رەنگە ببیە نیاشا دەستپێكی بۆ كەسێن نەخوشیا پەنجەشێرێ هەین، ب رەنگەكی كو شانەیێن دەستپێكێ نەیا زانراوە. ل ڤی دەمی ب كارئینانا بویاغاێن كیمیایی یێن شانەیی یێن بەرگریێ IHC گەلەك یا گرنگە، ئەوژی ب هاریكاریا خشتەیێن ماركەرێن بەرگریێ بۆ زانینا جورێ پەنجەشێرێ یانژی شانەیا دەستپێكی ژ پێخەمەت دانا چارەسەریەكا گونجایی بۆ كەسێ نەخوش ل سەنتەرێن چارەسەریێ.

ئارمانج :

ب كارئینانا بویاغێن IHC بۆ خشتەیان ل دەمێ دەستنیشانكرنا نەخوشیێ ب هاریكاریا شروڤەكرنا شانەیی یێن نەخوشیا ڤەگوهێزەر وەك نەخوشیا پەنجەشێرا ڤەگوهێزەر ئەوژی ژ بۆ زانینا شانەیا دەستپێكی و خواندنا هندەك سیفەتێن ڤان جورە پەنجەشێران، وەك جورێ پەنجەشێران و ژێدەرێن سەرەكی یێن وان و ئەو جهێن سەرەگكی یێن ئەڤ نەخوشیە لێ بەلاڤەدبن.

نەخوش و رێك :

پشتی چاڤپێكەفتنێ دگەل 1316 حالەتێن نەخوشیا پەنجەشێرێ یێن كو ل تاقیگەها ناڤەندی ل پارێزگەها دهوكێ هاتینە دەستنیشانكرن هەر ژ هەیڤا تەباخا 2009 هەتا كانونا ئێكێ یا سالا 2012، دناڤ ڤان حالەتاندا دیاربوو كو 175 حالەت ژ جورێ پەنجەشێرا ڤەگوهێزەرن یێن كو ژێدەرێ وان نەهاتیە زانین، ئەوژی ب هاریكاریا شروڤەكرنا شانەیی بۆ نەخوشان. هەردیسان خشتە بۆ ماركەرێن جوداجودا یێن IHC هاتنە بكارئینان ژ بۆ دەستنیشانكرنا جور و ئەگەرێ وەرمینێ. ئەڤ گروپە هاتنە هەلبژارتن لسەر بنەمایێ ئەنجامێن بۆ خشتەیێن جوداجودا.

ئەنجام :

ژ سەرجەمێ 1316 حالەتان، 175 حالەت وەك نەخوشیا پەنجەشێرێ یا ڤەگوهێزەر هاتنە دەستنشانكرن ئەوژی ب هاریكاریا تەكنیكا شروڤەكرنا شانەیی. پشتی ب كارئینانا IHC دیاربوو كو بتنێ 162 حالەت (12.3%) ژ جورێ پەنجەشێرا ڤەگوهێزەربوون. جهێ سەرەكی یێ ڤەگوهاستنێ ژی ل دەمێ دەستنیشانكرنێ ڤالاهیا زكی ل نێزیك هەستیكان، گرێیێن لیمفاوی، مێلاكا ڕەش، مێلاكێن سور، پەردەیێ مێلاكێن سور دنخیڤیت و هێلكەدان. شروڤەكەرێ IHC دیاركر پەنجەشێرێن خانەیێن نافپوش جورێ ئێكێ یێ پەنجەشێرێن ڤەگوهێزەرن كو دهێنە هەژمارتن پەنجەشێرێن نەدیار و بەرنیاس، پاشی پەنجەشێرا لیمفاوی و پەنجەشێرا هناڤان و پەنجەشێرا دەماری. ژێدەرێ سەرەكی یێ پەنجەشێرێن ڤەگوهێزەر سیستەمێ هەرسكرنێ بوو كو ب شێوەیەكێ سەرەكی دهاتە ڤەگوهاستن بۆ ڤالاهیا زكی و گرێیێن لیمفاوی و مێلاكا رەش و هێلكەدانێ.

دەرئەنجام :

ب هاریكاریا ڤێ ڤەكولینێ گرنگیا تەكنیكا IHC هاتە دیاركرن وەك دەستنیشانكەرەكێ هاریكار یێ گرنگ بۆ جودانكرنا و نیاسینا جورێن پەنجەشێرا ڤەگوهێزەر و ژ جورێ دەستپێكێ و دیاركرنا جورێ پەنجەشێرێ و شانەیا دەستپێكێ یا تووشبوی ئەوژی ژ پێخەمەت دانا چارەسەریەكا گونجایی.

معلمات الصبغات الكيميائية النسيجية المناعية في معرفة النسيج المنشأي للسرطانات المنتشرة داخل الجسم

الخلاصة

الخلفية: يمكن للسرطانات المنتشرة ان تمثل العارض الأول لمرضى السرطانات, حيث يكون النسيج المنشأ غير معروف. في مثل هذه الحالات يكون استخدام الصبغات الكيميائية النسيجية المناعية (IHC) ضروريا, عن طريق مجموعة متعاقبه للمعلمات المناعية لمعرفة نوع السرطان أو النسيج المنشأ لأعطاء العلاج المناسب في مراكز العلاج.

الهدف:استخدام IHC ب مجموعة متعاقبه لحالات تشخص بواسطة التحليل النسيجي المرضي المعتاد كسرطانات منتقلة وذلك لمعرفة النسيج الأولي ودراسه بعض خصائص هذه السرطانات, مثل نوع السرطانات والمصادر الرئيسيه لها والأماكن الرئيسيه لأنتشارها.

المرضى والطرق: بعد مراجعة1316 حاله سرطان تم تشخيصهم في المختبر المركزي في دهوك / العراق، من اب 2009 إلى كانونالأول 2012, وجد أن 175 حاله منهم شخصت على أنها سرطانات منتشرة غير معروفة الأصل بواسطة التحليل النسيجي المرضي. تم استخدام جداول لمعلمات مختلفة من IHC لتحديد نوع وأصل الورم. تم اختيار هذه المجموعات اعتمادا على النتائج لمختلف جداول المعلمات.

النتائج: من أصل 1316 حالة سرطان, تم تشخيص 175 حاله كسرطان منتشرة بواسطة التحليل النسيجي المرضي. بعد استخدام IHC وجد ان فقط 162 حاله (12,3%) منهم هي فعلا سرطان منتقل. الموقع الرئيسي للأنتقال في وقت التشخيص هوالتجويف البطني يعقبه العظم, العقد اللمفاويه, الكبد, الرئه, غشاء الرئه والمبيض. كشف تحليل IHC أن سرطانات الخلايا البطانيه هوالنوع الأول للسرطانات المنتشرة, يليه السرطان الغير متمايز, ثم السرطان اللمفاوي, والسرطان الحشوي, والسرطان العصبي الصماوي. لقد كان المصدر الأولي للسرطانات المنتقله هوالجهاز الهضمي حيث كان انتقاله بشكل اساسي الى التجويف البطني يعقبه العظم, العقد اللمفاويه, الكبد والمبيض

الاستنتاج: لقد تم تاكيد اهمية تقنية IHC كتشخيص مساعد هام للتمييز بين السرطان المنتقل والأولي وللتحقق من نوع السرطان والنسيج الأولي له وذلك لأعطاء العلاج المناسب.

SPECTROPHOTOMETRIC DETERMINATION OF MASALAMINE USING 9-CHLOROACRIDINE REAGENT–FOR SOME PHARMACEUTICAL FORMULATIONS

SUZAN AHMED ALI* , Shrieen Othman** and Theia'a Najim Al-Sabha***
*Directorate of Education-Sumeal
** Dept. of Chemistry , Faculty of Science, University of Zakho, Kurdistan Region-Iraq
*** Dept. of Chemistry , College of Education , University of mosul-Iraq

(Received: June 23, 2013; Accepted for publication: February 3, 2014)

ABSTRACT

A spectrophotometric method is proposed for the determination of mesalamine drug in their pure forms and in pharmaceutical formulations, based on the product formation reaction with 9-chloroacridine (9-CA). The molar absorptivity values are 1.8×10^3 $L.mol^{-1}.cm^{-1}$ and the lower limit of detection (LOD) and limit of quantitation (LOQ) are 1.8733 and 5.676 µg/ml respectively. The stoichiometry of the drug-9-CA product was found to be 1:1. The procedure is characterised by its simplicity with good accuracy and precision and no interference was observed from common pharmaceutical excipients. The proposed method was applied successfully for the determination of mesalamine in their pharmaceutical formulations and the obtained results were statistically compared with those given by the official method.

KEYWORDRS: Spectrophotometric, Mesalamine, 9-Chloroacridine.

INTRODUCTION

Mesalamine also known as mesalazine, chemically known as 5-aminosalicylic acid(5-ASA) was used for its local effects in the treatment of inflammatory bowel disease, including ulcerative colitis and Crohn's disease [1,2]. Despite the fact that it has been used for over 50 years, the mechanism of action of this drug remains unkown. Mesalamine has been shown to be a potent scavenger of reactive oxygen species that play a significant role in the pathogenesis of inflammatory bowel disease, inhibition of natural killer cell activity, inhibition of antibody synthesis, inhibition of cyclo-oxygenase and lipoxygenase pathways and impairment of neutrophil function [3,4].

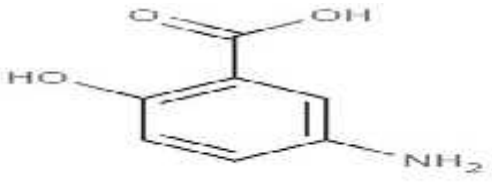

5-Aminosalicylic acid
(5-ASA)

Many Spectrophotometric methods depending on using various reagent have been reported for the determination of mesalamine drug. p-Dimethyl amino benzaldehyde, 2,2^{-}–bipyridyl or potassium ferricyanide in the presence of ferric chloride[5], N-(1-naphthyl)ethylenediamine dihydrochloride[6], tetracyanoethylene (TCNE) and 2,3-dichloro-5,6-dicyano-1,4-benzoquinone (DDQ)[7] are used for the determination of mesalamine. The HPLC method, for the determination of mesalamine, adopted by the British Pharmacopoeia (BP) was used the mobile phase containing glacial acetic acid, methanol and methyl isobutyl ketone (10:40:50 v/v)[8]. Nanostructured nickel-aluminum layered double hydroxide (Ni-Al LDH) was synthesized and the potential of the obtained material, as solid-phase extraction (SPE) sorbent, for the separation and pre-concentration of the trace amount of mesalamine was assessed using column method. The retained analyte on Ni-Al LDH was eluted with NaOH solution and the concentration of the elueted mesalamine was then spectrofluorometrically determined at λem = 480 nm with excitation at λex = 340 nm. The calibration graph for the pre-concentration system was linear in the range of 0.1-45.0 µg/ml [9].

The oxidative behavior of mesalamine has been investigated by differential pulse voltammetry using a glassy carbon electrode in different buffer systems. Linear sweep voltammetry was used to study the influence of pH on the peak current and peak potential. The Britton-Robinson buffer of pH 1.81 was selected as a suitable analytical medium in which mesalamine exhibited a sensitive diffusion controlled oxidative peak at 0.564 V (vs. Ag/AgCl). The peak current varied linearly with drug concentration in the range between 1 x 10^{-6}

M and 2 x 10^{-4} M [10]. The present work is a simple and selective spectrophotometric method for determination mesalamine and application to pharmaceutical formulations. The method is based on the reaction of mesalamine with 9-CA as chromogenic reagent without any derivatisation or catalysis.

EXPERIMENTAL

Apparatus

Spectral and absorbance measurements were made with U.V double beam spectrophotometers (Perkin-Elmer, lambda 25) with 1-cm matched silica cells.

The pH measurements were made by using both Cyber Scan 510 pc. pH meter with a combined glass electrode. Heating of solutions was carried out on a water bath of frost instruments, LTD. Weighing was carried out on a sensitive balance type of Mettler H 54AR.

Reagents

All chemicals used of the highest purity available which are provided by BDH , Fluka and Molekula companies. 9-CA (Eastman chemical co.) was used as the chromogenic reagent.

Stositis 9-Chloroacridine Reagent (1×10^{-3} M) Solution:

This solution was prepared by dissolving 0.0053 g of 9-CA in absolute ethanol and then the volume was completed to 25 ml in a volumetric flask. This solution was prepared daily and used immediately [11].

Sodium Hydroxide(1×10^{-2}M) Solution: This solution was prepared by appropriate dilution of the concentrated solution (1N) with distilled water.

Hydrochloric Acid (1×10^{-2}M) Solution: This solution was prepared by appropriate dilution of the concentrated solution (1N) with distilled water.

Mesalamine Pure Standard Solution : 100 µg/ml solution was prepared by dissolving 0.01g of pure mesalamine in 100 ml absolute ethanol in volumetric flask.

Preliminary Investigation

In the preliminary investigation work, it was found that 9-CA reagent reacted selectively with mesalamine in alcoholic medium of ethanol and produced a yellowish-green colored solution immediately with maximum absorption at λ_{max} in visible region 436 nm. The intensity of this color increased when the reaction mixture was heated and in contrast to the reagent blank which showed a maximum absorption at 392 nm. However, the wavelength of maximum absorption 436 nm was used in all subsequent experiments.

Study of the Optimum Reaction Conditions

The effect of various parameters on the absorption intensity of the colored 9-CA-mesalamine product has been investigated and the reaction conditions have been optimised

Effect of pH

The effect of pH on color intensity was first examined by mixing 0.5ml of 100 µg/ml mesalamine and 1 ml of 1×10^{-3} M 9-CA, in a 5 ml calibrated flask. The reaction mixture was diluted to the mark with absolute ethanol and the absorbance was measured at 436 nm after leaving the solution for 10 min at room temperature against the reagent blank and the pH of the final solution was measured and found 8.92.

A range between 2.15 and 10.50 pH value obtained in the final volume, by addition of 0.01 M of HCl and NaOH, was examined. It was found that the sensitivity of the product was not affected by the addition of HCl but decreased in the case of NaOH (Table 1, Table 2).

Table (1) : -Effect of pH on color intensity of mesalamine-9-CA product using HCl

Conditions	Consentrations					
HCl (0.01M),ml	**0**	**0.2**	**0.4**	**0.6**	**0.8**	**1.0**
Absorbance	0.106	0.103	0.102	0.102	0.101	0.100
pH	8.92	2.34	2.30	2.27	2.21	2.15

Table (2) :- Effect of pH on color intensity of mesalamine-9-CA product using NaOH

Conditions	Consentrations					
NaOH (0.01M),ml	**0**	**0.2**	**0.4**	**0.6**	**0.8**	**1.0**
Absorbance	0.105	0.099	0.096	0.095	0.075	0.073
pH	8.92	9.31	9.52	9.82	10.05	10.50

A series of different buffer solutions, such as sodium hydrogen carbonate, borate and phosphate of pH (8.92) were prepared with NaOH sodium hydroxide and examined. The results in Table (3) show a negative effect on the absorbance of the product

Table (3) :- Effect of buffer solution on color intensity

Type of Buffer	Absorbance
Without	0.105
($Na_2B_4O_7.10H_2O$+KCl)+NaOH	0.100
Na_2HPO_4+NaOH	0.065
$NaHCO_3$+NaOH	0.077

Effect of Reagent Concentration

Different volumes of (1×10^{-3} M) 9-CA were added to a solution containing 10 µg/ml of mesalamine in a final volume of 5 ml. The absorbance was measured at 436 nm after 10 min at room temperature against reagent blank. It was evident that the absorbance increases with increasing reagent concentration and reached maximum on using a volume of 3.0-3.4 ml of 9-CA (Table 4) and 3 ml was selected in the subsequent experiments

Condition	Reading of differentue as wents							
9-CA 1×10^{-3}M (ml)	**0**	**1.0**	**1.5**	**2.0**	**2.5**	**3.0**	**3.2**	**3.4**
Absorbance	0.0058	0.106	0.109	0.129	0.149	0.176	0.174	0.173

Table (4) :- Effect of the concentration of reagent on absorbance.

Effect of Surfactants

Effect of various surfactants including SDS, CTAB, Tween-80 and Triton x-100, of 0.2 % concentration, on the absorption intensity of the mesalamine-9-CA product has been investigated. As shown in Table (5), there was no effect of these surfactants on the absorbance of mesalamine-9-CA product.

Table (5) :- Effect of surfactant on color intensity

Surfactant	Absorbane
Without	0.175
SDS	0.161
CTAB	0.172
TritonX-100	0.173

Effect of Temperature and Development Time

The effect of temperature on the rate of reaction for mesalamine-9-CA product was studied at room temperature (22°C), 40°C, 50°C and 60°C under the previous optimum reaction conditions. The results indicated that product was formed after addition of reagent immediately and reached its maximum absorbance at 50°C after 15 min and remain constant for 55 min after which the absorbance was decreased indicating dissociation (Table 6). Whereas, a decrease in

absorbance with increased temperature was ating dissociation.
notic
ed
indic

Time(min)	Absorbance			
	R.T	40 °C	50 °C	60 °C
0.0	0.055	-----	-----	-----
5	0.105	0.107	0.110	0.108
10	0.175	0.180	0.182	0.183
15	0.180	0.183	0.195	0.185
20	0.183	0.185	0.195	0.187
25	0.183	0186	0.195	0.189
30	0.185	0.186	0.195	0.190
40	0.185	0.189	0.195	0.192
50	0.187	0.193	0.195	0.191
60	0.188	0.193	0.195	0.191
70	0.191	0.190	0.193	----
80	0.191	----	----	----
90	0.190	----	----	----

Table (6) : - Effect of temperature on the formation and stability of the mesalamine-9-CA product

However; the optimum reaction conditions for determination of mesalamine have been summarized in Table (7).

Table (7) :- Summary of optimum conditions for the determination of mesalamine

Compound	λ_{max} (nm)	Abs.	Temp. (°C)	9-CA 1×10^{-3} M (ml)	Development time(min)	Stability period(min)	Final pH
mesalamine	436	0.195	50	3.0	15	55	8.92

Final Absorption Spectra

Using the optimum condition described previously, the absorption spectra were recorded within 382 and 600 nm(Fig. 1). The yellow dye formed gave maximum absorption at 436 nm for mesalamine-9-CA product against reagent blank which showed low absorbance at the above λ_{max} and maximum absorption at 392 nm. These wavelength at maximum absorption have been selected for the recommended procedure.

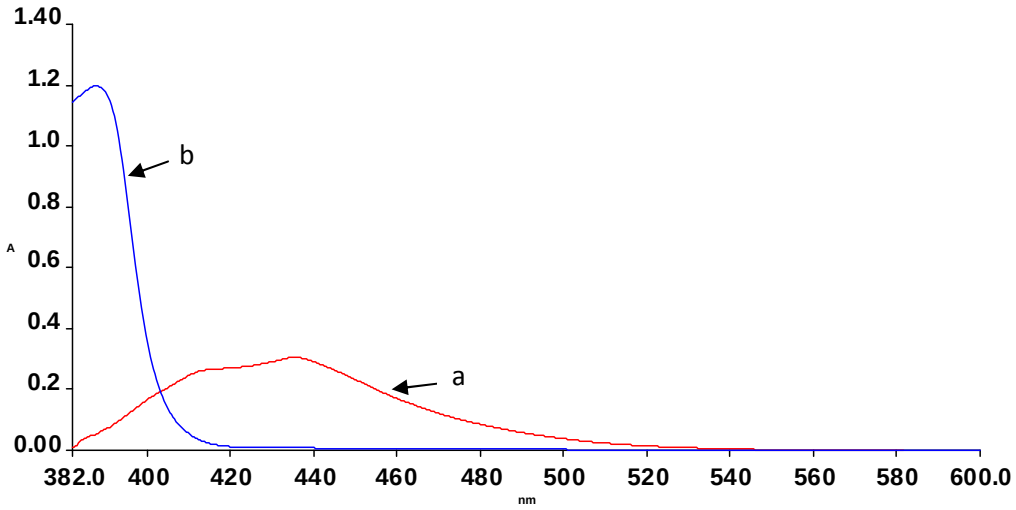

Fig (1): Absorption spectra of:
a) 25 µg/ml mesalamine versus reagent blank and
b) reagent blank versus ethanol.

Recommended Procedure

To a series of 5 ml calibrated flasks, increasing volumes of the working mesalamine solution (100 µg/ml) were transferred to cover the concentration range 2-28 µg/ml, followed by addition of 3 ml of 1×10^{-3} M 9-CA . The solutions were diluted to the mark with absolute ethanol and the blank solution was prepared in a similar way without mesalamine. The solutions were kept at 50°C for 15 min in a water bath and the absorbance was measured at 436 nm after cooling the room temperature.

Quantitation

A plot of absorbance versus determined concentration Fig. (2) shows that Beer's law was obeyed over the range 2-28 µg/ml and molar absorptivity was 1.8×10^{3} L. $mol^{-1}.cm^{-1}$, Table (9), which indicating that the method was sensitive. The linearity was represented by the regression equation and the corresponding correlation coefficient for the studied mesalamine determined by the proposed method represents excellent linearity (Table 8). LOD and LOQ were determined as described in chapter two and the values are cited in Table (9)

Fig (2) :- Calibration graph for determination of mesalamine

compound	slope	Intercept	Correlation Coefficient
mesalamine	0.012	0.018	0.994

compound	Linearity range (µg/ml)	Molar absorptivity ($L.mol^{-1}.cm^{-1}$)	LOD (µg/ml)	LOQ (µg/ml)	Sandell's Sensitivity ($\mu g.cm^{-2}$)
mesalamine	2.0-28	1.8×10^{3}	1.8733	5.676	0.08333

Table (8):- Slopes, intercepts and correlation coefficients for the determination of mesalamine

Table (9): Summary of the quantitation values of the proposed method

Accuracy and Precision of the Method

To check the accuracy and precision of the method , the recovery % and RSD for the determination of mesalamine were estimated at four replicates of three different concentrations. The results shown in Table (10) indicated reasonably good accuracy (average recovery 100.4 %) while RSD ≤4.3 % .

Table (10) :- Accuracy and precision of the method

compound	Amount added (µg/ml)	Recovery* %	Average recovery %	Error %	R.S.D* %
mesalamine	4.0	95.32	100.4	-4.68	4.3
	14.0	104.46		4.46	2.5
	22.0	101.42		1.42	2.0

*Average of four determinations.

Study of Interferences

The extent of interference by some excipients which often accompany pharmaceutical preparations were studied by measuring the absorbance of solutions containing fixed amount of drug (14 µg/ml) and various amounts of diverse species in a final volume of 5 ml. It was found that the studied excipients did not interfere seriously (Table 11). Slight positive interference was observed in the presence of large excess of excipients. However; an error of 5.0 % in the absorbance readings was considered tolerable. Typical results are given in Table (11).

Table (11) :- Effect of exciepient on the determination of 14 µg/ml mesalamine

Exciepient	Recovery % of 14 µg/ml in the presence of						
	40	120	200	280	400	480	560
NaCl	96.59	93.66	95.61	96.59	96.1	99.52	98.05
Lactose	100	----	105.37	103.41	102.43	103.90	103.41
Glucose	99.03	----	105.34	104.47	97.57	95.63	96.60
Acacia	104.37	----	----	105.83	103.88	103.88	103.39
Sucrose	98.05	105.85	104.88	103.90	100	100.98	97.07

Nature of the Colored Product

The most wiely applied method is that of continuous variation introduced by Job's and molar ratio methods [12] . The mesalamine with 9-CA have been studied by these methods using the recommended procedure.

Job's Method

Job's method of continuous variation was employed to establish the stoichiometry of the colored product. A $1x10^{-3}$ M standard solutions of mesalamine and 9-CA reagent were used. A series of solutions were prepared in which the total volume of mesalamine and reagent was kept at 2 ml. The reagents were mixed in various proportions diluted to volume in a 5-ml calibrated flask with absolute ethanol and the general procedure followed.

As shown in Fig. (3), the result indicated that the stoichiometric composition of the product was 1:1 (mesalamine : 9-CA) was formed. This indicates that aromatic amino group presented in the compound was responsible for the formation of the product.

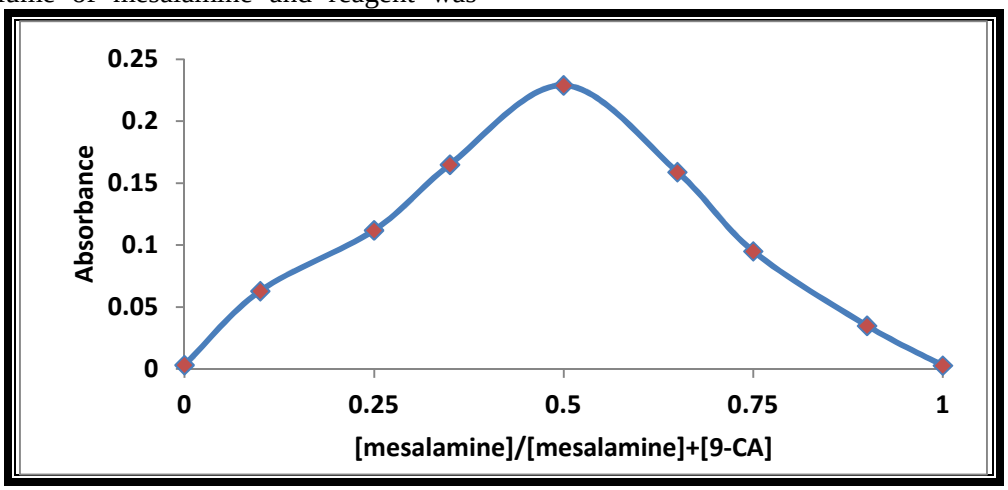

Fig. (3) :- Continuous variation plot for the mesalamine– 9-CA

Mole Ratio Method

Application of a molar ratio method was determined by the inflection point in a plot of the absorption versus the molar ratio of the reactants. Different volumes of $1x10^{-3}$ M 9-CA were added to the fixed volume (1ml) of $1x10^{-3}$ M mesalamine, then the solution was diluted to the mark in 5-ml volumetric flask with absolute ethanol and the general procedure followed. The intersections of the obtained straight lines indicate the molar ratio of the product. As shown in Fig.(4), the result also proved the formation of the 1:1stochiometry.

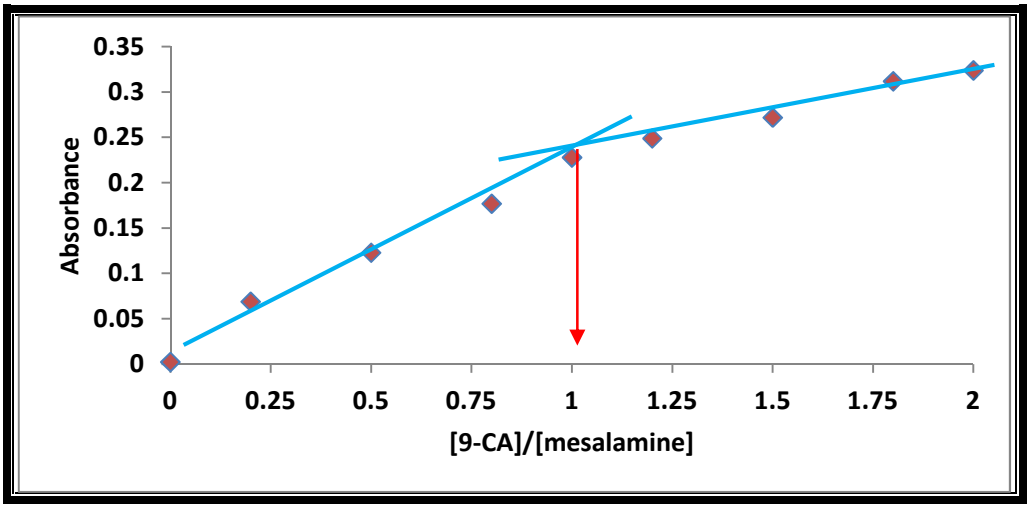

Fig. (4):- Mole ratio plot for mesalamine–9-CA product (1:1)ratio

Solutions were carefully formulated so as to contain one proportion of mesalamine to one of the 9-CA reagent exactly. Under these conditions, the complex was appreciably dissociated, and as it has been expected, it was found of low absorbance, that is A_s, is obtained. Similar solutions were then prepared containing the same amount of mesalamine, but with an optimum amount of 9-CA reagent. It can be assumed, in the latter case, that the mesalamine – 9-CA product has been largely associated and it would consequently have a higher absorbance, i.e. A_m. The difference between the two absorbances however, represents a measure of the degree of dissociation of the product.

$$\alpha = A_m - A_s / A_m$$

Where:

α = degree of dissociation

A_m= the absorbance of the solution containing excess amount of reagent relative to the mesalamine.

A_s= the absorbance of the solution containing stoichiometric amount of mesalamine and reagent.

The conditional stability constant of the 1:1 mesalamine-9-CA product, the reaction between the amine (A) and reagent (B) proceed according to :

$$\begin{array}{ccccc} A & + & B & \rightleftharpoons & AB \\ \alpha & & \alpha & & 1-\alpha \end{array}$$

They can be expressed by the rats constant as:

$$K = (1-\alpha) / \alpha^2 C$$

Where:

K= Stability constant of the product.

C= final molar concentration of mesalamine (1×10^{-3}M).

The results cited in Table (12) indicated that the product is stable.

Table (12):- Stability constant of mesalamine – 9-CA product at concentration(1×10^{-3})M.

Compound	Vol. of mesalamine	Absorbance		α	Average K_{st} ($L.mol^{-1}$)
		A_s	A_m		

mesalamine	0.5	0.135	0.210	0.35714	4.53×10^4
	1.0	0.226	0.289	0.21799	
	1.5	0.314	0.343	0.08455	

Proposed Chemical Reaction

The method was based on the reaction of mesalamine with 9-CA to form colored product with maximum absorption at 436 nm. The molar ratio of mesalamine to reagent was 1:1. This can be explained by the proposed following reactions. Scheme (1).

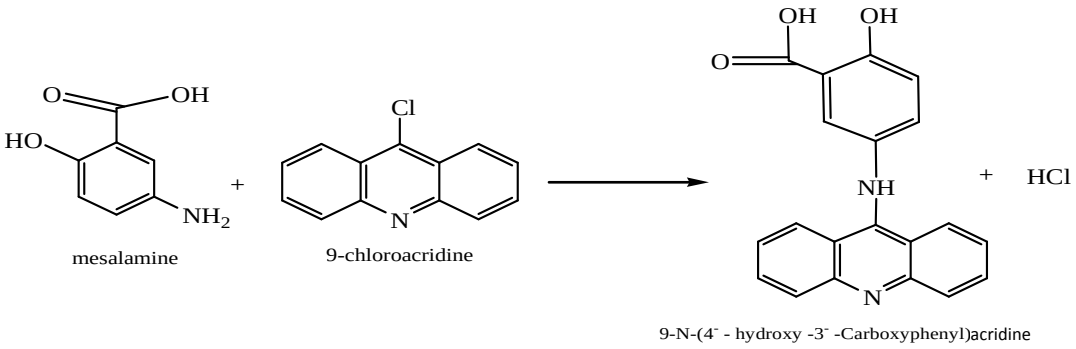

Scheme (1):- Proposed mechanism of formation reaction for assay of the mesalamine by 9-CA, HCl

Analysis of Pharmaceutical Formulations

Tablets and Capsules

Ten tablets or capsules content for each drug were weighed and finely powdered, an accurately weighed portion of the powder equivalent to 400 mg of mesalamine was dissolved in ethanol. Shaking for 10 min, then filtered through Whatmann no. 42 filter paper into 50 ml standard flask and the filtrate was diluted to the mark by repeated washing with ethanol. Solutions of lower concentrations were prepared by appropriate dilution with ethanol. The concentration of drug per capsule and tablet was determined using its respective calibration graph constructed for pure drug by the following general procedure**.**

The proposed method was successfully applied to determine mesalamine in pharmaceutical capsules and tablets formulations. The obtained results were compared statistically by a Student's *t*-test for accuracy and a variance ratio *F*-test for precision with the official method[13] procedure, as cited below, at the 95% confidence level with four degrees of freedom, as shown in Table (13). The results showed that the experimental *t*-test and *F*-test were less than the theoretical value (t= 3.182, F= 9.12), indicating that there was no significant difference between the proposed method and official method. The proposed method was compared favorably with other reported methods as shown in Table (14).

British Pharmacopeia Procedure

The British pharmacopeia 2008 procedure were based on a potentiometric titration and the end point was determined by the following variation of potential difference between two electrodes (indicator and reference electrodes) immersed in the 100 ml solution containing 50 mg mesalamine (this solution was prepared by dissolving mesalamine in boiling water and then cooled rapidly to room temperature). This solution was titrated against 0.1 M NaOH and the graph of the variation of the potential difference as a function of the quantity of NaOH added has been plotted. As shown in Fig. (5), the end-point corresponds to sharp variation of potential difference was 3.3 ml NaOH and by applying the equation (1ml of 0.1 M sodium hydroxide was equivalent to 15.31 mg of

mesalamine) the recovery amount was found 50.523 mg mesalamine.[14]

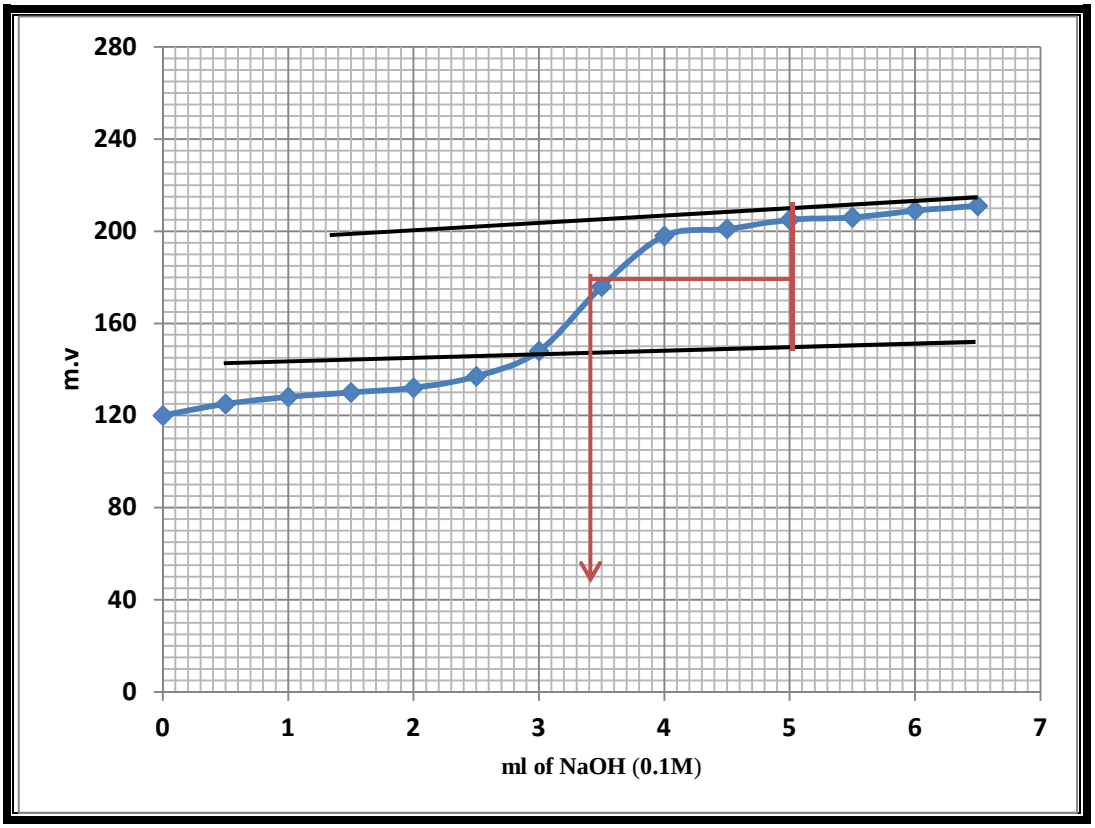

Fig. (5):- Potientiometric titration of mesalamine using British pharmacopeia procedure

Table(13): Assay of mesalamine in pharmaceutical preparations using the proposed method and comparison with the official method

Procedure applied	Pharmaceutical formulations	Drug amount present («g/ml)	Recovery[a] (%)	Average recovery (%)	Drug content found (mg)	Certified value (mg)
Proposed 9-CA method	Tablet Mesacol[d]	8 16 20	101.05 101.56 102.50	101.70	406.8 (1.00)[b],(7.54)[c]	400
	Capsule Mesacol[d]	8 16 20	100 102.50 97.35	99.95	399.8 (2.10)[b],(4.62)[c]	400
British Pharmacopoeia	Pure form mesalamine	50 mg	101.06	-	50.532	50

a Average of four determinations.
b Figure in parenthesis are the calculated values for t.
c Figure in parenthesis are the calculated values for F
d Manufactured by Universal Pharmaceutical Industries unipharama–Damascus – Syria

COMPARISON OF THE METHODS

Table (14) shows the comparison between some of analytical variables obtained from the present method with that of the recent spectrophotometric methods.

Table (14):- Comparison of the proposed method with other spectrophotometric methods

Analytical parameters	Present method	Literature method		
	9-Chloroacridine	o-Chloranil[15]	Fe-bipyridyl[16]	Vanillin[17]
λ_{max}(nm)	436	571.5	520	320
pH	8.92	9.8	-	acidic
Temp.(°C)	50	25	100	R.T
Development time (min)	15	5	15	-
Stability period (min)	55	45	-	120
Beer's law (µg/ml)	2-28	1.25-30	4-24	2-30
Molar absorptivity ($L.mol^{-1}.cm^{-1}$)	1.8×10^3	3.4×10^3	3.8×10^3	1.3×10^4
Recovery(%)	100.40	100.44	99.93	100.34
RSD(%)	≤ 4.3	1.67	0.684	0.409
Application	Tablet, Capsule	Tablet, Capsule	Tablet	Tablet

CONCLUSIONS

A simple, precise, selective and sensitive spectrophotometric method has been developed for the determination of microgram amounts of mesalamine range between 2-28 µg/ml with an accuracy (average recovery %) 100.4% and RSD ≤4.3%, indicating that the method is relatively accurate and precise. The method is based on the reaction of mesalamine with 9-CA reagent to form colored product having maximum absorption at 436 nm. The molar absorptivity 1.8×10^3 L. mol^{-1}. cm^{-1} indicating that the method is sensitive. The method does not require any pretreatment or extraction steps. The proposed method was applied successfully for the assay of the pharmaceutical formulations for tablets and capsules of mesalamine.

REFERENCES

- C. QX, Z. KJ, D. Chen and LP. Gao, (2003), Eur. J. Pharm. Biopharm., 55, 203-208.
- R. Gotti and et al; (2001), J. Chromatogr. A, 916: 175- 183.
- DL. Geier, Miner PB. ,(1992), Am. J. Med , 93, 208-298.
- G. Palumbo, G. Carlucci and P. Mazzeo, (1995), J. Pharm. Biomed. Anal. Oxford, 14, 175-180.
- Narala S. R.; K. Saraswathi, Int. J. Res. Pharm. Biomed. Sci., 2010, 1, 10-13
- Patel K. M.; Patel C.N.; Panigrahi B.; Parikh A.S.; Patel H.N., Pharm Analysis, 2010, 2, 284-288.
- Al-Sabha T. N.; . Altaee O. A, J.Edu & Sci., 2008, 21, 49-62.
- British Pharmacopoeia Commission, British Pharmacopeia, London, Stationery Office, (2003), 2, 1257.
- H. A. Zadeh and S. Kohansal , (2012), J. Braz. Chem. Soc., 23, 473-481.
- B. Nigović , B. Simunić, (2003), J. Pharm. Biomed. Anal. 31,169-174.
- A. Albert, "The Acridines," 2nd Ed., (1966), St. Martin's press, New York, N. Y., p. 254.
- L. G. Hargis, (1988), "Analytical Chemistry", Prentice- Hall. Inc., New Jersey, 424-427.
- Seize, T. K. ,(1977), Student's t-test. Southern Medical J. , 70, 1299.
- British Pharmacopoeia, (2008), II, 1403.
- S. Narala1 and K. Saraswathi, (2010), Int. J. of Res. in Pharmaceutical and Biomedical Sci., 1, 10-13.
- B. S. Chandra et al., (2011), Quim. Nova, 34, 1068-1073.
- M. S. Al-Enizzi, T. N. Al-Sabha, T. S. Al-Ghabsha, (2012), J. Chem., M. U, 7, 87-102.

ڕێکەیەکا شە بەنگی بۆ پێڤانا میسالامینی بکارئینانا دیارکەرێ 9- کلوروئەکردین وکارئێنا نا وان لەسەر دەرمانێن دەرمانخانێ

پوختە

با س ل ڕێکا شەبەنگی دکەت بۆ خەملاندنا میسالامینی ب هەر دوو شیوە پی پاك ودەرماندا ئو ژ ب کارلێکی دگەل دیارکەری 9- کلوروئەکردین .وهاوگولکەیێ مژینا مولاری 1.8×103 لتر. مول$^{-1}$.سم$^{-1}$ وب سنوری دیارکەر وسنوری شیوەی 1.8733 و 5.676 مایکروغرام/مللتر ولدویڤ ئێك. و دێت ئەو بەرهەم یێن هاتێە چێکرن بڕێژا 1:1 ب کارئینانا هەردوو ڕێکا جوب و ڕێژا مولی. وئەڤ ڕێکە یا ئاسانە دگەل ووردبینەکە باش ژ بر کو دێت چ ناڤ ئێك دا چوون وئالوزی نەبوون. وئەڤ ڕێکە بکارهات ب سەرکەفتنەکە پاش بۆ خەملاندنا میسالامینی دناڤ دەرمانی دەرمانخانی و جیوازی نەبوون دگەل ڕێکێن دی ئووین جێگیر د ناڤ پرتووکەدا.

طريقة طيفية لتقدير الميزالامين باستخدام الكاشف 9- كلوراكردين وتطبيقاتها على المستحضرات الصيدلانية

الخلاصة

يشمل طريقة طيفية لتقدير الميزالامين بشكله النقي وفي مستحضره الصيدلاني، وذلك بمفاعلته مع الكاشف 9- كلوراكردين وكانت الامتصاصية المولارية 1.8×103 لتر. مول$^{-1}$. سم$^{-1}$ وبحد كشف وحد كمي 1.8733 و 5.676 مايكروغرام /مللتر وعلى التوالي. ولقد وجد أن الناتج يتكون بنسبة 1:1 بتطبيق طريقتي جوب والنسبة المولية. لقد تم تطبيق الطريقة بنجاح لتقدير الميزالامين في مستحضراته الصيدلانية (الحبوب والكبسول) بنجاح من دون حدوث تداخل مع المضافات كما تمت مقارنة الطريقة المقترحة مع طرائق طيفية أخرى.

FPAA BASED PID CONTROLLER FOR TEMPERATURE CONTROL OF BABY INCUBATOR

ABDUL-KAREEM Z. MANSOOR* and ASMAA E. HAMDOON**

* Dept. of Electrical Power Technology Engineering, Technical College of Mosul-Iraq

** Dept. of Computer Technology Engineering, Technical College of Mosul-Iraq

(Received: July 16, 2013; Accepted for publication: March 2, 2014)

ABSTRACT

The factors affect the child within incubator is mainly the temperature, moisture and oxygen, the organization of temperatures is one of the basic criteria for building a stable environment for the child. The present work presents a development of temperature control of the environment inside the incubator. Temperature control is obtained through using the field programmable analog array (FPAA) card. The Anadigm (AN221E04) FPAA card permits a media for designing and implementing the PID controller together with the PWM controller used to operate the solid state relay (SSR) which is in turn is used to control the operation of the heater.

KEY WORDS: Premature infant Incubator, Temperature control, FPAA, PID controller, Pulse Width Modulation (PWM).

1- INTRODUCTION

One of the most important elements in a newborn's survival is the infant's temperature regulation. However a preterm newborn infant needs special care because some vital organs and/or biochemical/enzyme systems may not have developed society, or because the growth of the fetus may have been disturbed, with the result that the infant is unlikely to survive undamaged without special protection. An infant is called preterm if it is born following a gestation period of less than 37 weeks. The preterm infant has several disadvantages in terms of thermal regulation (Carlos, 2009).

Since the premature infants are at risk to develop hypoxia, hypothermia and many other associated adverse conditions, hence they need special care and attention. One of the major problems that newborns face is improper thermoregulation. The temperature inside the mother's womb is 38^0C (100.4^0F). Leaving the warmth of the womb at birth, the wet new born finds itself in a much colder environment and immediately starts losing heat.

In the first 10-20 minutes, the new born who is not thermally protected may lose enough heat for the body temperature to fall by 2-4^0C (3.6-7.2^0F), with even greater falls in the following hours if proper care is not given. If heat loss is not prevented and is allowed to continue, the baby will develop hypothermia and is at increased risk of developing health problems and of death. Therefore an infant incubator is necessary which attempts to create the necessary environment for the baby's survival (Tamanna et al., 2012).

Temperature regulation is of primary importance in an incubator. The present work therefore focuses on the temperature control of an incubator.

2- TEMPERATURE CONTROL SYSTEM:-

Temperature regulation is one of the most important factors affecting survival of newborn infants. Temperature control system is an important integral part of a baby incubator.

Selection of an appropriate temperature sensor is important for effective control of temperature in the incubator.

Comparing the sensitivity and response time of available temperature sensors like thermistor, thermocouple, RTD in the range of temperature 25^0C-40^0C along with accuracy, repeatability, term stability, linearity, self-heating; thermistor is the best choice in this case (Tamanna et al., 2012).

The air inside the incubator is warmed by a heater and is continually circulated by a fan.

The air temperature inside the incubator is controlled by a thermostat which is set by the nursing staff (incubator operator). Having decided that a baby requires care in an incubator, the nurse must choose an appropriate air temperature.

The average temperature needed to provide a suitable thermal environment for a healthy baby cared for in an incubator is shown in Table 1 (Mohamed et al., 2008).

Table (1) :-Air Temperature

Birth-weight (kg)	35ïC	34ïC	33ïC	32ïC
1.0-1.5	For 10 days	After 10 days	After 3 eeks	After 5 weeks
1.5-2.0		For 10 days	After 10 days	After 4 weeks
2.0-2.5		For 2 days	After 2 days	After 3 weeks
Greater than 2.5			For 2 days	After 2 days

3-OVERVIW OF COMPLETE SYSTEM:-

The incubator is provided with an **AC**-powered heater, motor and fan that sucks the air through it. Then the air-pass through a heating grid followed by a water evaporator to gets the required humidity. The LM35DZ sensor is used to convert the temperature degrees to electrical quantities, which will be the input to the proposed PID controller presented and applied by Anadigm (AN221E04) FPAA used to regulate the temperature inside a neonatal incubator. The closed loop implementation is a combination of sensing devices and actuators that operate synchronously to provide a stable thermal environment inside the incubator.

The actuators, which produce the stable environment inside the incubator, are the heater and the motor that propels the fan.

3.1 OVERVIEW OF FUNCTIONAL MODELS:

The system mainly consists of: the incubator chamber, temperature sensor (LM35DZ) circuit, FPAA kit that used to design a PID controller and Pulse Width Modulation (PWM), firing circuit, solid state relay, **AC**-powered heater, and fan. Figure 1 shows the overall view of the system along with the implemented modules on FPAA.

As the actual temperature inside the incubator varies, the control signal produced from the PID controller varies also, which leads to variable PWM signal. The PWM signal operates the solid state relay, which works in an ON-OFF control strategy. System operation is limited by the difference between the set value and the actual value of temperature.

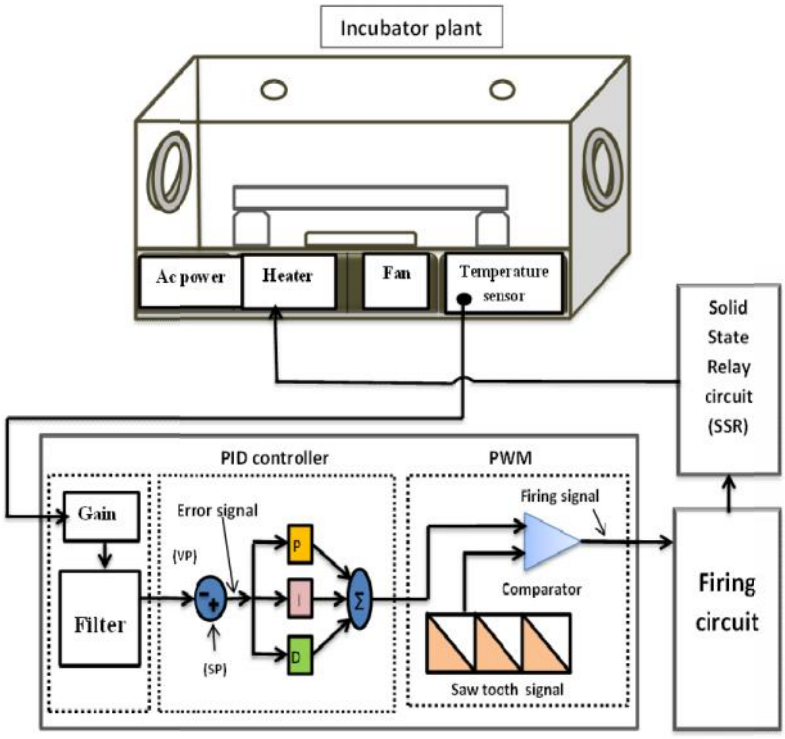

Fig. (1) :-The overall view of close-loop temperature control system for baby incubator

The Anadigm Software used for configuring the chip , to maintain a specific degree of temperature of an incubator , the output of PID controller is compared with a saw tooth wave generated using FPAA to generate pulse width modulation signal(PWM) given by FPAA.

The PWM generator is directly connected to the firing circuit to drive the solid state relay circuit to control the heater voltage.

If the temperature falls below the set value then an appropriate amount of heat energy needs to be supplied to the incubator to maintain the temperature at that level. This can be done by a simple turn ON and OFF control system which will turn ON the heater when the temperature is below the set level and turn OFF otherwise according to a variable duty cycle of PWM that depending on the error signal coming from the PID controller.

3.2 PID CONTROLLER:

Proportion Integration Differentiation (PID) control method is one of the widely used and always the important problem in the automatic control field, for it does not need to know the mathematical model of the controlled object, and it has simple algorithm, good robustness and high reliability (Ying Chen et al., 2013).

The structure of the PID controller system is shown in Figure 2.The system is mainly composed of PID controller and controlled object. As a linear controller, it generates the system deviation e(t) which is produced according to the difference between the set value r(t) and the actual output value y(t),in equation (1).

A control volume is the linear combination of the proportional, integral and differential operation of the deviation e(t), and the control volume work on the object. The PID controller output is in equation (2), and the Laplace transfer function is shown in equation (3).

$$e(t)=r(t)-y(t) \quad \text{..... (1)}$$

$$u(t) = K_p\left(e(t)+ \frac{1}{T_i}\int_0^t (t)dt + T_d \frac{de(t)}{dt}\right) \quad \text{... (2)}$$

$$G(S) = \frac{U(S)}{E(S)} = K_p\left(1 + \frac{1}{T_i s} + T_d s\right) \quad \text{... (3)}$$

where Kp is proportional coefficient, Ti and Td are the integral and differential time constants.

The effect of the individual parameters of the PID controller is described as: Kp is introduced in order to timely reflect the deviation signal of the control system. Once the error appears, the proportional link immediately plays a regulatory role, and then the error of the system will rapidly decrease.

When Kp is large, PID controller may accelerate the speed for adjustment. While too large value of Kp may create an overshoot will appear in the system, and it will reduce the stability of the system.

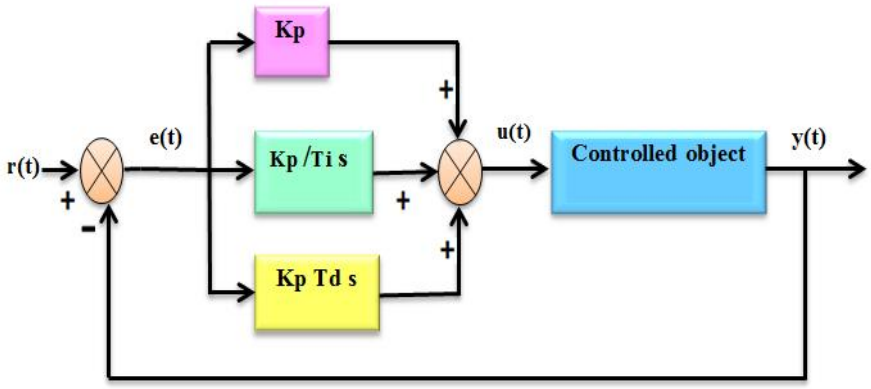

Fig. (2):- The structure of conventional PID control system

The parameter Ti is mainly used to eliminate static error, to improve the degree of no error of the system, to ensure the settings can be tracked with zero steady-state error. The strength of the integral role is depending on integrator time constant Ti. When Ti is greater, the integral action is weaker, otherwise stronger.

The parameter Td can reflect the trend (the rate of change) of the deviation signal, and introduce an effective correction signal before

the deviation signal becomes too large, it can accelerate the operation speed of the system, reduce regulation time (Ying Chen et al., 2013).

3.3 TEMPERATURE SENSOR:

This section presents the sensor type that is used in this work for controlling temperature. The output voltage of this sensor is used to fed the PID controller needs to be maintained at a constant level of temperature inside incubator according to the set point.

The LM35 series are precision integrated-circuit temperature sensors that rated to operate over a range of (-55 °C to 150°C). These sensors do not require any external calibration and the output voltage is linearly proportional to the Celsius (Centigrade) temperature (10mv / degree C).

The sensor circuit is shown in figure (3) .Since the sensor output is in mv, therefore it is connected to gain and filter circuit in FPAA kit to give an output voltage computable with the saw tooth signal (for PWM generation) designed according to Min and Max voltage from the sensor. Assuming a normal incubator temperature range of(28°C -38°C) , a gain of (9) is required to give Min and Max voltage input to FPAA as shown in Table 2.

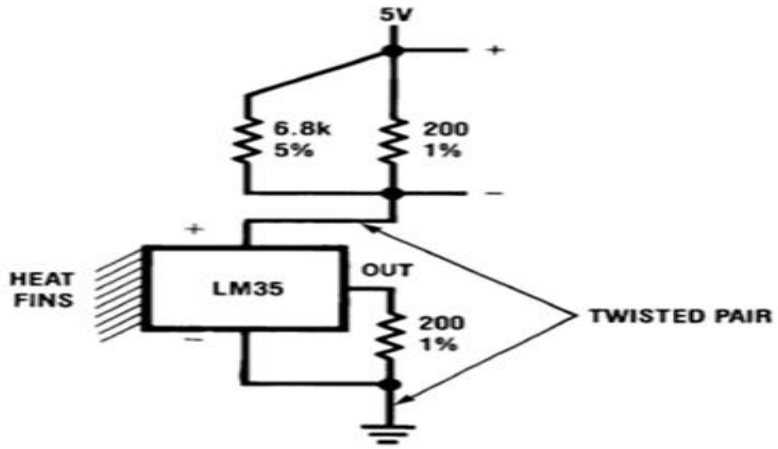

Fig. (3):- Sensor circuit diagram

Table (2) :-Min and Max voltage input to FPAA

Temperature(ic)	(mv)	(v)
28	280	2.52
29	290	2.61
30	300	2.7
31	310	2.79
32	320	2.88
33	330	2.97
34	340	1.06
35	350	3.15
36	360	3.24
37	370	3.33
38	380	3.42

3.4 FPAA Implementation for PID Controller and Pulse Width Modulation (PWM) Design:

The PID controller circuit was designed using the FPAA media. The output of the PID controller will be crossed with the saw tooth wave which is generated in the FPAA module as shown in figure (4).

The PID controller circuit output is intersected with the triangular wave circuit gives the PWM wave as shown in figure (5). The output of the PWM circuit is directly connected to the firing circuit to drive the solid state relay which is used to drive the AC-powered heater.

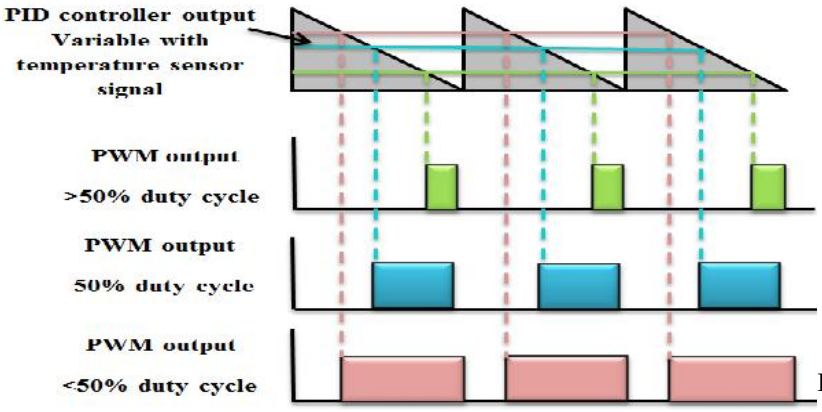

Designer 2

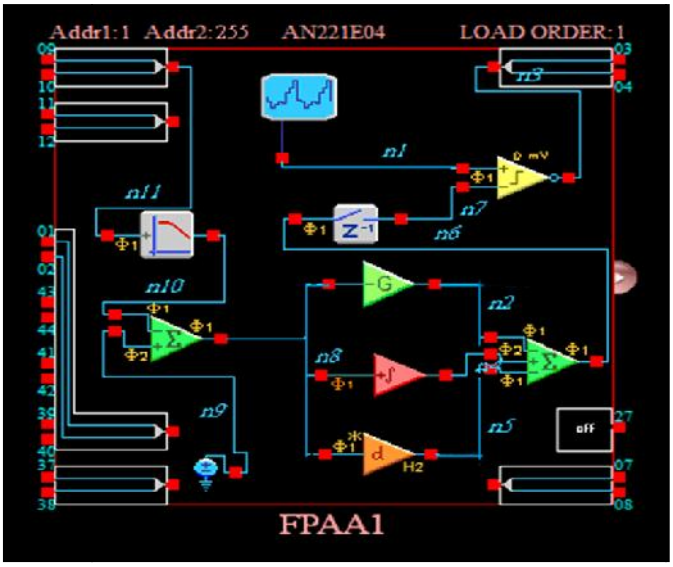

Fig. (5):- Generating PWM by comparing PID controller to a saw tooth waveform

3.5 FIRING CIRCUIT:

To drive the solid state relay it needs a gate voltage in the range of (3V to 32V), and the PWM output voltage from the FPAA kit does not exceeds (4V) which is enough to drive the solid state relay. To protect the FPAA from being overloaded by excessive currents and to be isolated from the 220V appearing on the power switches terminals, therefore the firing circuit is constructed.

This circuit consists of three stages, buffer circuit, optocoupler circuit, and matching circuit, as shown in Figure (6).

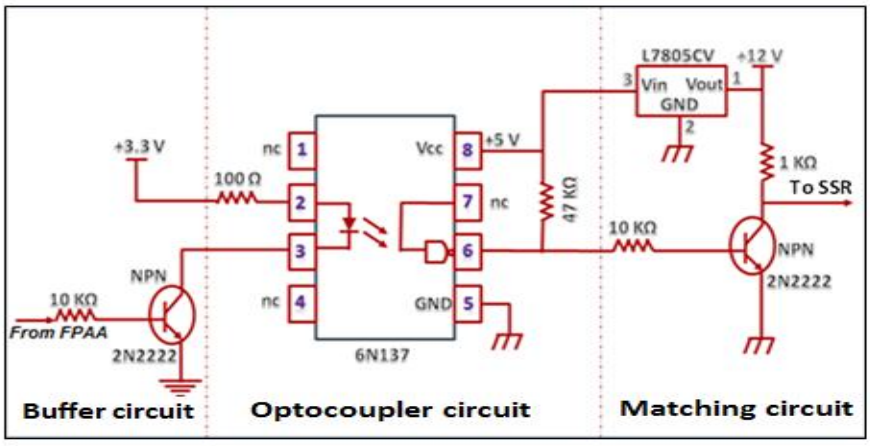

Fig. (6):- Firing circuit

3.6 SOLID STATE RELAY (SSR) CIRCUIT:

The solid-state relay is an ON-OFF control device in which the load current is conducted by one or more semiconductors - e.g., power transistors, an SCR, or a TRIAC. The SSR requires a relatively low control circuit energy to be switched ON and OFF.

When the voltage is applied to the input of the SSR, the relay is energized by a light emitting diode. The light from the diode is beamed into a light sensitive semiconductor which, in the case of zero voltage crossover relays, conditions the control circuit to turn on the output solid state switch at the next zero voltage crossover.

In the case of nonzero voltage crossover relays, the output solid state switch is turned on at the precise voltage occurring at the time.

Removal of the input power disables the control circuit and the solid state switch is turned off when the load current passes through the zero point of its cycle. As shown in figure (7).

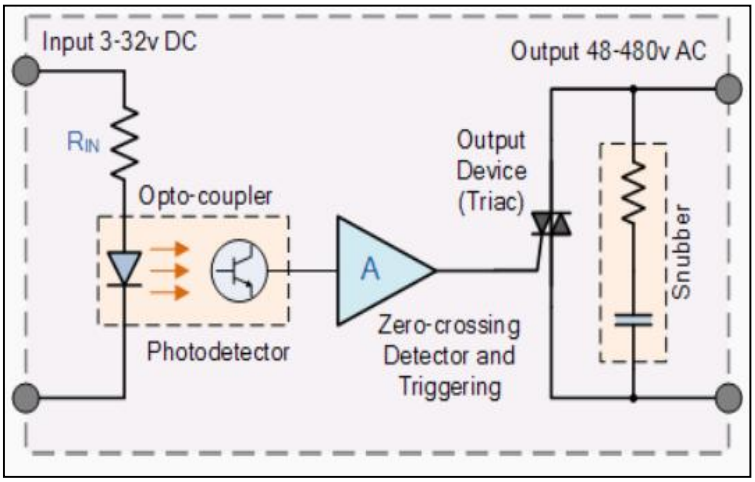

Fig. (7):- Solid state relay circuit

Figure (8) Shows a solid state relay circuit using a photocoupler. The figure includes an input circuit, photocoupler, thyristor for triggering, rectifying diode bridge, snubber circuit, and high power triac.

During the operation, the photocoupler turns on the thyristor for triggering and its ON-current activates the high power triac to drive the load. Because of a low collector withstand voltage and low output current of the photocoupler, a thyristor for triggering is needed to interface it with power control devices such as a power triac or power thyristor (Handbook. 2006).

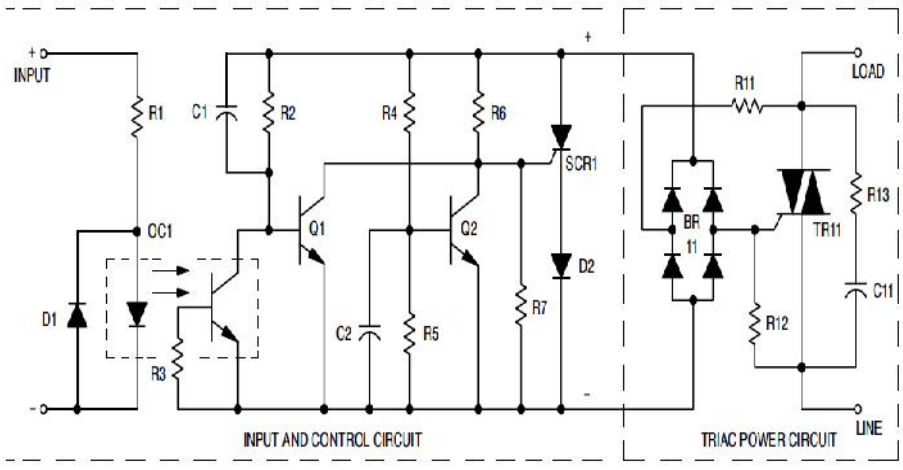

Fig. (8):- Solid State Relay with Built-in Zero-Crossing Circuit.

The complete hardware circuit of the work is shown in figure (9).

4. RESULTS AND DISCUSSIONS:-

The PID controller output used to control the temperature inside the incubator system depends on the temperature difference between the set value and the actual value given by temperature sensor inside the incubator.

The variable output of the PID controller to generates a variable PWM signal which in turns used to switch on and off the solid state relay to control the heater operation. In this work, the set point value is (36°C) and the saw tooth signal frequency is used to be (100HZ).

The PID controller parameters KP, KI, KD are taken initially as (KP=30, KI=0.007, KD=0.0) by ref. (Yasser, 2006),then the values are adjusted by trial and error method to be settled on the final values of (KP=10, KI=5.23e-005, KD=0.484).

The results given in the figures (10, 11, 12, and 13) show the variation of the operating periods of the heater due to the changes in the error signal which come from the difference between the set value and the actual value.

The figures show as the error signal becomes smaller the heater operating period also becomes smaller, and as the error becomes zero, the heater is completely turned off.

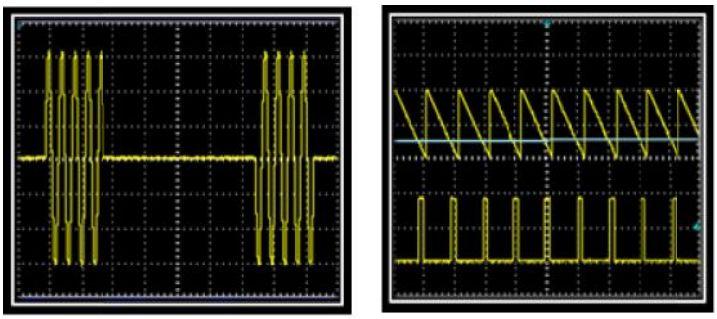

Y =10V/div, X =50 ms/div. **Y=2V/div, X =10 ms/div.**

Fig. (10):- Actual temp.(34.5°C) , Duty cycle 25% , Ton=100ms and Toff=300ms .

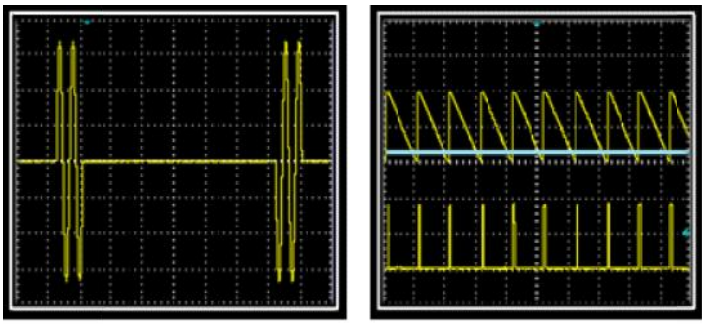

Y =10V/div, X =50 ms/div. **Y=2V/div, X =10 ms/div.**

Fig. (11) :-Actual temp.(35°C) , Duty cycle 12.5% , Ton=50ms and Toff=350ms .

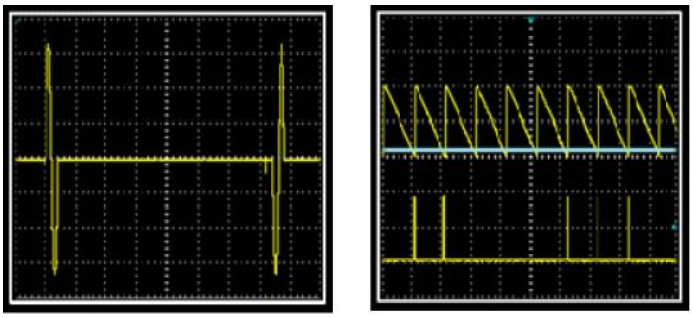

Y =10V/div, X =50 ms/div. **Y=2V/div, X =10 ms/div.**

Fig. (12):- Actual temp.(35.5°C) , Duty cycle 5.5% , Ton=25ms and Toff=425ms .

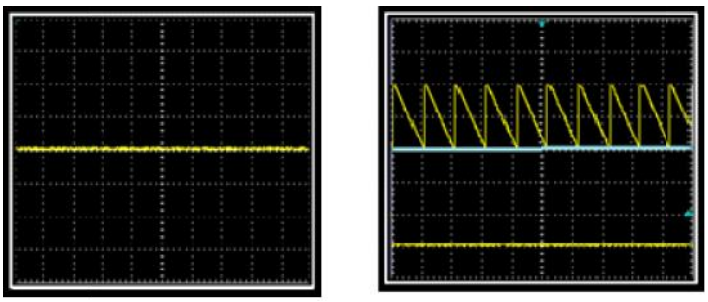

Y =10V/div, X =50 ms/div. **Y=2V/div, X =10 ms/div.**

Fig. (13) :-Actual temp. (36°C), Duty cycle 0%, Ton=0.

5. CONCLUSION:

1. The proposed system is represented by the implementation of the proportional-integral-derivative (PID) controller algorithm in a reconfigurable manner using a circuit based on field-programmable-analog-array (FPAA) technology.

2. FPAA implementation in designing the PID controller and PWM generator minimizes the number of electronic circuits used by the PID controller and generator when they are designed by the general approach.

3. FPAA implementation is an easy way for accurate circuit realization without need for priory analysis for the designed circuit.

6. REFERENCES

-Carlos Paternain Soler, "Prototyping a closed loop control system for a neonatal incubator", A master thesis in Helmholtz-institute for biomedical engineering ,2009.

-Tamanna Afrin Tisa, Zinat Ara Nisha ,Md. Adnan Kiber, "Design Of An Enhanced Temperature Control System For Neonatal Incubator". Bangladesh Journal of Medical Physics, Vol.5,pp.53-62, 2012.

-Mohamed Zahran, Mahmoud Salem, Yousry Attia, Aref Eliwa, "Design and Implementation of a Digital Control Unit for an Oxygenaire Servo Baby Incubator", Journal of Power Electronics, Vol. 8, pp. 121-130, 2008.

-Ying Chen , Yong-jie Ma, Wen-xia Yun, "Application of Improved Genetic Algorithm in PID Controller Parameters Optimization". Northwest Normal University, Vol.11, pp.1524 -1530,2013.

-Thyristor Theory and Design Considerations, Handbook, http://onsemi.com, 2006.

-Yasser Amer Al-TaweelA ,"Simulation Model of Infant Incubator Feedback System with Humidification and Temperature Control", A master thesis in Faculty of Engineering and Science of Auckland University of Technology, 2006.

استخدام المسيطر التناسبي–التفاضلي–التكاملي للسيطرة على درجات الحرارة لحاضنة الطفل بالاعتماد على المصفوفات التناظرية القابلة للبرمجة

الخلاصة :

العوامل الرئيسية التي توثر على الطفل داخل الحاضنة هي درجة الحرارة بشكل رئيسي والرطوبة والاوكسجين , ان تنظيم درجات الحرارة هي احد المعايير الأساسية لبناء بيئة مستقرة للطفل. يقدم البحث تطوير نظام التحكم في درجات الحرارة داخل الحاضنة باستخدام بطاقة المصفوفات التناظرية القابلة للبرمجة (FPAA) . حيث يتم تصميم وتنفيذ مسيطر نوع تناسبي– تفاضلي– تكاملي (PID) وبناء (PWM) معا داخل بطاقة (FPAA) للتحكم بعمل ريلاى الحالة الصلبة (SSR) التي من خلالها تتم السيطرة على عمل المسخن.

IMPROVE MICROSTRUCTURE AND MECHANICAL PROPERTIES OF AL-A332–ALLOY REINFORCED AL_2O_3 MICRO AND NANO COMPOSITES FABRICATED BY STIR CASTING

IBTIHAL **A.** MAHMOOD ,**A**DNAN **D**AWOOD **M**OHAMMED and **R**AWNAQ **A**HMED **M**OHAMMED
University of Technology
Minstery of Water Resorce

(Received: July 24, 2013; Accepted for publication: March 2, 2014)

ABSTRACT

Aluminium matrix composites (AMCs) reinforced with micro and nano-sized Al_2O_3 particles are widely used for high performance applications such as automotive, military, and aerospace and electricity industries because of their improved physical and mechanical properties. The major problem in fabricating metal matrix composites by liquid phase is the poor readability which leads to the non-uniform distribution of the particles. In order to improve the microstructure and mechanical properties of composite, firstly improve the wettability and distribution of reinforcement particles within the matrix. Three steps were applied in stir casting process to avoid agglomeration and segregation of particles. The process included heat treatment of micro and nano Al2O3 particles, injection of heat-treated particles within the molten A332 aluminium alloy by inert argon gas and stirring the melt at suitable speed. In the present work, nano and micro-composites (A332/Al_2O_3) with different weight percent of particles were fabricated by stir-casting techniques. Micro structural characterization was investigated by optical (OP) and scanning electron microscopy (SEM). Tensile, hardness tests were carried out in order to identify mechanical properties of the composites. The results of micro structural study revealed uniform distribution, grain refinement and low porosity in micro and nano-composite specimens. The mechanical results showed that the addition of alumina (micro and nano) led to the improvement in yield strength, ultimate tensile strength, and hardness. It was indicated that type of fabrication process and particle size were the effective factors influencing on the mechanical properties. Decreasing alumina particle size and using steps of stir casting method- process obtained the best mechanical properties.

KEY WORDS: - metal–matrix composite-nano Al2O3- stir **casting**

INTRODUCTION

The Ceramic reinforced aluminium alloys exhibit a unique combination of properties not found in monolithic aluminium alloys. Recent investigations find that the incorporation of nano-particles into the aluminium matrix could enhance the hardness, the yield and ultimate tensile strength considerably, while the ductility is retained **(Mazahery 2009, Habibnejad 2009)**. The great enhancement in strength values of these composites is attributed to good distribution of the nano and micro particulates. The addition of high modulus ceramic particles to conventional aluminium alloys results in increased strength, elastic modulus, wear resistance, as well as other desirable engineering properties Liquid metallurgy technique is the most economical of all the available routes for metal–matrix composite production and generally can be classified into four categories: pressure infiltration, stir casting, spray deposition and in situ processing **(Kok 2005)**. Compared to other routes, melt stirring process has some important advantages, e.g., the wide selection of materials, better matrix–particle bonding, easier control of matrix structure, simple and inexpensive processing, flexibility and applicability to large quantity production and excellent productivity for near-net shaped components **(M. Rosso 2001)**, but there are some problems associated with stir casting of AMCs such as: poor wettability and heterogeneous distribution of the reinforcement material. Poor wettability of reinforcement in the melt means that the molten matrix cannot wet the surface of reinforcement particles therefor, when the reinforcement particles are added into the molten matrix, they float on the melt surface **(J. Hashim 2001, J. Hashim 1999**).and a another problem is the heterogeneous distribution of the reinforcement material . This is because when the particles were wetted in the metal melt, the particles will tend to float to the molten melt due to the density differences between the reinforcement particles and the matrix alloy melt, so that the dispersion of the ceramic particles is not uniform

and the particles have high tendency for Agglomeration and clustering .Wettability and distribution of reinforcement particles becomes more difficult when the particle size decreases to the micro and nano scales, this is due to the increasing surface area and surface energy of nano particles which cause an increasing tendency for agglomeration of reinforcement particles. Moreover, several structural defects such as porosity, particle clusters,oxide inclusions and interfacial, there for there are some methods to improve the wettability and uniform distribution of the reinforcement particles within the molten matrix alloy; for example heat treatment of the particles before dispersion into the melt caused removal of the adsorbed gases from the particle surface **(W. Zhou 1997),**and in order to improve uniform distribution partials using the injection particles with an inert carrier gas into the melt. It has been reported that the technique is helpful in improving the distribution of the reinforcement particles within the melt as well as string the molten metal at suitable speed **(N. Valibeyglooa 2012, Bharath V2012)**.

The aim of the present investigation is to study the mechanical properties of A332/ reinforced Al_2O_3 (12 μm, 1 μm, 50 nm) at different wet fraction (0.05-0.1-0.5-1) wt% respectively. The nano composites were fabricated using a combination of stir casting techniques. The effect of micro and nano particles size and weight fractions on the microstructure and mechanical properties of the composites was investigated.

EXPERIMENTAL WORK

Preparation A332 alloy

Master alloys were prepared through conventional foundry method from (pure aluminium and pure cooper). The details of the theoretically selected alloy composition (design composition) and manufacturing processing are given in Tables (1, 2, 3, 4). For manufacturing of alloys A332 putAl 12%Si, master alloy and 0.1% Al-Ti alloyed (grain refinement). The chargh was melted in a pit furnace using graphite crucible and inert gas the Design of experimental rig as shown in Fig. 1. 0.25% slag remover were added by injection tube and mixed by stirrer for 10 minutes. The prepared molten alloys were cast in steel mold at 700°c.

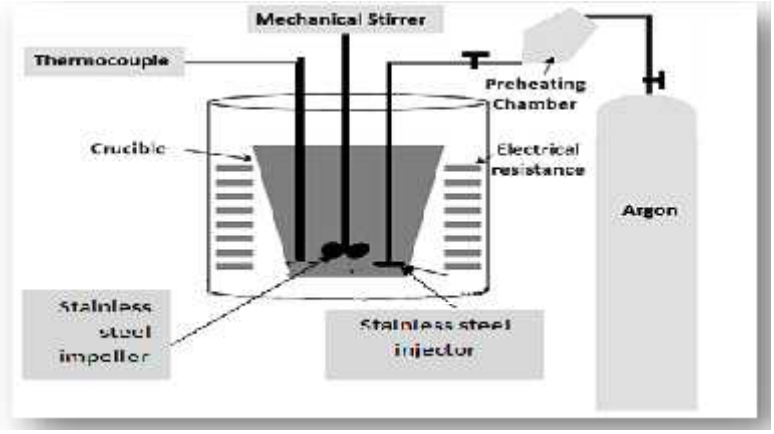

Fig (1):-Design of experimental rig

Table (1):- Chemical composition (wt %) of the Al-12%Si

Si%	Fe%	Cu%	Mn%	Mg%	Pb%	Zn%	Al%
11.54	0.806	1.05	0.27	0.113	0.033	0.409	Bal

Table (2):-Chemical composition master alloy (wt %) of the Al-Cu

Cr%	Pb%	Mg%	Mn%	Si%	Fe%	Cu%	Al%
0.019	0.041	0.041	0.301	0.204	0.339	48.98	Bal

Table(3):- Chemical composition (wt %) of the Al-Ti

Ti%	Si%	Fe%	Cu%	Mg%	Mn%	Cr%	Al%
5	0.5	0.5	0.1	0.1	0.1	0.1	Bal

Table(4):- Chemical composition (wt %) of the A332

Material Alloy	Si%	Cu%	Fe%	Mg%	Zn%	Mn%	Al%
Nominal Chemical composition	8.5-10.5	2-4	1.2	0.5-1.5	1	0.5	Bal
A332 fabric	9.62	3.2	1.1	1.2	1	0.1	Bal

MANUFACTURING AND CASTING OF COMPOSITE SAMPLES

A332 aluminium alloy and particulate alumina powder with size of (12 µm, 1 µm, 50 nm) respectively, were used as the matrix and reinforcement phases the chemical composition for composites. Composite specimens were manufactured by stir casting methods using mechanical mixing of the molten alloy. Micro and nano-particles were heated treatment of reinforcement particles at 1000 ◦C for 20 min in an inert atmosphere and then injected into the melt by using a stainless steel injection tube and inert argon gas in a graphite crucible inserted in a resistance heating furnace. The wet fraction of alumina powder injected into the composites were chosen (0.05-0.1-0.5-1) wt% micro-alumina and (0.05-0.1-0.5-1) wt% nano-alumina respectively. The stirring was continued for 15 min to produce homogenous mixture. The speed of impeller was 400 rpm .Stirring process was started 10 min before addition of reinforcement particles in the melt and continued 15 min after that. Then, the stirrer was turned off and finally composite slurry was poured in a preheated steel mold .The pouring temperature for the processes was 700 °C.

MEASUREMENTS AND TESTING

To study the microstructure of the specimens they were cut by an automatic cutter device. The specimen surfaces were prepared by grinding through 600 and 1200 grit papers and then by polishing with 3 µm diamond paste. Microscopic examination of the composites was carried out by optical and scanning electron microscopy. The density of the samples was measured by the Archimedes's method, while the theoretical densities calculated by taking the densities of A332 aluminium alloy and Al_2O_3 particles were equal to 2.7 and 3.9 g/cm3, respectively. The porosity percentage in the materials was calculated according to the difference between the theoretical and measured density .To investigate the mechanical properties of the composites The Brinell hardness values of the samples were measured on the polished samples using a ball with 5 mm diameter at a load of 250 kg. The tensile tests were carried out using Instron testing machine according to ASTM.B 557 and ASTM E9-89a, respectively as shown in fig 2. The cross head speed was set at 3 mm/min on the round specimens. Each test was repeated two times to obtain a precise average value for each property.

G-gage length (30 mm ï0.06). D-diameter (6.0 mm ï0.1).

R- radius of fillet (6mm)min. A-length of reduced section (36mm)

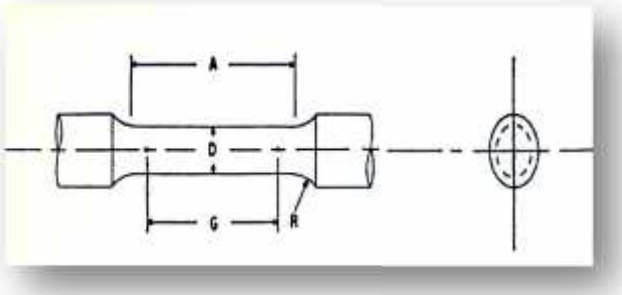

Fig(2):- tensile test sample

RESULT AND DISCUSSION

1-Microstructure analysis

The morphology of the microstructural constituents, their orientation, bonding, distribution, presence of porosity and impurities have strong influence on strength.Their appearance of the microstructural features depends upon the composition and processing method**.** In general as shows in Fig.3 the microstructures of the manufactured sample. According to optical microscopic observation, in case of A332, without additives of any element, the microstructure of Aluminum-Silicon alloy 332 consists of two phases, the white phase α-Al and the dark cubic phase β-Si in a soft matrix of ternary eutectic formed from the white phase α-Al, dark cubic phase β-Si **(Ali Mazahery 2012)** .

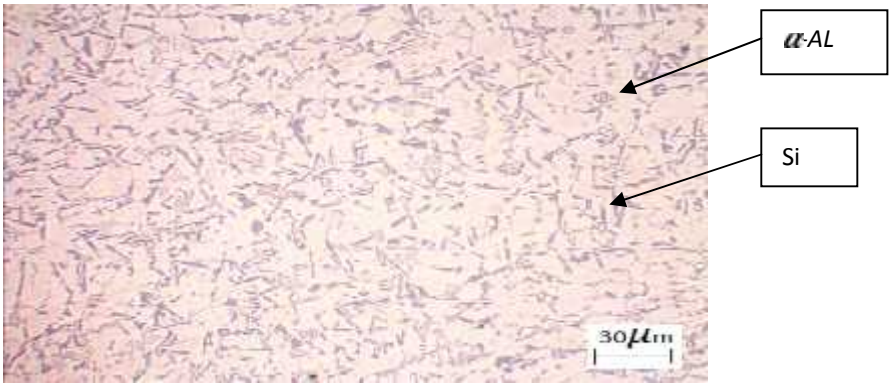

Fig (3): the microstructure of A332

The microstructure of composite samples containing four weight percent (0.05-0.1-0.5-1) of micron and nano size (12 µm, 1 µm, 50 nm) Al2o3 particles fabricated by stir casting processes. During solidification of A332–Al2O3 composites, nucleation of α -Al phase starts in the liquid at a distance away from the particles, where the temperature is lower. The growth of α -Al nuclei leads to enrichment of Si and other solutes in the remaining melt. Because of Si enrichment in the zones near Al2O3 particles, surface of Al2O3 particles can act as the suitable substrates for nucleation of Si phase **(Ali Mazahery 2012).** Therefore, the microstructure of the composites contains primary α -Al dendrites and eutectic silicon, while Al2O3 particles are separated at inter-dendritic regions and in eutectic silicon therefore, the microstructure of the composites contains primary α-Al dendrites and eutectic silicon, while Al2O3 particles are separated at inter-dendrite regions and in eutectic silicon.fig 4(A-B-C-D) shown the microstructures of some samples.

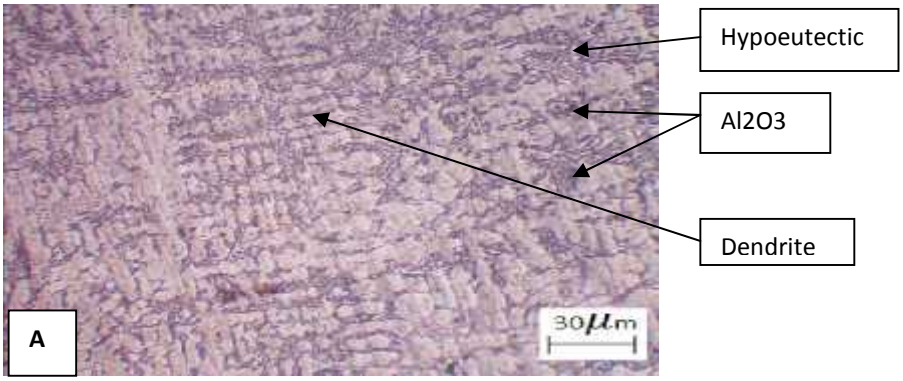

A: 0.05wt% Al2O3 (1micron)

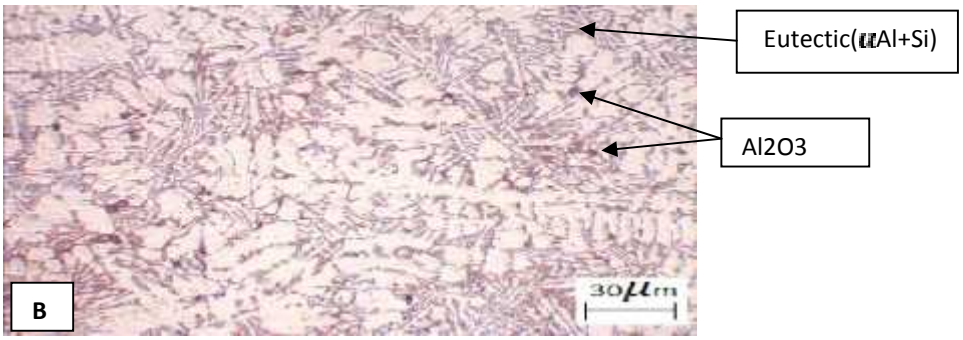

B:1wt% Al2O3 (12 micron)

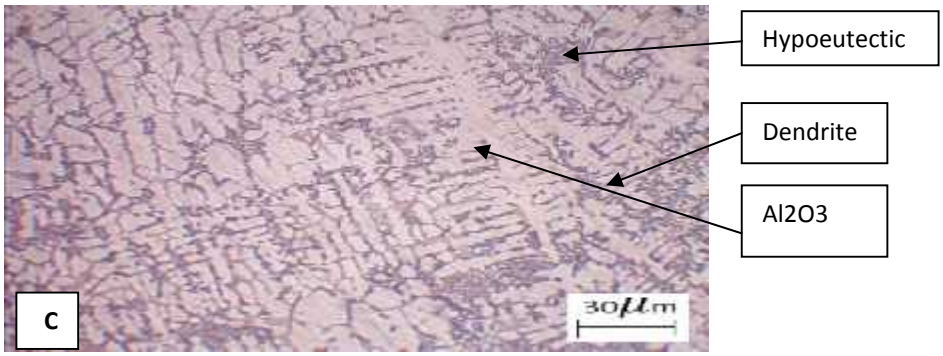

C: 0.1wt% Al2O3 (1micron)

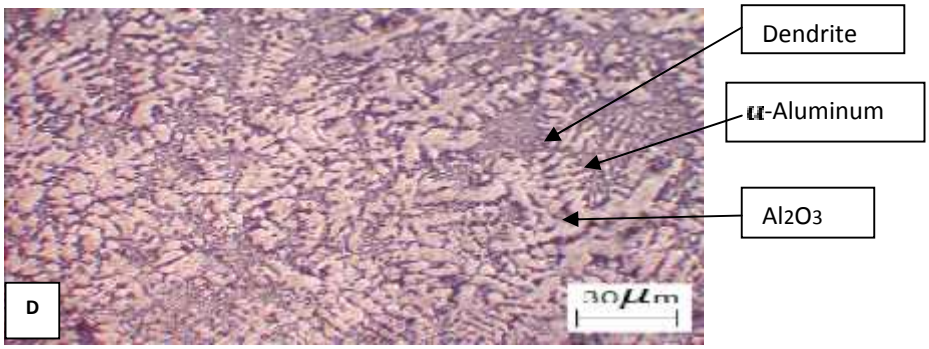

D: 1wt % Al2O3 (1 micron)

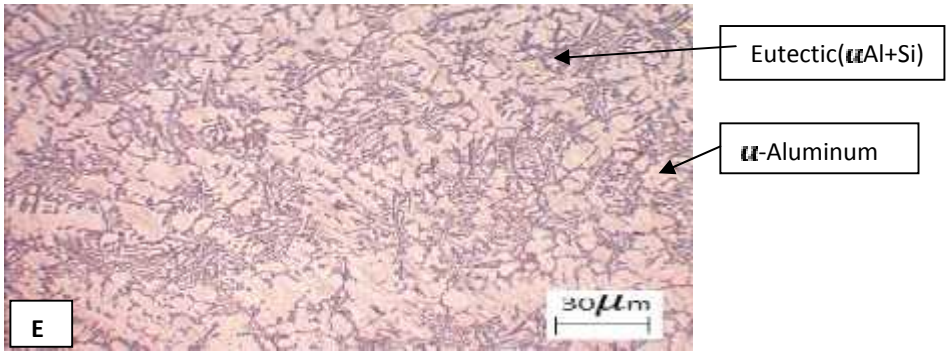

E:0.5wt% Al2O3 (nano)

Fig 4: (A-B-C-D-E) microstructures of some samples

Fig (5 a-b) the typical SEM images of nano and micro composite samples and see some agglomeration for Al2O3 in matrix structures .

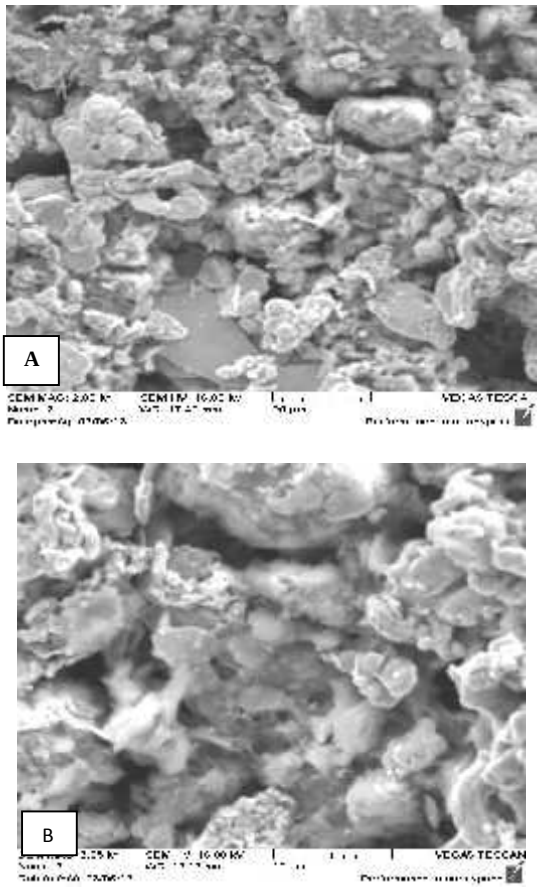

Fig 5 (A-B):- Typical SEM images of nano and micro composite

2- Tensile strength

The strength has prime importance in engineering design such as yield strength, ultimate tensile strength and modulus of elasticity. The most of these properties are determined by using ASTM standardized testing method.Table 5 shows mechanical properties of alloy 332 produced by casting. Mechanical properties (σ_t & σ_y) and elongation are recorded. After preparation A332 we compare it with nominal mechanical properties standard from **(ASM Handbook 2004).**

Table(5):- standard and properties of fabricated A332

Property	Alloy	σT MPa	σY 0.2% MPa	E %
Nominal	A 332	248	193	1
Fabricated	A332	250	195	1.5

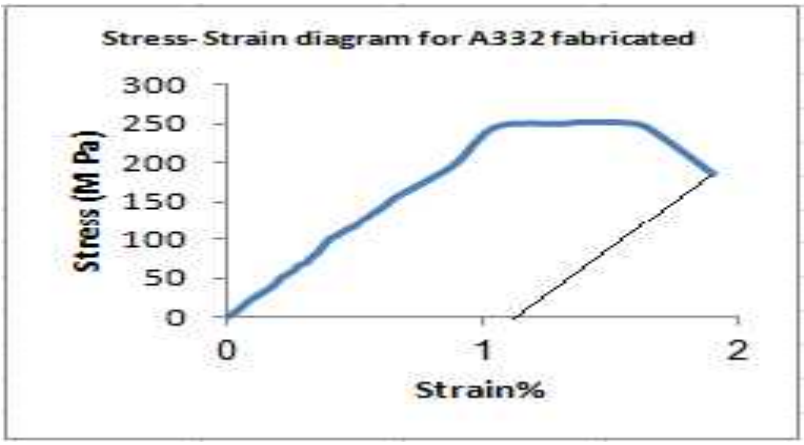

Fig (6):- stress-strain diagram of A332 fabricate

Fig 6 shows the tensile properties of A332 unreinfrced matrix at room temperature, the A332 alloy exhibited average UTS and YS of about 250 and 195 MPa respectively as shown in table 5.

Table (6):- tensile strength of A332+ 12 micron practical size(Al_2O_3)

property	0.05wt%	0.1wt%	0.5wt%	1wt%
Tensile strength(Mpa)	**259**	**262**	**265**	**258**
Yield strength(Mpa)	**202**	**205**	**221**	**225**

Table(7): -tensile strength of A332+ 1 micron practical size(Al_2O_3)

property	0.05wt%	0.1wt%	0.5wt%	1wt%
Tensile strength(Mpa)	**249**	**262**	**268**	**262**
Yield strength(Mpa)	**201**	**210**	**223**	**228**

Table(8):- tensile strength of A332+ 50 nanometer practical size(Al_2O_3)

property	0.05wt%	0.1wt%	0.5wt%	1wt%
Tensile strength(Mpa)	**258**	**263**	**269**	**280**
Yield strength(Mpa)	**205**	**214**	**224**	**234**

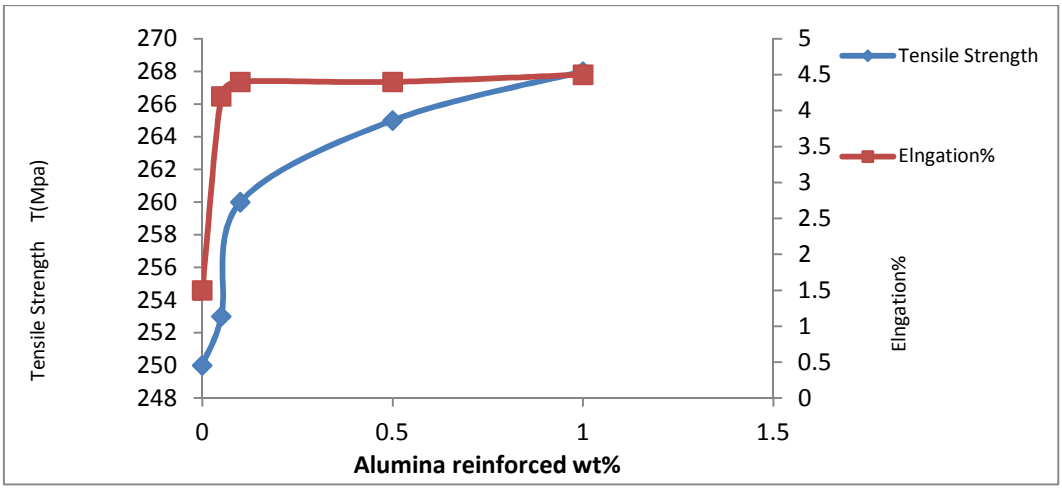

Fig (7):- Tensile strength and elongation for12 micron

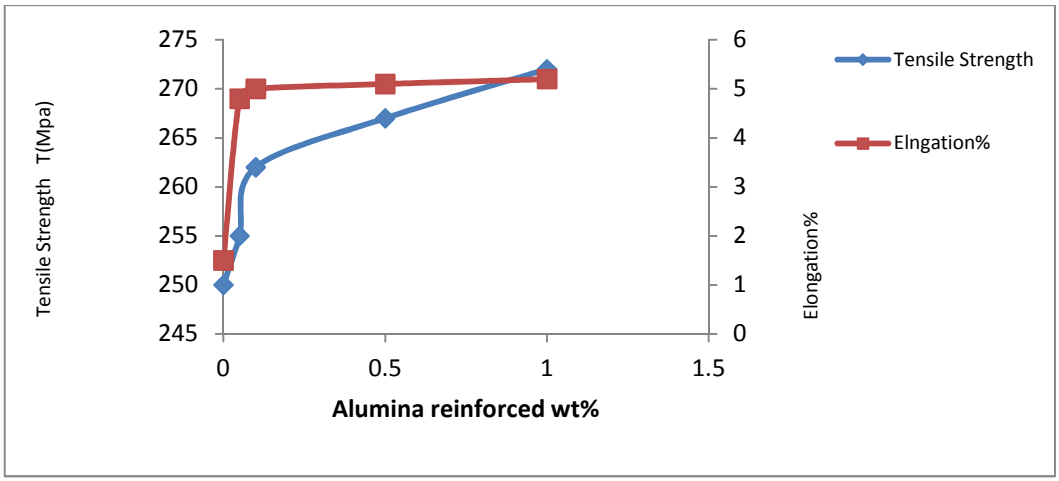

Fig (8):- Tensile strength and elongation for1 micron

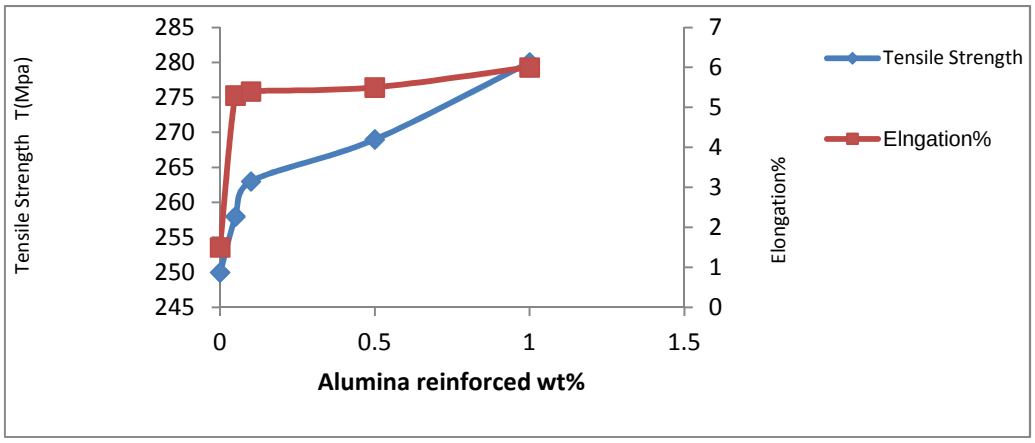

Fig (9):- Tensile strength and elongation for nano composite

Figures 7, 8 and 9 display the tensile curves and elongation of the composites respectively. It is believed that the great enhancement in tensile stress observed in these composites is due to good distribution of the nano- Al_2O_3 particles and low degree of porosity, which leads to effective transfer of applied tensile load to the uniformly distributed strong Al_2O_3 particulates. The grain reinforcement and strong multidirectional thermal stress at the Al/ Al_2O_3 interface are also important factors which play a significant role in the high strength of the composites. Al2O3 particles have grain-refined strengthening effect, which is improved with increasing volume fraction since they act as the heterogeneous nucleation catalyst for aluminium this result agree with the same result **(Bharath V 2012, (Ali Mazahery 2012)**.

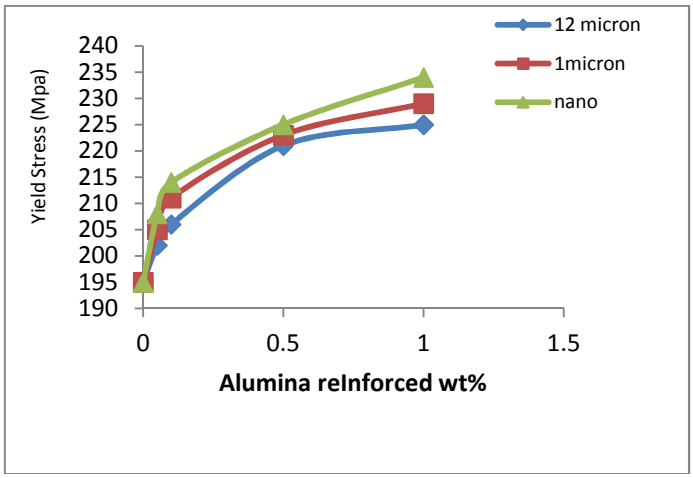

Fig (10):- Yield strength for composite

The best yield strength is composite A332+1wt% Al2O3 in different nano size of alumina. The rate of increasing in yield strength is 11%for 12 micron, 17% for 1 micron and 20% for nano alumina. From the above it is concluded that the modulus of elasticity, yield strength and ultimate tensile strength of aluminum cast composite materials is largely controlled by the selection of strong matrix composition, smaller particles size, increasing volume fraction of particles. Further improvements in mechanical properties in aluminum alloy based casting composite can be achieved by modifying the process parameters metal treatment, the bonding between the dispersions and matrix and also reducing micro porosities in the casting. In general the yield stress increases with the particle volume fraction and a better orientation of the particle along the tensile axis. The addition of alumina don't effect on young modulus of all sample which is about 72GPa (_±2%).Higher elongation percentage value was obtained for A332 with 1wt% nano alumina. It is observed that agglomeration increases with increase in volume fraction but if the agglomeration is well bonded with matrix, it can contribute to strengthen of composites. The measure of the ductility in stress strain diagram also represents the materials toughness which is important property needed for composite materials, the best elongation is 6 in A332 with 1 wt% nano alumina. The improvements in the ductility can be achieved through the control of porosity, mechanical working deformation processes, reducing the particle size and increasing the uniformly distribution of particle in aluminum composites **(Daouda 2002, Madeva Nagaral 2013)**.

3-Density

The density of A332 and their composite were computed by mass- volume relation and plotted against wt % of alumina. As shown in fig (11) the density decreases with an increase in weight percentage of alumina in the composite.Also, according to the measured and theoretical densities of composite samples, it is revealed that the amount of porosity in the composite samples increases with increasing weight percentage of Al2O3 particles and decreasing the size of particles **(El-Sayed 2011)**.

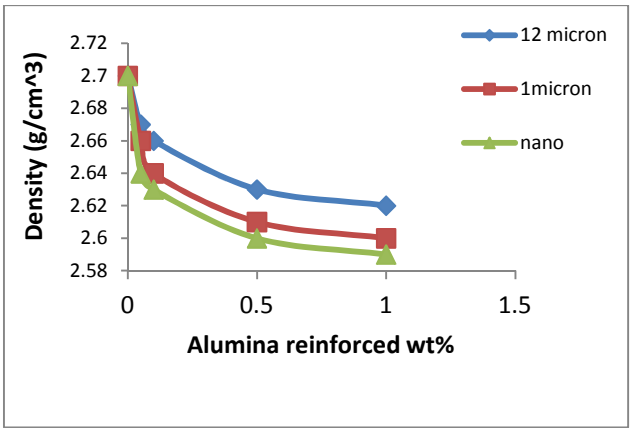

Fig (11):- Density for composite

4- Hardness Measurements

Fig12 shows the results of micro hardness tests conducted on A332 alloy composite containing different weight percentage of Al2O3 particles. A significant increase in hardness of the alloy matrix can be seen with addition of Al2O3 particles. Higher value of hardness is clear indication of the fact that the presences of particulates in the matrix have improved the overall hardness of the composites. This is true due to the fact that aluminium alloy is a soft material and the reinforced particle especially ceramics material being hard, contributes positively to the hardness of the composites. The presence of stiffer and harder Al2O3reinforcement leads to the increase in constraint to plastic deformation of the matrix during the hardness test. Thus increase of hardness of composites could be attributed to the relatively high hardness of Al2O3 itself. As shown in fig (12).The best composite in hardness is A332+1wt% Al2O3 (50nano alumina). The percentage value of increasing hardness is 50% between 0.05wt% to 1wt% (nano alumina), 37% between 0.05wt% to 1wt% (1 micron) and 25% between 0.05 wt % to 1 wt % (12 micron) so **(Daouda 2002, H.R.Ezatpoura 2011, S.A. Sajjadi 2012)** reached the same result ,the hardness of the composites is increased with increased wt% and decrees of particle size.

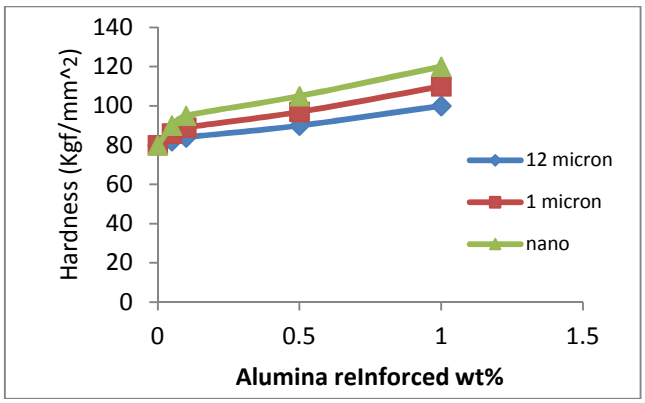

Fig (12):- Hardness for composite

CONCLUSION

1. The results showed use of heat-treated particles, injection of particles and the stirring system were improved the wettability and distribution of the nano particles more than micro particles within the aluminum melt.

2. The addition of nano particles results in significant improvement in hardness, yield strength and ultimate tensile strength of the composites more than micro particales.

REFERENCES

- ASM Handbook, “Properties and Selection: Nonferrous Alloy and Special-Purpose Materials”, Vol.2, 2004.
- Ali Mazahery, Mohsen Ostad Shabni Trans. Nonferrous Met. Soc. China 22(2012) pp275−280.
- Bharath V, Mahadev Nagaral and V. Auradi* International Journal of Engineering Research & Technology (IJERT) Vol. 1 Issue 6, August - 2012 ISSN: pp 2278-0181.
- Daouda A. and Reif W., Journal of Materials Processing Technology, Vol. 123, (2002) pp. 313–318.
- El-Sayed Youssef El-Kady, Tamer Samir Mahmoud, Mohamed Abdel-Aziz Sayed Materials Sciences and Applications, 2011, 2, 390-398.
- H.R.Ezatpoura,H.Beygia,S.A.Sajjadia,M.Torabi Parizib"Conferences on applications of Nanotechnology in Sciences,Engineering and Medicine(NTC2011), 16-17 May 2011Mashhad-Iran.
- Habibnejad-Korayema M, Mahmudia R,Pooleb W J,"Enhanced properties of Mg-based nano composites reinforced with Al2O3 nano – particles. Mater Sci Eng A,2009, 519(1-2):pp198-203.
- J. Hashim, L. Looney, M.S.J. Hashmi, Journal of Materials Processing Technology 92-93 (1999) pp 1-7.
- J. Hashim, L. Looney, M.S.J. Hashmi, Journal of Materials Processing Technology119 (2001) pp 324–328.
- Kok, Journal of Materials Processing Technology 161 (2005) pp 381–387.
- Mazahery A, Abdizadeh,Baharvandihr, "Development of high- performance A356/ nano Al2O3 composite. Mater Sci EngA, 2009, 518 ,pp61-64.
- M. Rosso, Journal of Materials Processing Technology 175 (2006) pp 364–375.
- Madeva Nagaral1*, Bharath V2 and V Auradi1 Nagaral et al., J Material Sci Eng 2013, 2:1
- N. Valibeyglooa, R. Azari Khosroshahib* Proceedings of the 4th International Conference on Nano structures (ICNS4) 12-14 March, 2012, Kish Island, I.R. Iran
- .S.A. Sajjadi a, H.R. Ezatpour a, M. Torabi Parizi b Materials and Design 34 (2012) pp-06–111.
- W. Zhou, Z.M. Xu, Journal of Materials Processing Technology 63 (1997) pp 358–363.

پێش ئێخستنا سالوخه تێت میکا نزمی وبناغی دیربینی بو پارچا (A332) ب هاریکاری هێز ئێخستنا (مایکرویی) دەنگێت گەلەك هویر زکه رستی (Al2O3)یی تێکەلی یا ئەلەمنیومی یا ب هێزکری ب پارچێت تەنك یێت (مایکرویی) و دەنگێن (نانوی) یێت گەلەك گەلەك هویر .

پوختە:

بشێوەکی بەرفرە دهێنە بکار ئینان دجێ بە جێکرنێت لەشکەری وگەردونی وپێشە سازی یێت ئەلکتریکی دا (کەهرەبێ دا). چنکو سالوخێت وی یێت فیزیایی ومیکا نیزمی گەلەك دپێش کەفتی نە ئاریشە دچێکرنا ڤێك لێگدایێت (مرکبات) توخمێت ئاسنی دا (مەعدەنی) ئەوە کو ئەو بەرهەمێ رونکری وحەلاندی بزەحمەت خو ب وان پارچێت تەنك ڤە بنسێین یان خولێك بدەن ژبەر وی چەندێ شێوەکێ نەرێك وپێك ونە گونجای پەیدادبیت بو وان پارچێت تەنك وێیت (نانوی) یێت گەلەك هویر.

ڤێجا داکو بناغەکی (مجهەری) یێ دویر بینی وسالوخێت میکا نزمی بو ئەوان توخمێت کەرستا باشتر لێ بکەن دەست دانە چاك کرنا شیانێت نەرم کرنێ بو پارچێت تەنك وچاك کرنا شیانێت بەلاف کرن وگونجاندنا وان دەنگێت زێدە هویر دناڤـ کەرەستێت لێگدای کری دا (متراکبات).

و ب وێ چەندێ سێ پێنگاڤ هاتنە بجھ ئینان بو کارێ پێـگڤە نساندن وگونجاندنێ داکو ئەو دەنگێت زێدە هویر بە بنە کوم تلك ودا ژێگڤە نەبن دیسا ئەڤـ چەندە گەرماتی دگەل هاتە بکار ئینان بەری کو دناڤـ ئالافێ حەلاندنێ دا بهێنە تژی کرن (عملیه الحقن).

دڤی کاری دا (غازا ئەرکون) یا سڤك هاتە بکار ئینان دگەل کارێ تێکەل کرنا وان کەرستا دیسا پارچێت تەنك ێیت (مایکرویی) وێیت (نانەوی) ێیت گەلەك هویر کرنە دگەل پارچا ئەلـەمنیومی (A332)دا وب سەنگاتیەکا جور بە جور وتەکەنیکا (Stir Casting) بو ڤێ چەندێ هاتە بکار ئینان پاشی هەمی پارچێت چێکەری هاتنە تاقیکرن ل ژێر دویربینەکا جورێ (OP) ویا ئەلکترونی جورێ (SEM).

دیسا تاقیکرنێت گڤاشتنێ و موکوم یێ ژی هاتەکرن داکو سالوخێت وێ ێیت میکانزمی دیار دبن و ل دوماهیکێ دیار بو کو ئەو پارچێت تەنك ێیت (مایکرویی) وێیت (نانوی) پاشی پێگڤە نسیاینە وێیت پێگڤە ماین وگونجاین بێ چ ئاریشە و چ کێماسی لێ نەبون دیسا ژ هەمی رەخا ڤە درێك و پێك بون.

تحسين الخواص الميكانيكية والبنية المجهرية لسبيكة (A332) مقواة بدقائق مايكروية ونانوية من (Al2O3)

الخلاصة

ان مركبات الالمنيوم المعززة بدقائق مايكروية ونانوية تستخدم على نطاق واسع في اغلب التطبيقات العسكرية والفضائية والصناعات الكهربائية بسبب تحسن خواصها الفيزيائية والميكانيكية. المشكلة الرئيسية في تصنيع المتراكبات المعدنية هو ان الطور السائل السائل يكون ضعيف الالتصاق مع الدقائق فيحدث توزيع غير متجانس للدقائق المايكروية والنانوية. من اجل تحسين البنية المجهرية والخواص الميكانيكية للمتراكبات تم تحسين قابلية الترطيب للدقائق وتحسين قابلية توزيع الجسيمات داخل المتراكبة.حيث طبقت ثلاث خطوات اثناء عملية السباكة لتجنب التكتل والفصل بين الجسيمات وشملت المعالجة الحرارية للدقائق قبل عملية الحقن داخل المنصهر واستخدام غاز الاركون الخامل واستعمال عملية الخلط.في هذا البحث تم اضافة دقائق مايكروية ونانوية الى سبيكة الالمنيوم A332بنسب وزنية مختلفة باسخدام تقنية السباكة (stir casting) وتم فحص المسبوكات مجهريا (OP)والكترونيا (SEM) كذلك تم اجراء فحوصات الشد والصلادة من اجل تحديد الخواص الميكانيكية .وقد اظهرت النتائج الى ان توزيع الدقائق المايكروية والنانوية كان متجانس اضافة الى تحسن في خواص مقاومة الخضوع وقوة الشد وزيادة الصلادة.

EOG SIGNAL ACQUISITION USING RECONFIGURABLE ANALOG DEVICES AND USE IT TO CONTROL WHEELCHAIR MOVEMENT

THAIR ALI SALIH and MOHAMMED TALAL GHAZAL
Dept. of Computer Technology Engineering, Technical College, Technical institution of Iraq, Mosul, Iraq

(Received: July 24, 2013; Accepted for publication: June 25, 2014)

ABSTRACT

This paper present an electrooculography (EOG) acquisition system based on reconfigurable devices. The field programmable analog array FPAA is used for extract the EOG signal which makes it possible to design flexible and adaptable EOG applications with the functionality that can be dynamically changed or extended. The EOG signals in this system have been acquired using a five-lead configuration. The FPAA has online Programmable feature that can dynamically be adapted the amplifier to detect the signal, it is reduced the circuit complexity and succeeded in detect these weak signals which coupled with huge noise. The system is established and its performance was tested. It is used to guide an autonomous robot (wheelchair) as a system to help the people with severe disabilities. It was found that the proposed system could produce clear EOG signals which are suitable for many activates and the success percentage of the system is 95%.

KEY WORDS: FPAA, EOG, Wheelchair, Control, Robot.

INTRODUCTION

Robot applications or more commonly technologies and know how derived from robotic researches have quickly developed through the last years to actual products for medical uses (Colle et al., 2002). There has been an increase in the development of assistive technology for people with multiple disabilities, and has made significant developments in communication systems between humans and machines (Barea et al., 2002, Barea et al., 2010).

The development of a wheelchair represents the most important applications useful to increase the mobility of persons with disabilities and / or elderly (Barea et al., 2002). The persons with a serious disability or handicap may find it difficult or impossible to guide wheelchair so the eye movements can be used to develop new system between humans and machines. Previously the implementation of eye signals and other bio signals acquisition circuits were a challenge for electronic circuit design. But this research have been presents a new methodology of detecting the eye movement using reconfigurable analog devices. The design incorporates many salient features including a novel algorithm, which learns the eye signal level of the user and helps in minimizing the noise due to the user. It also provided with obstacle avoidance system, which is used to help in guiding the patient user and prevent accidents. These features described are however not limited to wheelchair control alone but can be applied to many control system in general.

The Electrooculography (EOG) signals have been widely used in biomedical and rehabilitation engineering applications, particularly in wheelchair control system. Many efficient wheelchair control using EOG signals have been developed in the last decades, such as electrical powered wheelchair control system (Barea et al., 2002). Also, on the basis of the physiological and morphological data of the EOG, a previous model of the ocular motor system based on EOG was proposed (Bidimensional dipolar model EOG, BiDiM-EOG) (Barea, Boquete, Bergasa, Lopez, & Mazo, 2003), and many useful human- computer interface (HCI) systems, such as activity recognition based on eye movement analysis (Bulling et al., 2011), multitask gadget control (Gandhi et al., 2010), computer cursor control (Septanto et al., 2009), home automation (Harun and Mansor, 2009), computer animation application (Krupiński and Mazurek, 2009), eye writing recognition (Tsai et al., 2008), mobile robot control (Kim et al., 2007), visual improvement system for the elderly (Yu et al., 2005), and hospital alarm system (Venkataramanan et al., 2005). Many techniques have been proposed to develop all of these HCIs,

which can be divided into two main types: pattern recognition and non-pattern recognition. In pattern recognition, features extracted are discriminated by a suitable classifier (Brunner et al., 2007). Time-domain features that have been frequently used are mean value, peak duration, peak polarity and slope (Kherlopain et al., 2006). In addition, spectral analysis has been deployed as the useful features for eye movement classification (Bukhari et al., 2010; Lv et al., 2010). All of these features are usually implemented with two classifier types, that is, neural networks (Güven and Kara, 2006; Kikuchi and Fukushima, 2000; Lee and Lee, 1993) and support vector machine (Bulling et al., 2011; Shuyan and Gangtie, 2009).

Indeed, the computational times and implementation complexity become a major limitation of algorithm based on pattern recognition, particularly for implementing in microcontroller devices. Many research studies have established better performance of EOG signal classification based on non-pattern recognition (Deng et al., 2010; Gandhi et al., 2010). This technique has a simple structure. The classifier module of pattern recognition algorithm has been degraded to a simple threshold comparison module. In this study, non-pattern recognition algorithm has been implemented in order to be used in microcontroller devices.

EOG signal conditioning and acquisition systems are consist of an analog conditioning stage that amplifies and filters the signal, followed by a digital stage performing the control of wheelchair movement [since EOG signal features (low differential voltage amplitude, high noise level and low frequency band) suit perfectly the front-end ports of a Field Programmable Analog Array (FPAA) device.] [The use of FPAA device provide the system with the ability to modify any feature that has to be altered, as a function of the EOG signal quality being processed and the information that is needed to extract at any time.] Moreover, minimal processing noise is achieved due to the presence of a single analog device (Morales et al., 2011).

This paper has been divided into the following sections: Section 2 describes electrooculography (EOG) and the technique of sensing electrical signals from the eyeball and suitability to detect eye movements. Section 3 includes EOG signal acquisition and processing requirements. A study of FPAA suitability for EOG signal acquisition, and the FPAA features that may be used for reliable analog conditioning explained in section 4. A microcontroller (Arduino mega 2560) system that enables standard electric wheelchair control by eye movement is developed and a novel algorithm to guide the wheelchair movement is proposed in section 5. In section 6 the results and finally the conclusions and points to future research work in section 7.

ELECTROOCULOGRAPHY

The human eye is a spherical structure with a radius of 12mm. The signals that can be sense from the movement of the human eyes can be known as Electrooculography. The EOG is derived from the Cornea Retinal Potential (CRP) that is generated within the eyeball by the metabolically active retinal epithelium. The production of CRP comes from the hyperpolarization and depolarization's of the nervous cells in the retina. EOG is the electrical recording corresponding to the eye movement. The eye has a resting electrical potential, with the front of the globe positive and back with globe negative (Fig.1). This phenomenon was first observed by Emil du Bois-Reymond in 1848 and has been the foundation in electrooculography (Bukhari et al., 2011).

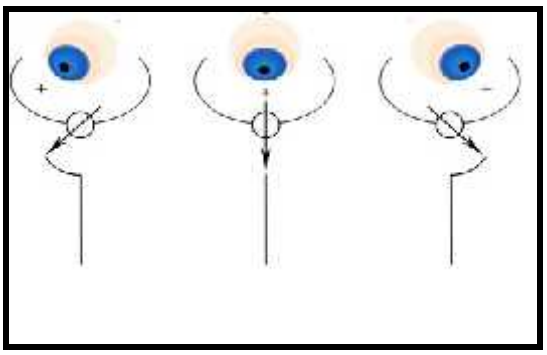

Fig. (1) Ocular dipole.

The EOG value varies from 50 to 3500 μV with a frequency range of about DC-100 Hz. Its behavior is practically linear for gaze angles of ±30◦ and changes approximately 20 μV for each degree of eye movement. It should be pointed out here that the variables measured in the human body (any biopotential) are rarely deterministic. Its magnitude varies with time, even when all possible variables are controlled (Barea et al., 2010). This means that the variability of the electrooculogram reading depends on many factors that are difficult to

determine: perturbations caused by other biopotentials such as EEG (electro-encephalogram), EMG (electromyogram), in turn brought about by the acquisition system, plus those due to the positioning of the electrodes, skin-electrode contacts, head and facial movements, lighting conditions, blinking, etc (Barea et al., 2002). a system build on FPAA kit for acquiring the EOG signal is used to eliminate or minimize these defects.

THE EOG SIGNAL ACQUISITION AND PROCESSING REQUIREMENTS

When EOG signal is acquired, it is always mixed with artifacts, which in electrocardiography refer to something that is not produced by eyes movement themselves. These artifacts include, but are not limited to, electrical interference by external sources, electrical noise from muscle tremor (electromyography) produces an artifact that is an electric noise added to EOG signal, In addition to a wide band noise which is generated over all the stages in the signal acquisition path. The most appropriate amplifier characterizing parameters are a high voltage gain, up to 1000 or even greater, and a common-mode rejection ratio (CMRR) over 140 dB, which attenuates the common-mode noise, a high input impedance, which does not attenuate considerably the electrooculography signal under measurement, and low drift and noise, both generated within the amplifier circuitry.

Fig.2 show the EOG signal acquisition path. A typical instrumentation amplifier AD623AN for EOG implementation makes use of commercial off-the-shelf low voltage and high precision. The amplified signal is fed to the filtering stage collected by the modules needed to select the band of interest. These modules include a high pass filter with the cut frequency set to 0.0159 Hz, which eliminates the DC component and lower frequency noise, i.e., signal wandering, a notch filter that suppresses the power line noise with its central frequency set to 50 Hz, and finally a low pass filter with the corner frequency set to 9 Hz, which attenuates the high frequency noise.

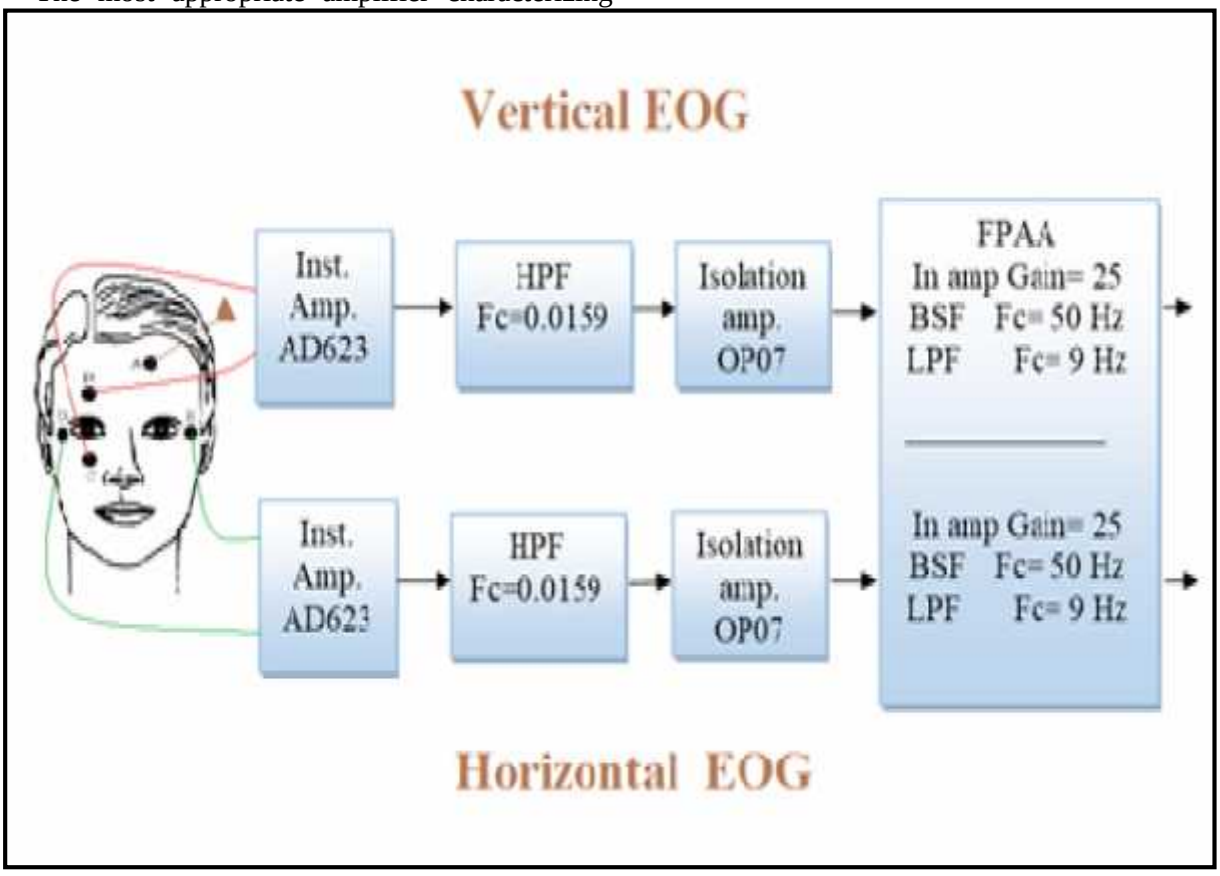

Fig. (2) EOG signal acquisition pat.

.

FPAA FOR EOG ANALOG SIGNAL CONDITIONING

This section explores the fitness of FPAA for EOG analog signal acquisition and conditioning. The following presentation of the Anadigm® FPAA architecture and functionalities allows to tie with EOG signals conditioning requirement. The EOG acquisition system is toughly conditioned by the external signal features, like amplitude, noise level and frequency bandwidth requirements. So that the circuit implementation would have to allow changing the gain to deal with the lowering in the amplitude of the signal, also it must be capable to adjust the behavior of the filters in response to multiple noise intensities. The FPAA can be simply meets those requirements. As well, the FPAA offer an interesting balance between performance and circuit design time. Practically the FPAA AN221E04 reconfigurable device from Anadigm was used to get high accuracy results. The AN221E04 device involves a 2x2 matrix of fully Configurable Analog Blocks (CABs), enclosed by a fabric of programmable interconnect resources. Configuration data is stored in an on chip SRAM configuration memory (Fathima et al., 2008). An AN221E04 Chip Overview is shown in (Fig. 3).

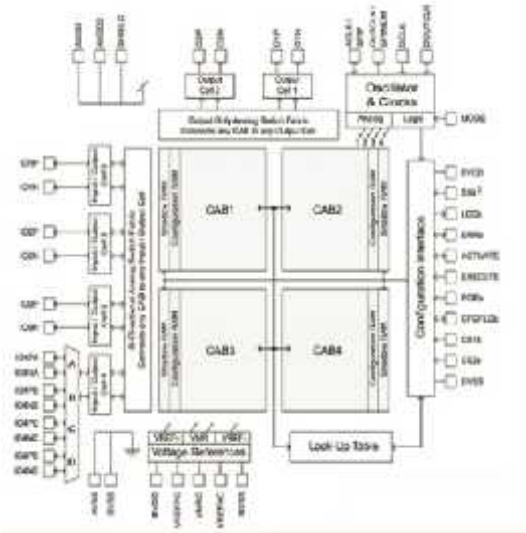

Fig. (3) Structure of the FPAA.

The four CABs have access to a single Look Up Table (LUT) which offers a new method of adjusting any programmable element within the device in response to a signal or time base. It can be used to implement arbitrary input-to-output transfer functions (companding, sensor linearization), generate arbitrary signals, and even perform voltage dependent filtering. A voltage reference generator supplies reference voltages to each of the CABs within the device and has external pins for the connection of filtering capacitors. Analog input signals can be connected from the outside world via the four Configurable Input/output Cells (AN221E04 manufacture data).

FPAA CONFIGURATION FOR EOG SIGNAL CONDITIONING

This section will present the elements of FPAA that will be used for conditioning the EOG signal. A high pass filter was used to eliminate ground shifting problem occurs in the EOG signals before FPAA stage. A passive RC filter was designed for that purpose with the cut frequency set to 0.0159 Hz followed by isolation stage with OP07 operational amplifier to provide safety relating to the electrodes and reduce hazards. The FPAA configuration is made by the subsequent resources: the input cell chopper amplifier is employed by the lowest existing gain (16), chopper amplifier offerings a CMRR of 102 dB in addition to the input cell antialiasing filter is employed by its lowest allowable corner frequency (76 kHz). This filter eliminates the noise caused by the chopper amplifier switching clock. The EOG signal is processed in the internal CABs after it has been amplified and filtered in the input cell.

The configuration of analog modules are reported in Table 1, which are defined in the following. The notch filter that eliminates the AC line interferences is accomplished by the Biquadratic Filter CAM with gain set to (1). The Biquadratic Filter CAM makes a full cycle, biquadratic (two pole) band stop filter with its switching clock set to 7.352 kHz. This clock frequency allows the band-stop center frequency to be set to 50 Hz. A quality factor (Q= 5) jams other EOG signal components. Lastly the low-pass filter that eliminates noise components over 9 Hz has been accomplished by a Bilinear Filter CAM in low pass configuration and with unity gain. The switching clock for this module is set to 7.352 kHz. This election enables the antialiasing filter hosted in the output cell to eliminate the noise generated by the switched capacitors within this CAM. The output cell antialiasing filter is set to its lowest possible corner frequency (76 kHz). The overall architecture provides a good signal to noise ratio. This circuit implementation occupies two CABs, leaving unused two complete CABs, so

that, another full EOG analog processing path could be fitted within the same device which is suitable to acquire both vertical and horizontal channels of the EOG acquisition system in the same device.

Table 1: Configurable Analog Modules: FPAA

Name	Options / Parameters	
FilterBiquad1	Filter Type	Band Stop
	Filter Topology	Type II
	Corner frequency [KHz]	0.0501
	DC Gain	1.00
	High Frequency Gain	1.000
	Quality Factor	5.00
	ClockA	7.353 KHz
FilterBilinear2	Filter Type	Low Pass
	Input Sampling Phase	Phase 1
	Polarity	Non-inverting
	Resource Usage	Minimum Resources
	Corner frequency [KHz]	0.00897
	DC Gain	1.00
	ClockA	7.353 KHz
FilterBiquad2	Filter Type	Band Stop
	Filter Topology	Type II
	Corner frequency [KHz]	0.0501
	DC Gain	1.00
	High Frequency Gain	1.000
	Quality Factor	5.00
	ClockA	7.353 KHz
FilterBilinear3	Filter Type	Low Pass
	Input Sampling Phase	Phase 1
	Polarity	Non Inverting
	Resource Usage	Minimum Resources
	Corner frequency [KHz]	0.00897
	DC Gain	1.00
	ClockA	7.353 KHz

MICROCONTROLLER SYSTEM

The EOG signal is processed by Arduino mega 2560 microcontroller circuit which is used to decide the direction flow for the wheelchair (right, left, forward or backward). To allow the wheelchair robot to detect obstacles in its way, an obstacles avoidance circuit has been attached to the system as shown in (Fig.4). The Arduino worked as a join part between the EOG signal acquisition circuit and the wheelchair movement control system, in addition to obstacles avoidance circuit.

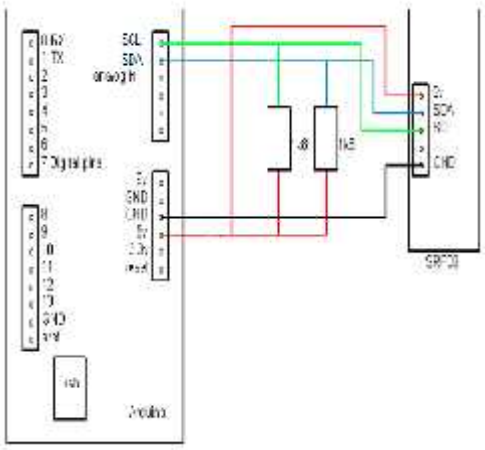

Fig. (4) The Ultrasonic ranger SRF08 connection diagram with Arduino.

The microcontroller programmed according to the following algorithm:

- Initial inputs/output ports and SRF08 Ultrasonic sensor.
- Train the microcontroller by the acquired eye signals (Up, Down, Right and left) from the user eye at the first 10 seconds.
- Check the distance between the wheelchair and obstacles to avoid collision.
- Acquire new signals and compare it with the trained signals to determine the direction of wheelchair movement.
- Delay 50 msec.
- Repeat checking the distance and comparing new acquired signals.
- End.

The output of the system is connected with the wheelchair controller, which is position the wheelchair in accordance with the user's command. Sensor data is processed by a novel algorithm, implemented within the microcontroller. Thus, user eye movement is translated into electric wheelchair position. Through the performed experiment, the system's ability to correctly recognize user's command is verified. The system block diagram is shown in (Fig.5).

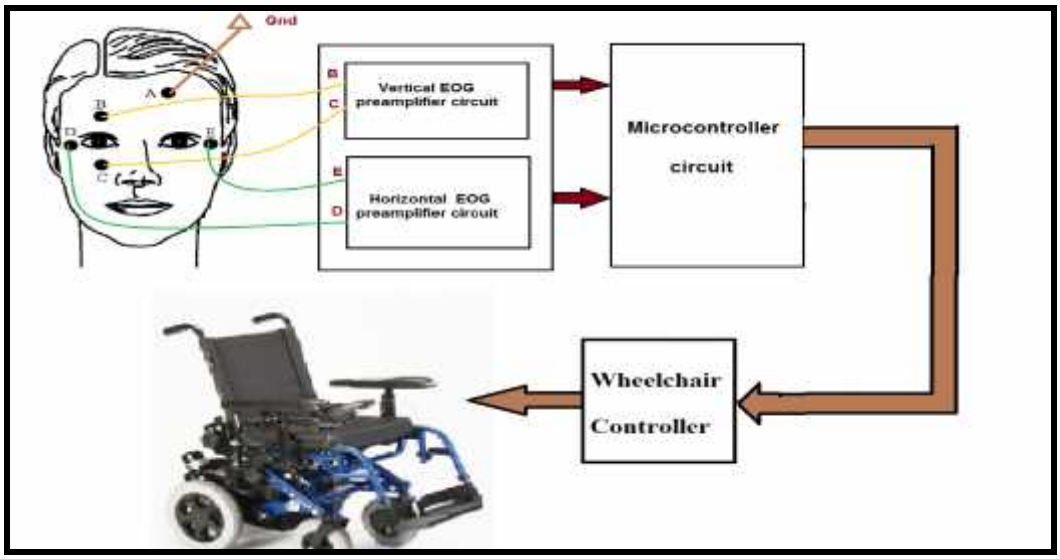

Fig. (5) Wheelchair controlled by eye movement block diagram.

SYSTEM IMPLEMENTATION TEST & RESULTS

Firstly, the testing of the EOG circuit was used as a way to not only improve the performance of the circuit, but also make sure that the circuit was working with the desired requirements. The oscilloscope measurement tool has been used to test physical building of the EOG circuit. The EOG signal obtained by vertical EOG channel has been tested in several states as shown in (Fig. 6).

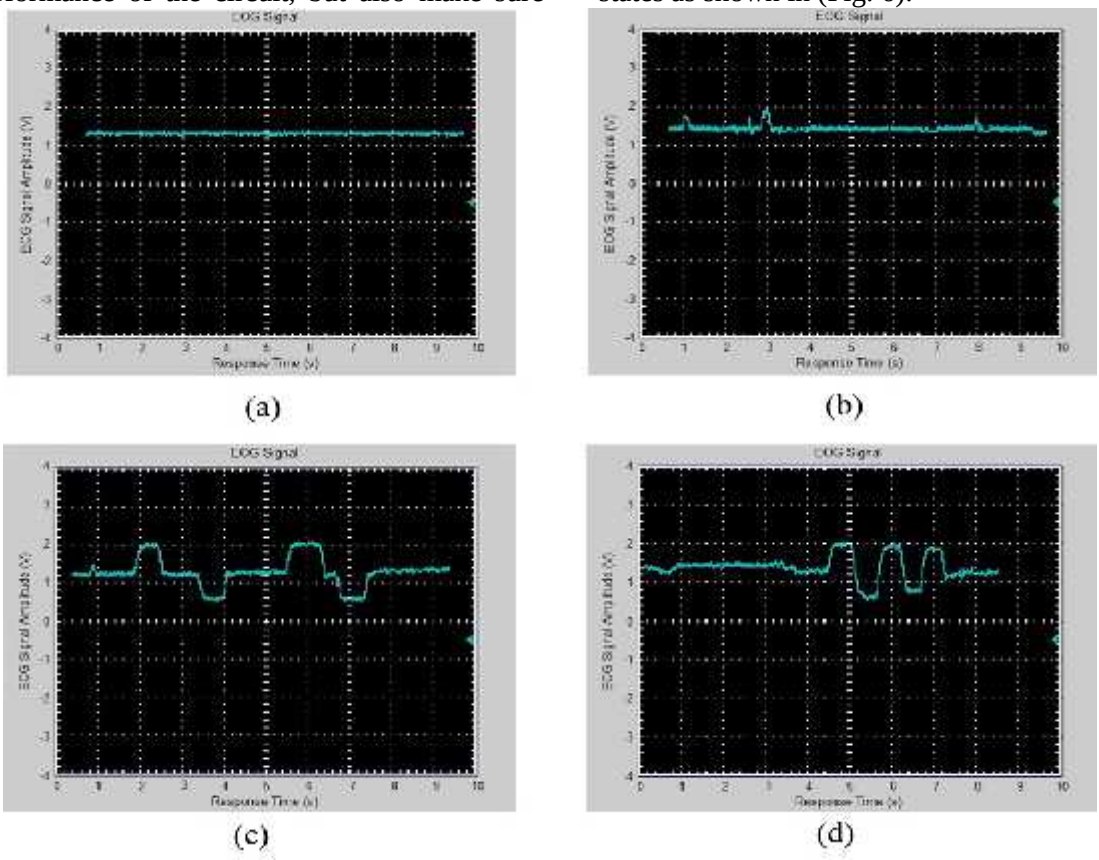

Fig. (6) EOG signal tests for vertical channel: (a) Looking straight, (b)Blinking, (c) Moving UP and DOWN, (d) Moving UP and DOWN Continuously.

As a results, a differential potential have been occurred when move the eyeballs, also, the EOG signal amplitude increase with the increasing of the degree of movement. To test the overall system, select a suitable environment is important, the senior design lab represent the best place for test because it has all of the software simulation and hardware tools needed to assemble any parts that need it and test each individual part to make sure it arrived in good working condition, the test must begin on how well it follows as well as its ability to avoid obstacles.

- The first test of the navigation system is to move in a straight line. The chair moves forward by moving the eyeball UP then moving the eyeball to the CENTER to stop the chair. Then return back to the starting point by moving the eyeball to the DOWN position.
- In the second test the wheelchair rotating to the right and left respectively. The chair moves right by moving the eyeball to RIGHT then moving the eyeball to the CENTER to stop the chair. And finally, rotate to left by moving the eyeball to the LEFT.
- The third test is to determine what will happen if a static obstacle is placed in front of the chair such as a box. The chair will need to go away of the box while checking the output on the sensor to determine if chair has clear way to move.

CONCLUSION

This paper has been proposed a flexible EOG acquisition system using FPAA Anadigm AN221E04, which processed the detected bioelectric signals generated from eye movement. The EOG signal was successfully used to generate driving and steering commands for a wheelchair. Which help many disabled persons to control the wheelchair without help of a caretaker. The system is tested and the probability of command error is less than 5%.Various user interfaces can be developed to control different tasks using EOG signal like painting and drawing on the intelligent board.

REFERENCES

- Barea R, Boquete L, Mazo M, Lopez E (2002). System for assisted mobility using eye movements based oelectrooculography. IEEE Trans. Neural Syst. Rehabil. Eng., 4: 209-218.
- Barea R, Boquete L, Mazo M, Lopez E, Bergasa LM (2002). EOG guidance of a wheelchair.Journal of Intelligent and Robotic Systems, vol. 34, p. 20, 2002.
- Barea R, Boquete L, Rodr?guez-Ascariz J,Ortega S, and Lopez E (2010). Sensory System for Implementing a Human—Computer Interface Based on Electrooculography. Sensors, vol. 11(1), pp. 310-328.
- Brunner S, Hanke S, Wassertheuer S, Hochgatterer A (2007). EOG pattern recognition trial for a human-computer interaction. In: Stephanidis C (ed.) UAHCI 2007. LNCS, 4555: 769-776.
- Bukhari WM, Daud W, Sudirman R (2010). A wavelet approach on energy distribution of eye movement potential towards direction. In Proceedings of the IEEE Symposium on Industrial Electronics and Applications, pp. 181-185, IEEE Press.
- Bukhari, W.,Daud, W., and Sudirman, R (2011). Time Frequency Analysis of Electrooculograph (EOG) Signal of Eye Movement Potentials Based on Wavelet Energy Distribution.fifth Asia Modelling Symposium, pp.81-86.
- Bulling A, Ward JA, Gellersen H, Tr?ster G (2011). Eye movement analysis for activity recognition using electrooculography. IEEE Trans. Pattern Anal. Mach. Intell. 33: 741-753.
- Colle, E., Rybarczyk Y., and Hoppenot P (2002). ARPH: An assistant robot for disabled people. IEEE Systems, Man and Cybernetics'02. Hammamet, Tunisia.
- Deng LY, Hsu DL, Lin TC, Tuan JS, Chang SM (2010). EOG-based human-computer interface system development. Expert Syst. Appl. 37: 3337-3343.
- Dynamically Reconfigurable FPAA AN221E04 with Enhanced I/O http://www.anadigm.com/_doc/DS030100-U006.pdf, last accessed July 05, 2013.
- Fathima, A., and Sanavullah, D (2008). Autonomus Reconfiguration using FPAA for Bandwitdh Recovery in Satellite Subsystems. International Journal of Computer Science and Network Security, VOL.8 No.7, pp.132-137.
- Gandhi T, Trikha M, Santhosh J, Anand S (2010). Development of an expert multitask gadget controlled by voluntary eye movements. Expert Syst. Appl., 37: 4204-4211.
- Güven A, Kara S (2006). Classification of electro-oculogram signals using artificial neural network. Expert Syst. Appl., 31: 199-205.
- Harun H, Mansor W (2009). EOG signal detection for home appliances activation. In Proceedings of the 5th International Colloquium on Signal Processing and Its Applications, pp. 195-197, IEEE Press.

- Kherlopian AR, Gerrein JP, Yue M, Kim KE, Kim JW, Sukumaran M, Sajda P (2006). "Electrooculogram based system for computer control using a multiple feature classification model", In Proceedings of the 28th IEEE EMBS Annual International Conference, IEEE Press. pp. 1295-1298.
- Kikuchi M, Fukushima K (2000). Pattern recognition with eye movement: a neural network model. In Proceedings of the International Joint Conference on Neural Networks, ACM Press. pp. 37-40.
- Krupiski R, Mazurek P (2009). Estimation of eye blinking using biopotentials measurements for computer animation applications. In: Bolc L, Kulikowski JL, Wojciechowski K (eds.) ICCVG 2008. LNCS, 5337: 302-310.
- Lee J, Lee Y (1993). Saccadic eye-movement system modelling using recurrent neural network. In Proceedings of the International Joint Conference on Neural Networks, pp. 57-60, IEEE Press.
- Lv Z, Wu XP, Li M, Zhang D (2010). A novel eye movement detection algorithm for EOG driven human computer interface. Pattern Recognit. Lett., 31: 1041-1047.
- Morales, D., Garcia, A., Castillo, E., Carvajal, M., Banqueri, J. and Palma, A (2011). Flexible ecg acquisition system based on analog and digital reconfigurable devices. Sensors and Actuators 165, 261–270.
- Septanto H, Prihatmanto AS, Indrayanto A (2009). A computer cursor controlled by eye movements and voluntary eye winks using a single channel EOG. In Proceedings of the International Conference on Electrical Engineering and Informatics, pp. 117-120, IEEE Press.
- Shuyan H, Gangtie Z (2009). Driver drowsiness detection with eyelid related parameters by support vector machine. Expert Syst. Appl., 36: 7651-7658.
- Tsai JZ, Lee CK, Wu CM, Wu JJ, Kao KP (2008). A feasibility study of an eye-writing system based on electrooculography. J. Med. Biol. Eng., 28: 39-46.
- Venkataramanan S, Prabhat P, Choudhury SR, Nemade HB, Sahambi JS (2005). Biomedical instrumentation based on electrooculogram (EOG) signal processing and application to a hospital alarm system. In Proceedings of the 2nd International Conference on Intelligent Sensing and Information Processing, pp. 535-540, IEEE Press.
- Yu M, Piao YJ, Kim YY, Kwon TK, Hong CU, Kim NG (2005). Study of the characteristic of eye movement for visual improvement of the elderly. In Proceedings of the International Conference on Control, Automation and systems.

نظام اكتساب اشارة العين بأستخدام الاجهزة التناظرية القابلة لاعادة التشكيل برمجياً واستخدامها للسيطرة على حركة عربة المعوقين

الخلاصة

هذا البحث يقدم نظام اكتساب اشارة تخطيط حركات العين الكهربائية (EOG) بالاعتماد على الاجهزة القابلة لاعادة التشكيل برمجياً. لقد استخدمت البوابات التناظرية القابلة للبرمجة FPAA لاكتساب اشارة العين مما يسهل عملية تصميم تطبيقات مرنة تقبل التغيير ديناميكياً. استخلصت اشارات العين باستخدام خمسة اقطاب حول العينين. ان البوابات التناظرية لها القابلية على تغيير وظيفتها برمجياً وبصورة ديناميكيا بحيث يكيف المكبر لكشف الاشارة المطلوبة مما يسهل عملية البناء المادي للدائرة الالكترونية بنجاج وخصوصاً في التقاط تلك الاشارات الضعيفة المقترنة بضجيج. تم انجاز النظام واختبار ادائه من اخلال استخدامه لقيادة عربة للمعاقين كنظام لمساعدة الناس من ذوي الاحتياجات الخاصة. لقد تمكن النظام المقترح من الحصول على اشارة العين بصورة واضحة كما ويمكن استخدامها في العديد من التطبيقات حيث وصلت نسبة نجاحه الى 95%.

SEASONAL VARIATIONS OF RAW WATER OF TIGRIS RIVER AND EFFECT ON QUALITY WATER PLANTS

LILYAN YAAQUB MATTI ALSAKAJ
College of Environmental science and technology, Mosul University-Iraq

(Received: August 4, 2013; Accepted for publication: June 2, 2014)

ABSTRACT

The study present an extensive investigation of physic-chemical parameters of water samples of Tigris river at Baghdad. Water samples under investigations were collected from eight station during spring season(march, April, May), summer season(June, July, August) and autumn season (September, October - November)and winter season (December January, February) in the year 2008.

This study aimed at using 18 ecological parameters in evaluating the quality of the Tigris River for public usage, by choosing eight sampling sites along the river in Baghdad area. These parameters included are Temperature ^{0}C, Turbidity, pH value, Total hardness, Iron, Chlorides, EC, TDS, TSS, calcium, Sulfate, Nitrate, Fluoride, Total Alkalinity, Magnesium, DO, BOD_5 and PO_4

Parameters were used for calculating water quality seasonal variation in the Tigris River at study area. water temperature showed high seasonal variations, ranging from 12-17 °C in the winter, to 25.3-31.67°C in the summer, pH values in all stations in Tigris River showed slightly alkaline, Conductivity distribution along the river showed high values in the East Tigris, Rashed and Karam. Seasonally, the highest conductivity levels were observed in winter, Turbidity values in all stations in Tigris River were higher in the autumn and winter during irrigation period, The lowest TH values were detected in Karkh for all season while the highest value of TH at Rashed in autumn season, The calcium concentration values fall between 65 to 179.33 mg/l and the average is 122.165 mg/l. The magnesium concentration values fall between 29 to 39 mg/l and the average is 34 mg/l. the lowest chloride values were detected in winter ,Chloride values varied from 32 to 113.87 mg/l, Total dissolved solids varied between (75 – 1324.7) mg/l in all study stations minimum of 75 mg/l in spring to a maximum of 1324.7 mg/l in Autumn , Seasonally, the highest TSS values in all stations were observed in spring, while the lowest ones were detected in Summer , DO concentrations varied from 3.47 mg/l at Wethaba in autumn to 7.9 mg/l . Qadisiya in Summer, The highest BOD_5 values in all stations except Karkh were observed in season. Sulfate values did not show large variations among stations in the same season, ranging from 190 mg/l at Karkh in winter to 405 mg/l at Al Qadisiya autumn, the highest NO_3 values were observed in autumn in all stations. Al Karkh showed the highest NO_3 values.

The phenomenon of water quality degradation along Tigris was generally evident throughout the year's results. Therefore, the authorities should practice more efforts in controlling various activities along the river bank. The urgent water management rules should be applied, enforcing waste-water treatment systems among the factories and other activities

***KEY WORDS*:** Environmental monitoring; seasonal variation; Water quality; Baghdad city, Tigris River.

INTRODUCTION

The city is located on a vast plain bisected by the River Tigris. The Tigris splits Baghdad in half, with the eastern half being called 'Risafa' and the Western half known as 'Karkh'. The land on which the city is built is almost entirely flat and low-lying, being of alluvial origin due to the periodic large floods which have occurred on the river.

Baghdad has a hot arid climates, in terms of maximum temperatures, one of the hottest cities in the world. In the summer from June to August, the average maximum temperature is as high as 44 °C accompanied by blazing sunshine: rainfall is almost completely unknown at this time of year. Temperatures exceeding 50 °C in the shade are by no means unheard and even at night temperatures in summer are seldom below 24 °C. Because the humidity is very low (usually under 10%) due to Baghdad's distance from the marshy Shatt al-Arab, dust storms from the deserts to the west are a normal occurrence during the summer.

Winters boast mild to warm days and variable nights. From December to February, Baghdad has maximum temperatures averaging 15.5 to 18.5 °C though highs above 21 °C are not unheard of. Low temperatures can be chilly: the average January low is 3.8 °C but lows below freezing only occur couple of times per year.

Annual rainfall, almost entirely confined to the period from November to March, averages around 120 mm, but has been as high as 575 mm and as low as 23 mm. On January 11, 2008, light snow fell across Baghdad for the first time in memory table (1) (AEP 2008).

Table (1): Climate data for Baghdad [2,3]

Climate data for Baghdad													
Month	**Jan**	**Feb**	**Mar**	**Apr**	**May**	**Jun**	**Jul**	**Aug**	**Sep**	**Oct**	**Nov**	**Dec**	**Year**
Average high °C	16.0	18.5	23.6	29.9	36.5	41.3	44.0	43.5	40.2	33.4	23.7	17.2	30.6
Average low °C	3.8	5.5	9.6	15.2	20.1	23.3	25.5	24.5	20.7	15.9	9.2	5.1	14.9
Rainfall (mm)	27.2	19.2	22.0	15.6	3.2	0	0	0	0	3.3	12.4	20.0	122.9
Avg. precipitation days	8	7	8	6	4	0	0	0	0	4	6	7	50
Sunshine hours	186	198	248	270	310	360	341	341	330	279	210	186	3,259

Squillqace,et.al.studied the determination of volatile organic compound, VOCs, pesticides, Nitrate and their mixtures in groundwater used for drinking Water (Squillqace, et al 2002). Nitrate at levels above 45 mg/L is a health risk for infants of less than six months of age and pregnant women with certain specific enzyme deficiencies. Nitrate can interfere with the capacity of blood to carry oxygen (Squillqace, et al 2002).

Fluoride has beneficial effects on teeth at low concentrations in DW, but excessive exposure to fluoride in drinking-water, can give rise to a number of adverse effects. These ranges from mild dental fluorosis to crippling skeletal fluorosis which is a significant cause of morbidity (Fawell, et al 2006). The significance and health effects of some water pollutants and ingredients like sulfate, lead, fluoride, nitrate and organic compounds have been reported (Kendall, 1992).

In Iraq, the municipalities are responsible for the production and delivery of drinking water. During 2004 and 2005 the quality of drinking water in Iraq was greatly deteriorated because of the war operation in this country. The analytical laboratories of the environment and water and health authorities carry out chemical and bacteriological test on drinking water in Iraq. The failure of the analyzed water samples reached about 40% of the collected samples, (Barbooti, et al 2005). Some efforts were put to improve the infrastructure and reconstruction of DW treatment systems. Many projects were established in Iraq to supply bottled DW and manufacture of home water clarification, disinfection units in Iraq. A comprehensive study was carried out during 2006 for the evaluation of bottled DW and home purification units. Some bottled DW failed to match the minimum contaminant level (Barbooti, *et al* 2006).

Ion chromatography was used successfully for the determination of major anions, $PO4^{3-}$, $SO4^{2-}$, $NO3^{-}$, NO2-, Cl^{-}, Brand F^{-} in drinking water samples from Baghdad area and

Kualalampur (Alsudany, *et al* 2009).

Soylak *et al.*, 2002, studied the determination of metal ions in the drinking water samples from Yozgat, Turkey. They concluded that the concentrations of the investigated major ions and metal ions in the drinking water samples were below the guidelines for DW standards (Water Pollution Control Regulation of Turkish Authorities, 1989 and WHO, 2004. No correlations were found between metal concentrations in the drinking water sample (Soylak *et al.*, 2002).

This study aimed Seasonal Variations of raw water of Tigris River and effect on quality water plants at using 18 ecological parameters in evaluating the quality of the Tigris River for public usage, by choosing eight sampling sites along the river in Baghdad area.

THE STUDY SITES

In this study, eight stations along Tigris River in Baghdad were chosen Fig (1): Karkh works is in the north of Baghdad on the west bank of the Tigris. East Tigris treatment plant is located close to the northern suburb of the city approximately (1Km) downstream of the north bridge , Karam treatment plant is located within the city on the west bank of the Tigris. Wethba treatment plant is situated within the city area on the east bank of the Tigris river downstream of the Sarafiya rail way bridge near the madenat Al-Tub, Qadisiya treatment plant is situated within the city area on the west bank adjacent to Umm Al Qanazir land , the intake polluted location and condition due it because a small channel located between the island and the west bank ,a short distance downstream from the Al Kair river outlet into the river channel , Doura treatment plant, on the west bank of the river just downstream of Dora power station, within the city area, Rashed treatment plant is located close to the present downstream limit of city development on the east bank of the river between port of Al Rashed Army Comp and the river , short distance downstream of Al Dora

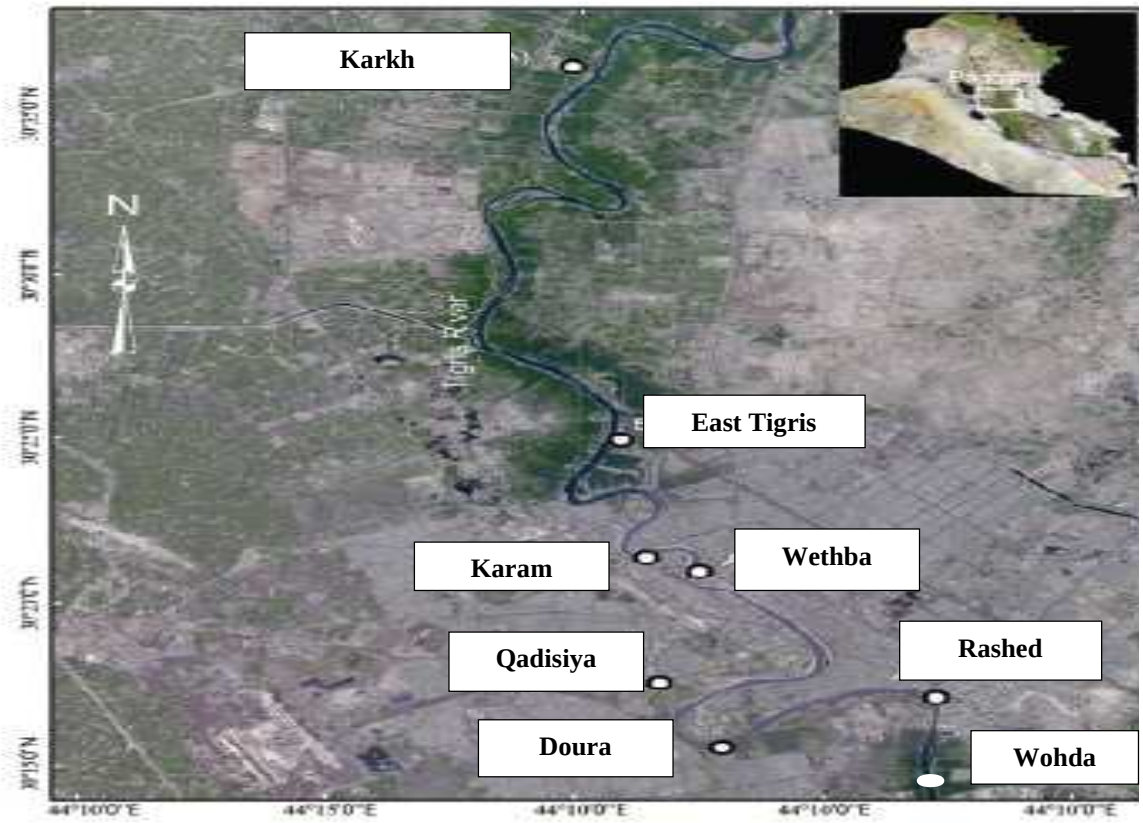

Fig (1): Map of Iraq showing the sample sites on Tigris River (A. M. RABEE *ET AL*.2011)

MATERIALS AND METHODS

All data in research collected from laboratories water treatment plants, through 2008 year , the data covered the physical and chemical properties of the water of the river Tigris at eight water supply intakes these are Temperature, Turbidity, pH value, Total hardness, Iron , Chlorides , EC, TDS , TSS, Calcium, Sulfate, Nitrate, Fluoride, Total Alkalinity, Magnesium ,Oxygen dissolved , BOD_5 and PO4 table(2).

Table (2): The average values of physic- chemical parameters of Tigers River water at r HDL: Highest Desirable Limit; MPL; Maximum Permissible Limit

NO.	PARAMETERS	UNITS	DRINKING WATER WHO Standard		Experimental value (range)
			HDL	MPL	
1	Temperature	°C	---	-----	12-31.67
2	Turbidity	NTU	5	10	0.497-90
3	pH value	-	6.5 to 8.5	No relaxation	7.8-8.16
4	Total hardness (as CaCO3)	mg/l	300	600	290.7-523.3
5	Iron	mg/l	0.3	1.0	0.153- 2.23
6	Chlorides	mg/l	250	1000	32 - 113.87
7	Total Dissolved Solids	mg/l	500	2000	75 – 1324.7
8	Calcium	mg/l	75	200	65 - 179.33
9	Sulphate	mg/l	200	400	190-405
10	Nitrate	mg/l	50	No relaxation	0.24 - 0.568
11	Fluoride	mg/l	1.0	1.5	0.06 - 0.26
12	Total Alkalinity	mg/l	200	600	
13	Magnesium	mg/l	30	150	29 -39
14	Oxygen Observed from KMnO4 at 37°C in 3 hrs.	mg/l	3.0	No relaxation	3.47 - 7.9
15	Total Suspended Solids	mg/l	20	150	26.83 - 131
16	EC	µS/cm	250		607.16- 3269
17	BOD_5	mg/l	10	40	……..
18	PO_4	mg/l	10	10	…….

RESULTS & DISCUSSION

The spatial and temporal variations of monitored parameters in the surface waters of the Tigris River are shown in Figures (2 – 19).During the study period, water temperature showed high seasonal variations, ranging from 12-17 °C in the winter, 25.3-31.67 °C in the summer table (5),Wethba showed high water temperatures, while low water temperatures were detected in Doura, Fig (2).

pH values in all stations in Tigris River showed slightly alkaline. The lowest pH values were detected in Doura Fig (3). It is obvious that the pH was relatively stable among and within stations during the year. It ranged between 7.8-8.16. Seasonal variation of the pH values did not show significant differences, all the results are

within the acceptable limits (6.5 – 8.5). However the WHO regulations do not include limits for the pH values for drinking water. European standard includes a range of 6.5 – 9.5 for the pH of drinking water.

Conductivity distribution along the river showed high values in the East Tigris, Rashed and Karam. Seasonally, the highest conductivity levels were observed in winter table (3). Conductivity values ranged from 607.16-to 3269 µS/cm. Fig (4). The EC measurement of the samples indicated that the raw water characterized by relatively high and fluctuating EC values. The Iraqi standard does not include limits for the EC values of drinking water. Meanwhile, the WHO and the European standards recommended value of EC is 250 µS/cm. This matter needs to be studied to correlate the EC values with human health and to manage for the introduction of EC limits within the Iraqi Standard. The increase in EC is related to the increase in chloride and sulfate ions.

Turbidity values varied from 0.497 at Karkh in summer table (5), to 90 NTU at Wohda in autumn table (6) .Turbidity values in all stations in Tigris River were higher in the autumn and winter during irrigation period Fig (5) .Autumn and Winter recorded the highest values, this could be attributed to presence of organic matter pollution, other effluents, runoff with a high suspended matter content and heavy rain fall. The lower values re-corded in summer can be that, at that time, all the tributaries had dried up, thus, reducing the influx of suspended matter.

From our experience, the water hardness of the Baghdad aqueduct of calcium carbonate equivalent dissolved in water. As for the stations analyzed for 2008, the water hardness is waving between 290.7- 523.3 The lowest TH values were detected in Karkh for all season Fig (6), while the highest value of TH at Rashed in autumn season table 6 In theory this parameter should be more homogeneous but it is not influencing the properties of the drinking water. The only effect is on the cleaning performances during washing. It is interesting that the hardness values for water samples taken in Turkey which is located upstream of Tigris River ranges between 50 – 300 mg/l (Soylak, et al 2002).

The results of the major cations, Ca^{2+}, Mg^{2+}, concentrations are given in fig7, 8. The calcium concentration values fall between 65 to 179.33 mg/l and the average is mg/l. The magnesium concentration values fall between 29 to 39 mg/L and the average is mg/l.

Chloride values varied from 32 to 113.87 mg/l, Qadisiya and Wethaba showed high chloride concentrations, while the lowest values were observed in Karam ,Karkh and Wohda Fig(9). Seasonally, the lowest chloride values were detected in winter table 3. Chloride values varied from 32 to 113.87 mg/l.

The various levels of iron in different samples between 0.153- 2.23 mg/l Fig (10), original pH of the river water is between 7.5 and 8.16. Corrosion of the pipes could partly explain this observation, because flocculation is seldom performed in Iraq by ferric chloride ($FeCl_3$). In any case, the relatively high levels of iron are not impacting the quality of the drinking water except the taste and the red residues on basins, showers, toilets.

Fluoride has beneficial effects on teeth at low concentrations in drinking water, but excessive exposure to fluoride in drinking-water, can give rise to a number of adverse effects. These ranges from mild dental fluorosis to crippling skeletal fluorosis which is a significant cause of morbidity (Fawell, *et al.*,2006).The significance and health effects of some water pollutants and ingredients like sulfate, lead, fluoride, nitrate and organic compounds have been reported (Kendall, 1992). Values varied from 0.06 to 0.26 mg/l, Whoda and Rashed showed high fluoride concentrations, while the lowest values were observed in Karam Fig (11). Seasonally, the lowest chloride values were detected in summer table (5) while the highest value autumn table (6).

Total dissolved solids varied between 75 – 1324.7 mg/l in all study stations Fig (12) and ranged from a minimum of 75 mg/l in spring Table 4to a maximum of 1324.7 mg/l in autumn table (6) as average. The high dissolved solids recorded in autumn could be because of domestic effluent discharges and surface runoff from the cultivated fields which might have increased the concentration of ions. The observed high concentration of dissolved solids in the surface water is a pointer to the fact that there are intense anthropogenic activities along the course of the river and run-off with high suspended matter content (UNESCO, WHO, UNEP, 2001).

Seasonally, the highest TSS values in all stations were observed in spring table (4), while the lowest ones were detected in summer table (5). TSS values varied from 26.83 to 131 mg/l.

Karam showed the highest TSS value in spring, while Karam exhibited the lowest one in autumn Fig (13).

DO concentrations varied from 3.47 mg/l at Wethaba in autumn to 7.9 mg/l.at Qadisiya in summer. DO values were higher in summer and autumn Tables (5, 6) all Stations above 3mg/l of all season variation Fig 14. According to the USDA, 1992, the level of oxygen depletion depended primarily on the amount of added waste, the size, velocity and turbulence of the stream, the initial DO level in the water and in the stream, and the temperature of the water.

BOD_5 values varied from 3.6 mg/l at Karkh in winter to 60.7 mg/l at Wethba in autumn Fig (15). The highest values in all stations except Karkh were observed in season.. The high BOD_5 value Table (6), may be due to discharge of organic wastes (e.g. refuse, human and animal excreta, soap, etc.) into the water, resulting in the uptake of oxygen in the oxidative breakdown of these wastes (Abdul, et al 2009). It is obvious that the BOD_5 concentration decreases gradually during the river passage downstream of the river. This phenomenon can be attributed to the natural self-purification of the river and the lack of outfalls along this stretch.

Sulfate values did not show large variations among stations in the same season, ranging from 190 mg/l at Karkh in winter to 405mg/l at Qadisiya Autumn Fig (16).People that are not used to drinking water with high levels of sulfate can experience dehydration and diarrhoea. Babies are more sensitive to sulfate than adults. As a safety measure, water with a sulfate level exceeding 400 ppm should not be used in the preparation of baby food (WHO directives). Older children and adults become used to high sulfate levels after a few days. In any case, water with high sulfates should be avoided for the rehydration of people with diarrhoea. To confirm this hypothesis, it is necessary to carry out some checks on the raw water. Only these analyses will confirm the real origin of sulfates. Relatively high level of magnesium, if compared with the Calcium content, should maintain the sulfate in solution. This is the reason why the addition of Calcium Hydroxide should help to remove the excess of sulfates.

NO_3 values varied from 0.24 to 0.568 mg/l Fig (17). Seasonally, the highest NO_3 values were observed in autumn in all stations. Karkh showed the highest NO_3 values. The high levels of nitrate recorded in winter might have been because of surface runoff from agricultural activities into the river from the rains. All the nitrate values were within the “no effect” range of (0 – 6) mg/l for drinking water use (WRC, 2003). This indicates that no adverse health effects were expected during the sampling months.

The phosphate values obtained is within the tolerable limits. The total phosphate concentrations in study period varied between (0.001 - 0.30) mg/l Fig (18), with recorded high values in winter table (3), which suggest that phosphorus is rarely found in high concentrations in waters as it is actively taken up by plants. High concentrations of phosphates can indicate the presence of pollution and are largely responsible for eutrophic conditions (WHO, 1998). The phosphate levels increased during winter due to agricultural runoff containing phosphate fertilizers as well as waste water containing detergents.

Table (3): The value, rang, average and standard deviation for recorded parameters in studied stations in winter.

Winter 2008	Karkh	East Tigris	Karam	Wethba	Qadisiya	Doura	Rashed	Wohda	max	min	average	ST
Temperature °C	15.33	15.67	12.67	14	12	17	12.33	13	17	12	14	1.817
Turbidity NTU	0.67	23.33	35.33	20.67	35	35	35	38	38	0.67	27.8754	12.666
pH value	8.04	8.05	8.08	8.03	7.96	7.98	8.08	7.94	8.08	7.94	8.02	0.053
Total hardness (as CaCO3) mg/l	370	466	446	471	471	450	462.5	396.33	471	370	441.603	41.952
Iron mg/l	0.353	0.44	0.39	0.52	0.46	0.47	0.46	1.09	1.09	0.353	0.52287	0.282
Chlorides mg/l	70	101.67	93.33	100.67	100	94.33	93.33	86	101.67	70	92.4166	10.420
EC µS/cm	906.6	3269	1183	1105.3	1134.3	1142.67	1253.67	1034.33	3269	906.6	1378.60	770.790
TDS mg/l	228.33	739.33	715	734.67	742.3	704	791.3	725	791.3	228.33	672.491	218.827
TSS mg/l	26.83	33.67	55.67	31.33	39	51.3	76.33	54.67	76.33	26.83	46.1	18.777
Calcium	91.67	130.67	127.67	131.67	129.33	137.67	129.33	97	137.67	91.67	121.875	17.314
Sulfate SO4 mg/l	190	366.67	320	354.33	345	273.6667	323.5	252.33	366.67	190	303.187	60.187
Nitrate NO3 mg/l	0.905	0.44	0.9733	0.4567	0.42	0.763333	0.54	0.833	0.9733	0.42	0.66645	0.2268
Fluoride mg/l	0.15	0.14	0.193	0.127	0.087	0.103	0.236	0.086	0.236	0.086	0.13885	0.056
Total Alkalinity mg/l	132.67	132.33	131.67	142	134	148.67	131.33	151.33	151.33	131.3	138	8.733
Magnesium mg/l	33.67	34.67	32	33.67	37	39	39	36.33	39	32	35.6666	2.588
DO (dissolved oxygen) mg/l	5.96	4.5	5.1	4.03	5.85	4.93	5.2	5.26	5.96	4.03	5.10375	0.726
BOD_5 mg/l	3.6	21.67	6.47	36.67	13.33	9.33	6.13	3.73	36.67	3.6	12.6162	13.120
PO4 mg/l	0.031	0.076	0.12167	0.0683	0.09	0.095	0.061	0.01	0.1217	0.01	0.06937	0.035

J. Duhok Univ., Vol.17, No.1 (Pure and Eng. Sciences), Pp 55-71, 2014

Table (4): The value, rang, average and standard deviation for recorded parameters in studied stations in spring

Spring 2008	Karkh	East Tigris	Karam	Wethba	Qadisiya	Doura	Rashed	Wohda	max	min	average	ST
Temperature °C	**23.6**	**24.3**	**22**	**24.3**	**23.3**	**21.67**	**22.3**	**22.67**	**24.3**	**21.67**	**23.017**	**1.013**
Turbidity NTU	**0.895**	**36**	**70.33**	**44.33**	**67**	**45**	**36**	**59**	**70.33**	**0.895**	**44.82**	**22.133**
pH value	**8.16**	**8.01**	**8.1**	**8.07**	**8**	**8.07**	**8.14**	**7.97**	**8.16**	**7.97**	**8.0653**	**0.067**
Total hardness (as CaCO3) mg/l	**365**	**368**	**340.3**	**350.33**	**356.7**	**349.7**	**372**	**339.3**	**372**	**339.3**	**355.16**	**12.381**
Iron mg/l	**0.78**	**1.06**	**0.31**	**0.97**	**1.52**	**2.23**	**2**	**1.89**	**2.23**	**0.31**	**1.345**	**76.846**
Chlorides mg/l	**50**	**76**	**69. 33**	**87.33**	**82.67**	**75**	**69**	**67**	**87.33**	**50**	**72.067**	**11.332**
EC µS/cm	**671.6**	**889.3**	**897.3**	**892**	**816.3**	**858.3**	**1005**	**793.67**	**1005**	**671.6**	**852.93**	**96.884**
TDS mg/l	**75**	**597.7**	**551.7**	**599**	**561**	**484**	**649.33**	**580**	**649.33**	**75**	**512.2163**	**182.884**
TSS mg/l	**65**	**56.3**	**131**	**51.67**	**103.3**	**81.67**	**74.83**	**115**	**131**	**51.67**	**84.846**	**28.7844**
Calcium	**65**	**96.67**	**98. 67**	**94.33**	**96.67**	**100.33**	**102.17**	**88.33**	**102.17**	**65**	**92.77**	**11.975**
Sulfate SO_4 mg/l	**140**	**251. 67**	**223.33**	**268.33**	**245**	**193.33**	**242.67**	**175**	**268.33**	**140**	**217.41**	**44.031**
Nitrate NO_3 mg/l	**0.413**	**0.643**	**0.848**	**0.603**	**0.65**	**0.767**	**0.825**	**0.867**	**413.**	**0.603**	**52.31**	**145.87**
Fluoride mg/l	**0.133**	**0.123**	**0.213**	**0.133**	**0.097**	**0.1**	**0.204**	**0.08**	**0.213**	**0.08**	**0.1255**	**0.063**
Total Alkalinity mg/l	**139.3**	**146**	**144.7**	**144.7**	**149**	**170**	**147.3**	**156**	**170**	**139.3**	**149.62**	**9.485**
Magnesium mg/l	**26.33**	**30.67**	**25.67**	**30.67**	**28**	**34.33**	**31.33**	**28.33**	**34.33**	**25.67**	**29.417**	**2.871**
DO (dissolved oxygen) mg/l	**5.87**	**5.1**	**6**	**4**	**5.3**	**5.9**	**6**	**6.1**	**6.1**	**4**	**5.533**	**0.71**
BOD_5 mg/l	**4**	**18.83**	**5.56**	**40**	**14**	**9.73**	**7.2**	**4.13**	**40**	**4**	**12.93125**	**12.090**
PO_4 mg/l	**0.0416**	**0.0867**	**0.113**	**0.0813**	**0.1033**	**0.143**	**0.061**	**0.01**	**0.1433**	**0.01**	**0.08**	**0.042**

Table (5): The value, rang, average and standard deviation for recorded parameters in studied stations in summer

Summer 2008	Karkh	East Tigris	Karam	Wethba	Qadisiya	Doura	Rashed	Wohda	max	min	average	ST
Temperature °C	30.7	31.67	28.67	31.67	30	25.3	31.33	31	31.67	25.3	30.04	25.3
Turbidity NTU	0.497	37.33	25.33	24.33	26.67	27.33	25	59	59	0.497	28.18	0.497
pH value	8.03	8.02	8.1	8.04	7.9	7.88	8.07	7.97	8.1	7.88	8.001	7.88
Total hardness (as CaCO3) mg/l	290.7	496.3	462.3	485.7	348.97	473.3	475.3	407	496.3	290.7	429.94	290.7
Iron mg/l	0.42	0.76	0.29	0.54	0.153	1.33	0.937	0.817	1.33	0.153	0.65	0.153
Chlorides mg/l	75	98	99	101	107	95.33	90	67	107	67	91.54	67
EC µS/cm	813.3	1120.7	1236.7	1110.3	1179.3	1194.3	1200.3	1023	1236.7	813.3	1109.74	813.3
TDS mg/l	722	746.7	727.67	767.7	759.3	707.3	831.3	733.3	831.3	707.3	749.41	707.3
TSS mg/l	34	52.7	52.5	45.67	56.3	47.67	51.83	45	56.3	34	48.21	34
Calcium	66.33	179.33	148	154.67	153.67	151.33	133.33	88.33	179.33	66.33	134.37	66.33
Sulfate SO_4 mg/l	188.33	382	349.67	393	388. 33	253.33	315.33	175	393	175	305.62	175
Nitrate NO_3 mg/l	0.33	0.26	0.507	0.267	0.24	0.43	0.395	0.87	523.33	0.24	65.79	0.24
Fluoride mg/l	0.14	0.143	0.177	0.153	0.123	0.113	0.223	0.06	0.223	0.06	0.14	0.06
Total Alkalinity mg/l	129	106	113	108	121	123	117.83	143	143	106	120.10	106
Magnesium mg/l	27	30	24.33	28.67	28	35	36.67	28.33	36.67	24.33	29.75	24.33
DO (dissolved oxygen) mg/l	5.97	6.13	7.03	4.17	7.9	7	7	7.17	7.9	4.17	6.54	4.17
BOD_5 mg/l	5.17	25.83	8.17	54.67	15.5	12.87	8	5.37	54.67	5.17	16.94	5.17
PO_4 mg/l	0.045	0.06	0.073	0.051	0.088	0.043	0.083	0.01	0.088	0.01	0.056	0.01

Table 6. The value, rang, average and standard deviation for recorded parameters in studied stations in Autumm

Autumm 2008	Karkh	East tigris	Karam	Wethba	Qadisiya	Doura	Rashed	Wohda	max	min	average	ST
Temperature °C	25.3	25.67	24.3	25.7	23.7	22	25	24.33	25.7	22	24.5	1.23
Turbidity NTU	0.63	53.33	51.33	54	50.33	46.67	50.33	90	90	0.65	49.58	24.12
pH value	8.1	7.96	8.03	7.85	7.84	7.8	8.06	7.94	8.1	7.8	7.9475	0.11
Total hardness (as CaCO3) mg/l	310.67	513	455	516	519.7	490.7	523.3	367.3	523.3	310.67	461.95	80.48
Iron mg/l	0.68	0.78	0.34	0.75	0.27	1.5	0.5	0.81	1.5	0.27	0.70	0.38
Chlorides mg/l	82	104.33	101.33	103.67	113.67	100.33	99	88.67	113.67	82	99.12	9.77
EC µS/cm	891.67	1264.3	1324.7	1214	1277	1268.7	1283.3	1040.7	1324.7	891.67	1195.54	150.12
TDS mg/l	68.7	829.7	752.7	814.7	801	730	902	698.3	902	68.7	699.63	262.73
TSS mg/l	62	69.33	86.67	64	68.7	79.7	100.7	65	100.7	62	74.51	13.51
Calcium	71.33	150.33	155.33	153.33	156	150.67	158	88.67	158	71.33	135.45	34.63
Sulfate SO_4 mg/l	211.67	405	349.67	403.33	389	277.33	365.33	261	405	211.67	332.79	73.28
Nitrate NO_3 mg/l	0.3	0.346	0.648	0.343	0.26	0.47	0.47	0.49	568.33	0.26	71.42	200.78
Fluoride mg/l	0.14	0.14	0.23	0.18	0.097	0.117	0.26	0.076	0.26	0.076	0.15	0.064
Total Alkalinity mg/l	0.14	0.14	0.23	0.18	0.097	0.117	0.26	0.076	0.26	0.076	0.15	0.064
Magnesium mg/l	32.33	30.33	29	30.67	30.33	39	38.33	34	39	29	33	3.80
DO (dissolved oxygen) mg/l	6.4	4.497	5.47	3.47	7.84	5.3	5.5	5.6	7.84	3.47	5.50	1.27
BOD_5 mg/l	5.77	29.6	9.87	60.7	17.3	14.3	8.6	6.07	60.7	5.77	19.02	18.55
PO_4 mg/l	0.047	0.06	0.07	0.067	0.12	0.04	0.07	0.01	0.12	0.01	0.065	0.03

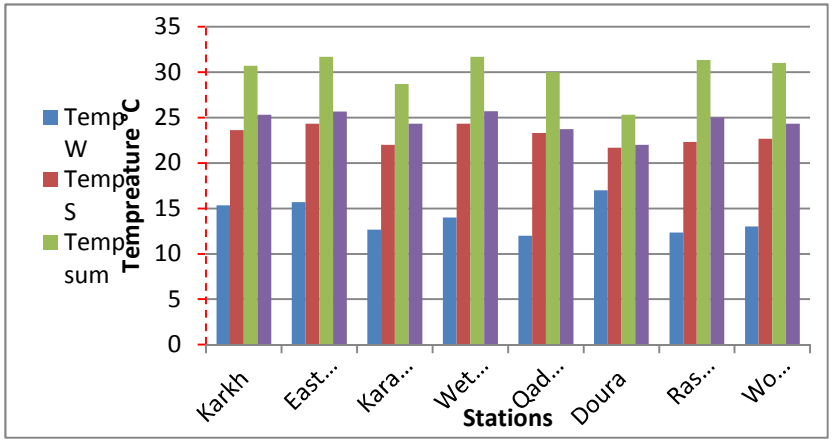

Fig (2): Spatial and temporal variations of temperature

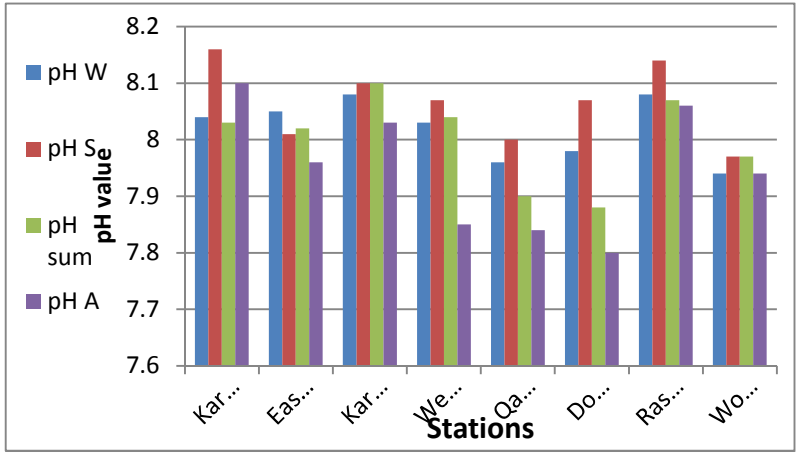

Fig (3): Spatial and temporal variations of pH

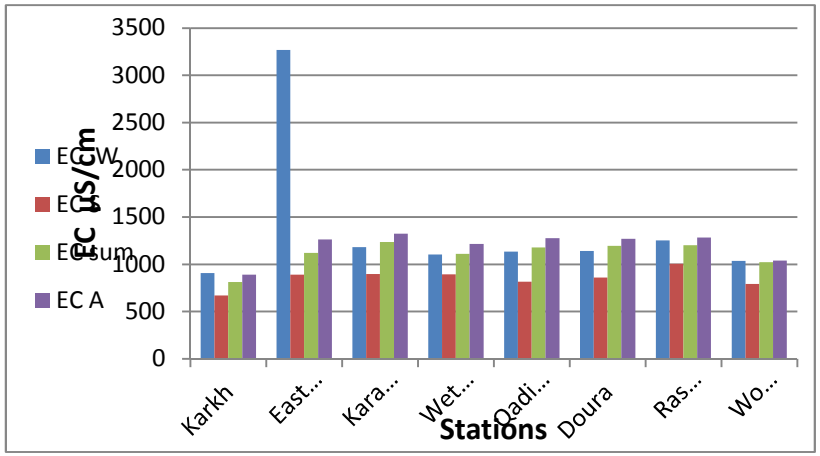

Fig (4): Spatial and temporal variations of EC

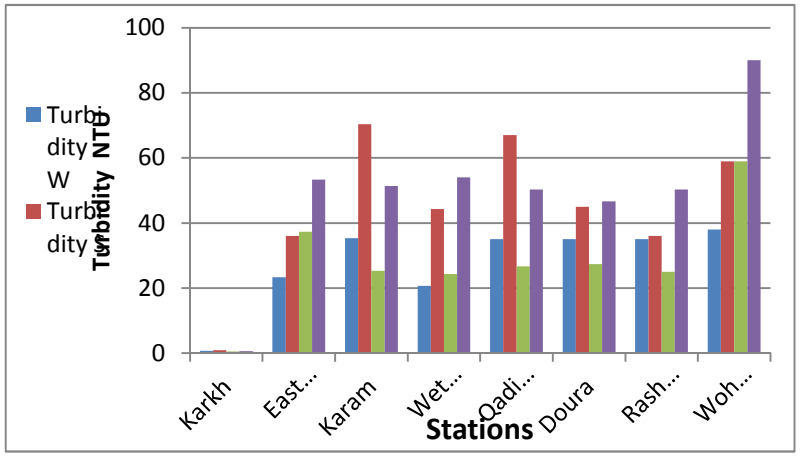

Fig (5): Spatial and temporal variations of turbidity

W Winter S Spring Sum Summer A Autumn

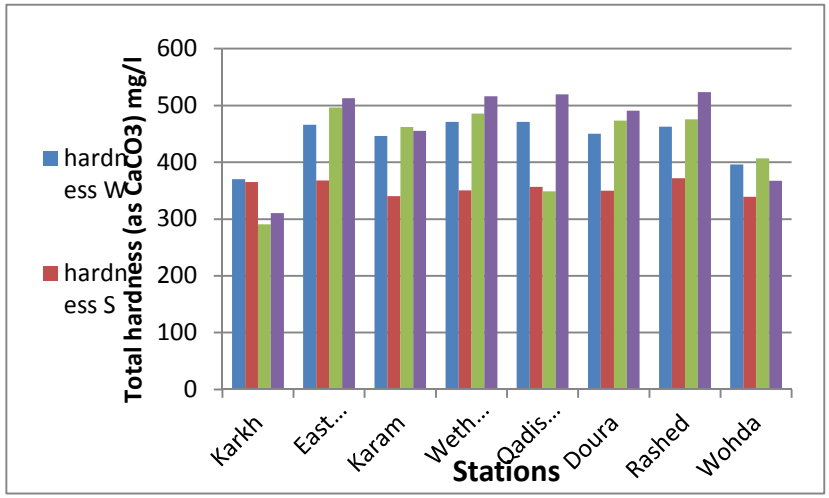

Fig (6): Spatial and temporal variations of total hardness

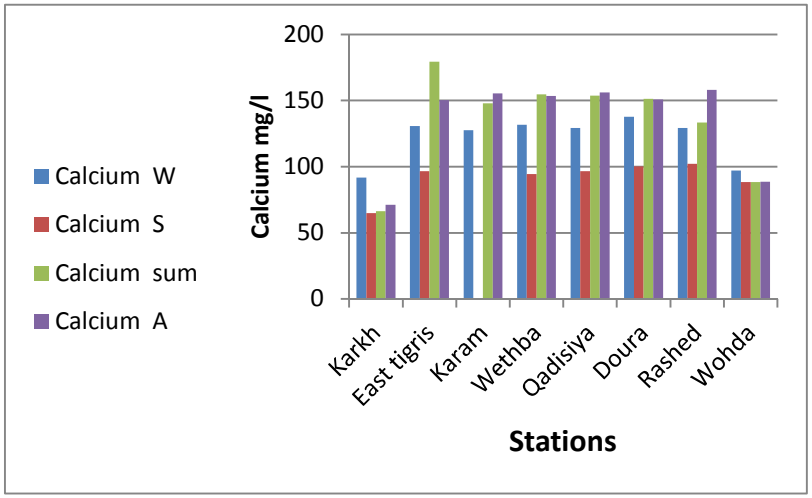

Fig (7): Spatial and temporal variations of Calcium

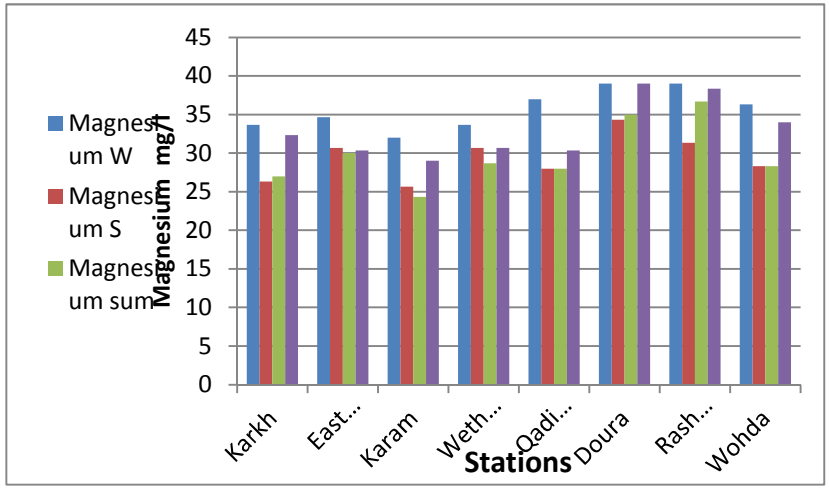

Fig (8): Spatial and temporal variations of Magnesium

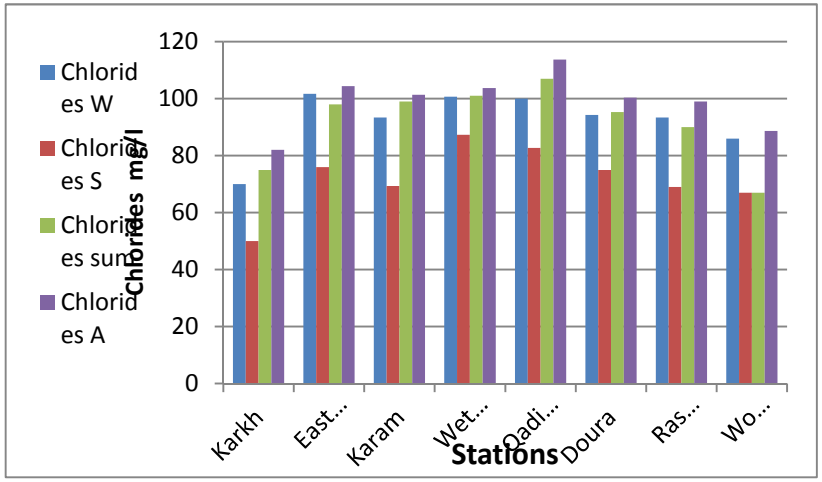

Fig (9): Spatial and temporal variations of Chlorides

J. Duhok Univ., Vol.17, No.1 (Pure and Eng. Sciences), Pp 55-71, 2014

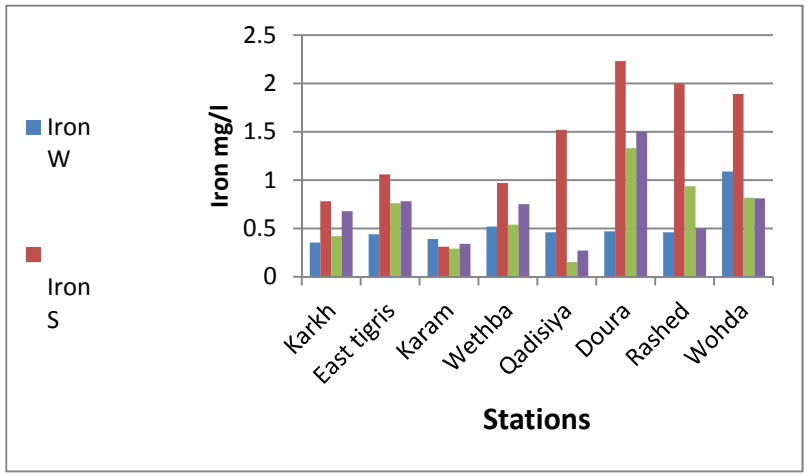

Fig (10): Spatial and temporal variations of Iron

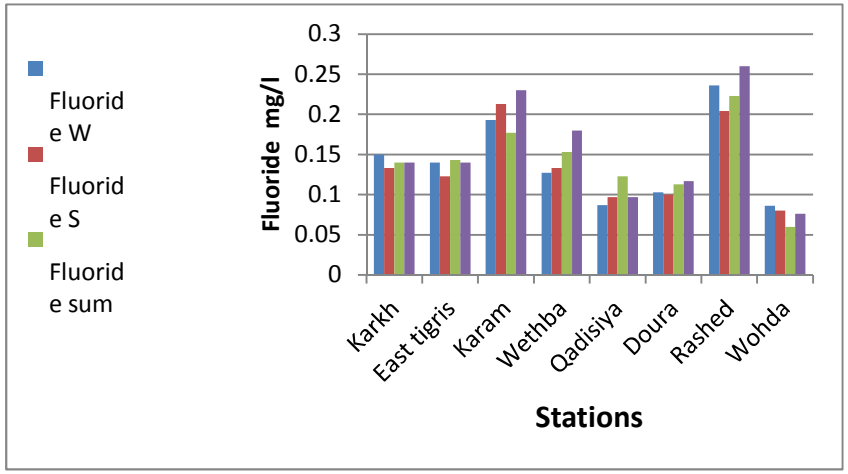

Fig (11): Spatial and temporal variations of Fluoride

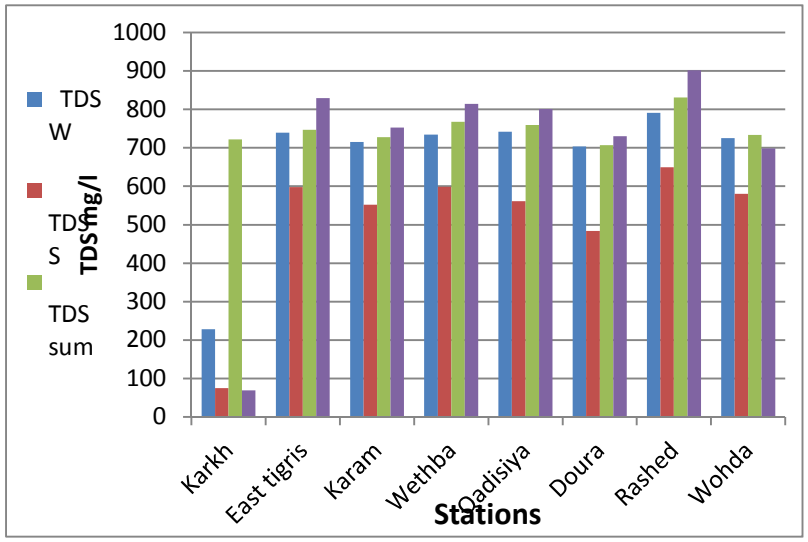

Fig (12): Spatial and temporal variations of TDS

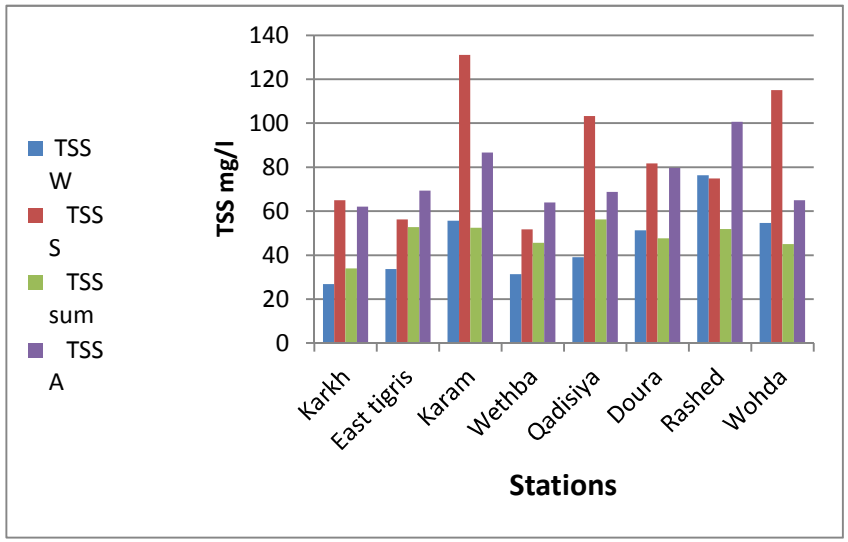

Fig (13): Spatial and temporal variations of TSS

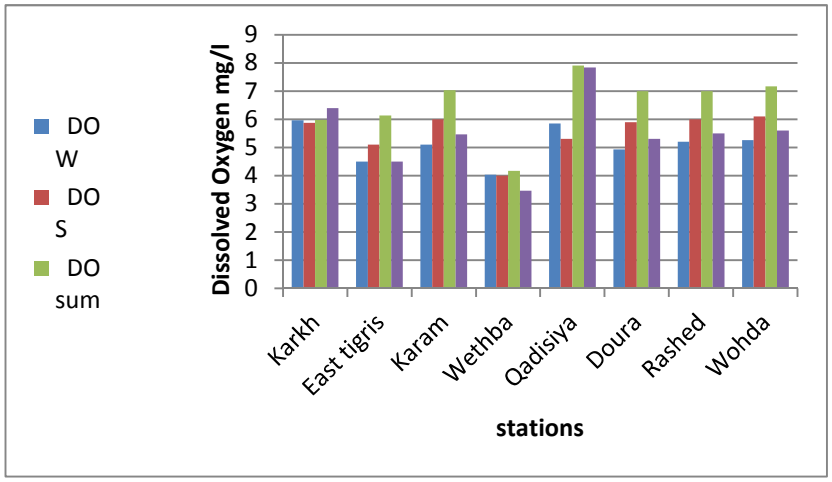

Fig (14): Spatial and temporal variations of DO

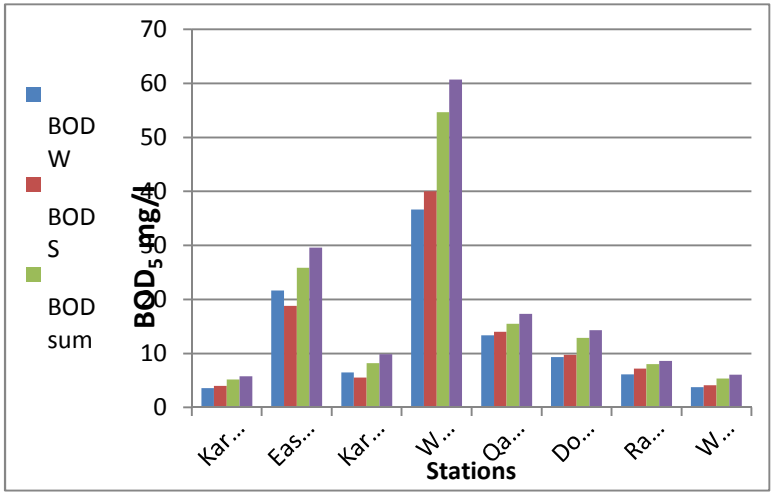

Fig (15): Spatial and temporal variations of BOD_5

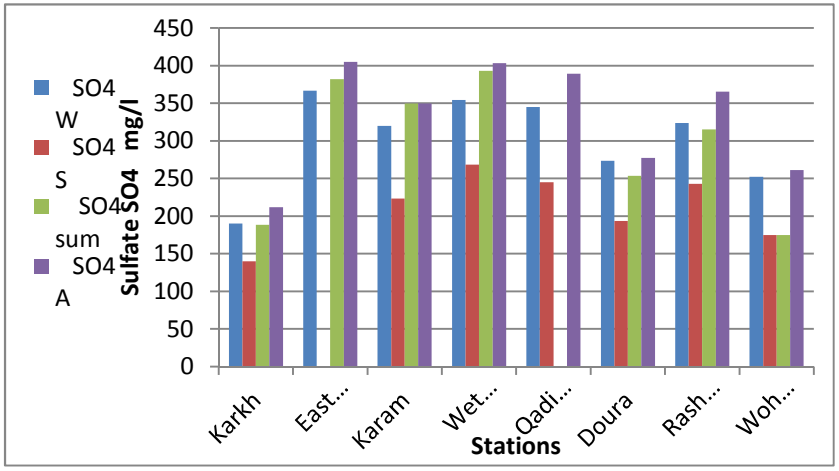

Fig (16): Spatial and temporal variations of Sulphate

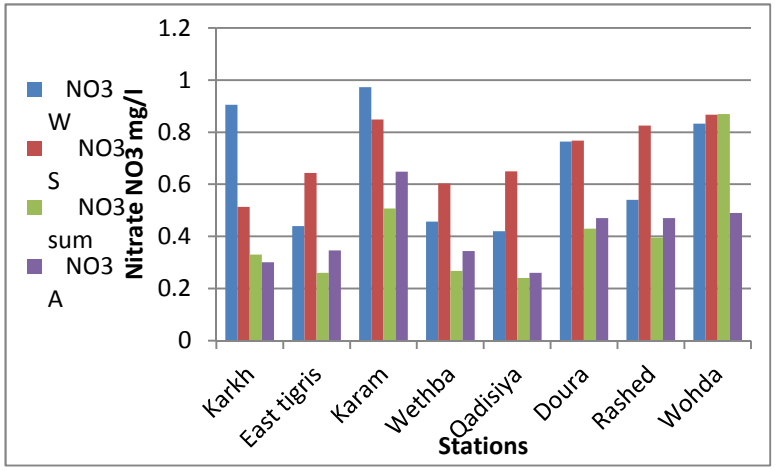

Fig (17): Spatial and temporal variations of Nitrate

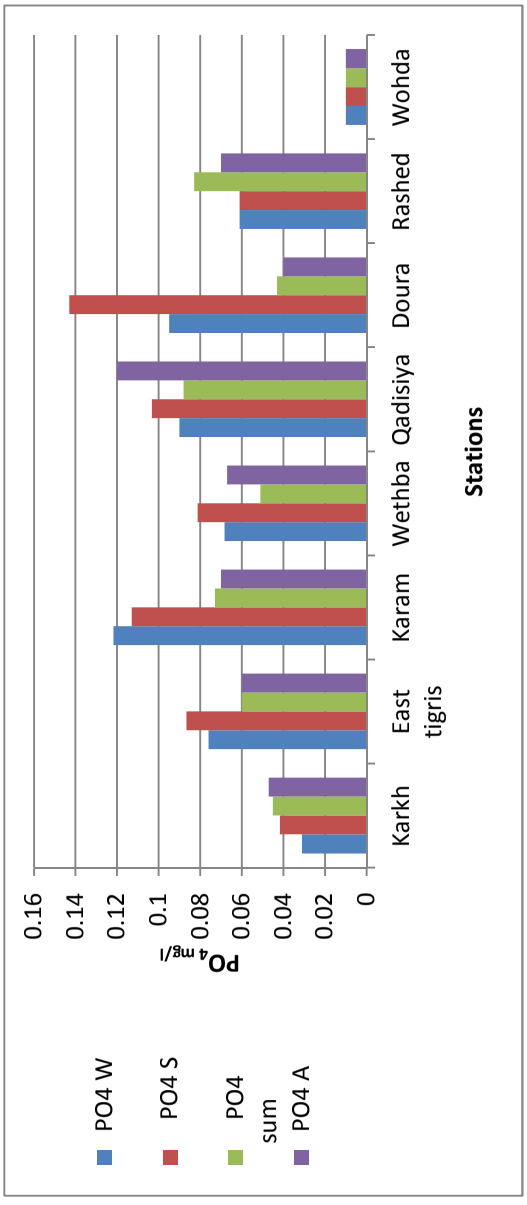

Fig (18): Spatial and temporal variations of PO_4

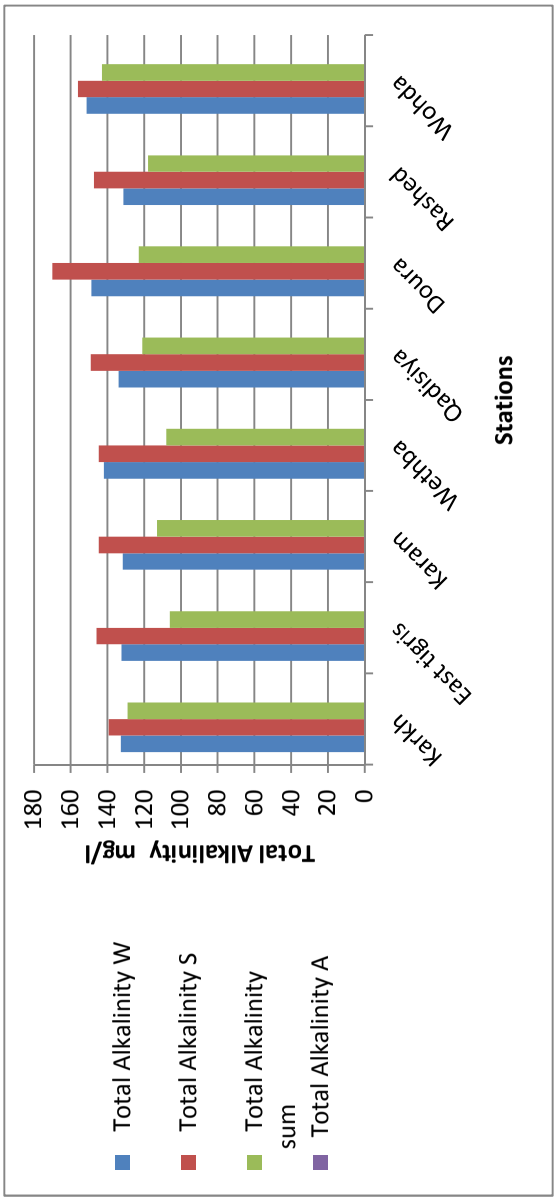

Fig (19): Spatial and temporal variations of Total Alkalinity

CONCLUSION

water temperature showed high seasonal variations, ranging from 12-17 °C in the winter, to 25.3-31.67°C in the summer , pH values in all stations in Tigris River showed slightly alkaline, Conductivity distribution along the river showed high values in the East Tigris, Rasheed and Karam. Seasonally, the highest conductivity levels were observed in winter, Turbidity values in all stations in Tigris River were higher in the autumn and winter during irrigation period, The lowest total hardness values were detected in Karkh for all season while the highest value of TH at Rasheed in autumn season, The calcium concentration values fall between 65 to 179.33 mg/l and the average is mg/l The magnesium concentration values fall between 29 to 39 mg/l and the average is 34 mg/l.

the lowest chloride values were detected in winter ,Chloride values varied from 32 to 113.87 mg/l, Total dissolved solids varied between 75 – 1324.7 mg/l in all study stations minimum of 75 mg/l in spring to a maximum of 1324.7 mg/l in autumn , Seasonally, the highest TSS values in all stations were observed in spring, while the lowest ones were detected in summer , DO concentrations varied from 3.47 mg/l.at Wethaba in autumn to 7.9 mg/l at Qadisiya in summar, The highest BOD_5 values in all stations except Karkh were observed in season., Sulfate values did not show large variations among stations in the same season, ranging from 190 mg/l at Karkh in winter to 405mg/l at Al Qadisiya autumn, the highest NO_3 values were observed in autumn in all stations. Al-Karkh showed the highest NO_3 values,

REFERENCES

- (AFP) ,Afp.google.com, First snow for 100 years falls on Baghdad, Afp.google.com. http://afp.google.com/article/ALeqM5huPkYk4bGVvo1Sa1tWeH-tgENiFw. Retrieved 2010-04-27.
- World Weather Information Service-Baghdad. http://worldweather.wmo.int/154/c01464.htm. Retrieved 2010-03-29.
- BBC-WeatherCentre-World Weather-Average Conditions - Baghdad, http://www.bbc.co.uk/weather/world/city_guides/results.shtml?tt=TT002400. Retrieved 2010-05-06.
- Squillqace, J.; Scott, J. C., Moran, M. J.; Nolan, B. T. & Kolpin, D.W., VOCs, Pesticides, Nitrate, And Their Mixtures In Groundwater Used For Drinking Water In The United States.*Environmental Science and Technology, 36*. (2002), 1923-1930.
- Fawell, J.; Bailey, K.; Chilton, J.; Dahi, E.; Fewtrell, L. & Magara, Y., Fluoride in Drinking-water, WHO, TJ International (Ltd), Cornwall, UK. (2006).
- Kendall, P. ,Drinking Water Quality and Health, Food And Nutrition Series, No. 9.307, (1992).Colorado State University, Cooperative Extension. 10/92. www.colostate.edu/Depts/CoopExt.
- Barbooti, M. M., Hatam, N., Akram, B., Joseph, F., Ibraheem, S. & Fadhil, A. ,The Quality Of Drinking Water In Baghdad Area After-The War, Proceedings of the 1st International Conference on Environmental Health in Iraq, Amman, (2005), 19-22.
- Barbooti, M. M., Jassem, I. A. & Kadhum, R., Evaluation of DW purification units in Iraq, Report No. 261, (2006), Ministry of Environment, Iraq.
- Alsudany, H. M. L., Al-Bayati, R. I. & Barbooti, M. M.,Determination of anions by ion chromatography in water samples of Baghdad city, *African Journal of Pure and Appl chemistry*, 3.(2009).165-169.
- Water Pollution Control Regulation of Turkish Authorities (WPCRTA) (Su Kirliligi Kontrol Yonetmeligi), (1989), No:19919, T.C. Resmi Gazete.
- World Health Organization (WHO), , Guidelines for Drinking Water Quality, Chap. 8, (2004).Geneva.
- Soylak, M.; Armagan Aydin, F.; Saracoglu, S.; Elci, L. & Dogan, M. Chemical Analysis of Drinking Water Samples from Yozgat, Turkey, *Polish Journal of Environmental Studies, 11*.(2002).151- 156.
- A. M. RABEE *ET AL*. Seasonal Variations of Some Ecological Parameters in Tigris River Water at Baghdad Region, Iraq , *Journal of Water Resource and Protection*, 2011, 3, 262-267 .
- World Health Organization, Guidelines for drinking water quality-,Recommendations, 2nd Ed. Geneva WHO, 1993. www.lenntech.com/drinking-water-standards.htm.
- UNESCO/WHO/UNEP,Water quality Assessment-AGuide to Use Biota, Sediment and Water in Environmental Monitoring," 2nd Edition, (2001), pp. 10-14.
- USDA (United States Department of Agriculture), "Agri-cultural Waste Management Building Design Hand-book," Soil Conservation Service, Washington, DC, (1992).
- A. B. Abdul-Razak, R. E. M. Asiedu, and K. A. A. de-Graft-Johnson, "Assessment of the Water Quality of the Oti River in Ghana," *West African Journal of Applied Ecology*, Vol. 15, 2009.
- WRC (Water Resources Commission), "Ghana Raw Water Criteria and Guidelines," *Domestic Water*, Vol. 1, CSIR-Water Research Institute, Ghana, (2003).
- WHO (World Health Organization), "Guidelines for Drinking Water Quality," 2nd Edition, Geneva, (1998).

الخلاصة

الدراسة الحالية تحقيق نطاق واسع للمعايير الفيزيائية والكيميائية والبايولوجية لعينات اياه نهر دجلة في بغداد .تم جمع عينات المياه من ثمانية محطات خلال فصل الربيع (مارس وأبريل ومايو)، وفصل الصيف (يونيو، يوليو، أغسطس) وفصل الخريف(سبتمبر، أكتوبر حتي نوفمبر) وفصل الشتاء (ديسمبر يناير وفبراير) في عام 2008.

هدف الدراسة استخدام 18 معير في تقييم جودة نوعية مياه نهر دجلة للاستخدام العام، عن طريق اختيار ثمانية مواقع لأخذ العينات على طول النهر في منطقة بغداد. هذه المعايير المدرجة هي درجة الحرارة، العكارة، قيمة الرقم الهيدروجيني، العسرة والحديد والكلوريدات، التوصيل الكهربائي، المواد الصلبة الذائبة،المواد الصلبة الكلية ، الكالسيوم، كبريتات، نترات، الفلوريد، القاعدية، المغنيسيوم، الاوكسجين المذاب، المتطلب الاوكسجين الحيوي والفوسفات.

استخدمت المعايير لحساب نوعية المياه لتغيرات الموسمية في نهر دجلة في منطقة الدراسة. ابدت درجة حرارة الماء تغيرات موسمية عالية ، والتي تتراوحت 17–12 درجة مئوية في فصل الشتاء، 25 ،31–3، 67درجة مئوية في فصل الصيف، وأظهرت قيم الرقم الهيدروجيني في جميع المحطات في نهر دجلة قاعدية قليلة، قيم عالية لتوصيلية الكهربائية في محطة شرق دجلة، والرشيد والكرامة، موسميا، لوحظ أعلى مستويات لقيم التوصيلية في فصل الشتاء، وكانت قيم العكورة عالية في كل المحطات في نهر دجلة وفي فصل الخريف والشتاء خلال فترة الري، اوطى قيمة للعسرة الكلية فيمحطة الكرخ ولجميع المواسم في حين أن أعلى قيمة للعسرة الكلية في محطة الرشيد في موسم الخريف، تركيز قيم الكالسيوم بين 65– 179.33 ملغم /لتر والمعدل هو 122. 165ملغ /لتر. قيمة تركيز المغنيسيوم 39–29 ملغم /لتر ومعدل 34 ملغ /لتر . أدنى قيةم للكلوريد في فصل الشتاء، تباينت قيم كلوريدات 32– 113.87 ملغم /لتر، تراوحت قيمة المواد الصلبة الذائبة بين (1324.7–75)ملغم /لتر في جميع محطات الدراسة سجل أدنى قيمة 75ملغ /لتر في فصل الربيع و أقصى قيمة 1324.7ملغم /لتر في الخريف، موسميا، لوحظت أعلى القيم المواد الصلبة في جميع المحطات في الربيع، في حين سجل أقل منها في فصل الصيف، تفاوتت تراكيز من 3. 47 – 7.9 ملغ /لتر في محطة الوثبة في الخريف قادسية في الصيف، وقد لوحظت أعلى قيم للمتطلب البايولوجي في جميع المحطات باستثناء محطة الكرخ .لم تظهر قيم الكبريتات اختلافات كبيرة بين المحطات في نفس الموسم، بدءا من 190ملغ /لتر في الكرخ في فصل الشتاء إلى 405 ملغ /لتر في محطة القادسية في فصل الخريف، أعلى قيم للنترات لوحظت في فصل الخريف في جميع المحطات .أظهرت الكرخ أعلى القيم للنترات.

ظاهرة تدهور نوعية المياه على طول نهر دجلة واضح عموما في جميع أنحاء النتائج لهذا العام .وبالتالي، يتعين على السلطات ممارسة المزيد من الجهود في السيطرة على الأنشطة المختلفة على طول ضفة النهر .ينبغي تطبيق قواعد إدارة المياه، وعزل نظم معالجة مياه الصرف الصحي للمصانع وغيرها من الأنشطة.

SOIL TESTING FORECASTING USING TIME - SERIES ANALYSIS TECHNIQUES

MUTHAINA **.A. M**USTAFA
Dept. Environmental technologies, College of Environmental Science and Technology , University of Mosul-Iraq
(Received: November 21, 2013 ; Accepted for publication: May 4, 2014)

ABSTRACT

Factor analysis is one of the most important methods usually used to identify the most important methods usually used to identify the most important factors affecting the phenomenon of forecasting soil testing along a different periods of time, announced in this study. In this study, interpretation of the different inter-related factor or variables related to soil investigation on testing all classifications along different soil depths are analyses. Soil metal compositions of each layer according to Iraqi Environment during the last two decades changed due to different circumstauses forced people to change their life style, all behavior, and produced pollutions all soil chemical changes specially in effected agricultural prediction.

For the above reasons, the open ion of uses born in mineral to predict soil future behavior using some well-known methods such as Brown Double exponent ion and Box-Jenkins times analysis techniques.

INTRODUCTION

Factor analysis is a mathematical process aimed at simplifying the links between different variables entering in the analysis and access to common factors that describe the relationship between these variables.

the Approach to a statistical analysis of multiple data is related with each other at different degrees from the link so that it starts calculating correlations between the number of variables to get the matrix of correlations between these variables moving forward after that to analyze this matrix correlation universally to get to the lowest possible number of axes or the factors that enable to express the greatest contrast between these variables, in the form of an independent classifications list on the basis of the quality of the rating.(Wikipedi)

the Forecasting process propagated by the method of Brown's Double Exponential Smoothing Method, is one of the modalities of the exponential smoothing, to estimate parameters specific to the model which represents the weights is equal and that is given previous observations and range values of these parameters between zero and one. Values of primary for the purpose of starting the process of forecasting to select the optimum values is done by minimizing the mean squares error or using logarithmic non-linear optimization to find the best values and the most recent attribute values having larger weights in the prediction of the previous observations. (Arsham,2002)(Brocklebank,2003).

(Box & Jenkins) prediction method main objective is to find a suitable formula to predict so as to make Residuals very small by minimizing MSE. (Al-Tai ,2004)

CORRELATION IN THE TIME SERIES

Uses the estimate Autocorrelation and Partial Autocorrelation estimate Time series in determining the appropriate model of the time series measures and the statistical relationship between the series Views Can be illustrated as follows: (Al-Shakurji ,2010)

AUTOCORRELATION ANALYSIS

describe autocorrelation functions as a measure of linear relations between the time series is used in this study the relationship between the present and past series and is known as the autocorrelation function measure for the degree of correlation between Views coming in the time series {Xi: 1, 2, ---, n} the estimator function the link can be estimated by the following equation:

$$r_k = \frac{\sum_{t=k=1}^{n} x_t - \bar{x}\ (x_{t-k} - \bar{x})}{\sum_{t=1}^{n}(x_t - \bar{x})^2} \qquad k1, 2, - -, n - 1 \quad (1 - 1)$$

That's where:

r_k: Represent the links between self X_t,X_{t-1}
r_k: Distributed natural zero rate as variation 1/n.

AUTOCORRELATION ANALYSIS PARTIAL

The partial autocorrelation function kkØ to the k measure correlation between X_t, X_{t-k} certified as the value of X_t in the rest periods and is defined as follows:

$$\emptyset_{kk} = \mathbf{Cov}(X_t, X_{t+k} / X_{t-1}, - -, X_{t+k-1} (2 - 1)$$

FACTOR ANALYSIS

Factor analysis approach aims to summarize fewer variables called factors so that each of these factors function with which some or all of these variables and thus can give an explanation for this factor, according to the strength of variables that are associated with.

The basic idea of this analysis is to work to draw a range of factors related to the original variables
these factors explain the largest possible proportion of the variance in the original variables which can be represented by the equation following: (Mohamed, 2004) (Mustafa, 2012)

$$\begin{aligned} Y_1 &= h_{11}f_1 + h_{12}f_2 + - - + h_{1p}f_p + \varepsilon_1 \\ Y_2 &= h_{21}f_1 + h_{22}f_2 + - - + h_{2p}f_p + \varepsilon_2 \\ &\ \ .\quad .\quad .\quad . \\ &\ \ .\quad .\quad .\quad . \\ Y_k &= h_{k1}f_1 + h_{k2}f_2 + - - + h_{kp}f_p + \varepsilon_k \end{aligned} \qquad (3-1)$$

Where:

f1,f2,---,fp: represent the general factors that have been selected from K variables.

hij: represents the coefficients general factors fi in Xj linear structure and called Working to download the i variable Xj .

$\varepsilon_1, \varepsilon_2, - - -, \varepsilon_k$: represent specific factors and therefore can be represented using matrices as follows:

$$X_{kxp} = B_{kxp}F_{px1} + \varepsilon_{kx1} \qquad (4 - 1\ )$$

Brown's Double Exponential Smoothing Method

Suppose that we have a time series represents Views $Z_1,Z_2,\ldots,Z_{n-1},Z_{n-2}$ static pave $0<\alpha<1$
In order to predict the data contained direction in the meaning that the new value be either greater or less than the previous values. (Makridkis,1998), (Wikipedia)
equations in this method are :

$$L_{t=}\alpha Z_t + \alpha\ 1 - \alpha\ Z_{t-1} + \alpha\ 1 - \alpha\ ^2 Z_{t-2} \pm - - - \quad t = 1, 2, - -, n \quad (5 - 1)$$

$$\text{Level} = L_t^{(1)} = \alpha Z_t + \ 1 - \alpha\ L_{t-1}^{1} \qquad t = 1, 2, - -, n \qquad (6 - 1)$$

as the $L_t^{(1)}$ represents an exponential smoothing to simple

$L_t^{(1)} = L_t$ Symbolizes the degree to the smooth &(1)

$$L_t^{(2)} = \alpha L_t^{(1)} + 1 - \alpha\ L_{t-1}^{2}\ (7-1)$$

as the L_t^2 represents a double exponential smoothing and (2) to symbolize the degree the smooth

$$a_t = 2L_t^{1} - L_t^{(2)}$$

$$\text{Trend} = b_t = \frac{\alpha}{1-\alpha}\ L_t^{1} - L_t^{2} \qquad 8-1$$

$$\text{Forecast} = F_{t+m} = a_t + b_{t.m}\ (9-1)$$

Represents the equation (6-1)modification so that represents Views of the most recent L_t weights equal to (α) and give value to smooth the previous weight equal (α-1). the Equation (8-1) function to update the direction in which interpreted as the difference negative values smooth This is useful in case of specific direction of the data, which modify and multiply the amount by $\frac{\alpha}{1-\alpha}$.

Finally, equation (9-1)used to predict where the direction multiply b_t number of future interval (m), in addition to the base value of a_t.

It should be noted that this method requires giving initial values to (b_t,α ,a_t)and the initial values are calculated $L_0^{(1)}, L_0^{(2)}$ as follows:

$$L_{(0)}^{(1)} = a_0 - \frac{1-\alpha}{\alpha} b_0$$

$$L_0^{(2)} = a_0 - 2\frac{1-\alpha}{\alpha} b_0$$

The Style of Time-Series Analysis Using Factor Analysis

Method was used factor analysis to find transactions regressions desired, as well as to get rid of the problem of multiple linear relationship between variables where Y containing K of the independent variables . Components less than K are derived from the original values of Y to replace these variables so that they are qualified to explain most of the total original values variation and those components are orthogonal with each other depending on the covariance matrix of the fact that the data has the same classes and units of measurement.

Using the SPSS statistical program and the results obtained are shown in table (1). (Mustafa, 2012)

Table (1): values of the Factor Analysis of Soil Tests for 10&25 cm layers

Values of factor analysis For the first layer depth of 10 cm			***Values of factor analysis For the second layer depth of 25 cm***			***Values of factor analysis For the first layer depth of 10 cm***			***Values of factor analysis For the second layer depth of 25 cm***		
Pb	**Ni**	**Zn**	***pb***	***Ni***	***Zn***	***pb***	***Ni***	***Zn***	***pb***	***Ni***	***Zn***
-1.35	-20.90	-6.90	*-1.10*	*-9.45*	*-8.38*	*-0.69*	*-10.32*	*3.39*	*1.08*	*-13.89*	*-3.94*
-1.47	-20.87	-6.87	*-1.09*	*-9.41*	*-8.35*	*-0.72*	*-10.30*	*3.35*	*1.09*	*-13.77*	*-3.91*
-1.53	-20.82	-6.84	*-1.07*	*-9.38*	*-8.31*	*-0.66*	*-10.25*	*3.32*	*1.07*	*-13.74*	*-3.87*
-1.61	-20.77	-6.86	*-1.08*	*-9.34*	*-8.28*	*-0.63*	*-10.28*	*3.37*	*1.06*	*-13.68*	*-3.84*
-1.32	-20.92	-6.89	*-1.11*	*-9.39*	*-8.30*	*-0.70*	*-10.23*	*3.38*	*1.08*	*-13.73*	*-3.88*
-1.48	-20.85	-6.91	*-1.09*	*-9.42*	*-8.32*	*-0.75*	*-10.29*	*3.40*	*1.05*	*-13.84*	*-3.92*
-0.07	0.42	-4.71	*0.76*	*-3.27*	*-2.73*	*-3.36*	*-27.19*	*-19.90*	*-3.90*	*-25.13*	*-3.90*
-0.09	0.40	-4.66	*0.73*	*-3.24*	*-2.71*	*-3.31*	*-27.20*	*-19.86*	*-3.88*	*-25.11*	*-3.88*
-0.1	0.37	-4.63	*0.77*	*-3.21*	*-2.68*	*-3.25*	*-27.17*	*-19.85*	*-3.84*	*-25.15*	*-3.84*
-0.11	0.33	-4.57	*0.68*	*-3.25*	*-2.65*	*-3.29*	*-27.15*	*-19.77*	*-3.82*	*-25.09*	*-3.81*
-0.12	0.39	-4.51	*0.63*	*-3.29*	*-2.61*	*-3.38*	*-27.13*	*-19.74*	*-3.78*	*-25.07*	*-3.75*
-0.15	0.41	-4.72	*0.71*	*-3.28*	*-2.64*	*-3.41*	*-27.17*	*-19.72*	*-3.72*	*-25.12*	*-3.71*
-0.50	-2.18	-4.19	*-3.00*	*10.29*	*-14.62*	*0.44*	*-20.60*	*-10.17*	*-1.01*	*-8.57*	*-7.01*
-0.57	-2.20	-4.16	*-3.01*	*10.25*	*-14.61*	*0.47*	*-20.56*	*-10.13*	*-1.0*	*-8.59*	*-7.02*
-0.44	-2.17	-4.13	*-2.96*	*10.23*	*-14.57*	*0.50*	*-20.52*	*-10.15*	*-1.03*	*-8.60*	*=7.03*
-0.59	-2.15	-4.15	*-2.94*	*10.22*	*-14.53*	*0.42*	*-20.48*	*-10.12*	*-1.02*	*-8.57*	*-7.04*
-0.61	-2.19	-4.17	*-2.97*	*10.26*	*-14.59*	*0.39*	*-20.43*	*-10.14*	*-1.04*	*-8.54*	*-7.05*

-0.64	-2.21	-4.18	-3.02	10.30	-14.60	0.43	-20.41	-10.6	-1.05	-8.58	7.06
-0.72	-23.38	0.26	-0.83	-15.7	-2.27	2.60	-11.31	-3.68	-2.39	-17.15	-1.80
-0.77	-23.34	0.28	-0.81	-15.8	-2.30	2.58	-11.27	-3.70	-2.41	-17.13	-1.82
-0.81	-23.31	0.30	-0.79	-15.5	-2.24	2.54	-11.24	-3.67	-2.37	-15.17	-1.83
-0.85	-23.28	0.27	-0.74	-15.6	-2.23	2.50	-11.21	-3.63	-2.35	-15.14	-1.78
-0.74	-23.36	0.24	-0.77	-15.7	-2.21	2.55	-11.27	-3.65	-2.33	-15.12	-1.76
-0.69	-23.39	0.25	-0.82	-15.6	-2.24	2.61	-11.30	-3.68	-2.38	-15.11	-1.79
3.77	-5.98	-15.20	7.60	0.30	-20.37	8.2	19.0	8.1	7.1	9.2	3.00
3.80	-5.94	-15.25	7.55	0.33	-20.35	8.16	18.94	8.2	6.94	8.95	3.05
3.71	-5.91	-15.29	7.52	0.36	-20.31	8.14	18.88	7.92	6.93	8.84	3.04
3.65	-5.87	-14.91	7.47	0.29	-20.27	8.12	18.83	7.95	6.86	8.81	2.99
3.69	-5.82	-14.87	7.58	0.27	-20.25	8.17	18.91	7.87	7.94	8.77	2.93
3.70	-5.90	-15.0	7.74	0.31	-30.1	8.19	19.1	7.99	7.2	8.93	2.91

The Practical Work :

This includes the Viewing the results of lab tests of samples of soil, which represented lead, nickel and zinc, which were taken from different areas of agricultural land in the Nahrawan area in the city of Baghdad, for the period from 1/1/2012 until 30/10/2012 and by six samples per month and the10 cm surface layer deep and the second of 25 cm deep.

Factor Analysis Sample Selection :

One of the first steps that should followed to describe or analyze any time series is drawn by what is known as drawing time to see the general direction of the series stability and show the following forms of time series variables first and second layer as follows:

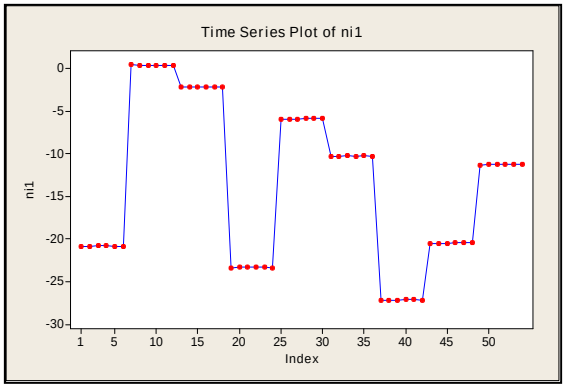

Fig. (1.1): Time Series for the lead of the First Layer

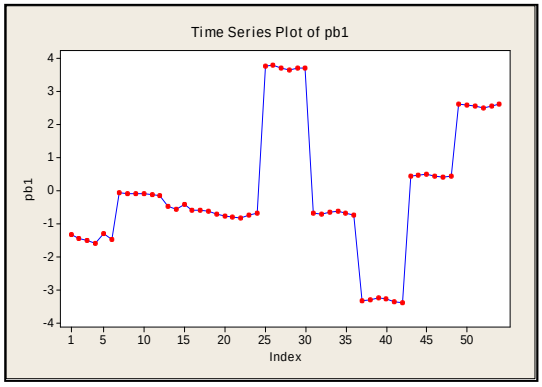

Fig. (2.1): Time Series for the nickel of the First Layer

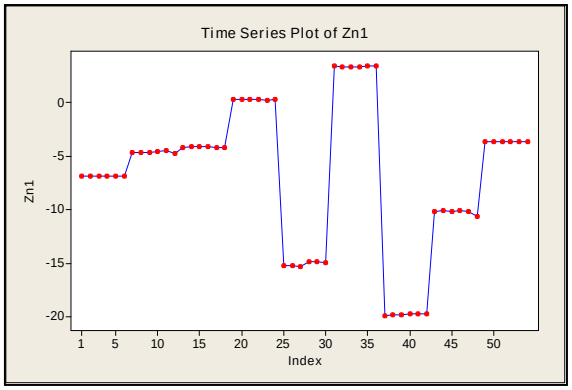

Fig. (3.1): Time Series for the zinc of the First Layer

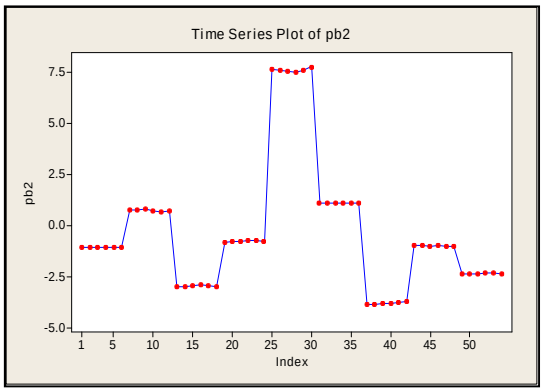

Fig. (4.1): Time Series for the lead of the Second Layer

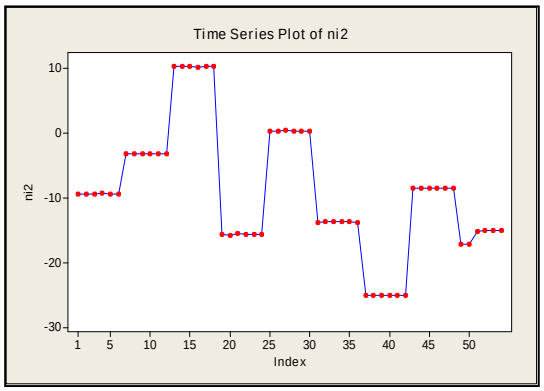

Fig. (5.1): Time Series for the nickel of the Second Layer

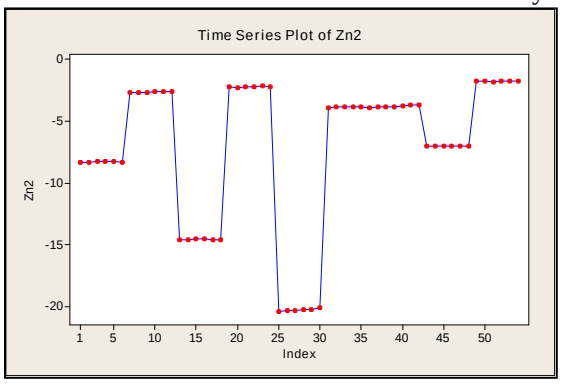

Fig. (6.1): Time Series for the zinc of the Second Layer

We note from the drawing time series for the first layer a fixed variance, the arithmetic mean and to increase the

the accuracy of the knowledge of stability of the data was used chi squared and the value calculated are (χ^2= 64.21), (χ^2=72.33),(χ^2=56.32) For examinations and comparisons with the value of chi squared tabular we find that it is.

Significant, which refers to the stability of time-series. the second layer it was fixed in contrast, but the first sequential difference was taker as (d=1) to prove stability, For the arithmetic mean for both lead and zinc nickel either fixed in the mean and variance then find the appropriate form of the data with the knowledge he is as Rate were excluded the last six samples for each examination and layers to find her prediction follows:

Table (2): Appropriate Forms for Factor Analysis of the Data Layers Tests

first layer			
test	sample	MSE	(k AIC)
Lead	(0,0, 2)	0.0230	-478.342
Nickel	(2,0,0)	0.5361	-483.864
Zinc	(1,0,2)	0.2153	-484.938
second layer			
Lead	(0,1,2)	0.04801	-492.964
Nickel	(2,1,1)	0.2369	-497.926
Zinc	(0,0,2)	0.2440	-465.873

Partial Autocorrelation Functions for the First Layer as Follows:

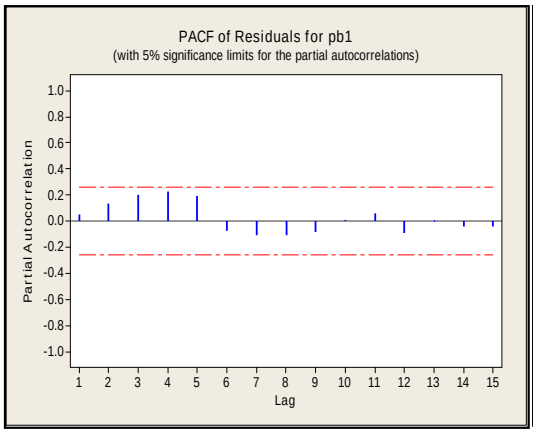

Fig. (7.1): partial autocorrelation function of the residuum of lead

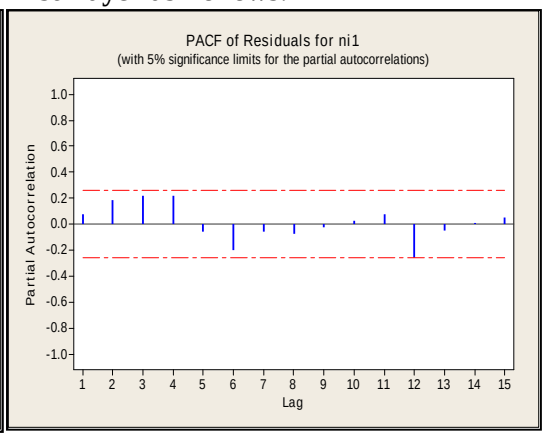

Fig. (8.1): partial autocorrelation function of the residuum nickel

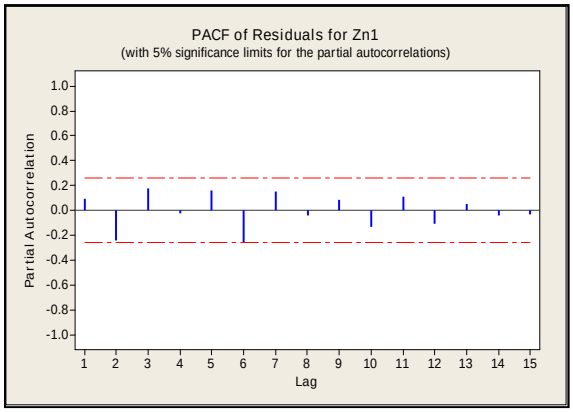

Fig. (9.1): partial autocorrelation function of the residuum of zinc

The partial autocorrelation functions for the second layer were as follows:

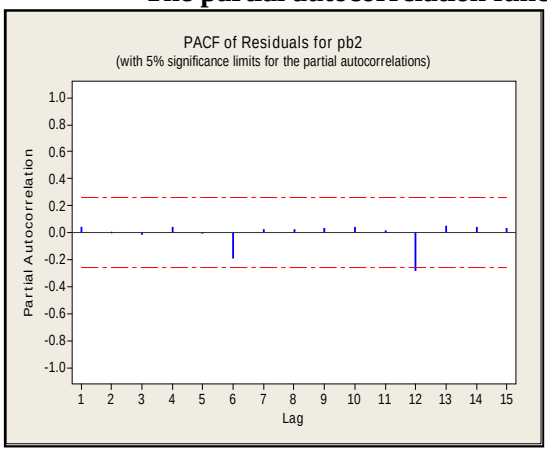

Fig. (10.1): partial autocorrelation function of the residuum of lead

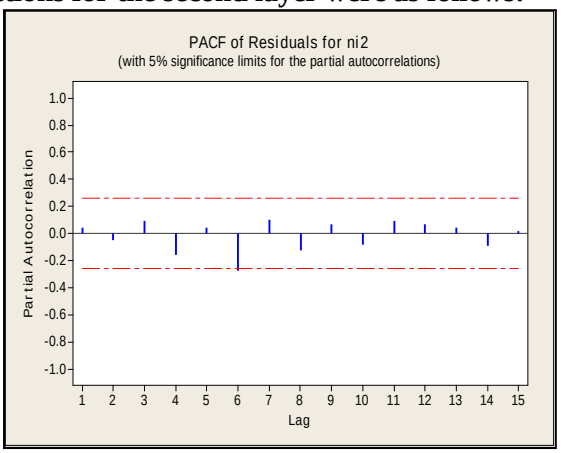

Fig. (11.1): partial autocorrelation function of the residuum nickel

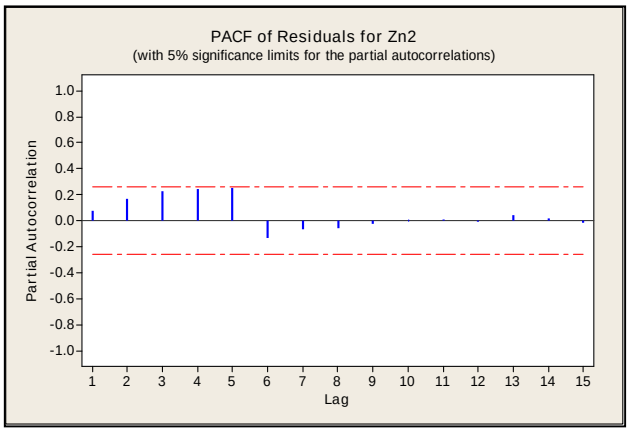

Fig. (12.1): partial autocorrelation function residuum of zinc

Estimate Transactions of the Factor Analysis Samples Values

Moments method has been used to find an estimate of the factor analysis models parameters for each layer and using the program ready Minitab Version(14) was reached following sample:

Prediction equation for the lead of the first layer

$$Z_t = 3.252 + 0.634 a_{t-1} + 0.421 a_{t-1} + a_t$$

Prediction equation of nickel of the first layer

$$Z_t = 5.463 + 1.673 z_{t-1} - 1.754 z_{t-1} + a_t$$

Prediction equation for zinc of the first layer

$$Z_t = 2.252 - 7.842 a_{t-1} + 1.342 a_{t-1} + 2.354 z_{t-1} + a_t$$

Prediction equation for the lead of the second layer

$$Z_t = 3.475 + 0.773 a_{t-1} - 2.754 a_{t-1} + a_t$$

Prediction equation of the second layer of nickel

$$Z_t = 4.213 - 5.442 a_{t-1} + 0.334 z_{t-1} - 0.798 z_{t-1} + a_t$$

Prediction equation for zinc of the second layer

$$Z_t = 2.385 + 0.563 a_{t-1} - 2.851 a_{t-1} + a_t$$

We test the hypothesis that the parameter where we selected sample ($\square, \hat{\theta}$) are not moral different from zero, use the (t) test as follows:

$$t = \frac{\theta_1}{\frac{S_1^2}{n}} \quad OR \quad t = \frac{\square_1}{\frac{S_1^2}{n}}$$

as the:

$\hat{\theta}_1$:The estimated value for the moving average parameter

$\square_1$:estimated value for the regression parameter self

S_1^2 : Parameter variation SMA

S_1^2:Self-regression parameter variation

The application on the first layer we get the following results :

The calculated value of the (t) test to lead ($\hat{\theta}_1$ &$\hat{\theta}_2$) were respectively (11.23,15.34) and the calculated value to (t) test nickel ($\hat{\theta}_1$& $\hat{\theta}_2$) are respectively (9.78,10.53) The calculated value of the (t) test zinc ($\square_1$&$\hat{\theta}_1\hat{\theta}_2$) was (12.77,13.22 ,15.65) By comparing the calculated value with the values tabular to (t) test when the level of moral 95% degrees of freedom (n-1) reject the null hypothesis that the parameters of the sample model is no different morally from zero test was applied (t) test on the second layer**.** The calculated values of the (t) test to lead ($\hat{\theta}_1$& $\hat{\theta}_2$) were respectively (10.13, 18.53)and the calculated value to (t) test nickel ($\square_{2}$و $\square_1$&$\hat{\theta}_1\hat{\theta}_2$) and (17.87 ,13.56,20.25,18.91) respectively , The calculated value of the (t) test zinc ($\hat{\theta}_1$& $\hat{\theta}_2$) was (13.54,21.32) compared with the calculated value from tables to (t) test on under moral level of 95% degrees of freedom (n-1)and reject the null hypothesis that the parameters of the proposed sample is no different morally from zero.

Find Predictions of the Values of Factor Analysis

After sample has been found appropriate for each examination parameters moral tested of these samples , it was found that predictions of the values of the analysis factor using these samples for both layers to predict the rate of the last six samples for each test and each layer for the year 2012 compared with the original values as well as finding predictions for the year 2013 in a method to smooth Brown and exponential way Box – Jenkins.

Table (3): First Layer Soil tests Predictions for 2012

Examination	Value prediction	The actual value	Minimum 95% trust interval	maximum 95% trust interval
Lead	-1.46	-1.11	-2.62	0.83
Nickel	-9.12	-9.46	-3.17	1.46
Zinc	-7.29	-8.38	-3.21	2.67

Table (4): Second Layer Soil tests Predictions for 2012

Examination	Value prediction	The actual value	Minimum 95% trust interval	maximum 95% trust interval
Lead	-0.96	-1.48	-2.78	1.65
Nickel	-22.65	-20.81	-2.45	1.53
Zinc	-7.22	-6.72	-2.89	1.77

For the purpose of reaching a calculated values to predict for the year 2014 calculations accurately been used sampling rate selected for the first layer using Brown exponential smoothing through the use of system-ready MINITAB For the purpose of access to the values of prediction and calculators accurately has been selected an

experience of all Combinations through average error squares through thβ) , (α optimum values for the possible on an equation to predict the time series and extract less (MSE) and then get the parameters smooth 0.2), After the smooth process the data and compensation for the value of a_0=3.542& b_0=0.326 (β = 0.2)(α=

been getting on the values of prediction as well as the method was used Box - Jenkins for sampling rate selected layer second so that been getting in which the best values for the parameters and the lowest average error squares through the use of the system ready MINITAB and then it is the comparison between the two layers to reach the best layer as follows:

Table(5): First Layer Soil tests Prediction Using Brown Method in 2013

Value prediction of Zinc	Value prediction of Nickel	Value prediction of Lead	Minimum 95% trust interval	maximum 95% trust interval	months
-5.61	-21.53	-1.67	-2.87	2.98	Jan
-3.93	1.06	-0.21	-2.56	2.76	Feb.
-4.67	-2.32	-0.92	-2.85	2.58	Mar.
0.84	-20.12	-0.46	-2.98	2.84	Apr.
-15.68	-4.24	4.02	-2.92	2.56	May.
3.89	-9.31	-1.03	-1.77	1.77	Jun.
-20.21	-28.09	-2.22	-1.95	1.94	Jul.
-8.34	-18.34	1.02	-1.64	1.96	Oug.
13.85	-12.22	3.11	-1.76	1.87	Seb.

Table(6): second Layer Soil tests Prediction Using Box - Jenkins Method in 2013

Value prediction of Zinc	Value prediction of Nickel	Value prediction of Lead	Minimum 95% trust interval	maximum 95% trust interval	months
-8.92	-10.03	-1.22	-3.76	2.543	Jan.
-1.84	-3.51	1.14	-3.85	2.87	Feb.
-13.23	-8.14	-3.54	-392	2.66	Mar.
-2.67	-13.62	-0.77	-3.85	2.83	Apr.
-21.45	1.01	6.13	-3.21	2.96	May.
-4.07	-14.63	1.15	-2.68	1.63	Jun.
-2.64	-27.21	-4.01	-2.57	1.94	Jul.
-8.04	-9.12	-0.86	-2.63	1.82	Oug.
-2.11	-15.46	-2.97	-2.82	1.57	Seb.

For comparison between the two layers Which is better, following standards were used:

1-RMSE (Root Mean Square Error)

2-Mean Absolute Error(MAE)

3-Mean Absolute percentage Error (MAPE)

Table(7): Statistical Standards for Both layers Included in the Study

Layers	RMSE	MAE	MAPE
First layer	86.38	0.45	2.29
Second layer	65.06	0.39	1.09

is clearly from the above results, the second layer is better for the fact that the three statistical criteria are less.

CONCLUSIONS

1- The original time series of three tests the soil is un stationary and it is unfixed in variance, there is a difference in the arithmetic mean of both layers.

2- after studying the autocorrelation function and partial autocorrelation function tests for the first layer and the second layer, to determine the appropriate models. Showing significant parameters of the models suggested by the results of t-test of the two layers.

3- observed through the results to predict the mean of the last six samples, the values of factor analysis for the three tests for the first layer and the second approach is that the results of the original values were within the confidence interval specified.

4-Through statistical criteria used was reached that the best layer is the second layer in which the concentration of heavy metals are few, as well as the proportion of affected small erosion factors and therefore is reflected positively on the agricultural output..

5- The method of (Box – Jenkins) proved its efficiency in the possibility of time-series study using factor analysis to predict the testing soil through the use of computer applications and utilization optimally solve some of the complex issues in real life, especially in the environmental pollution.

REFERENCES

- Mustafa .M. .Abdala (2012) : Comparison of independent components analysis and Fuzzy logic prediction in TIME SERIES, "Iraqi Journal of Statistical Sciences, folder (12), number (21).

- Al-Sukrge.Th. Younis. (2010) : The use of factor analysis to predict the time series with the application on series Rainfall and relative humidity in the city of Mosul ", Tikrit magazine for Economic and Administrative Sciences, Folder (6) Number (20).

- Al-Tai .F .G. Ahmed (2004) : A comparative study between Box Jenkins methods and Adaptive filtering method to predict ", unpublished Ph.D. thesis, Faculty of Computer Science and Mathematics, University of Mosul..

- Mohamed, M. ,Bahjet, M.,(2004): "Using Factor Analysis to Measure the key Factors Affecting the Performance of The Students in the First University Degree A Field Study Applied on The High institute of Computer and Management at Port Said.

- Brockle bank , John C. Dickey, David A. 2003 "SAS for Forecasting and Time Series "SAS Institute Inc., Cary, NC, USA.

- Arsham's Hossein (2002): "Time Series Analysis and Forecasting Techniques" http://ubmail.ubalt.edu/~harsham/stat-dataforconstructing amirror site .

- Makridkis, S., Wheel Wright, S. and HYdman, R. (1998): "Forecasting Methods and Application",3rd ed. , john Wiley ,New york.

CONCEPTS OF WATER MANAGEMENT AMONG RIPARIAN COUNTRIES (IRAQ - TURKEY - SYRIA) AND IT'S IMPACT ON WATER QUALITY AND QUANTITY

LILYAN YAAQUB MATTI ALSAKA
College of Environmental science and technology, Mosul University-Iraq

(Received: January 14, 2014 ; Accepted for publication: June 2, 2014)

ABSTRACT

Demographically, the MENA region is enveloped in a period of fairly sweeping changes, all of which will have major implications for water governance. The highly contentious Tigris-Euphrates River, shared by upper riparian Turkey and downstream states Syria and Iraq, is one example. By 2050, Iraq's population-and projected water needs-will soar, as the country grows 2.6 times its current size, its population increase from 32.6 million to more than 83 million. Syria, which also depends on the Euphrates as an important economic lifeline, will see its population by mid-century grow 1.5 times its current size, from 22.5 million to 33.6 million. Combined, this population growth in Syria and Iraq will increase water demand for irrigation, industrial development, and domestic usage, placing pressure on Turkey to ensure an ample flow of water downstream throughout the year. As the effects of climate change lengthen drought and alter the time of snow melting and precipitation, tensions could easily flare throughout the basin, as they have in the past.

The problems in Iraq are more pressing than in Turkey and Syria. Iraq is very dry and more flat making it prone to evaporation. Iraq has extremely dry periods, sometimes lasting up to six months from May to October. The temperature during this time can get up to 120 degrees Fahrenheit. The climate is a major factor in producing high evaporation, but the artificial lakes upstream the dams, which have large open water areas that increase the quantity of evaporation and increase the pollutant concentration in the storage water, also contributes in water losses from the system through evaporation.

Urbanization, industrialization, increase in population, and expansion in farming with using traditional irrigation systems, all these factors lead to increase water demand in these three countries. With the construction of many dams in Turkey and Syria, the quantities of water that enter Iraq decreases with the execution of an ambitious water management plan for Turkey (GAP), the quantities of water will decrease more and more.

Key Word: Tigris-Euphrates River, quality, quantity, Iraq, GAP

INTRODUCTION

The water resources in Iraq are concentrated in Tigris and the Euphrates Rivers, which are representing together 98% of the water resources in the country (FAO, 1994). Euphrates and Tigris are two of the largest three rivers in the Middle East, figure (1). These two rivers play an extremely important role in providing water for these areas. Within this area, just these two rivers together with the Nile are classified as large by the world standards (Al-Hadithi, 1978). Euphrates and Tigris (with some of their tributaries) originate in the highlands of Turkey, and flow through a region between 45° N and 25° North latitude. Euphrates crosses Syria before flowing into Iraq and meeting Tigris, which also crosses Syria, and together they form Shat Al Arab in the south of Iraq, jointly flowing 190 km before pouring water into the Gulf. Iraq is located between latitudes 29° and 38°N, and longitudes 39° and 49°E (a small area lies west of 39°E), encompassing 438,320 km^2. includes 924 km^2 of inland waters and it is the 58th largest country in the world(http://en.wikipedia.org/wiki/Iraq#Geography Jon 2011.).

The Tigris and Euphrates rivers are the main sources of water in Iraq with a river basin area of 126,900 km^2 for Tigris and 177,600 km^2 for Euphrates without tributaries (Frenken, 2009). Both these rivers originate in the highlands of Turkey and share their physical, climatic, hydrologic, and geomorphologic characteristics.

However, there are different perspectives on to how treat these two river basins, and some specialists the identified these rivers as twins. Thus, for purposes of integrated water resources management, it is useful to treat them as belonging to a single basin, tables (1, 2). (Kliot, 1994).

Fig. (1): Tigris-Euphrates Rivers

Table (1): Length of the river reaches in the basin by country (in km))(UNESCO, 2002)

River	Turkey		Syrian Arab Republic		Iraq		Iran		Total
Euphrates	**1,230**	**41%**	**710**	**24%**	**1,060**	**35%**	**0**	**0%**	**3,000**
Tigris	**400**	**22%**	**44**	**2%**	**1,418**	**76%**	**0**	**0%**	**1,862**

Table 2: Distribution of the Tigris-Euphrates (Shatt Al-Arab) river area by country (km^2)(UNESCO,2002)

River	Turkey		Syrian Arab Republic		Iraq		Iran		Total
Euphrates	**124,320**	**28%**	**75,480**	**17%**	**177,600**	**40%**	**0**	**0%**	**444,000**
Tigris	**46,512**	**12%**	**776**	**0,2%**	**209,304**	**54%**	**131,784**	**34%**	**387,600**
Total	**170,832**	**22%**	**76,256**	**10%**	**386,904**	**51%**	**131,784**	**17%**	**765,600**

Turkey, in the last few decades has tended to develop their water use plans unilaterally, without careful consideration for the environment and the actual water potentiality of the river basin, causing a severe shortage of water in Iraq and sometimes in Syria. Two of the main objectives in Turkey are to use the rivers for hydroelectric power and irrigation. A new project called GAP was started there in the 1960s (Dagan, 2004). This project was first introduced to provide irrigation water and electricity power to the poorest districts within Turkey. It involves the construction of 22 new dams and hydroelectric power plants (about 19) on the Euphrates River alone (Bagis, 1989).

Before the 1950s Syria made little use of the Euphrates and Tigris rivers. After 1970 Syria executed large-scale projects to utilize the water of these rivers, and at present time 80-90% of the surface water in Syria comes from the rivers (Beaumont, 1996).

The flow contribution percentage-wise for each country to the Tigris and Euphrates rivers is illustrated in figure (2).

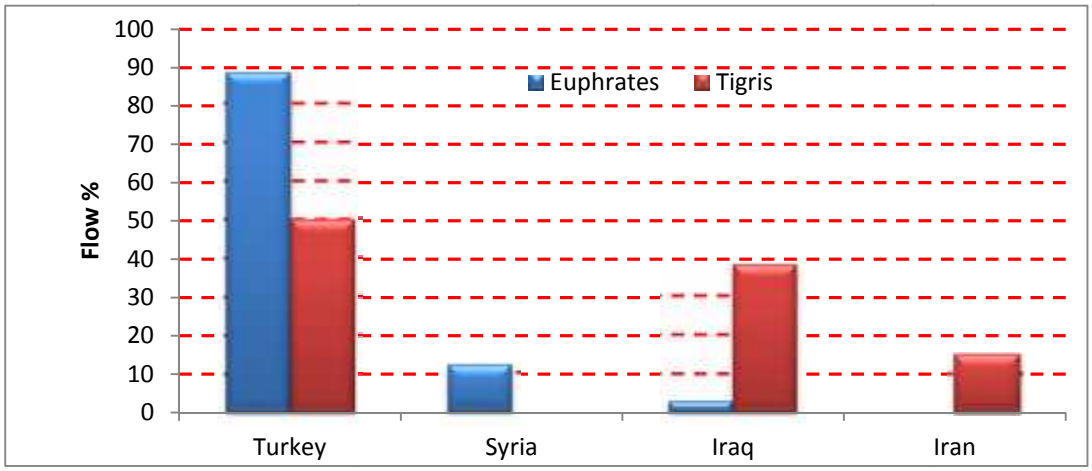

Fig.(2): Contribution percentage-wise of countries in the water flow in the Tigris and Euphrates rivers (Al Bomola., 2011).

THE OBJECTIVES OF THIS STUDY ARE:
Study the effect of upstream project on quality and quantity on Tigris and Euphrates rivers water.

GEOGRAPHY AND CLIMATE

Iraq is located at 33°00' N, 44°00'E spanning 437072km^2, Iraq mainly consists of desert, but near two rivers (Euphrates and Tigris) are fertile alluvial plains, as the rivers carry about 60 million cubic meters of colloids annually to the delta. The north of the country is mostly composed of mountains, Iraq has a small coastline measuring 58 km along the Arabian Gulf, close to the coast and along the Shatt al-Arab there used to be marshlands. The local climate is mostly desert, with mild to cool winter and dry, hot, cloudless summer. The northern mountainous regions have cold winters with occasional heavy snows, sometimes causing extensive flooding. Most of Iraq has hot arid climate. Summer temperatures average above 40°C for most of the country and frequently exceed 48°C. Winter temperatures infrequently exceed 21°C with maximums roughly 15 to 16°C and night time lows occasionally below freezing. Typically precipitation is low; most places receive less than 250mm rainfall annually, with maximum rainfall during the months of

November to April. Rainfall during the summer is extremely rare except in the very north of the country (http://en.wikipedia.org/wiki/Iraq)

The climate in Turkey (upstream) is characterized by long harsh cold winters with abundant precipitation, where the temperature increases gradually from north to south. Winter rains are more excessive than the summer rains. Extremely cold temperatures of down to -45 °C occur in the winter, while the hottest month in Turkey is August with a mean maximum temperature of 24-28 °C (Beaumont, 1996) The prevalent climate types in Syria (river basin part) and in Iraq (downstream) are the continental, subtropical, and semi-arid types. The average temperatures in Iraq range from higher than 48 °C in July and August to below freezing in January,figure (3). Minimum temperature in the winter season range from near freezing in the northern parts to 2 °C in the western desert and to 4 ° C in the alluvial plain of southern Iraq. Summer is dry and extremely hot with a shade temperature of 43 °C during July and August, dropping at night to 26 °C. The winter in Iraq is cold while the summer is very hot resulting in a high rate of evaporation in the middle and southern part of the country which reaches 17 mm per day during summer (Dagan, 2004).

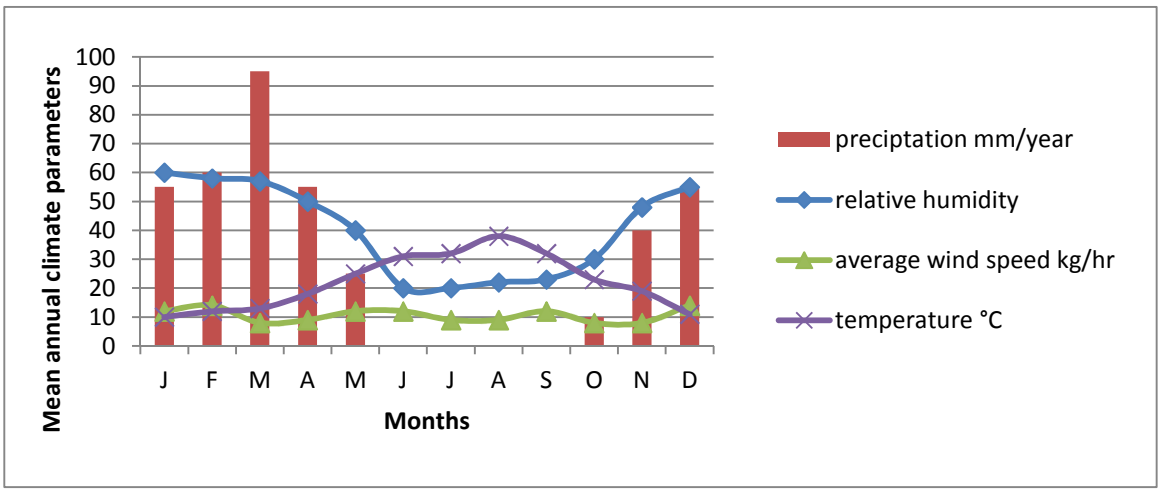

Fig. (3): Mean annual climate parameters over Iraq (FAO. 1994)

HYDROLOGIC CHARACTERISTIC

Almost the origin of all the major rivers and tributaries crossing Iraq is located in Turkey and Iran. Iraq only contributes with a tiny quantity of flow to the Euphrates River, however, on the Tigris River, Iraq contributes the majority of the total flow via greater and lesser Zab, the Adhaim, and the Diyla River. Iraq contributes 48.1% of water potential to the Tigris (some tributaries have their heads out of Iraq which reduces the Iraq contribution) and 2%-3% to the Euphrates. Iraq has much greater control of the water in the Tigris than it has of the Euphrates. Approximately more than 98% of the Euphrates flow originates outside Iraq compared to only 52% of the Tigris flow.

The river is largely fed from the snow precipitation over the upland of eastern Turkey, where the annual total precipitation is more than 1000 mm, while the precipitation over Syria and Iraq is much less than this quantity. The flow of Euphrates is highly regulated and controlled by a series of dams and reservoirs constructed by Turkey, Syria, and Iraq.

The Euphrates and the Tigris river hydrology is to a large degree determined by the snow melt and is largely linked to the precipitation in the highlands of Turkey (and to less extent in Iran, for some of the tributaries to Tigris River). The annual flow of the

Euphrates River is highly seasonal. The value exhibits a wide range, estimated to be between 33% and 75% of the annual average flow, which range, from31 to 33 BCM (983 to 1046 m^3/s). Turkey contributes with about 88%, and Syria contributes with 10%, and the remaining 2% comes from Valleys inside Iraq (FAO, 1994). Precipitation in the river basin is confined to winter time from October through April, and a large proportion of the total precipitation falls as

snow on the uplands, stay in solid state on the mountain slopes until an increase in temperature occurs in early summer (April and May). The river flow during these two months is estimated to be 42% of the annual total flow (Beaumont, 1996) and (Shahin, 2007).

A schematic description of the hydrologic and water allocation schemes for Euphrates River and its relationship with Tigris River within Iraq is shown in (diagram 1) The management and operation of the whole system is done in accordance with the water balance, the climatic conditions (dry-wet year), and the dam operation policies (storage- release) in the upstream countries.

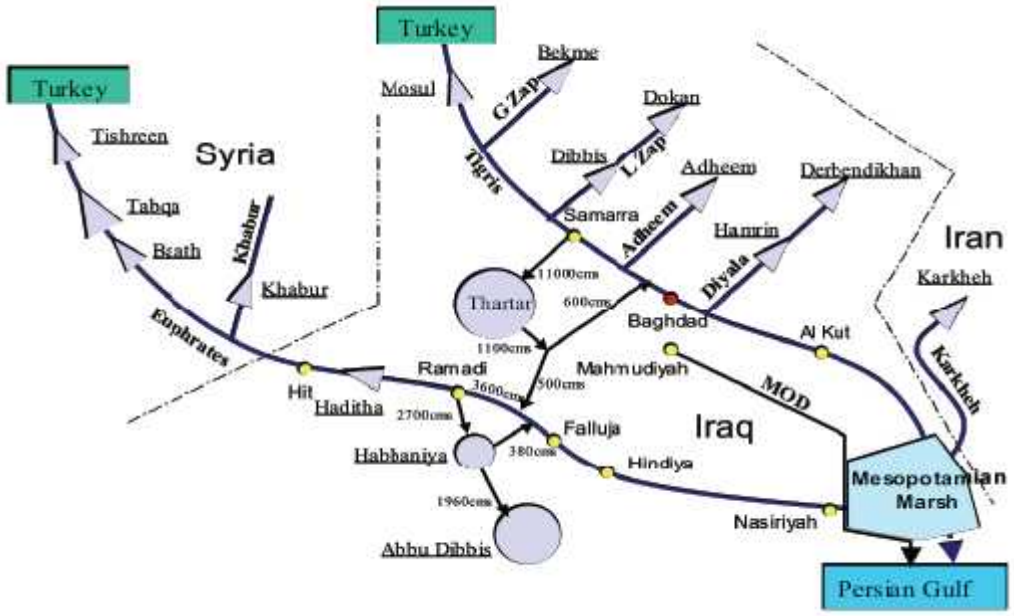

Diagram (1): Major reservoir systems in the Tigris-Euphrates watershed (improved from Kavvas et. al, 2006)

EFFECT OF THE UPSTREAM PROJECT

The dam projects of Turkey on the Euphrates and Tigris River could affect negatively on the irrigation and power production in Iraq, as well as the environment, recreation, fisheries, and generate health hazards. The decrease in river flow rates and the effects of drought and evaporation of water that is stored in reservoirs will cause deterioration in water quality due to increasing concentration of pollutants and salts in the remaining water. What makes the quality of water worse is the relative increase in industrial wastewater, return irrigation wastewater, and untreated sewage water that reach the waterway, which has led to the disqualification of 1.3 million acres in Iraq. (FAO, 1994).

Dam Constructions and Conflict on the Tigris and Euphrates before the GAP

In the case of the Tigris and Euphrates rivers, the dams play an important role in exacerbating conflict between the major riparian States –

Turkey, Syria and Iraq

- is clear. All three countries rely on the waters of the Euphrates and Tigris for their agriculture, energy and future development, table (3) (PWA, 2001).

Dam Constructions and Conflict on the Tigris and Euphrates together with GAP

Since the 1980s Turkey and Iraq have started to implement ambitious water development schemes on both the Tigris and the Euphrates, transforming the river and the lives of people who depend on it. Iraq completed the large multi-purpose

Mosul Dam

with a reservoir capacity of **10 BCM** in the late 1980s, and has started to construct the other big **Samara dam**

on the Tigris with a similar storage capacity. (Allan, 2000).

Table (3): Major Turkish and Syrian Dams that Reduce Downstream Flows

(Global Food and Water Crises, 2012)

Major Turkish and Syrian Dams that Reduce Downstream Flows

Atatürk (Turkey)	Completed in 1990 on the Euphrates River Almost led to armed conflict between Turkey and downstream countries Syria and Iraq
Ilisu (Turkey)	Under construction on the Tigris River Due for completion in 2015 Strongly opposed by Iraq due to projections of significant decreases in downstream flows
Tabqa (Syria)	Completed in 1975 on the Euphrates River Largest dam in Syria Created severe objections from Iraq and almost led to armed conflict between the two nations

1-REDUCING THE FLOW

Covering an area of 126,900 km^2 and 177,600 km^2 respectively, the Tigris and the Euphrates Rivers are the primary sources of surface water in Iraq. Historically, the rivers played a central role in sustaining Iraq and contributed to the birth and development of flourishing civilizations in the Fertile Crescent. In the last few years, however, water levels in Iraq's rivers have rapidly decreased to less than a third of their normal capacity. Water levels may fall further in the coming years due to declining precipitation, gradual desertification, and upstream water use and damming. The long-term average annual precipitation in Iraq is equal to 216mm per year with high variability across time and governorate. In 2011, 507.4mm of water fell in Suleimaniyah while only 65.3mm fell in Basrah. Lakes, reservoirs, and minor rivers are also experiencing diminished levels of water. If present conditions remain unchanged, Iraq will experience a water shortage of over 33 million cubic meters a year by 2015. The Tigris and Euphrates Rivers, originating in Turkey and crosses both Syria and Iraq, have experience cross drastic reductions in water flows in recent years due, primarily, to Turkish hydro-engineering and regional drought. This is of significance for Iraq, which has historically prospered because of the rich agricultural harvests based on water supplies source from these waterways. Turkish initiatives aimed at massively expanding their exploitation of the water from the two rivers have coincided with severe droughts in the region and resulted in a burgeoning water-shortage crisis in Iraq. This problem threatens an environmental catastrophe. Political negotiations between the three countries have so far fallen short of reaching agreement on providing the necessary increases in flow rates to address the deteriorating situation in Iraq, Figure (4).

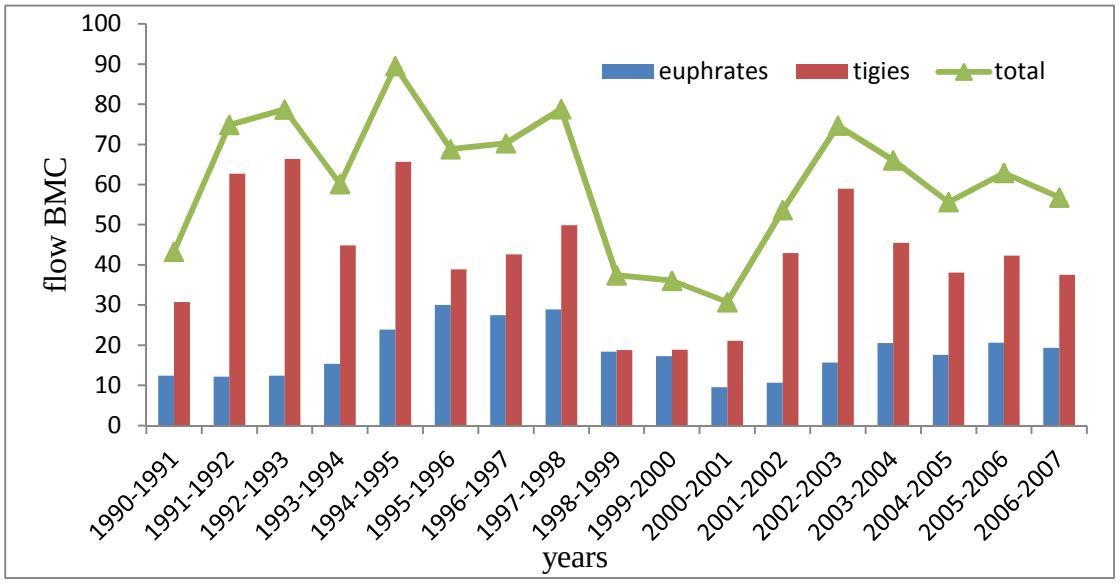

Fig. (4): Annual average flows via Euphrates & Tigris River in Iraqi during period (1990-2007). ((Jawad ,2003 Al Bomola., 2011).

Much of the water stored in GAP dams is intended for irrigation. All GAP dam reservoirs are planned to irrigate a total of almost 1.82 million hectares of land, Iraq calculates that the Tigris irrigation projects will reduce the flow of the Tigris as it passes the border into Syria at Cizre by 46% - considering that there is an annual mean flow rate of 17 BCM figure (5) (Letter of Iraq Foreign Minister, 2007).

Fig. (5): The GAP project region (Kolars, 1994).

-Since 1975, Turkey's extensive dam and hydropower construction has reportedly reduced water flows into Iraq and Syria by approximately 80 per cent and 40 per cent respectively.
-Approximately 90 per cent of the water flow in the Euphrates and 50 per cent in the Tigris originate in Turkey.
-Low flow rates in Iraq have allowed salt water to infiltrate nearly 150 km inland from the Persian Gulf.
-Lack of international agreement is hampering progress on a deal between Turkey, Iraq and Syria. (Global Food and Water Crises, 2012)

The Tigris is also expected to experience high stress levels of development in Turkey. Iran on the other hand has implemented a number of water resources projects on tributaries of Tigris including major reservoirs that are now in place causing reduction of transboundary flows of the Tigris and its tributaries. Although not as substantial as far the Euphrates, but will be significant in view of the growing demands. Figure(6) shows the annual volume of the Tigris inflow to Iraq for the years 1933-2011. The average annual flow volume of the Tigris River at the Iraqi-Turkish border dropped from 49.22 BMC for the period 1933-1998 to 33.10 BMC for the period 1999-2011(Jawad, 2003).

Figure(6) shows the annual volume of the Euphrates inflows to Iraq for the years 1933-2011. This may be divided into three distinct periods. The first is 1933-1971 which represented the annual, or predevelopment, periods. The average annual inflow volume to Iraq during this period was 30.44 BMC. The second period is 1976-1989 and covers the construction and filling of Kiban and Tabaka Dams. The average annual inflow volume to Iraq during this period was 26.23 BMC. The average annual inflow volume following the filling of Ataturk Dam (1994-2007) dropped to 19.69 BMC. The last four years (2008-2011) represent the realization of some GAP projects in Turkey in addition to the consequence of weather change in the region. The average annual inflow volume to Iraq during this period was 12.75 BMC(Jawad,2003),and the reducing flows shows in diagram(2)

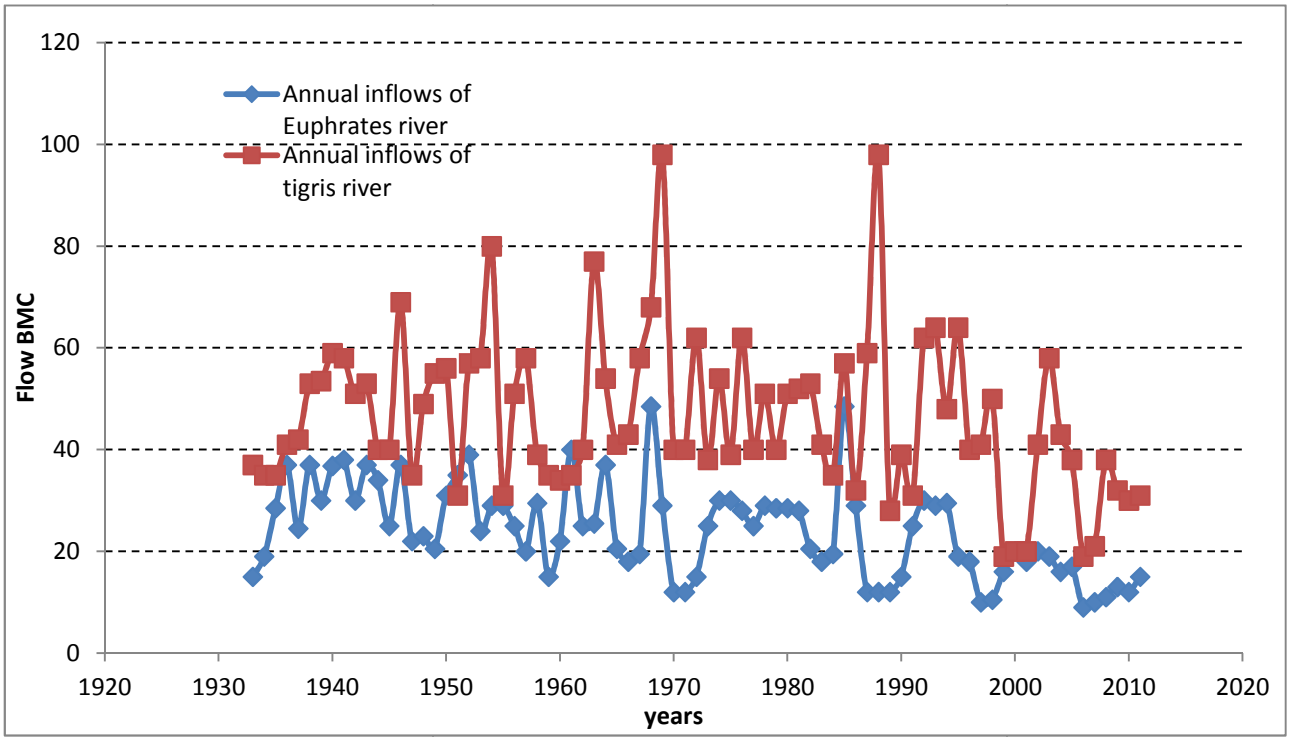

Figure 6: Annual Inflows of Tigris River and Euphrates River

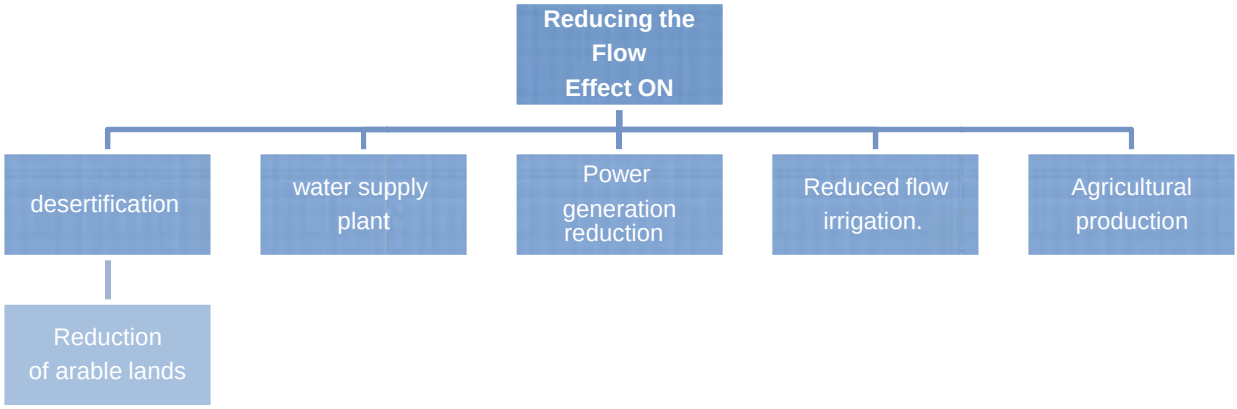

Diagram2: shows the effect of reducing flow in rivers

2-DECREASED WATER QUALITY

The quality of the water or which release from Turkey to Syria and Iraq will significantly deteriorate to be of less quality than before entering the dam reservoirs within Turkey. This is due to increasing waste water entering rivers from urban areas and increasing water use for irrigation.

The original planning for the GAP project appears to have paid little attention to the problem of return flows from irrigation schemes. Both Syria and Iraq fear that the result will be increased levels of salinity in the waters of the Tigris and Euphrates, a problem which will be compounded by pesticide and fertilizer run-off and by increased sewage discharges from the new urban centers that GAP is seeking to stimulate. Already before reaching Syria and Iraq the water quality in the most large dam reservoirs of GAP will be decreased enormously. So in Syria and Iraq the use of contaminated water in irrigation results in the transmission of contaminants to the irrigated plants and consequently to humans, as well as increasing soil salinity, reducing productivity and converting areas of agricultural land into barren land. The deterioration of water quality definitely reduces the uses to which the water

can be put, even if it does not render the water completely unusable for human or agricultural consumption. This can create a shortage in water supply,converting the quality problem into aquantity problem (www.amarappeal.org,1994). Estimates vary, but one independent study has predicted that insecticide levels in the Syrian portion of the Euphrates and its tributaries could increase by 35% (Kolars ,et al,1991). Technical studies conducted by Iraq have also forecast a doubling of salinity levels in the Tigris as a result of upstream irrigation in Turkey.Iraq also believes that existing dam projects on the Tigris and Euphrates will affect about 1.3million hectares of agricultural land (40 per cent of the agricultural land available) as a result of declining water quality. Turkey's Regional Ambitions; Controlling the Water There are also fears that the dams that Turkey has built - and intends to build - will enable Turkey to exercise control over its downstream neighbors. Such fears for an hydro hegemony by Turkey are not without foundation. The potential to hold water back, which the GAP - even uncompleted -gives Turkey over its downstream neighbours, is huge. Turkey's three major dams on the Euphrates - Keban, Karakaya and Ataturk - have a storage capacity (some 90-100 billion cubic metres of water), which greatly meets almost the three time of annual flow of the Euphrates. If all dams in the Tigris Basin are built, Turkey will have a storage capacity of 22 BMC which is more than the annual mean flow of 17 BMC (Frenken,2009).

In Iraq, the quality of water used for drinking and agriculture is poor and violates both Iraqi National Standards and World Health Organization guidelines. In 2010, the Biological Oxygen Demand (BOD) representing the degree of water pollution by organic materials—was equal to 36.2 mg/L, more than three times the national limit of 10 mg/L, indicating an alarming increase in water pollution, the BOD was between (1.04-12.12). The Total Dissolved Salts (TDS) in the Euphrates' river water increased from 457 parts per million (ppm) in the 1980s to 1200ppm in 2009 reflecting a quick deterioration of incoming water, high pollution and salinity had devastating effects on livestock, agriculture, and fishing in the Muthanna, Missan Basra, and Wassit governorates(Al Bomola,2011).

3-ISSUES OF WATER QUANTITY AND QUALITY

From tables (4,5) and diagram (3) Appear that water requirements generated from the GAP causes most severe strains in the waters of both rivers, but most drastically affect on the flow in the Euphrates. With the completion of the Ataturk Dam in 1990, Turkey declared that it will only guarantee a flow from its border equal to half the original flow of the river. Although this represents the "minimum" amount that will be provided from the Turkish border for use by Syria and Iraq, the more important issue will be the discharge patterns established by Turkey. Power production will likely be maximized during the winter months, resulting in the peak discharge from the dam occurring in the months of December – January. The river flow will consequently be at a maximum during these months as well, in contrast to the traditional peak discharge months of April – May (Beaumont, 1996). If the additional water released by Turkey during peak discharge periods is not adequately captured by both countries in reservoirs, they will be left with a significant shortage during periods of peak use by farmers. Even with reservoirs to hold such waters (Lake Assad, Lake Habbaniyah, etc), evaporation due to the extreme temperatures will continue to strain these resources. Furthermore, although irrigation is the primary culprit for the increased water demand, the increasing populations along the rivers and the potential increase in industries requiring significant water sources will place additional strain on water resources of the basin. The extensive use of water for irrigation and Industrial use will also undoubtedly lead to water re-entering the river system with higher levels of salinity, chemical content, and in generall untreated and contaminated state. This issue will most severely affect Iraq as they will be the beneficiaries of such abuse by both Turkey and Syria. Depending on the severity of such use in the future, Iraq could potentially experience drastic effects to their agricultural industry and on their ability to sustain populations and industry along the river.

CONCLUSION

The most important step toward solving the water issues of the Tigris-Euphrates river basin for all three riparian nations is to sit down to seriously negotiate the issues surrounding the water resources of the basin. Turkey unquestionably holds the most power in this situation, but both Syria and Iraq have shared interests that, if presented as a common front, may have more weight in political negotiations.

Iraq has the most to gain from developing some kind of a formal agreement on water use in the region as the historical heaviest user of a resource that will only continue to be consumed at an ever increasing rate upstream. The fact that Turkey controls much less of the Tigris than the Euphrates leaves the option of flow diversion as a possible solution to Iraq to supplement decreases flow rate from the Euphrates. Challenges of increased salinity levels of the water, As Iraq continues to stabilize and improve its infrastructure and economy,

Table (4): Some water quality parameters of Tigris and Euphrates rivers in 1981

River / test	Tigris (turkey & pesh khabur)1981	Tigris Mosul city Upper town 1981	Tigris Mosul city Lower town 1981	Euphrates Haditha 1981	Euphrates Ramadi 1981
Temperature C	**12.5**	**19.5**	**19.5**	**19**	**19.5**
pH	**9**	**8.5**	**8.8**	**8.7**	**8.9**
Conductivity *u*mh	**430**	**520**	**535**	**360**	**360**
Turbidity(NTU)	**25**	**75**	**56**	**35**	**40**
Dissolved oxygen concentration mg/l	**5.7**	**5.1**	**5.3**	**5.4**	**6**
Alkalinity mgCaCO3/l	**131**	**133.5**	**138.2**	**103.5**	**105**
Sodium concentration mg/l	**11**	**23**	**18**	**32**	**15**
Potassium concentration mg/l	**1.1**	**1.9**	**2.3**	**2.5**	**2.3**
Calcium concentration mg/l	**33.6**	**47.6**	**47.2**	**32.4**	**32.8**
Magnesium concentration mg/l	**20.1**	**22.5**	**21.1**	**19.9**	**22.5**
Nitrate concentration *u*g at .N/l	**41.5**	**44.4**	**43.9**	**39.9**	**35.3**
Nitrite concentration *u*g at .N/l	**0.21**	**0.58**	**0.54**	**0.09**	**0.19**
Silicate concentration *u*g at Si /l	**29.9**	**43.3**	**39.1**	**41.6**	**44.1**
Orthophosphate concentration *u*g at .p/l	**0.29**	**0.9**	**0.36**	**0.61**	**0.27**
Total number of phytoplankton cells/l	**199800**	**148160**	**555560**	**537080**	**814880**

Table (5): Some water quality parameters of Tigris and Euphrates rivers in 2000

River / test	Tigris (Turkey & pesh khabur)2000	Tigris Mosul city Upper town 2000	Tigris Mosul city Lower town2000	Euphrates Haditha 2000	Euphrates Ramadi 2000
Temperature C	**12.2**	**19.95**	**19.45**	**19.6**	**19.9**
pH	**8.45**	**7.79**	**7.65**	**8.9**	**8.85**
Conductivity *u*mh	**425**	**435**	**445**	**400**	**410**
Turbidity(NTU)	**35**	**89**	**105**	**55**	**100**
Dissolved oxygen concentration mg/l	**5.3**	**5.5**	**5.8**	**5.3**	**5**
Alkalinity mgCaCO3/l	**140**	**230**	**250**	**146**	**155**
Sodium concentration mg/l	**15**	**26.5**	**28.4**	**38**	**22**
Potassium concentration mg/l	**1.5**	**5.1**	**5.8**	**3.5**	**4.3**
Calcium concentration mg/l	**63.7**	**192**	**208**	**134**	**138**
Magnesium concentration mg/l	**30**	**85**	**92**	**39**	**45**
Nitrate concentration *u*g at .N/l	**85**	**182**	**215**	**40**	**135**
Nitrite concentration *u*g at .N/l	**0.26**	**0.98**	**1. 4**	**0.18**	**0.2**
Silicate concentration *u*g at Si /l	**30**	**32**	**45**	**46**	**51**
Orthophosphate concentration *u*g at .p/l	**0.49**	**105**	**98**	**4.6**	**7**
Total number of phytoplankton cells/l	**209100**	**150000**	**654560**	**648080**	**903280**

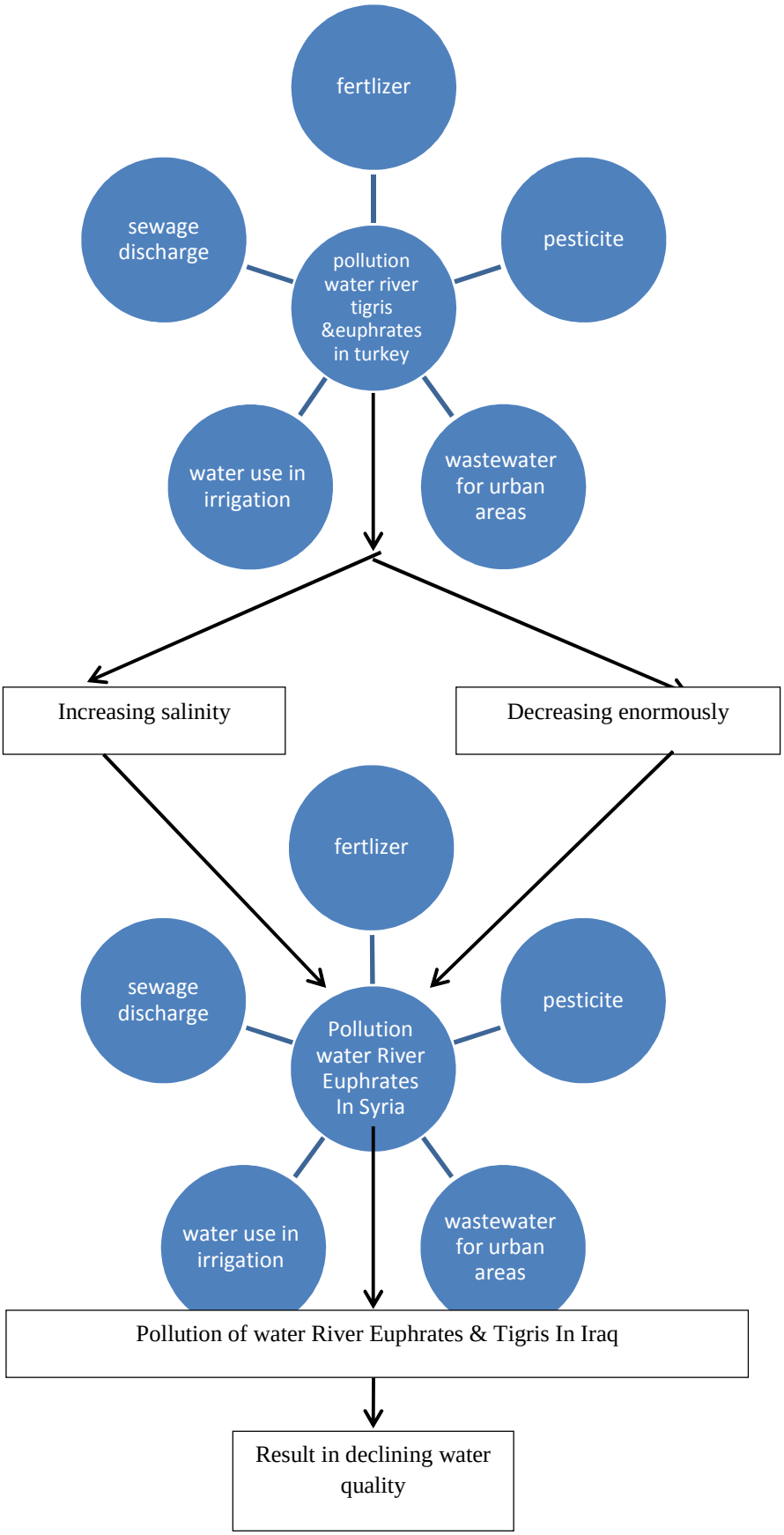

Diagram (3): pollution resources of water in Tigris &Euphrates rivers

REFERENCE

- FAO. 1994. Country information brief, Iraq. FAO-Representation in Iraq.
- Al-Hadithi A.H., Optimal utilization of the water resources of the Euphrates River in Iraq. Doctoral Dissertation. University of Arizona (1978).
-From Wikipedia, the free encyclopedia. Information about Iraq, available at http://en.wikipedia.org/wiki/Iraq#Geography, retrieved 21 Jon 2011.
- Frenken, Karen, Irrigation in the Middle East region in figures. AQUASTAT survey 2008, Water Reports, 34, Rome: FAO, (2009), ISBN9789251063163.
-Kliot, Nurit, Water Resources and Conflict in the Middle East, London: Routledge, (1994), p. 100.
- WATER RESOURCES IN IRAQ,(1999)**unesco.org/water/wwap/news/iraq.shtml**
-Dagan, A. ,Development and Management of the Euphrates-Tigris Basin, International Hydropower Association and Department of Civil Engineering, Middle East, Technical University, Ankara, Turkey, Water Resources Development, Vol. 20,No. 1, (2004), 15-33.
-Bagis, A.L.. South-eastern Anatolia Project—the cradle of civilization regenerated. Istanbul: Gelisim Yayinlari A.S(1989).
-Beaumont, P., Agricultural and environmental changes in the upper Euphrates catchment of Turley and Syria and their political and economic implications. Applied Geography, vol. 16, no. 2,(1996), 137-157.
-Shahin, Mamdouh, Water Resources and Hydrometeorology of the Arab Region, Dorecht: Springer, ISBN 9781 402054143. (2007),P251.
-Kavvas, M.L, Chen, R.Z.Q., Anderson, M.L., Ohara N., Yoon., A regional hdroclimatic data over the watershed.(2006).
- PWA ,Cited in Philip Williams and Associates: A Review of the Hydrological and Geomorphic Impacts of the Proposed Ilisu Dam, Report for the Corner House, San Francisco, July 2001.
-Turkish Ministry of Foreign Affairs, quoted in Allan, J.A., *The Middle East Water Question: Hydropolitics and the Global Economy*, I.B.Taurus, London, 2000, p.73.
-Global Food and Water Crises ,Tuesday, 28 August 2012)http://www.futuredirections.org.au/publications/food-and-water-crisis.
- Letter of Iraq Foreign Minister Hosyar Zebari to the German Foreign Minister Walter Steinmeier on the 21st July 2007.
-Kolars, J., Problem of International River Management. In: The case of the Euphrates, International Waters of the Middle East from Euphrates-Tigris to Nile, Biswas, A.K. (Ed.). Oxford University Press, Oxford, (1994), pp:44-49.
-Jawad, Laith A. ,Impact of environmental change on the freshwater fish fauna of Iraq International Journal of Environmental Studies 60 (6), (2003),: 581-593.
- UN General Assembly, Situation of Human Rights in Iraq, General Assembly Resolution 1994/203,available from www.unhchr.ch . For information on the persecution of the Marsh Arabs, see:www.amarappeal.org
- Al Bomola.A.H , TEMPORAL AND SPATIAL CHANGES IN WATER QUALITY OF THE EUPHRATES RIVER – IRAQ, Avdelningen för Teknisk Vattenresurslära TVVR-11/5013 ,ISSN-1101-9824,(2011).
-Kolars, J. and Mitchell, W.A., *The Euphrates River and the Southeast Anatolia Development Project"*, Southern Illinois University Press, Carbondale, 1991, cited in Daoudy, M., "The Development of the Euphrates and Tigris Basins: An Assessment of Upstream Development (Turkey) on Downstream Riparians (Syria)", Submission to the World Commission on Dams, Presented at the Africa/Middle-East Regional Consultation, December 1999, available from www.dams.org.

الخلاصة

ديموغرافيا، تعرضت منطقة الشرق الأوسط في الفترة الاخيرة الى تغييرات جذرية ، والتي سيكون لها آثار كبيرة على إدارة المياه. **وجدلا كبيرا حولمشاركة الدول االمتشاطئة لنهري دجلة والفرات تركيا سوريا والعراق، مثال على ذلك بحلول عام 2050، احتياجات السكان والمياه المتوقعة في العراق ترتفع، بسبب النمو السكاني لـ 2.6 ضعف حجمها الحالي، اي الزيادة في سكانها من 32.6مليون نسمة لأكثر من 83 مليون نسمة .سوريا، تعتمد أيضا على نهر الفرات باعتباره شريان الحياة الاقتصادية ، سوف نرى سكانها بحلول منتصف القرن ينمو 1.5 أضعاف حجمها الحالي، 33.6–22.5 مليون نسمة ، هذا النمو السكاني في سورية والعراق وزيادة الطلب على المياه لأغراض الري، والتنمية الصناعية، واستخدام المحلي، يضغط على تركيا لضمان تدفق وافرة من المياه على مدار السنة. كما آثار تغير المناخ و الجفاف وتغيير وقت تساقط الثلوج وهطول الأمطار، ممكن ان يثير المشاكل كما في الماضي.**

المشاكل في العراق هي أكثر إلحاحا مما كانت عليه في تركيا وسوريا،العراق جاف جدا وأكثر اماكنه مستويةة مما يجعله عرضة للتبخر .لديه فترات جفاف طويلة، وأحيانا لمدة تصل إلى ستة أشهر من مايو إلى أكتوبر. درجة الحرارة خلال هذا الوقت يمكن ان تصل إلى 120 درجة فهرنهايت . المناخ هو العامل الرئيسي في التبخر عالية، ولكن البحيرات لاصطناعية و السدود، والتي هي مناطق مياه مفتوحة كبيرة تزيد من كمية التبخر وزيادة تركيز الملوثات في مياه تخزين، ويسهم أيضا في فاقد من المياه من خلال نظام التبخر. لتحضر والتصنيع، وزيادة في عدد السكان، والتوسع في الزراعة باستخدام نظم الري التقليدية كل هذه العوامل تؤدي إلى زيادة الطلب على المياه في هذه الدول الثلاث. مع بناء العديد من السدود في تركيا وسوريا، وكميات من المياه التي تدخل العراق يتناقص مع تنفيذ خطة طموحة لإدارة المياه تركيا (GAP)، فإن كميات المياه تنخفض أكثر وأكثر.

GROWTH OF SCINTILLATOR MATERIALS OF CERIUM DOPED LANTHANUM BROMIDE SINGLE CRYSTALS VIA BRIDGMAN TECHNIQUE

FARIS **K**OCHARY

Dept. of Physics, Faculty of Science, University of Duhok, Kurdistan Region, Iraq- Iraq

(Received: January 26, 2014; Accepted for publication: February 27, 2014)

ABSTRACT

The capability to distinguish between gamma rays with somewhat different energies by scintillation is of extreme prominence for many applications such as medical imaging, X-rays astronomy, and gamma rays spectroscopy. Lately, various halide scintillators such as cerium doped lanthanum bromide have been discovered. There is a great importance in sensitive scintillator materials for use in homeland security and medical applications. These materials are very hygroscopic and therefore techniques are needed to reduce their hygroscopic nature. A look for non-hygroscopic materials is needed to advance the scintillator knowledge and technology. In this paper, I have had an attempt of a crystal growth for a new bulk single crystal of $LaBr_3$:Ce from melt using vertical Bridgman-Stockbarger technique with good conditions such as a growth rate of 10 mm a day. At the melting point of the mix, the occupied ampoule was lowered down over a temperature ramp of 10ºC/cm. The growth process via this technique is confirmed to be encouraging and hopeful for growing transparent $LaBr_3$:Ce single crystals with good optical quality. This work has been done at the Physics laboratory of Alabama Agricultural and Mechanical University (Normal, Alabama/USA). Outcomes of creation and crystal growth parameters shall be reported.

***KEYWORDS**:* Scintillators, Halides, Bridgman Technique, Single Crystal Grow*th*

1. INTRODUCTION

Recently, a lot of research is focusing on the development of new and improved scintillator detector crystals for use in detection and spectroscopy of energetic photons (gamma rays). The radiation detector requirements for many indicative ways vary significantly and are not always met by commercially available scintillators. Ideally, a scintillator should have a high light yield, a fast response time, a high density and atomic number. Obviously, there are many other criteria, such as transparency of the material to its own emission, ease of crystal growth, stability in air, and the matching of the scintillation wavelength spectrum with the sensitivity curve of the light detectors. However, there is no material that meets all of these criteria and the choice of a particular scintillator is often a compromise among these and other factors [1-5].

The continuing serious global threat is the spread of nuclear weapons. When examining the nuclear weapons, γ-ray spectrometers may help very well by recognizing the γ-ray and X-ray signatures of the greatly developed uranium and plutonium limited in them. The latest general cautions on such bombs have highlighted the necessity for a wider range checking of dangerous and active materials such as manufacturing and health waste. For examining places, γ-ray spectrometers must have these preferred features: great detection efficiency, high energy resolution, easy movability, compressed size, light weightiness, and low power necessities [6]. Current γ-ray spectrometers have some deficiencies in those needed properties. In the search for new and efficient scintillators, most efforts have been directed to cerium-doped crystals. In the (300-6000) nm wavelength region, the fast scintillation emitted by trivalent cerium which is ranged between (15-60) ns is well known for a long period of time and in many cases, the light output is high [7]. Because of the high density and effective atomic number of $LaBr_3$, $LaBr_3$:Ce will eventually become the scintillator of choice in the near future if it can be easily grown into large single crystals. The LaBr:Ce scintillator crystals have the favorite characteristics for γ-ray spectrometers which meet nowadays requests. Here, the latest outcomes for growth of $LaBr_3$:Ce single crystals via vertical Bridgman-Stockbarger technique are reported.

2. EXPERIMENTAL

3.1 SYNTHESIS AND PURIFICATION OF THE STARTING MATERIALS

Single crystals of cerium doped lanthanum bromide $LaBr_3$:Ce crystallize in the hexagonal close-packed structure (HCP) with atomic packing factor of 0.74, coordination number of 12, and space group $P6_3/m$ [8]. Based on this HCP crystal structure and other lattice parameters, the density of $LaBr_3$ is 5.29 g/cm^3 and it melts at about 783°C [9]. The lattice is not layered and does not cleave easily and the effective atomic number for $LaBr_3$ is 46.9 [10]. In fact, this atomic number is almost similar to sodium iodide with respect to energy detection efficiency. $LaBr_3$ is hygroscopic like NaI or $RbGd_2Br_7$, but react differently to moisture and air. It is seemed to be oxidized within moments forming a whitish wet powder. It is therefore essential that these crystals are sealed into a glass or quartz container to prevent hydration and oxidation of the crystal surface. The following requirements are important in selecting a material for use in high performance gamma ray scintillator crystals:

(a) High density and atomic number.
(b) High light output.
(c) Short decay time without afterglow.
(d) Convenient emission wavelength.
(e) Mechanical ruggedness.
(f) Radiation hardness and low cost [11-12].

The needed starting chemicals were commercially available as powders, but since a large amount of pure anhydrous lanthanum bromide material was needed for bulk crystal growth and because of the hygroscopic nature of this compound, I have synthesized it in the Physics laboratory of Alabama Agricultural and Mechanical University (Normal, Alabama/USA). Production of the anhydrous $LaBr_3$ was carried out via ammonium halide method. After overcoming initial problems and difficulties, I was capable of designing a new experimental set up to build the anhydrous compound by means of these two successive chemical reactions:

$$La_2O_3 + 12\,(NH_4)Br \rightarrow 2(NH_4)_3LaBr_6 + 6NH_3 + 3H_2O$$

$$2(NH_4)_3LaBr_6 \rightarrow 2\,LaBr_3 + 6(NH_4)\,Br$$

In our first batch, 81.45 g of 99.99% pure lanthanum oxide procured from Alfa Aesar was added to react with 293.79 g of 99.9% pure ammonium bromide from Cerac to form a lanthanum bromide complex. The first reaction proceeded with reasonable speed and carried out at 250°C. Both ammonia and water have been evaporated, Figure 1.

Fig. (1) A setup designed for the first step of synthesizing of anhydrous $LaBr_3$

In order to move out the excess ammonium bromide, a second reaction was carried out at a temperature of about 350ºC in vacuum. The anhydrous $LaBr_3$ was then effectively synthesized. The experimental set up shown in Figure 2 was made for this purpose.

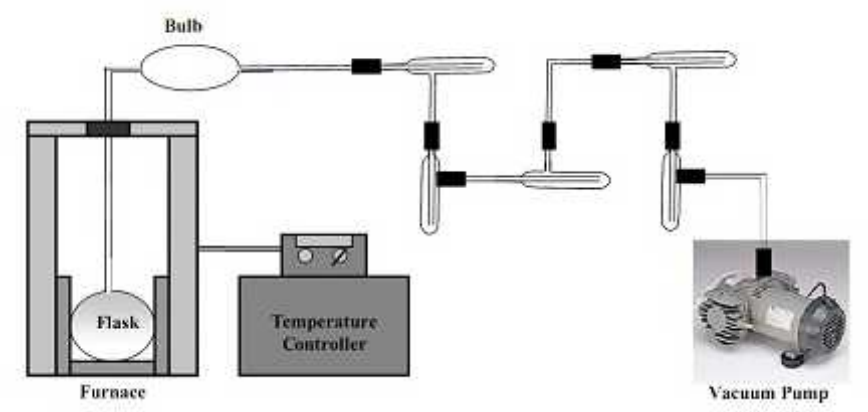

Fig. (2) Scheme for the 2nd step of synthesizing anhydrous lanthanum bromide

After both reactions mentioned in above, I was able to synthesize about 189.3 g of anhydrous lanthanum bromide. Initial tests of melting point and density were comparable to the literature values. This material was then used to grow bulk single crystals in a quartz tube of 16 mm outside diameter.

3.2 CRYSTAL GROWTH

Anhydrous $LaBr_3$ and a small amount of $CeBr_3$ (0.5%) were loaded into a quartz ampoule in the glove box. A vacuum pump was attached to the ampoule and the ampoule had been evacuated to about 0.001 Torr. Almost after 3 hrs of evacuation, the ampoule was sealed by an oxygen torch. Throughout the whole sealing process, the mixture was kept cool by covering a wet cloth around the ampoule. Because of heating gained from the torch, this step was necessary to prevent any thermal decomposition of the mixture. In order to lower it down through the furnace, the upper part of the ampoule was attached to a quartz nail. Single crystals of cerium doped lanthanum bromide were then grown. A photograph of the used vertical Bridgman furnace is shown in Figure 3:

Fig. (3) Multi-zone vertical Bridgman furnace

The transparent high temperature resistance furnace was fabricated from Thermcraft Inc., with a furnace muffle size of 37 mm (id) × 405 mm. For the scaling up of the growth method, the temperature ramp in the furnace was dynamically adjusted. The used transparent furnace could grow $LaBr_3$:Ce crystals up to 3 inches long and 1 inch diameter. A computerized motor was used to lower down the ampoule at a rate of 10 mm a day. At the start of

the growth process, I heated the quartz ampoule to around 800ºC (slightly above the melting point) to guarantee whole melting of the entire solid. The molten charge began to solidify gradually into single crystals when the tip of the tube fell below the melting point. When the temperature was underneath the melting point and in order to reduce the residual stress in the crystal, I cooled down the furnace very slowly (for about 48 hrs) to room temperature. Figure 4 shows a grown bulk single crystal of the material. After the end, I have unlocked the ampoule very cautiously by a diamond edge. The crystal was then encapsulated for the characterization purpose at the National Space Science and Technology Center of NASA. They seemed to be scintillating, but were not able to collect all the light due to scattering losses. Initial results were encouraging. It is believed that there may be some residual lanthanum oxide in the end product and therefore, steps need to be taken to avoid this problem during synthesis.

Fig.(4) A grown single crystal of cerium doped lanthanum bromide

3. CONCLUSION

A large size single crystal of anhydrous $LaBr_3$:Ce with attractive properties was grown successfully from melt using the vertical Bridgman-Stockbarger method. In comparison to other groups work in recent years, this work has provided an effective method to prepare such an anhydrous material and a modified process to grow crystals with desirable optical properties. These scintillator materials show unlimited potential and ability for use in γ-ray spectrometers for medical imaging and other environmental remediation. The vertical Bridgman technique in this work is confirmed to be a promising method to grow the cerium doped lanthanum bromide single crystals.

ACKNOWLEDGEMENTS

This effort was fully supported by NASA cooperative agreement NCC8-250 and NSF HBCU-RISE project HRD-0531183. The author would like to thank Professor Mohan D. Aggarwal for his scientific advices and assistance.

REFERENCES

J Moszynski, M., Nassalski, A., Syntfeld-Kazuch, A., Szczesniak, T., Czarnacki, W.,
Wolski, D.G. and Stein, J. (2006). Nucl. Instrum. Meth. A, 568(2), 739.

J W.W. Moses and K.S. Shah, Nucl. Instrum. Meth. A, 537(1-2), 317 (2005).

J J. Glodo, K. S. Shah, M. Klugerman, P. Wong and B. Higgins, Nucl. Instrum. Meth. A, 537(1-2), 93 (2005).

J Yu Pei, Xiaofeng Chen, Rihua Mao, Guohao Ren, J. Crystal Growth 279 (3-4), 390 (2005).

J O. Guillot-Noel, J.T.M. de Haas, P. Dorenbos, C.W.E. van Eijk, K. Kramer, H.U. Gudel, J. Lumin, 85, 21 (1999).

J K.S. Shah, J. Glodo, M. Klugerman, W.M. Higgins, T. Gupta, P. Wong, IEEE Trans, Nucl. Sci. 51 (5) (2004).

J S. Normanda, A. Iltis, F. Bernard, T. Domenech and P. Delacour, Nucl. Instrum. Meth. A, 572(2), 754 (2007).

J W.M. Higgins, J. Glodo, E. Van Loef, M. Klugerman, T. Gupta, L. Cirignano, P. Wong and K.S. Shah, J. Crys. Growth, 287(2), 239 (2006).

J C. Hoel, L.G. Sobotka, K.S. Shah, J. Glodo, Nucl. Instrum. Methods A 540 (2005).

J E.V.D. van Loef, P. Dorenbos, C.W.E. van Eijk, K. Kramer and H.U. Gudel, Appl. Phys. Lett., 79(10), 1573 (2001).

J W.W. Moses, Nucl. Instrum.Meth. A, 487(1-2), 123 (2002).

J E.V.D. van Loef, P. Dorenbos, C.W.E. van Eijk, K. Kramer and H.U. Gudel, Nucl. Instrum. Meth. A, 486(1-2), 254 (2002).

NATURAL RADIOLOGICAL HAZARDOUS OF ROCKS IN DUHOK GOVERNORATE, KURDISTAN REGION, IRAQ

REVINK **A**LI **R**AMADHAN[*] and **K**HAIRI **M-S. A**BDULLAH[**]
[*] Dept. of Physics, College of Science, University of Duhok, Kurdistan Region-Iraq
[**] Dept. of Water Resources, College of Engineering, University of Duhok, Kurdistan Region-Iraq

(Received: April 2, 2014; Accepted for publication: June 29, 2014)

ABSTRACT

We performed a study over the radiological impact on nine samples of natural rocks collected from various areas in the Duhok governorate. The governorate is located in the northwest Kurdistan region of Iraq. NaI(TI) gamma ray spectrometer for 30000 sec per sample was utilized to detect the concentration of radionuclide in rocked samples. The average activity concentration values of ^{226}Ra, ^{232}Th and ^{40}K obtained are 13.10 Bqkg^{-1}, 5.20 Bqkg^{-1} and 134.32 Bqkg^{-1} respectively. Gray Clay stone, Limestone, Fine sand, Silty clay and Marley shows relative high activity concentration whereas Chalky Limestone show low activity concentration while other rock formations were moderate in radioactivity level. By utilizing the standard analytical method the excess life time cancer risk and hazard indices were estimated. The average values obtained for absorbed dose, annual effective dose equivalent (Indoor, Outdoor), hazard indices (external, internal), excess lifetime cancer risk, representative (alpha, gamma) indices and radium equivalent are respectively 14.88 nGyh^{-1}, 73 µSvy^{-1}, 18.26 µSvy^{-1}, 0.084, 0.120, 0.064×10^{-3}, 0.115, 0.07 and 31 Bqkg^{-1}. After the values which obtained in this work are compared with corresponding world permissible values, it found that the values located below the standard limits for such environments. The rock from the study area provided no excessive exposure for the inhabitants and can be utilized as building material without posing any radiological threat or harm to the public users.

KEYWORDS: NaI(TI) spectrometer, Rock sample, concentration, Hazard indices and Excess lifetime cancer risk.

INTRODUCTION

Human beings are always exposed to background radiation that stems both from natural and artificial. Natural radioactivity, that is found in numerous geological formation for instance: rocks, earth crust, , soils, plants, air and water, widespread in the environment around. Natural radioactive concentration mainly depends on geographical and geological condition and appears at various level in soils of each different geological area (UNSCEAR, 2000). When rocks are disintegrated through natural process, radionuclides are carried to soil by rain and flows. In addition to the natural sources; soil radioactivity is also affected by man-made activities (Ramasamy 2009 and Surinder et al. 2005).

Primordial radiation exposure originates from the terrestrial radio-nuclides, whose half-lives are tantamount to the age of the earth, and the secondary radionuclides produced by their radioactive decay. The naturally occurring radionuclides include the three radioactive decay chains originating with ^{238}U, ^{232}Th, and ^{235}U and single ^{40}K. These radionuclides are ubiquitously present in low concentrations in water and soil as a result of weathering and drift of rock (Okeyode and Oluseye 2010).

Radioactive elements found in rock and soil from the earth makes their way into our bodies through the water we drink, food we eat, air we breathe which contains them. The largest contributor to our daily exposure of radiation is the natural radioactivity and the major form of natural radiation is Radon gas (Okeyode and Akanni 2009).

The long-term exposure to uranium and radium through inhalation has several health effects as chronic lung diseases, acute leucopoenia, anemia and necrosis of the mouth. Radium causes cranial, nasal tumors and bone. Thorium exposure can cause bone, hepatic, pancreas, lung, leukemia and kidney cancers. Therefore, gamma dose rates and radio-nuclides activity concentrations should be monitored (Ramasamy 2009).

Knowledge of natural radioactivity present in rocks enables one to estimate any possible radiological risk to mankind. Hence, the aim of

this study is to calculate the radioactivity concentrations as well as the environmental outdoor the absorbed dose rate, annual effective dose rate (Indoor, Outdoor), hazard indices (internal, external), excess life time cancer risk, gamma-index (I_γ, I_α) and radium equivalent activity are also calculated.

STUDAY AREA

Duhok governorate lies in the far northwest of Iraq and forms the western governorate in Iraqi Kurdistan Region. It confines with Turkey from the north, Syria from the west, Erbil governorate from the east, and Nineveh governorate from the south. It is located at the intersection of longitude 43° 00′ to the east and the latitude 36° 52′ in the north (Abdullah and Ramadhan 2011).

It is a part of the mountain and semi-mountain that orientated from west to east, in physiographic diversity from the middle and south of Iraq. The governorate is divided administratively into the following four districts: Duhok-district with area (1092) km^2, Sumel-district with area (1327.7) km^2, Zakho-district with area (1521.51) km^2, Akre-district with area (6418) km^2 and Amadi-district with area (2582.8) km^2. The climate of the Region is of semi-arid type, designated as continental and subtropical. The elevation is quite different ranging from lower than 300 to more than 1300 meters above the sea level. (Dilshad 2008). The geological formations consisting of limestone, red beds of silt, hard clay stone with some beds of siltstone and conglomerate and formation of well bedded chalky, partly dolomite limestone with thin beds of yellowish-green marl (Abduljabbar 2003).

SAMPLE COIIECTION AND PREPARATION

According to the geological characteristics of Duhok governorate as shown in Figure1, samples have been carefully collected from each type of the geological formations. A total of nine samples have been collected (Table 1) which represent the predominant rock formations of Duhok. Measured samples were dried in an oven at 110 C° till constant dry weight was obtained, crushed, sieved through 0.2-*mm* mesh to homogenize them, stored in standard 1000 *ml* beakers, dry weighed and stored for at least one month before counting in order to permit the in-growth the production decay of thorium and uranium to achieve the equilibrium for ^{232}Th and ^{238}U with their respective progeny. While, important disequilibrium is uncommon in rocks older than 10^6 years, and the ^{232}Th series may be considered in equilibrium in most geological surrounding (Tzortzis et al, 2003).

Fig 1: Locations of the rock samples in Duhok Governorate.

SAMPLE COUNTING

For the radioactive concentration, the detection assembly set up for this study consist of thallium activated sodium iodide 3″×3″ well type NaI(Tl) detector, the photo multiplier tube and multi-channel analyzer (MCA). The detector was surround in 6 cm lead shield. The counting time of each sample was set to 30000 seconds. Background count was measured for the same length of time. The net count was used for subsequent analyses. As in energy calibration the same multi source (^{155}Eu, ^{137}Cs and ^{22}Na) gamma rays standard sources are used to determined detector efficiency. Both sources have known activity, energies and gamma decay fraction f_γ needed in calibrated process. These data are fitted exponentially and plotted using EXCEL program system, as shown in Figure 2, to get the following relationship between the efficiency and gamma energies.

$$£_E = 15.975\, e^{-0.0015 \times E_i}$$

With R^2=0.994

Where ε_E is the efficiency as a function of γ-ray energies, E_i is γ-ray energies for nuclide *i* and R is standard deviation.

From the counting spectra, the specific activity of ^{238}U, ^{232}Th and ^{40}K was determined. The peak corresponds to 1460.8 keV for ^{40}K, 352 keV (^{214}Pb) for ^{238}U and 238.6 keV (^{212}Pb)

for ^{232}Th were considered in arriving at the activity levels (Bq/kg).

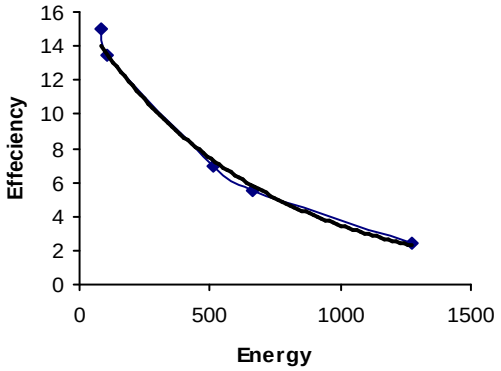

Figure 2: Energy efficiency as a function of γ-ray energies for 3"×3" well type NaI(TI) detector.

RESULTS AND DISSCUTION

1. Activity Concentration

Based on the measured γ-ray counts (N_{Ei}) of full width at half maximum (FWHM) photo-peaks of specified radio-nuclides in the ^{226}Ra and ^{232}Th decay series and in a single ^{40}K, their specific activity or activity concentrations (activity per unit mass) in samples can be calculated from the following equation (Abdullah and Ahmed 2012):

$$C_e = \frac{1}{M_s \times n} \sum_{i=1}^{n} A_{Ei} \, (BqKg^{-1})$$

Where $$A_{Ei} = \frac{N_{Ei}}{£_E \times t \times f_¥} (Bq)$$

And N_{Ei} is the net peak area of a peak at energy E_i, ε_E is the energy detection efficiency E_i, t is the counting life time = 30000s, f_γ is gamma fraction, M_s is the mass in kg of the measured rock samples, and n is number of photo-peaks, such that of ^{40}K and the decay series of ^{238}U or ^{226}Ra and ^{232}Th (n=1).

The specific activity (Bqkg^{-1}) of ^{226}Ra, ^{232}Th and ^{40}K along with the mean values for the nine rock samples collected from Duhok governorate are presented in Table 1, The concentrations of ^{226}Ra ranged from 3.30 Bqkg^{-1} in chalky limestone to 32.66 Bqkg^{-1} in gray limestone, the concentration of ^{232}Th ranges from 1.5 Bqkg^{-1} in dolomitic limestone to 13.76 Bqkg^{-1} in silty clay while the concentration of ^{40}K ranges from 14 Bqkg^{-1} in chalky limestone to 395 Bqkg^{-1} in silty clay. The ratio radioactive concentrations, which we found in different types of rocks depends on the nature of the chemical elements such as (K^+, Na^+, Mg^+, Ca^+) and ratio of soil such as (sand, clay and silty) in the rocks. Where it is clear that the concentrations of ^{226}Ra are higher than that of ^{232}Th for all samples except sample R6. This perhaps attributed to the fact that ^{226}Ra is moderately soluble in water and is found greater abundantly than ^{232}Th in atmosphere. The average value of ^{226}Ra, ^{232}Th and ^{40}K is 13.10 Bqkg^{-1}, 5.20 Bqkg^{-1} and 134.32 Bqkg^{-1} respectively. The obtained results for three radionuclides are lower than the permissible levels of (35, 30 and 370) Bqkg^{-1} (UNSCEAR 2000).

It is interesting to compare the mean concentration of natural radioactivity in Duhok governorate region rock with the results from different parts of Iraq and other countries of the world, as given in Table 2. In Sulaimany and Mosul determined a higher activity concentration of ^{226}Ra, ^{232}Th and ^{40}K compared to this study. While the comparison of the ^{226}Ra with that of the worldwide shows that, nine countries have higher values and one have lower values activity concentration of this radionuclide than in the rock of the understudy region. It is found that the average value of ^{232}Th in the present study was less than reported for rock of all countries. The comparison of ^{40}K activity concentration shows that the values of this radionuclide in the rock of Nigeria, Turkey, Brazil, Egypt, Iran, Saudi Arabia and Word average are higher than the present study mean value and may be as a result of its relative abundance in the earth crust. All other countries in comparison with present study have a comparable activity concentration values. The variations in the concentrations of the radioactivity in the rock of the various locations of the world depend upon the geographical and geological conditions of the area and the extent of fertilizer applied to the agriculture lands (Tzortzis et al. 2003).

2. Absorbed Dose Rate

Radiation exposure are measured in terms of the quantity “absorbed dose rate”, which is equal to the energy deposited per unit mass in the irradiated medium. It is the major step for evaluating the health hazard and is expressed in gray (Gy). Nature of biological effect, clinical effects and radiological is directly related to the absorbed dose rate (Ramasamy et al. 2010).

Factors of conversion published by UNSCEAR (2000) are utilized to calculate

the total dose rate (*DR*) ($nGyh^{-1}$) in the equation below:

$$DR = 0.462C_{Ra} + 0.604C_{Th} + 0.0417C_K$$

The range of a calculated absorbed dose rates given Table 3 is from 3.10 $nGyh^{-1}$ to 29.31 $nGyh^{-1}$ with an average of 14.88 $nGyh^{-1}$. Mean absorbed dose rate for all samples is less than the world average value 57 $nGyh^{-1}$ (UNSCEAR 2000).

3. Annual Effective Dose Equivalent

The annual effective dose equivalent (AEDE) received outdoor by a member is calculated from the absorbed dose rate by applying dose conversion factor of 0.7 Sv/Gy and occupancy factor for indoor and outdoor were 0.8(19/24) and 0.2(5/24) respectively (Al-Zahrani 2012). AEDE was calculated from absorbed dose rate by using equation below :

$$AEDE\ (Indoor)(\text{«}Svy^{-1}) = D(nGyh^{-1}) \times 8760\ h \times 0.7\,SvGy^{-1} \times 0.8 \times 10^{-3}$$

$$AEDE\ (Outdoor)(\text{«}Svy^{-1}) = D(nGyh^{-1}) \times 8760\ h \times 0.7\,SvGy^{-1} \times 0.2 \times 10^{-3}$$

The calculated indoor and outdoor AEDE values are quoted in table 3. The average, minimum and maximum value for indoor and outdoor is found to be 73 μSvy^{-1}, 15.20 μSvy^{-1} and 143.78 μSvy^{-1} and 18.26 μSvy^{-1}, 3.80 μSvy^{-1} and 35.95 μSvy^{-1} respectively. So, one can note that the obtained value of indoor and outdoor is less than the average values of the world which are (450 μSvy^{-1} for indoor and 70 μSvy^{-1} for outdoor) (Avwiri et al. 2013).

4. Radiological Hazard Indices

The gamma ray radiation hazard indices from radionuclides in rock samples have been calculated. Even though total specific activity of radionuclides is calculated, it does not provide the exact indication about the total radiation risk. Also these hazard indices are used to select the right materials. Hazard Indices (H_{ex} and H_{in}), represent the external and internal radiation hazards as given in Table 3 according to the following criterion (Fares et al. 2012 and Ramasamy et al. 2010).

$$H_{ex} = \left(\frac{C_{Ra}}{370} + \frac{C_{Th}}{259} + \frac{C_K}{4810}\right) \le 1$$

$$H_{in} = \left(\frac{C_{Ra}}{185} + \frac{C_{Th}}{259} + \frac{C_K}{4810}\right) \le 1$$

The utmost value of H_{ex} equal to unity corresponds to the upper limit of Ra_{eq} (370 $Bqkg^{-1}$). The values of H_{ex} for the studied rock samples range from 0.018 to 0.161, with an average value of 0.084, are less than unity. While the values of H_{in} for the studied rocks samples range from 0.027 to 0.208 with an average value 0.120 are less than unity. This refers that the outcome will not effected to respiratory disease for example: cancer and asthma and external diseases such as erythematic, cataracts and skin cancer (Osimobi et al. 2013).

5. Excess Lifetime Cancer Risk

This distribute with the possibility of developing over a life-time at a specific exposure level. It is believed as a value representing the number of additional cancers regarded in a given number of people on exposure to a carcinogen at a given dose. Excess Life-time Cancer Risk (ELCR) has been calculated utilizing the equation below and is shown in Table 3.

$$ELCR = AEDE \times DL \times RF$$

Where effective dose equivalent is AEDE, the duration of life (70 years) is DL and fatal cancer risk per Sievert (Risk Factor) is RF. For stochastic effects, a value of 0.05 Sv^{-1} for the public is used (Avwiri et al. 2012). The range of ELCR is 0.013×10^{-3} to 0.126×10^{-3} with an average of 0.064×10^{-3}. The average ELCR for whole samples is lower than the average of the world 0.29 x 10^{-3} (Fares et al. 2012). This indicate that the probability of cancer production by drillers and the audiences in general are unimportant. For that reason, operations of drilling and utilize of rocks as materials for building is not creating any health problems on Duhok population.

6. Gamma-index and Alpha-index

These are used to evaluate the hazard of radiation related with the natural radionuclide in investigated samples specifically (Thabayneh and Jazzar 2012 and Laith et al. 2013). The representative gamma index **(I_γ)** is as :

$$I_\gamma = \frac{C_{Ra}}{300} + \frac{C_{Th}}{200} + \frac{C_K}{3000}$$

This gamma index is utilized as well to connect the annual rate of dose because of the surplus of external gamma radiation that caused by surface materials. It is an examination tool for identifying materials, which may be healthy of health concern when utilized for construction. (Osimobi et al. 2013).

The average values of I_γ calculated from the measured specific activity of ^{232}Th, ^{226}Ra and ^{40}K that are presented in Table 3. The calculated values of I_γ for the studied samples are ranged between 0.025–0.230. While, for the types of rock are fewer than the critical value of unity. The average calculated values of I_γ for the studied samples values was 0.115 for all rock types which were lower than the critical value of unity.

Several alpha indices are proposed to assess the level of exposure, yet. This is due to inhalation of radon originating from construction materials. The following formula were used to determine the alpha index (I_α) (European Commission 1999).

$$I_{\sim} = \frac{C_{Ra}\left(Bqkg^{-1}\right)}{200}$$

Where C_{Ra} is the ^{226}Ra activity concentration, which is assumed in equilibrium with ^{238}U. The exemption recommendation and upper level of activity concentrations of ^{226}Ra in construction materials are 100 and 200 Bqkg^{-1}, respectively, as proposed by the ICRP 1994. These considerations are reflected in the alpha index. The recommendation of upper limit concentration of ^{226}Ra is 200 Bqkg^{-1}, for which $I_\alpha = 1$.

The average computed I_α values for the studied samples are given in Table 3 for the varies types of rock and areas where they been collected. The values of I_α ranged from (0.017 to 0.163), with the mean value of 0.07. The values of Iα ranged between (0.017 and 0.163), with the average value of 0.07. For the safe use of a material in the building of housing, I_α should be fewer than unity. The average computed values were equal unity.

7. Radium Equivalent Activity

Radium equivalent (Ra_{eq}), which is a common index, was utilized to compare materials specific activities that containing ^{226}Ra, ^{232}Th and ^{40}K by a single amount, which takes into account the radiation dangerous related. Availability of activity index a beneficial directive in regulating the safety standard dwellings. The weighted sum of activities of the mentioned above natural radionuclides represented radium equivalent activity and is depend on the appreciation that 1 Bqkg^{-1} of ^{226}Ra, 0.7 Bqkg^{-1} of ^{232}Th, and 13 Bqkg^{-1}of ^{40}K produce the same dose rates of radiation (Thabayneh and Jazzar 2012). The radium equivalent activity is given as:

$$Ra_{eq} = C_{Ra} + 1.43C_{Th} + 0.077\,C_K$$

The world average of Ra_{eq} in soils is 89 Bqkg^{-1} (UNSCEAR 1998). As reference, the allowed dose limit for public, which is recommended by ICRP 1991, is 1.5 mSvy^{-1} or equivalent to 370 Bqkg^{-1}. The average calculated Ra_{eq} values are displayed in Table 3 for the different types of rock and areas from where they were collected. The minimum (6.67 Bqkg^{-1}) and the maximum (59.62 Bqkg^{-1}) values of Ra_{eq} were found in R2 and R6 rock kinds, respectively. The average 31 Bqkg^{-1} were almost lower than the limit value of 370 Bqkg^{-1} recommended by the Organization for Economic Cooperation and Development (Fares et al. 2012).

CONCLUSION

NaI(TI) gamma ray spectrometer was used to measure the radioactivity of rock samples collected from the Duhok governorate. ^{40}k was observed to be relatively high compare to other two natural radio-nuclides, as it is the most abundant radioactive element under consideration. Moreover, the excessive use of the Potassium containing fertilizers in the areas adjacent to the sampling sites may contribute to the higher values of ^{40}K activity. The radio-nuclides were observed to be distributed at an irregular pattern, which could be attributed to the mineralogy, carbonate content. The average activity concentrations of ^{232}Th, ^{226}Ra and ^{40}K are lower than the permissible levels of (30, 35 and 370) Bqkg^{-1}. Therefore no significant health threat to human lives is anticipated and the surrounding is safe radio logically. All obtained values show that the average outdoor absorbed dose rate, the annual effective dose rate indoor-outdoor, radiological hazard indices (H_{in} -H_{ex}), the excess lifetime cancer risk, gamma indices (I_γ), alpha indices (I_α) and radium equivalent activities (Ra_{eq}) are within the acceptable limits. This implies that Duhok rocks can be used safely for construction of buildings.

This information is important for local utilization of the rocks in house construction.

Table (1): Radionuclide activity concentration for different rock samples:

Sample No	Location	Rocks type	Activity concentration (BqKg^{-1})		
			^{226}Ra	Th^{232}	K^{40}
R1	Khanki	Gray Clay stone (Lower Fares Formation)	18.72±0.29	5.28±0.28	**117 ± 3.32**
R2	Seji	Chalky Limestone (Pelaspi Formation)	3.30±0.18	1.6±0.25	**14.0±1.1**
R3	Feshkhabor	Limestone (Pelaspi Formation)	11.15±0.33	4.70±0.28	**113.73±4.1**
R4	Geli Zaxo	Fine sand (Upper fares formation)	6.55 ±0.30	6.40±0.35	**234 ± 2.67**
R5	Akre	Gray limestone (Agra Formation)	32.66±0.64	5.22±0.35	**53.36±3.44**
R6	Feshkhabor	Silty clay (Lower Fares Formation)	9.53±0.32	13.76±0.34	**395±3.52**
R7	Sindor	Dolomite Khurmala formation	8.27±0.34	1.24±0.37	**45.75±2.36**
R8	Avrike	Dolomitic limestone Pelaspi formation	6.80 ±0.22	1.5±0.19	**44.32±1.77**
R9	Merga drij	Marley Kolosh formations	24.22±0.45	7.10±0.33	**191.67±2.90**
		Average	13.10±0.31	5.20 ± 0.30	**134.32 ± 2.8**

Table (2): Comparison of natural radioactivity concentration (Bqkg^{-1}) in the soil and rock Samples and dose rates for present study with previous study reported from different parts of Iraq and other countries of the world:

Country	Average activity concentration (BqKg^{-1})			Average Dose Rate (nGyh^{-1})	Reference
	^{226}Ra	^{232}Th	^{40}K		
Duhok, Kurdistan, Iraq	13.10	5.20	134.32	15	Present work
Sulaimany, Kurdistan, Iraq	83.337	19.147	284.86	-	Rasheed and Kamal 2013
Mosul, Iraq	91.90	50.4	482.37	81.83	Laith et al. 2013
India	57	87	143	86.54	Surinder, et al. 2005
Nigeria	9.67	112.38	961.49	119.3	Okeyode and Akanni 2009
Cyprus	15	11	178	14.9	Tzortzis et al. 2003
Turkey	21	23.5	363.5	40	Rıdvan et al. 2011
Egypt	199	36.39	1051	150.5	Fares et al. 2012
Brazil	31	73	1648	128.3	Orgun et al. 2005
Iran	28	22	640	71	Al-Zahrani 2012
Saudi Arabia	37	32	343	50	Al-Zahrani 2012
Palestine	34.5	23.8	120	35.5	Thabayneh and Jazzar 2012
Word average	35	30	400	57	UNSCEAR 2000

Table (3): Absorbed dose rate, Annual effective dose rate, hazard indices and Ra_{eq}:

Sample no.	Dose Rate ($nGyh^{-1}$)	AEDE(μSvy^{-1})		Hazard indices					Ra_{eq} ($Bqkg^{-1}$)
		Indoor	Outdoor	H_{ex}	H_{in}	ELCR×10^{-3}	I_γ	I_α	
R1	16.75	82.17	20.54	0.095	0.146	0.072	0.130	0.094	35.28
R2	3.10	15.20	3.80	0.018	0.027	0.013	0.025	0.017	6.67
R3	12.77	62.64	15.66	0.072	0.102	0.055	0.100	0.056	26.63
R4	16.72	82.02	20.50	0.091	0.109	0.072	0.130	0.033	33.72
R5	20.48	100.55	25.12	0.119	0.208	0.088	0.155	0.163	44.23
R6	29.31	143.78	35.95	0.161	0.187	0.126	0.230	0.048	59.62
R7	6.50	31.89	7.24	0.037	0.059	0.025	0.050	0.041	13.57
R8	5.91	29.0	7.97	0.033	0.051	0.028	0.045	0.034	12.36
R9	23.54	115.48	28.87	0.133	0.198	0.101	0.180	0.121	49.13
Average	14.88	73	18.26	0.084	0.120	0.064	0.115	0.07	31

REFERNCES

- Abdullah K. and Ramadhan R. (2011). Determination of gamma emitting radionuclides in Duhok city, Iraq. *Journal of The Nucleus*, 48 (4), 295-300.
- Abdullah K. and Ahmed M. (2012). Environmental and radiological pollution in creek sediment and water from Duhok, Iraq. *Journal of the Nucleus*, 49 (1), 49-59.
- Abduljabbar I. (2003). A study of Some Engineering Properties of Undisturbed and Eemolded Desiccated Soils in Duhok governorate. M.Sc. Thesis, College Engineering, Duhok University (2003).
- Avwiri G., Egieya J. and Ononugbo C. (2013). Radiometric assay of hazard indices and excess lifetime cancer risk due to natural radioactivity in soil profile in Ogba, Egbema, Ndoni local government area of rivers state, Nigeria. *Journal of Natural and Applied Sciences*, 4 (5), 54-65.
- Avwiri G. Osimobi J.and Agbalagba E. (2012) Evaluation of Radiation Hazard Indices and Excess Lifetime Cancer Risk Due to Natural Radioactivity in soil profile of Udi and Ezeagu Local Government Areas of Enugu State, Nigeria, J. of Environmental and Earth Sciences Vol. 1(1), pp. 1-10.
- Al-Zahrani J. (2012). Radioactivity Measurements and Radiation Dose assessments in Soil of Albaha Region (Saudi Arabia). *Journal of Life Science*, 9 (3), 2391-2397.
- Dilshad G. a. Ganjo nad EIa team (2008) Environmental Impact Assessment, (EIA) report, Deralok Hydropower project, Duhok/KRG-Iraq, Map. Com Company.
- European Commission (EC), Radiation Protection 112. (1999) Radiological Protection Principles Concerning the Natural Radioactivity of Building Materials, Directorate-General Environment, Nuclear Safety and Civil Protection.
- Fares S., Ashour A., El-Ashry M. and Abd El-Rahma M. (2012). Gamma Radiation Hazards and Risks Associated with Wastes from Granite Rock Cutting and Polishing Industries in Egypt. *Journal of* УДК, 1 (53), 64-73.
- ICRP, Annals of the ICRP. (1990). Recommendations of the International Commission on Radiological Protection, ICRP Publication 60, Oxford Pergamon Press, 1991.
- Laith A., Nada F. and Fouzey H. (2013). Measurement of Natural Radioactivity in Building Materials used in IRAQ. *Journal of Basic and Applied Sciences*, 7(1): 56-66.
- ICRP. 1994. Protection against Rn-222 at home and at work. No. 65; Ann. ICRP 23 (2), Pergamon, Oxford.
- Osimobi J., Avwiri G. and Agbalagba E. (2013). Evaluation of natural occurring radionuclide variation with lithology depth profile of Udi and Ezeagu local government area of Enugu state, Nigeria, Journal *of Engineering and Applied Sciences*, 4(3), 1-10.
- Okeyode I. and Oluseye A. (2010)Studies of the Terrestrial outdoor Gamma Dose Rate Levels in Ogun-Osun River Basins Development Authority Headquarters, Abeokuta, Nigeria. *Journal of Physics International*, 6 (1), 1-8.
- Okeyode I, and Akanni A. **(**2009). Determination of some physical parameters of Olumo rock, Abeokuta Ogun-State, Nigeria. *Journal of Science and Technology*. 2 (7), 6-10**.**
- Orgun Y**.,** Altənsoy N., Gultekin A., Karahan G. and Celebi N. (2005). Natural radioactivity levels in granitic plutons and groundwaters in Southeast part of Eskisehir, Turkey. *Journal of Appl. Radiat. Isot.*, 63, 267-275.
- Ramasamy V., Suresh G., Meenakshisundaram V. and Gajendran V.(2009). Evaluation of

Natural Radionuclide Content in River Sediments and Excess Lifetime Cancer Risk Due to Gamma Radioactivity. *Journal of Environmenal and Earth Sciences*, 1 (1), 6-10.
- Ramasamy V., Suresh G., Venkatachalapathy R., Ponnusamy V. and Meenakshisundaram V.(2010). Magnetic Susceptibility and Radiological Hazardous Nature of the River Sediments-Spectroscopical Approach. *Journal of Acta Physica Polonica*, 118 (4), 701-711.
- Rasheed M. and Kamal O. (2013). Measurement of Natural Radioactivity in Soil Collected from the Eastern of Sulaimany Governorate in Kurdistan–Region, Iraq. *Journal of Science and Technology*, 3 (7), 749-757.
- Rıdvan B., Hu¨seyin A. and Mustafa E. (2011). Radioactivity measurements and radiation dose assessments due to natural radiation in Karabu¨k (Turkey), *Journal of Radioanal Nucl. Chem*, 289, 297-302.
- Surinder S., Asha R. and Rakesh K (2005). ^{226}Ra, ^{232}Th and ^{40}K analysis in soil samples from some areas of Punjab and Himachal Pradesh, India using gamma ray spectrometry. *Journal of Radiat. Measurements*, 39, 431–439.
- Tzortzis M., Tsertos H., Christofider S., Christodoulides G. (2003). Gamma-ray measurements of naturally occurring radioactive samples from Cyprus characteristic geological rocks. *Journal of Radiat. Measurements*, 37, 221-229.
- Thabayneh K. and Jazzar M. (2012). Natural radioactivity levels and estimation of radiation exposure in environmental soil samples from Tulkarem province-Palestine. *Journal of soil science*, 2, 7-16.
- UNSCEAR. 2000. Sources and Effects of Ionizing Radiation. Report to General assembly, with Scientific Annexes, United Nations, New York.
- UNSCEAR. (1988). Sources Effects and Risk of Ionizing Radiation. United Nations Scientific Committee on the Effects of Atomic Radiation., New York.

الخطورة الإشعاعية الطبيعية للصخور في محافظة دهوك، اقليم كردستان، العراق

الخلاصة

أجرينا دراسة حول مدى تأثير الإشعاع في تسع عينات من الصخور الطبيعية التي تم جمعها من مناطق مختلفة في محافظة دهوك . تقع محافظة دهوك في إقليم كردستان في الشمال الغربي من العراق. تم قياس تركيزات النويدات المشعة في العينات الصخرية باستخدام (NaI(TI مطيافية اشعة كاما لمدة 30000 ثانية لكل عينة. ان معدل الفعالية النوعية للنويدات المشعة ذات قيم (13.10 , 5.20 , 134.32) Bqkg^{-1} لكل من النويدات الارضية(^{226}Ra , ^{232}Th , ^{40}K) على التوالي. الحجرالرمادي الطيني , الحجر الجيري , الرمل الرفيع, الطين الغريني و مارلي تظهرالنسبية تركيز نشاط عالية بينما في حالة الحجر الجيري الطباشيري تظهر انخفاضا بتركيز النشاط بينما كانت التكوينات الصخرية الأخرى معتدلة في مستوى النشاط الإشعاعي. قدرت مؤشرات الخطر و يزيد من مخاطر الاصابة بالسرطان مدى الحياة باستخدام الطريقة التحليلية القياسية. القيم التي تم الحصول عليها عن متوسط الجرعة الممتصة والمعدل السنوي للجرعة المكافئة (في الهواء الطلق وداخل) ، ومؤشرات الخطر (الخارجية والداخلية) ، يزيد خطر الاصابة بسرطان عمر ، مؤشرات (ألفا و كاما) و الراديوم يعادل على التوالي 14.88 nGyhr^{-1} , 18.26 μSvy^{-1} 73, μSvy^{-1} , , 0.12 , 0.084 0.064 × 10^{-3} , 0,115 , 0.07 و 31 Bqkg^{-1}. القيم، عندما قارنت بقيمهم الجائزة العالميا، تبين بأنها كانت تحت الحدود القياسية لتلك البيئات. الصخور من منطقة الدراسة لم تتعرض بشكل بما يؤثرعلى السكان ويمكن أَن تستعمل كمادة إنشائية بدون ان تشكيل أي تهديد أَو أذى إشعاعي إلى المستعملين لهذه المادة من العامة.

مەترسین تیشکێن سروشتی یێن کەڤرا ل پارێزگەها دهوکێ, هەرێما کوردستان ل عیراق

پوختە

دڤێ ڤەکولینێدا بزاڤ هاتیە کرن کارتێکرنا تیشکا نافۆکی بو نەهـ سمپلێن کەڤرێن سروسشتی ئەوێن هاتینە کومکرن ژ جهێن جێواز یێن پارێزگەها دهوکێ. پارێزگەها دهوکێ دکەڤیتە هەرێما کوردستانێ کو دکەڤیتە باکورێ روژئاڤایێ عێراقێ. هژمارتنا کارێگەریا جۆریا ناوکیدێن تیشکدەر دکەڤرێن دهوکێ داب هاریکاریا NaI(TI) شەبەنگبینێ تیشکا گاما هاتە ئەنجامدان بو ماوێ 30000 چرکا بو هەر سمپلەکێ پاراستی. تێکرایێ هژمارتنا کارێگەریا جۆریا ناوکیدێن تیشکدەر خوەدی بهایێن (134.32, 5.20, 13.10) $Bqkg^{-1}$ بو هەر ئێك ژ ناوکیدێن ئەردی (^{226}Ra , ^{232}Th, ^{40}K) لپەی ئێك. کەڤرێ رمادی تەقنی, کەڤرێ جیری, رەملا گر, تەقنا غەرینی ومارلی دیاربو رێژا کارێگەریا جۆری یابلند بو بەلی کەڤرێ جیریێ تەباشیری کو کێم بون دکارێگەریا جۆری دیاربو بەس پێکهاتنێن دی ژن کەڤرا یەکسان بون دکارێگەریا جۆری دا. بهایێ بدستڤەئینانا تێکرایێ قورچا وەرگرتی, تێکرایێ سالانە یێ قورچا یەکسانە (دەرەکی و نافخوی), نیشانا مەترسیا(دەرەکی و نافخوی), نیشانا زێدەبوونا مەترسیا توشبوونا شێرپەنجا ژیێ مروڤی, نیشانا (ئەلفا , گاما) و رادیوم وەکهەڤن لپەی ئێك 14.88 $nGyhr^{-1}$ 18.26 , μSvy^{-1} 73 ,μSvy^{-1} 0.084, 0.12 , 0.064 × 10^{3-} , 0,115 , 0.07 و31 $Bqkg^{-1}$. بهایێن بدستڤەئیناین هاتنە بەرەوارکرن دگەل هندەك بهایێن جیهانێ یت وەك هەڤ , کو دیار بو کێمتربون ژ ئاستێن باگراواندا تیشکدەرا وێ ژینگەهێ ل جیهانێ یارێ پێ دهێتە دان. کەڤرێن دڤێ ڤەکولینێ دا هیچ مەترسیێن هەژی گوتنێ لسەر ژیانا مروڤایەتیێ نینن ودشێن بکاربینن وەك کەرەستێن ئافاهیا بێکو هیچ گەفەك و مەترسیەکا تیشکی لسەر بکارهێنەرا بشێوەیەکێ گشتی هەبیت.

ANATOMICAL AND PALYNOLOGICAL STUDIES OF *Cissus Quadrangularis* AND *Cayratia Geniculata* (VITACEAE AND *Leea Angulata* (LEEACEAE)

CHNAR NAJMADDIN
Dept of Biology, Collage of Sciences, University of Salahaddin, Kurdistan Region-Iraq

(Received: May 4, 2014; Accepted for publication: August 19, 2014)

ABSTRACT

This study was conducted to evaluate anatomical comparison between three species belonging to two families (Vitaceae and Leeaceae). Two genera of the family Vitaceae (*Cissus quadrangularis* and *Cayratia geniculata*) and one species of Leeaceae family (*Leea angulata*) were investigated. Anatomically it has been shown that the shape of stem, petiole, midrib, margin and lamina were different. There were druses and raphid crystals in stem, petiole, midrib, margin of *Cissus quadrangularis* and *Cayratia geniculata*, however, in *Leea angulata* there was only druses crystals, except in lamina of *Cissus quadrangularis*, *Cayratia geniculata* and *Leea angulata* in which there were druses and raphid crystals. Leaf epidermis of *Cissus quadrangularis*, *Cayratia geniculata* and *Leea angulata* were investigated by using light microscope and scanning electron microscope. The shapes of leaf epidermal cells were usually polygonal; the types of anticlinal walls are straight and arched. The stomatal apparatus presented on the both side of the leaf (abaxial and adaxial). *Cissus quadrangularis* and *Cayratia geniculata* had different types of stomatal apparatus such as cyclocytic and hemiparacytic, and *Leea angulata* had anisocytic type.

KEY WORDS: Vitaceae, Leeaceae, Cissus quadrangularis, Cayratia geniculata, Leea angulata, stomata types.

INTRODUCTION

Vitaceae family includes woody climbers, sometimes vines, trees, and also involve shrubs and succulents (Timmons *et al*., 2007; Najmaddin, 2011 a,c). *Cissus quadrangularis* is climbing herb, excluding wings, fleshy, quadrangular with wings at the angles, broad, glabrous or pubescent; tendrils present and frequently leafless. The leaves are simple, fleshy and glabrous or sparingly pubescent and leaf-opposed cyme. The few flowered, cymes axillary, fruits are red when ripe and seeds are smooth with single dorsal crest (Wild and Drummond, 1966; Valkenburg and Bunyapraphtsara, 2002). *Cayratia geniculata* is woody, branches terete, slightly flattened, pubescent; tendrils bifurcate. The leaves are trifoliolate, fruits are berry nearly globose and semiglobose seeds (Valkenburg and Bunyapraphtsara, 2002; Lian-Mei, 2007).

Leeaceae includes shrubs, stem is unarmed, tendrils absent (Wen, 2007). *Leea angulata* is a weak strangler and bushy shrub. The leaves are pinnate with numerous leaflets and bearing greenish-white flowers that developed into lead-grey berries (Lok *et al*., 2011).

The stomata apertures in the epidermis, bounded by two guard cells, their main function is to allow gases as carbone dioxide, water vapours and oxygen to move rapidly into and out of the leaf (Perveen *et al.* 2007; Tay and Furukawa 2008; Najmaddin 2011 b, c). On the basis of arrangement of the epidermal cell neighbouring the guard cell (subsidary cells), more than 25 main types of stomata in dicots have been recognized (Perveen *et al*, 2007).

MATERIALS AND METHODS

Plant materials were collected from the field in Malaysia (UKM) and fixed in a mixture of formalin, alcohol and glacial acetic acid (Fathulla and Duhoky, 2008). Transverse sections through the middle region of petioles and midribs were made on the sliding microtome (Richard Jung or Leica Histolide 200) and stained in Safranin and Alcian Green. Following dehydration in an alcohol series the sections were mounted in Euparal (Johansen, 1940). Images were captured using a Video Camera (JVC) attached to a leica diaplan microscope using analysis docu software. Epidermal peels were prepared by mechanical scraping stained, dehydrated and mounted on the same way. For pollen morphological studies, the pollens

gathered from open flowers or mature flower buds and prepared for light microscope (LM) by methods described by Erdtman (1952) and were washed three times with phosphate buffer solution (PBS) 85%, the samples later dehydrated using series of aceton concentration percentages ranging from 50, 70, 80, 85, 90, 95% and three times in 100% aceton for 30min each, dried at critical point, coated with gold in a sputter coater and were observed under a Philips XL30 Scanning Electron Microscope (SEM), at 10 to 20 KV according to magnification requirements.

RESULTS

Anatomical description

T.S stems

In Vitaceae the outline in TS is different between species. It varies from adaxial and abaxial surfaces with long lateral projections adaxially and abaxially as in *Cissus quadrangularis* (A) to subcircular as in *Cayratia geniculata* (B) while in *Leea angulata* (D) is rounded. Collenchyma cells are present in the cortex beneath the epidermis in *Cayratia geniculata* and *Leea angulata*, while in *Cayratia geniculata* collenchyma cells exist below five layers of parenchyma cells. Secretory canals and druses are present in all genera. Trichomes are present in *Cayratia geniculata* and are multicellular non-glandular (Figure 1).

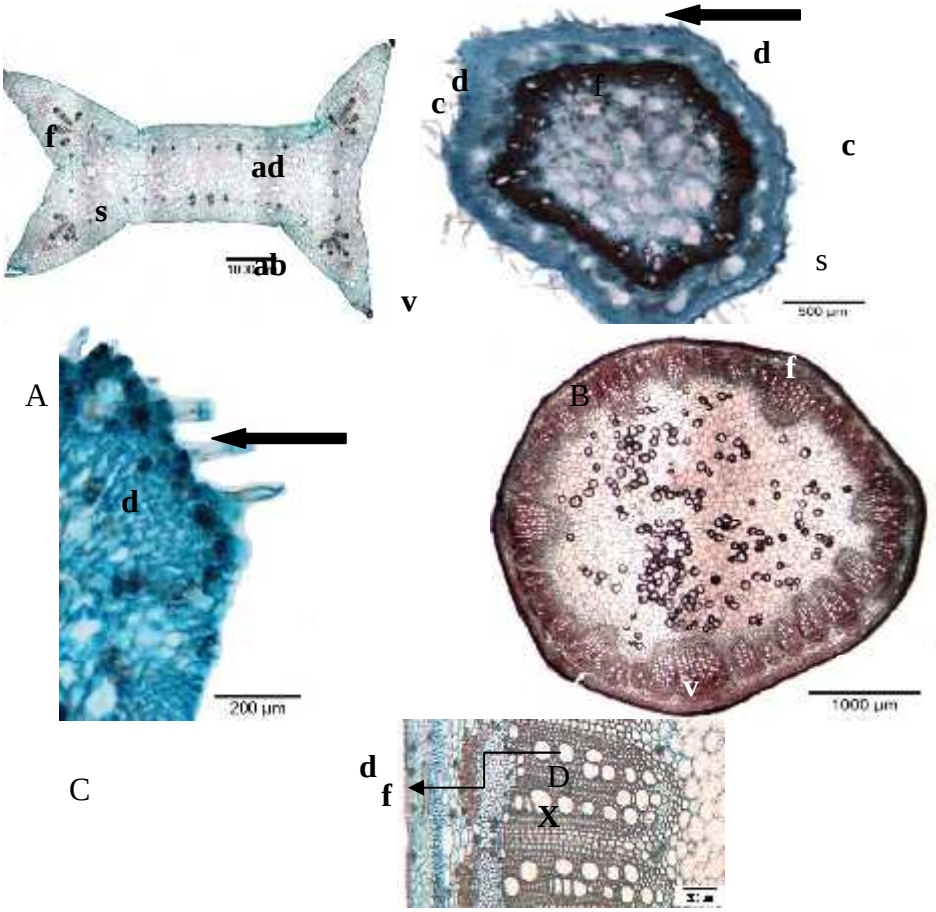

Fig. (1): TS of stems: A. *Cissus quadrangularis*, B. *Cayratia geniculata*, C. TS of *Cayratia geniculata* stem showing trichomes, D. *Leea angulata*, E. vascular bundle, s: secretory canal, d: druses, c: collenchyma cells, f: fibres, v: vascular bundles, trichomes (large black arrow), ad: adaxial surface, ab: abaxial surface, phloem (irregular small black arrow), x: xylem.

T.S petioles

Collenchyma cells present in the cortex beneath the epidermis in *Cayratia geniculata* (B) and *Leea angulata* (D), while in *Cissus quadrangularis* (A) collenchyma cells exist below five layers of parenchyma cells. Druses are present in the cortex, near vascular bundle and pith. The arrangement of vascular tissue system is closed and a fibrous layer occurs next to the phloem tissue which is present in both genera. Secretory cells are present, accessory vascular bundles are present in *Leea angulata* (B) but absent in *Cissus quadrangularis* (A) and *Cayratia geniculata* (B). Trichomes are present in *Cayratia geniculata* and are multicellular non-glandular (Figure 2).

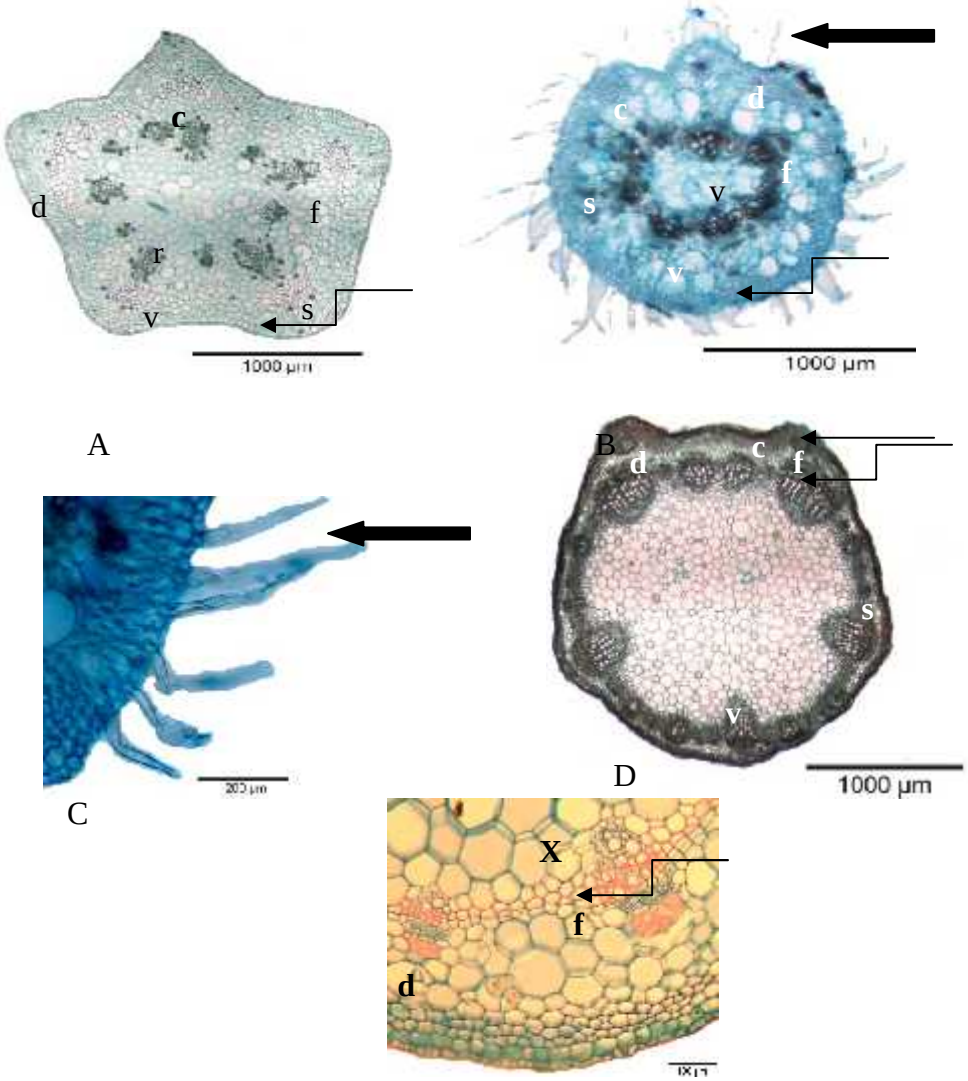

Fig. (2): TS of petioles: A. *Cissus quadrangularis*, B. *Cayratia geniculata*, C. TS of *Cayratia geniculata* petiole showing trichomes, D. *Leea angulata*, E. vascular bundle, s: secretory canal, d: druses, r: raphides, c: collenchyma cells, f: fibres, v: vascular bundles, trichomes (large black arrow), accessory vascular bundle (small black arrow), phloem (irregular small black arrow), X: xylem.

T.S midrib

The arrangement of midrib vascular tissue system is closed and a fibrous layer occurs next to the phloem tissue which is present in both genera. Secretory cells are present in the cortex. Collenchyma cells are present in the cortex beneath the epidermis. Trichomes are present in *Cayratia geniculata* (B) which are simple multicellular non-glandular. Druses are present in the cortex, near the vascular bundle and the pith (Figure 3).

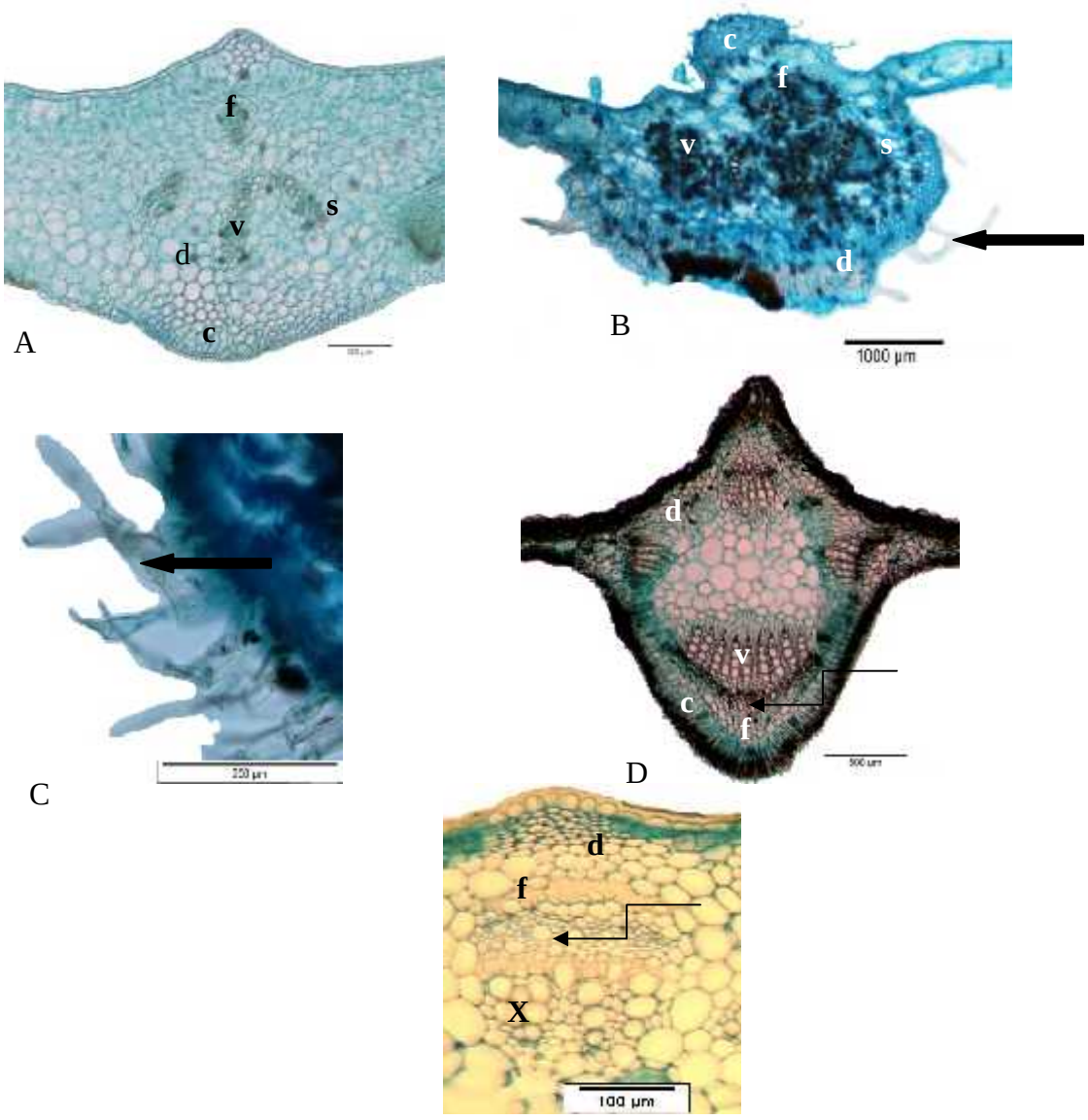

Fig. (3): TS of midrib: A. *Cissus quadrangularis*, B. *Cayratia geniculata*, C. TS of *Cayratia geniculata* midrib showing trichomes, D. *Leea angulata*, E: vascular bundle, s: secretory canal, d: druses, c: collenchyma cells, f: fibres, v: vascular bundles, trichomes (large black arrow), phloem (irregular small black arrow), X: xylem.

T.S lamina

In all species the palisade consists of two layers of cells; both raphides and druses are present while only raphides are present in the spongy mesophyll layer. Trichomes are present in *Cayratia geniculata* (B) which are simple and glandular multicellular (Figure 4).

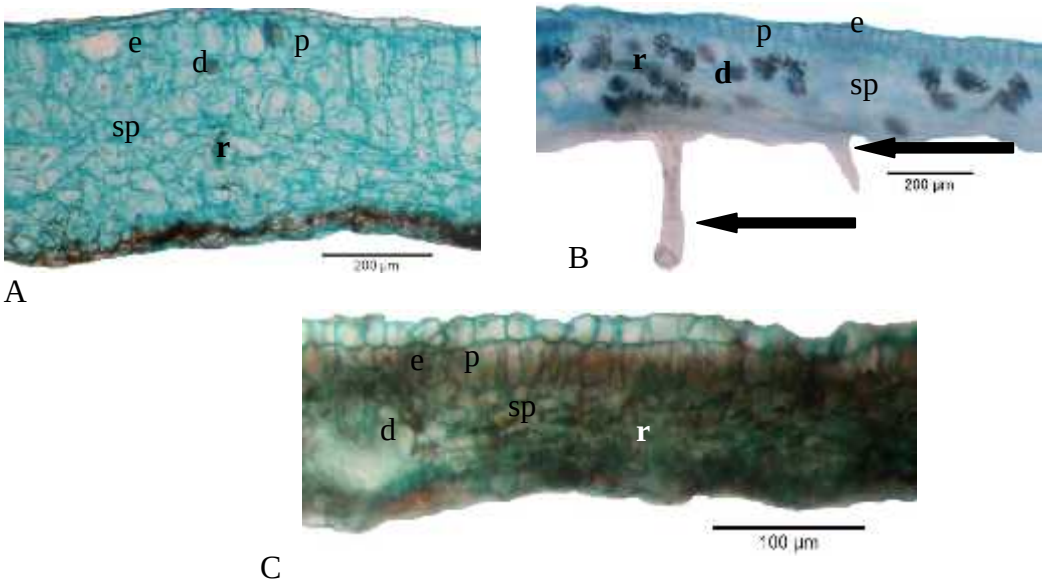

Fig. (4): TS of lamina: A. *Cissus quadrangularis*, B. *Cayratia geniculata*, C. *Leea angulata*, d: druses, r: raphides, e: epidermis, p: palisade layer, sp: spongy layer, trichomes (large black arrow).

T.S margin

The shape of the margin is straight in *Cissus quadrangularis* (A), pointing slightly downwards in *Cayratia geniculata* (B) and rounded pointing downwards in *Leea angulata* (D). Trichomes are present in *Cayratia geniculata* (B) which are simple multicellular non-glandular (Figure 5).

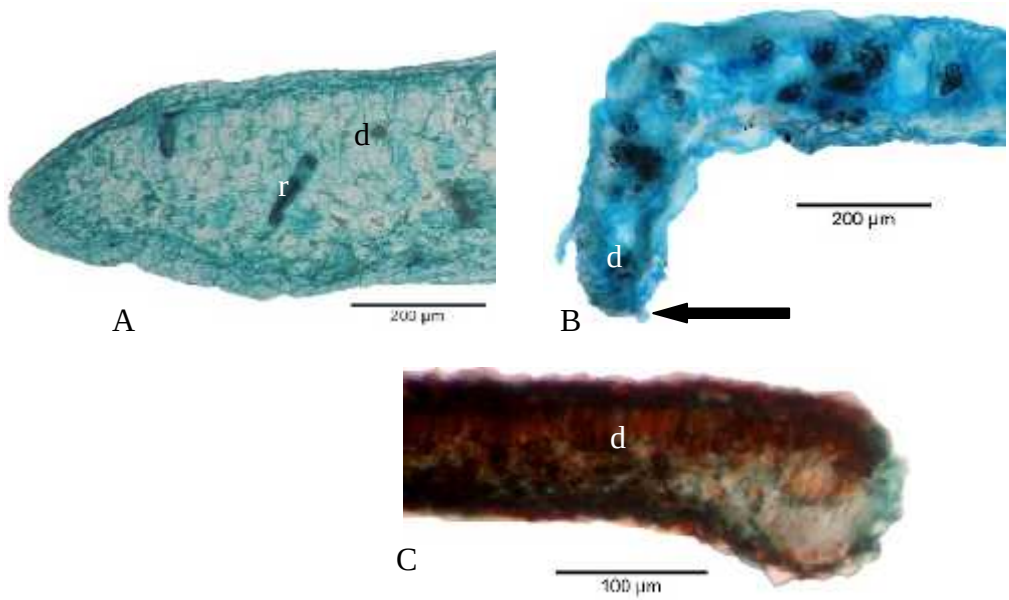

Fig. (5): TS of margin: A. *Cissus quadrangularis*, B. *Cayratia geniculata*, C *Leea angulata*, d: druses, r: raphides, e: epidermis, trichomes (large black arrow).

Stomata

The cuticle is striate (striped or granular) depending on the species. Adaxial anticlinal walls are straight or straight to wavy. The abaxial anticlinal wall is straight or straight to wavy; stomata are present in some species adaxially as in *Cissus quadrangularis* and *Leea angulata*. Stomata are cyclocytic (A,B,C), hemiparacytic (D,E,F) in Vitaceae and anisocytic in *Leea* (G,H) (Figure 6).

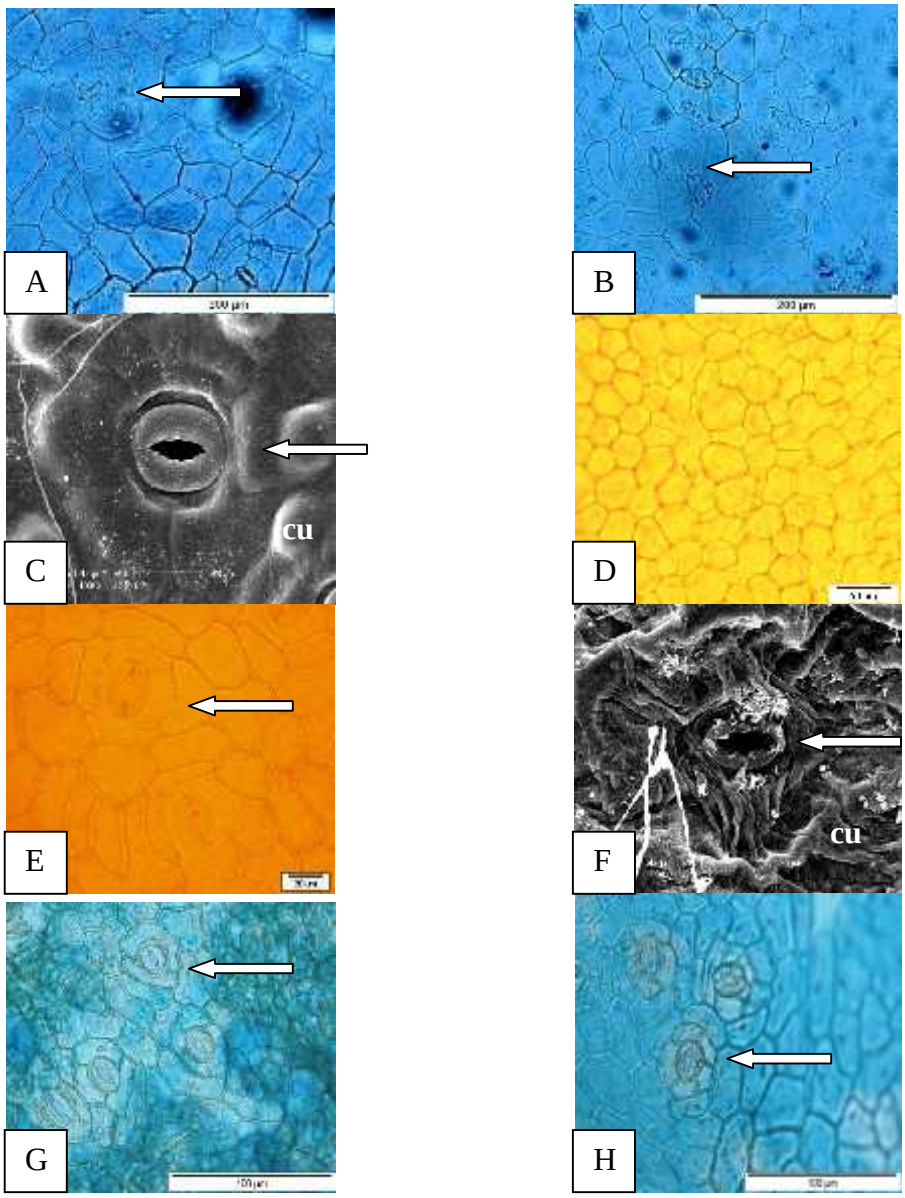

Fig. (6): leaf abaxial and adaxial surface showing the stomata and the cuticle layer. A. *Cissus quadrangularis* LM of adaxial epidermis, B. *Cissus quadrangularis* LM of abaxial epidermis, C. *Cissus quadrangularis* SEM of abaxial epidermis, D. *Cayratia geniculata* LM of adaxial, E. *Cayratia geniculata* LM of abaxial epidermis, F. *Cayratia geniculata* SEM of abaxial epidermis, G. *Leea angulata* LM of adaxial epidermis, H. *Leea angulata* LM of abaxial epidermis, stomata (large white arrow), cu: cuticle layer.

Flower: Flowers are hermaphroditic, calyx-5, petal-5. In Leeaceae petals or corolla at the base fused with stamen (C,D), while in Vitaceae the petals are free (A,B) (Figure 7).

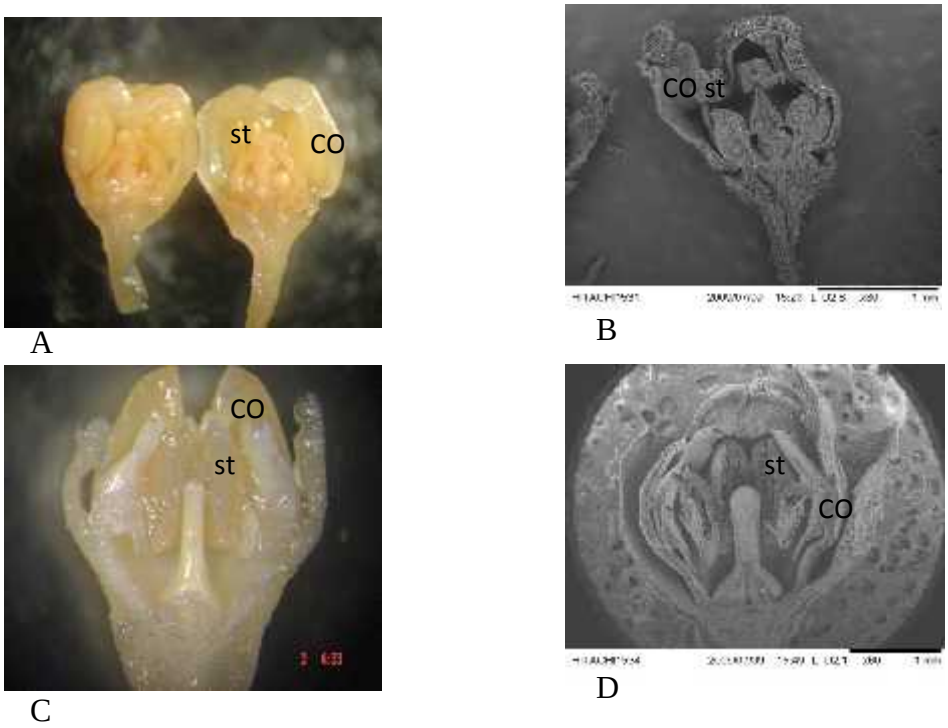

Fig. (7): flowers. A and B. Vitaceae flower, C and D. Leeaceae flower, CO: corolla, st: stamen

Pollen grains

Vitaceae pollen grains are tricolpate. The shape in equatorial view prolate as in *Cissus quadrangularis* and *Cayratia geniculata* (A,B,C), while in *Leea angulata* pollen grain tricolporate and equatorial view is triangular (D,E) (Figure 8). The shape, aperture, size and sculpture ornamentation of the pollen grains are good characters for differentiating between the genera as shown in the (Table 1).

in Vitaceae the pollen grains are circular in polar view and prolate in equatorial view as in *Cissus quadrangularis* (A) and circular in polar view and subprolate in equatorial view as in *Cayratia geniculata* (B,C), while in *Leea angulata* (D,E) the shape of the grain is trigonal in equatorial view and subprolate in polar view however, the size varies between genera e.g *Cayratia geniculata* pollen is bigger (0.781µm) than *Cissus quadrangularis* (0.659µm) and the porus is absent, while in *Leea angulata* the size is (1.087µm) and the porus or pore is present. There are certain characters present in certain species only such as the clava which is a long exine element more than 1 µm in diameter in *Cissus quadrangularis* (A).

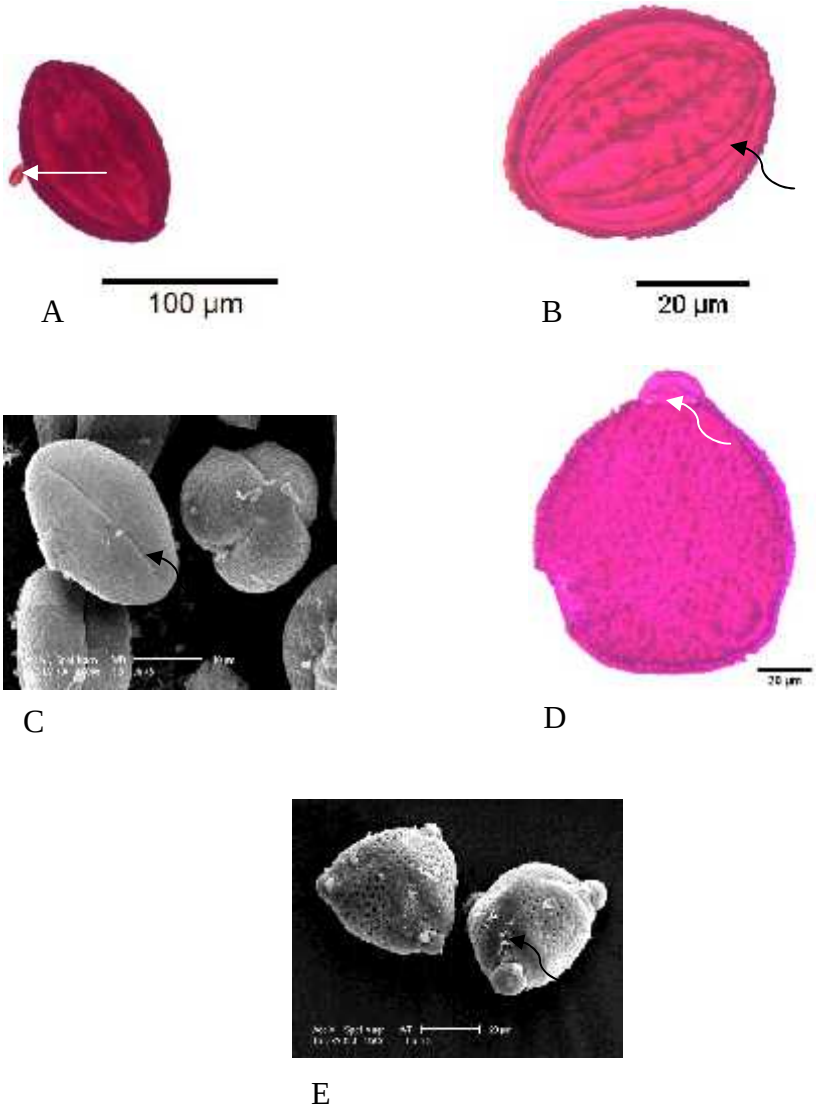

Fig. (8): Pollen grains. A. equatorial view of *Cissus quadrangularis* (LM), B. equatorial view of *Cayratia geniculata* (LM), C. polar and equatorial view of *Cayratia geniculata* (SEM), D. equatorial view of *Leea angulata* (LM), E. polar and equatorial view of *Leea angulata* (SEM), colpus (irrigular black arrow), porus (irrigular white arrow) .

Table (1): Pollen grains feature

Species	Polar view	Equatorial view	P/E	Porus	Clava
Cissus quadrangularis	circular	prolate	0.659	absent	present
Cayratia geniculata	circular	subprolate	0.781	absent	absent
Leea angulata	subprolate	trigonal	1.087	present	absent

DISCUSSION

The results of the present investigation showed that both Vitaceae and Leeaceae possess a few common characters such as the presence of druses and secretory cells as has been reported by Metcalfe and Chalk (1950). According to them the secretory cells with amorphous contents which are probably mucilaginous and tanniniferous are widely distributed in the parenchymatous tissues, and has also been found in *Leea angulata*, *Vitis vinifera* and probably in other genera and species. Both families have the closed vascular tissue system. When comparing

species based on a particular organ though, certain characters may be useful in confirming the species. The presence or absence of raphides in the stems, petioles midribs and lamina, raphides and druses in parenchymatous cells observed near the vascular bundle, beneath the epidermis as well as in the pith of stems are characteristic of the Vitaceae. In Leeaceae they are only present in the lamina. Raphides, however, have also been observed in the mesophyll tissue in the Leeaceae, as reported by Metcalfe and Chalk (1950) and Wen (2007).

The outlines of the stems and petioles as well as the pattern of vascular bundle arrangement differ between species and between both families. The present investigation revealed that the stem and petiole of Vitaceae and Leeaceae vary in shapes. The structure of the stem and petiole thus provides some useful characters for use in the identification of species. The presence of accessory vascular bundles in *Leea angulata* and absence in *Cissus quadrangularis* and *Cayratia geniculata*. According to Metcalfe and Chalk (1950) the petiole in transverse sections, exhibit a ring of isolated bundles, accompanied by two or less, cortical bundles on either side of the groove in the adaxial surface of the petiole in some species of *Vitis*, *Leea* and *Tetrastigma.*

Trichomes occur on the nodes and/or internodes of *Vitis berlandieri* and *Vitis rupestris* especially *Vitis riparia* and *Vitis rupestris* (Swanepoel 1984). Based on this Swanepoel (1984) constructed a key partly based on the presence of different trichome types on the shoot of 33 species of *Vitis* species. According to Lombardi (2007), glandular or nonglandular trichomes in Vitaceae are commonly present. They are very important for species identification, while Metcalfe and Chalk (1950) reported the trichomes to be unicellular 2-armed with or without stalks, notably in certain species of *Cissus*. These studies showed that simple multicellular non-glandular and glandular trichomes are present in Cayratia geniculata provide additional characters for identification. Trichome morphology when combined with other characters this character is can be helpful for identifying the species.

Mechanical collenchyma tissues in the stem, petiole and midrib were observed. The present investigation revealed that the stem and petioles of *Cissus quadrangularis*, *Cayratia geniculata* and *Leea angulata*. The vascular bundle is closed, a fibrous layer occurs next to the phloem tissue and secretory cells there are present in both families.

The present study further revealed that the midribs are characteristics by the outline of the adaxial surface which is slightly humped and arc to subcircular shape surface of the abaxial and the presence of collenchyma in both epidermis layers, while in *Leea angulata* the midrib is characteristic by the outline of the adaxial surface which is long humped by "V" shape surface of the abaxial and the presence of collenchyma in both epidermis layers. The vascular bundle is closed and the druses and raphides are present in Vitaceae and absent in *Leea*, while in *Leea* the raphides only present in lamina. However, the present study showed that the margin of the species were straight and slightly downwards with rounded or tapering tip. The druses and secretory cells are present. In addition, mesophyll layer contains calcium oxalate (druses) crystals and mucilage cells or secretory cells with raphides in bundle. Similary, this has also be reported in a study by Metcalfe and Chalk (1950), mucilaginous idioblasts in the mesophyll of leaf and cortex of the stem which was absent in the epidermis (Kannabiran and Pragasam, 1994).

The petiole, midrib, margin and lamina outline of these sections is smooth, while in *Cayratia geniculata* the trichomes are present and multicellular glandular and non glandular which is an important feature in determining the cultivars. The trichome complement of a particular organ can consist entirely of unbranched or branched hairs (Lombardi, 2007).

Vitaceae leaf epidermal characters have been studied by Ren *et al*. (2003) using light and scan electron microscope. The shape of leaf epidermal cells was irregular or polygonal; the anticlinal walls are straight, arched or sinuolate which are in conformity with the leaf epidermal cell of the present study. However, the present study reveals that leaf epidermis has anomocytic and are in conformity with Ren *et al*. (2003); Kannabiran and Pragasam (1994).

The flower of *Vitis* sp. has complex organ, arranged between 4 to 5 mm, bisexual, 5-numerous, pedicels mostly umbellate clustered (Townsend and Guest, 1980 and Al-Saady, 1982). However, the symmetry of the flower is pentamerous while Ampelopsis, *Cayratia* and *Cissus* have tetramerous flowers; herefore, they may have closely related features (Patil, 1998). *Vitaceae stenopalynous* in nature and is characterized by three colporate grains.

However, sufficient variation is found between pollen shape class and exine pattern. Base on this features the family divided into three pollen types, *V. parvifolia* type, *V. jacqumontii* and *Ampelopsis vitifolia* subsp., *hazaraganjiensis* type (Perveen and Qaiser, 2008). The shape and aperture of the pollen grains are good characters for differentiating between the genera in the Vitaceae as shown in the Table 1, in Vitaceae the pollen grains are prolate, while in Leeaceae are triangular. Intergeneric variations in the pollen structure have been observed in many other families. The pollen grains of the species were studied using scan electron microscope which show Vitaceae pollen grains consist of isopolar and tricolporate, and mostly sub-prolate or prolate to prolatespheroidal (Perveen and Qaiser, 2008; Marasali *et al*., 2005; Inceoglu *et al.*, 2000), exine foveolate-rugulate at the mesocolpia and distincly reticulate towards the poles and at the poles (Inceoglu *et al*., 2000). Pollen grains of the grapevine have been reported to be normally three zoncolporate, spheroidal to prolate with very long, narrow, slightly slit but distinctly sunken ectoaperture or colpus (Gallardo *et al*,. 2009 and Maria *et al*,. 1994 and Inceogul *et al*,. 2000). The colpi in the equatorial zone they are usually wide and deep, while in the polar zone they are narrower (Roytchev *et al*. 1994) and the exine is reticulate (Erdtman, 1952). The pollen grains in *Leea* species are triangular in shape and tricolporate. Patil (1998) used the pollen grain characters to isolate the position of *Leea* to a separate family Leeaceae.

CONCLUSIONS

The anatomical evaluation of the species of Vitacece was reported. The result shows that druses and raphid crystals were present in Vitaceae, while raphides were present in *Leea* only in lamina. Leaf epidermal cells in Vitaceae were straight or straight to wavy; stomata are present in some species adaxially as in *Cissus quadrangularis* and *Leea angulata*. Stomata are cyclocytic, hemiparacytic in Vitaceae and anisocytic in *Leea*. The trichomes were present in epidermis in *Cayratia geniculata*. Vitaceae pollen grains are tricolpate. The shape in equatorial view prolate as in *Cissus quadrangularis* and *Cayratia geniculata*, while in *Leea angulata* pollen grain tricolporate and equatorial view is triangular.

ACKNOWLEDGEMENTS

I would like to express my gratitude and sincere thanks to all who help me to complete this research.

REFERENCES

- Al-Saadi, I.H.M. (1982). Cultivation and Production of the grapevine. Mausel, Iraq: published in Ministry of Higher education and Scientific Research, Mausel University.
- Erdtman, G. (1952). Pollen morphology and plant taxonomy. Angiosperm (An introduction to palynology. I), stockholm: Almqvist and Wiksells.
- Fathulla, C.N. and Duhoky, M.M.S. (2008). Biological and anatomical study of different *Cuscuta* species. 1st Kurdistan Conference on Biological Sciences, Jur. Doh. Univ., 11(1): 22-39.
- Gallardo, A., Ocete, R., Lopez, M.A., Lara, M. and Rivera, D. (2009). Assessment of pollen dimorphism in populations o*f Vitis vinifera* L. subsp. *sylvestris* (Gmelin) Hegi in Spain. Vitis, 48 (2):59-62.
- Inceogul, O., Pinar, N.M. and Oybank-Donmez, E. (2000). Pollen Morphology of wild *Vitis sylvestris* Gmelin (Vitaceae). Tur. Jou. of Bot., 24:147-150.
- Johansen, D.A. (1940). Plant microtechnique. New Yourk: MC Graw,Hill.
- Kannabiran, B. and Pragasam, A. (1994). Foliar epidermal features of Vitaceae and taxonomic position of *Leea*. Jou. of In. Bot. Soc., 73: 81-87.
- Lian-Meri, X.Q.W. 2007. *Cayratia geniculata*. Flora of China Vol. 12:184, 345.
- Lok, A.F.S.L., Ang, W.F., Ng, B.Y.Q., Suen, S.M., Yeo, C.K., and Tan, H.T.W. (2011). *Leea* L. (Vitaceae) of Singapore. Nat. In Sing., 4:55-71.
- Lombardi, J. A. (2007). Systematic of Vitaceae in South America. Can. Jou. Bot., 85, p: 712- 721.
- Marasali, B., Pinar, M. and Buyukkartal, N. (2005). Palynological study on the pollen grains of selected Turkish grape (*Vitis vinifera* L.) cultivars. Tur. Jou. of Agri. and For., 29:75-81.
- Maria, F.C.S.S., Villota, P.D.L. and Tortola, M.E.T. (1994). Palynological study of the pollen grain of *Vitis vinifera* L. cultivars. Some aspects of sculpturing and pollination. Vitis, 33:57-61.
- Metcalfe, C.R., and Chalk, L. (1950). Anatomy of the dicotyledons. Clarendon Press, Oxford. Vol. 2: 413-419.
- Najmaddin, C., Hussin, K. and Maideen, H. (2011a). Comparative Anatomical Study between *Cayratia mollissima*, *Pterisanthe,s caudigera* (Vitaceae) and *Leea indica* (Leeaceae). Ame. Jou. App. Sc., 8 (9): 839-842.
- Najmaddin, C., Hussin, K. and Maideen, H. (2011b). Comparative study on the anatomy and palynology of the three variety of *Vitis vinifera*

(family Vitaceae). Afr. Jou. Biot.,10 (74):16866-16874.

- Najmaddin, C., Hussin, K. and Maideen, H. (2011c). Anatomical comparison between *Cissus repens*, *Cayratia japonica* (Vitaceae) and *Leea aequata* (Leeaceae). Jou. Duh. Uni., 14 (1):290-298.

- Patil, S.G. (1998). Inter-generic variations in pollen grains of the family Vitaceae and their taxonomic significance. Jou. of the Ind. Bot. Soc., 77:99-102.

- Perveen, A., Abid, R. and Fatima, R. (2007). Stomatal types of some dicots within flora of Karachi, Pakistan. Pak. J. Bot., 39(4): 1017-1023.

- Perveen, A. and Qaiser, M. (2008). Pollen flora of Pakistan-LVII. Vitaceae. Pak. Jou.of Bot., 40 (2): 501- 506.

- Ren, H., Pan, K-Y., Chen, Z-D. and Ren-QingWang, R-Q. (2003). Structural characters of leaf epidermis and their systematic significance in Vitaceae. Acta Phyto.taxo. Sin., 41 (6): 531-544.

- Roytchev, V., Terziisky, D., Dimova, D. and Karageorgiev, S. (1994). Scanning electron microscopy study of pollen morphology in seedless grape (*Vitis vinifera* L.) cultivars. Vitis, 33:105-108.

- Swanepoel, J.J., Delaharpe, A.C., and Orffer, C.J. (1984). A Comparative anatomical study of the grapevine shoot: I epidermis. Sou. Afri. Jou. Eno. and Viti., 5 (2):51-57.

- Tay, A., and Furukawa,A. (2008). Variations in leaf stomata density and distribution of 53 Vine species in Japan. Plant species Biology 23, 2-8.

- Timmons, S.A., Posluszny, U. and Gerrath, J.M. (2007). Morphological and anatomical development in the Vitaceae. X. Comparative ontogeny and phylogenetic implications of *Cissus quadrangularis* L. Can. J. Bot., Vol. 85: 860-872.

- Townsend, C.C. and Guest, E. (1980). Flora of Iraq part 1 ed. Baghdad, Iraq: Ministry of Agriculture and Agrarian Reform of Iraq. Vol. 4. pp. 443-450.

Valkenburg, J.L.C.H.V. and Bunyapraphatsara, N. (2002). Plant Resources of South-East Asia. Medicinal and poisonous plants 2. Bogor, Indonesia: Prosea Foundation, Bogor, Indonesia 2 ed. Vol. 12. pp. 439-230.

- Wen, J. (2007). The Families and Genera of Vascular Plants; Leeaceae. Leeaceae Dumortier, Anal. Fam. Pl.: 27 (1829), nom. Cons. Springer-verlag Berlin Heidelberg Vol.9. p. 221- 225.

- Wild, H., and Drummond, R.B. (1966). Vitaceae. Flora zambesiaca Vol 2,2.

CONCRETE SURFACE SEALANTS: A COMPARATIVE STUDY

KHALID **M.S**HAHEEN and **L**EENA **J**.**S**EDEEQ
Dept. of Building & Construction Technology Engineering Technical College, Mosul-Iraq

(Received: June 4, 2014; Accepted for publication: October 12, 2014)

ABSTRACT

This study investigates the ability of reducing water absorption of concrete surfaces by using powdered one component acrylic and tar epoxy. The effect of these waterproofing materials on concrete properties such as splitting, flexural strength was also studied. The mixing ratio of powdered one component acrylic to water of 1.5:1, and The mixing ratio of tar: epoxy of1:1, both achieved 100% waterproofing for the concrete surfaces. Maximum splitting and flexural strength were also obtained at these mixing ratios for the indicated materials. The influence of acidic solutions on the waterproofing materials was also studied.

KEYWORDS: Acrylic Coatings, Tar Epoxy, Initial Surface Absorption.

INTRODUCATION

Like any other material, concrete is subject to deterioration due to different factors. Among the factors leading to the deterioration of concrete structures are: fire events, humidity, water absorption, concrete porosity, corrosion of reinforcement, and climatic conditions, especially acid rain. It is essential that concrete be capable of withstanding the conditions for which it has been designed through the life of the structure without significant deterioration[1]. Water ingress is an important factor that enhances deterioration of concrete [2]. The surface of the concrete is the first line of defence against the ingress of water and aggressive agents into the concrete. There is an increasing awareness to this subject due to its serious consequences on mechanical properties of the concrete and performance of the related structures. One laboratory test that is usually used in evaluating the magnitude of water ingress into concrete is the initial surface absorption test (ISAT). The details of the test are presented in B.S. 1881: Part 5: 1970, [3].Prolonging the service life of concrete structures through the use of waterproof coatings has been emphasized [4, 5]. Also the performance of the coated concrete against chemically aggressive environments is generally better than the performance of the uncoated concrete [6]. This paper focuses on the effectiveness of powdered one component acrylic of different mixing ratios with water and different mixing ratios of tar: epoxy on water absorption of concrete surface. The effects of powdered one component acrylic coating and tar: epoxy on the flexural and splitting strength were also investigated and the degree of their affectedness by action of acidic solution.

METHODOLOGY

Fabricating The Isat Apparatus:

The first step in the experimental work was the fabrication of an apparatus for initial surface absorption test, shown in (Figure1), The apparatus was fabricated by the researchers according to British Standard BS 1881: Parts 5:1970 [3].

MATERIALS

The Concrete Mix Ingredients:

Coarse Aggregate: The coarse aggregate used was river bed gravel obtained from the Tigris river (Mosul/Iraq). The maximum aggregate size used was 20 mm. Table 1 shows the sieve analysis of the gravel according to the Iraqi Standard Specifications No.45/1984 [7].

Table (1): Sieve Analysis of Gravel

Sieve Size .S.(mm)	Weight Passing (%)	Total limits (Iraqi Standard Specification No.45/1984)
20	100	95-100
10	43	30-60
5	0.5	0-10

Fine Aggregate (Sand): The sand used in this study was natural sand supplied from Kanhash

region (Mosul). This type of sand conforms to the Iraqi Standard Specifications No.45/ 1984 limits [7], as shown in Table 2.

Table (2): Sieve Analysis of the Sand

Sieve Size B.S.	Weight Passing(%)	Total limits (Iraqi Standard Specification No.45/1984)
4.75 mm	100	90-100
2.36 mm	81	75-100
1.18 mm	66	55-90
600µ	52	35-59
300µ	24	8-30
150µ	7	0-10

Cement: Ordinary Portland cement produced by Badoosh Factory (Mosul) was used as the binding material. Table 3 shows the Chemical composition of the cement used [8]

Table (3): The Chemical composition of the cement used

Main Oxide	Cao	Sio2	Fe2o3	Al2o3	So3	Mgo
%	62.2	21.31	2.67	5.89	2.6	3.62
Iraqi Standard Specification No.5/1984	—	—	—	—	Max. 2.8%	Max. 5%

Water: Potable water was used in this study for both mixing and curing.

COATING MATERIALS:

The Primer:. It is a liquid agent used to improve the property of adhesion of the top layer of cement concrete surface. It is usually applied to the surface by a normal brush, a roller brush or by a sprayer. The concrete surface has to be free from oil, grease, dust, and any foreign materials before applying the prime. In order to avoid separation of the coating. Each coating used in this study has a specific Primer to be used with it, Figures2 and 3 show the primer used in this study.

Powdered One Component Acrylic: It is a water soluble powder used with different dissolution ratios. The powder and the water are mixed together until a homogenous mixture is obtained. Figure 4 shows the one component acrylic (Powder).

Tar Epoxy: Tar epoxy is generally an amine or polyamide epoxy modified with tar pitch resin to produce a high-build film that has good chemical resistance and excellent water resistance.

Table (4): Technical Data Sheet for Waterproofing Materials

Materials	Physical Properties					
	Color	Tensile strength (MPa)	Shelf life (Months)	Viscosity (Cp)	Specific Gravity (gm/cm3)	Elongation %
Powder One Component acrylic	gray	43	24	2500-3500	1.7 -1.9	218
Tar Epoxy	black	60	24	2150-3100	1.5-1.7	360

Concrete Mix Proportions: A predetermined compressive strength of 35 MPa was decided for the resulting concrete at the age of 28 days. Accordingly, the mix proportions obtained through the British mix design method were (1: 1.92: 2.95) with w/c of 0.47. The cement content of the mix was 380 Kg/m^3.

Mixing, Casting, and Curing of Concrete Specimens:A mechanical tilting mixer of a capacity of 134 liters was used for mixing the ingredients of the concrete. The interior surface of the mixer was cleaned and moistened before placing the materials. Mixing and casting were carried on according to ASTM C192 [9].Curing was accomplished according to ASTM C511 [10].Normal structural concrete will be used in this investigation.

Preparation of Concrete Specimens Surface:
The service life of a coating depends on the degree of surface preparation achieved as much as it depends on application [11]. Preparation of the specimens surface involves cleaning of the surface, removal of ridges and then drying of the

surface to be coated. Drying the sample to be coated is a very important step because the moisture will prevent adhesion of the coating to the surface.

Application of Coatings:

Application of Primer: After preparing of \\ coated with a layer of primer that is used with coatings using a roller brush

Application of Powdered One Component Acrylic coating: Different ratios of water and powdered acrylic were mixed together until a homogeneous mixture was obtained. The coating was then applied on the concrete surface using a roller brush and pinlevler.

Tar Epoxy: Here again the surfaces of specimens were prepared and coated with the specific primer that was used in case of tar based materials. The tar was mixed with epoxy until the homogeneous mixture was obtained. Then, the surface was coated with a layer of the mixture also using a roller and pinleveler. The two mixing ratios of tar: epoxy used are 1:0.5 and 1:1.Table 4 shows the specifications of coating of the concrete specimens and the given symbol to each type of coating.

Table 5: Coating specifications of the concrete specimens

Specimens	Description
A	Specimens of concrete without coating
B	Specimens of concrete coated with powdered one component acrylic in mixing with water is 1:1
C	Specimens of concrete coated with powdered one component acrylic in mixing with water is 1.5:1
D	Specimens of concrete coated with tar: epoxy with ratio1:0.5
E	Specimens of concrete coated with tar: epoxy with ratio1:1

The Testing Procedure: The tests performed on the concrete specimens a long with the related standards are given in Table 5. In each test three specimens were used and the average value was calculated.

Table (6): The tests performed on the concrete specimens

Test	Shape and dimension of molds used	Standards
Slump test	----------	ASTM (C143-98) [12]
Initial surface absorption test (ISAT)	Cube: 100mm x100mm x 100mm.	BS 1881: Parts 5:1970 [3]
Flexural strength	Beam: 100mmx 100mm x400mm.	ASTM (C 78-94) [14]
Splitting tensile strength	Cylinder: 100mm , 200mm.	ASTM (C 496-96) [15]
Resistance to acid attack	Cube: 100mm x 100mm x100mm.	----------

Fig. (1): An Image Showing the ISAT Apparatus

Fig. (2) The Primer Used With Acrylic Coating

Fig. (3) Powdered One Component Acrylic

Fig. (4) Tar Epoxy

RESULTS AND DISCUSSIONS

Slump test:

The predetermined slump value for the concrete was 70 mm.

Initial surface absorption test (ISAT):

The results of the ISAT for the reference concrete sample A and the coated concrete samples B, C ,D and E are shown in Figures 6,7,8,9 and10, respectively. The ISA values corresponding to each type of waterproof coatings are as shown below:

Powdered one component acrylic: Figure 7 suggests that the ISA values for the specimens coated with powdered one component acrylic were between 645 -137 ml/m2.s $*10^{-3}$ for the time range of 10 – 120 minutes. These values were for acrylic: water mixing ratio of 1:1 The 1.5:1 mixing ratio had zero initial surface absorption, as shown in Figure 8, as a result of increasing the fine material (the acrylic powder) in the coating mix. This led to high degree of polymerization which means more dense coating.

Tar Epoxy: The tar epoxy coating was tried in tar: epoxy ratios of 1:0.5 and 1:1 the corresponding ISA graphs are shown in Figures 9 and 10, respectively. The results given in Figure 10 show that the 1:1 mixing ratio resulted in zero ISA values at all exposure times.

Weight Loss: Results of weight loss which was calculated by the related equation are Weight Loss (%) = $[(m_1-m_2)/m_1]$ X100 illustrated in Figures 11-13 at the exposure time of 56, 90,and 120 days . The above results show that the percentage of weight loss for all the coated concrete specimens exposed to sulfuric acid solution was less than that of the uncoated specimens, especially at early ages. This means that all waterproofing coatings used have a good resistance to the action of the acidic solution but with varying degrees.

The tar:epoxy with ratio 1:1, in particular, was less affected by the acidic solution. This can be attributed to the high degree of polymerization of the coating.

Splitting Tensile Strength (Indirect, Brazilian Test):

The splitting tensile strength results for the specimens at 28 days are shown in Figure 14.Figure 15 demonstrated the percentage increase in splitting strength in coated specimens compared to the uncoated specimen A.

From the above results one can outline the following observations concerning the splitting tensile strength values obtained:

1. It can be observed that all coated specimens have splitting tensile strength more than the uncoated specimens. This is due to the use of acrylic coatings and tar epoxy which have good tensile strength and high ductility thus improving the performance of the coated concrete relative to the uncoated specimen A.

The powdered one component acrylic: water ratio of 1.5:1 it gave the highest splitting strength. This may be due to that the higher acrylic content results in higher plasticity of the coating.

Two different ratios of tar: epoxy that are, 1:0.5 and 1:1 were tried. Although the difference in splitting tensile strength was not big but the mixing ratio of 1:1 gave a higher result. The tar and epoxy gives good flexibility when mixed together

Flexural strength (modulus of rupture):
Figure 16 shows the results of the flexural strength at 28 days. Figure 17 demonstrates the percentage increase in flexural strength in coated specimens compared to the uncoated specimen The same discussion presented concerning splitting strength can be applied to the flexural strength.

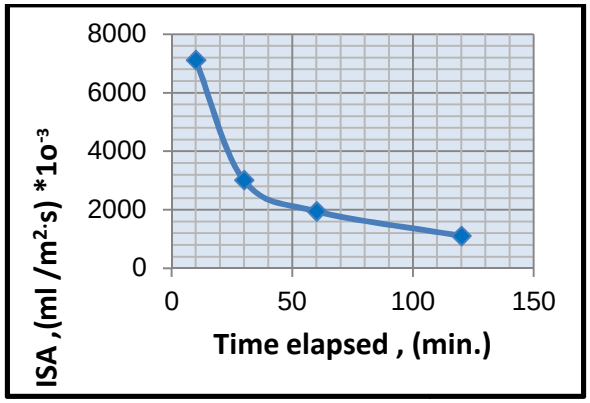

Fig. (6) ISA vs. Time for Specimen A at 28 Days

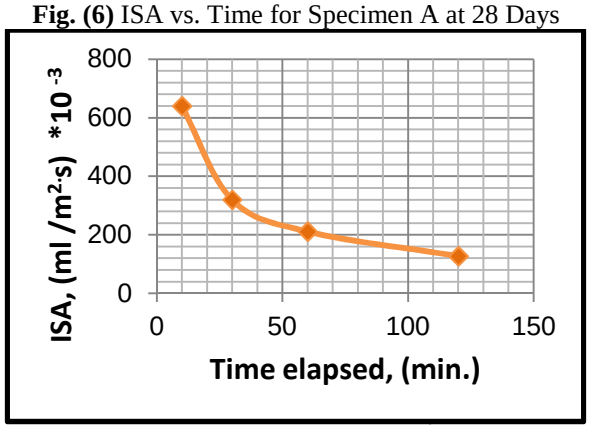

Fig. (7) ISA vs. Time for Specimen B at 28 Days

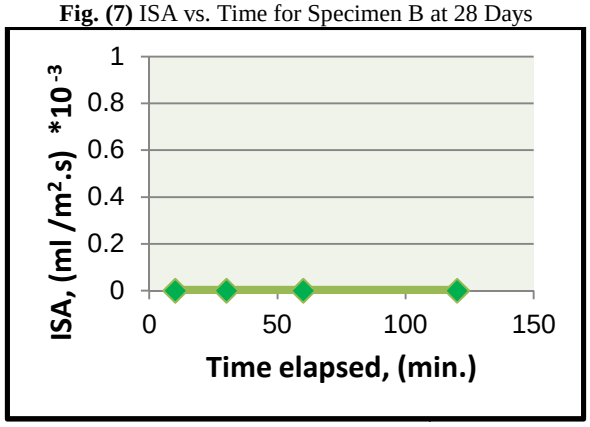

Fig. (8) ISA vs. Time for Specimen C at 28 Days

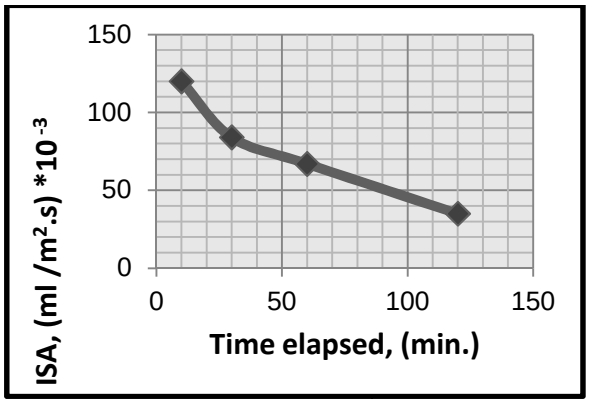

Fig. (9) ISA vs. Time for Specimen D at 28 Days

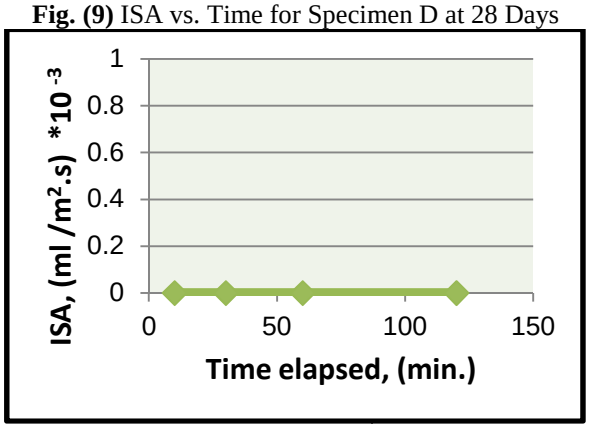

Fig. (10) ISA vs. Time for Specimen E

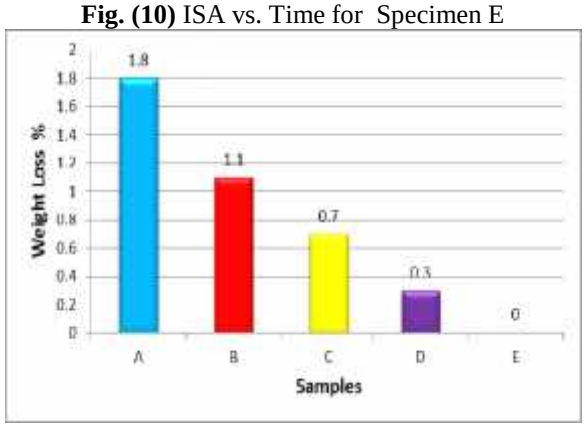

Fig. (11) Percentage of Weight Loss for all Specimens 56 Days

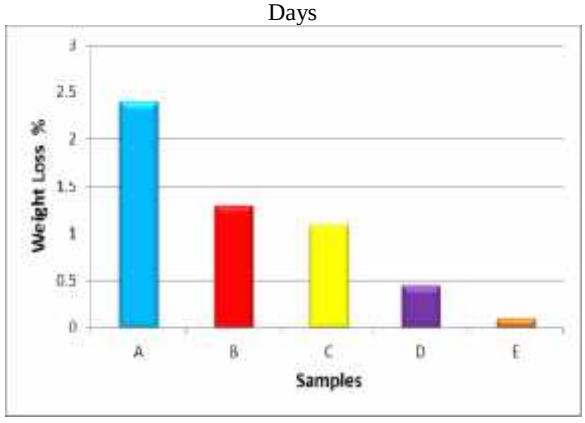

Fig. (12) Percentage of Weight Loss for all Specimens 90 Days

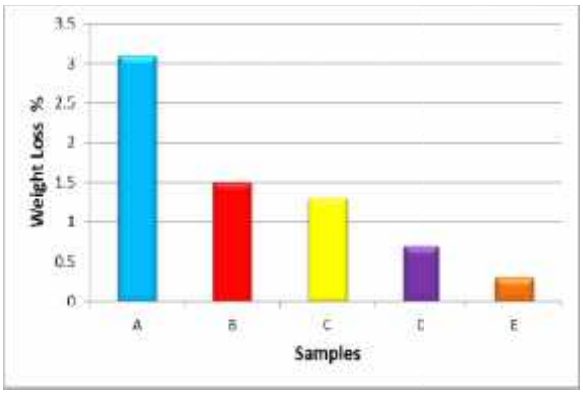

Fig. (13) Percentage of Weight Loss for all Specimens 120 Days

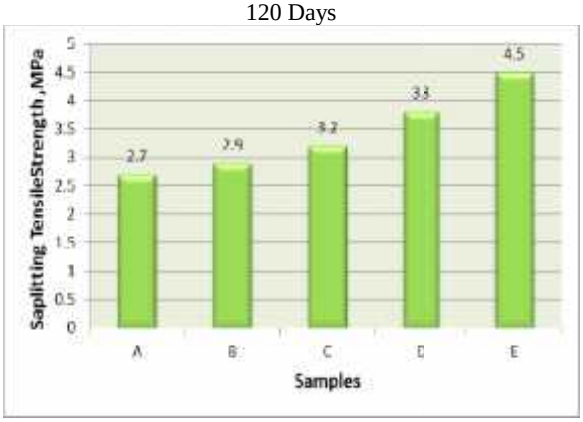

Fig. (14) Splitting Tensile Strength Values for all Specimens

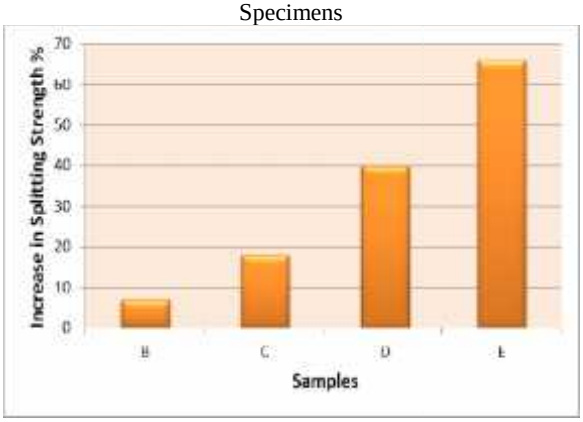

Fig. (15) Increase in Splitting Tensile Strength of the Coated Concrete Specimens Compared to the reference Specimens

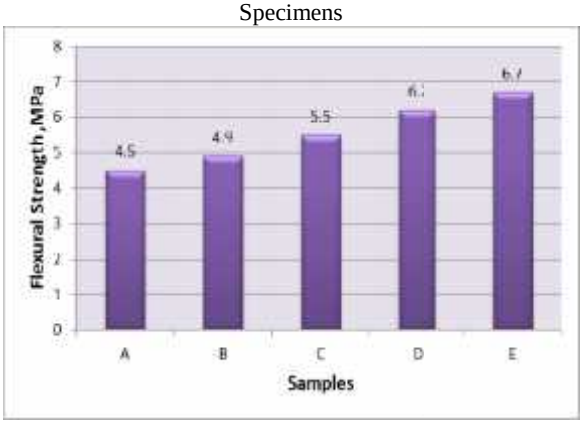

Fig. (16) Flexural Tensile Strength Values for all Specimens at 28 Days

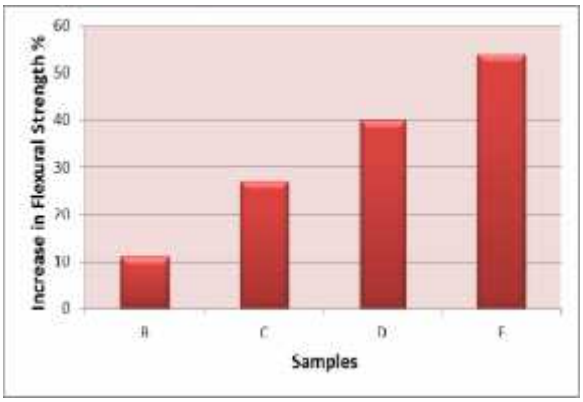

Fig. (17) Increase in: Flexural Tensile Strength of the Coated Concrete Specimens Compared to the reference Specimens

CONCLUSIONS

Based on the experimental tests results, the following conclusions were reached

1. Coating the concrete surface with acrylic and tar epoxy is effective in limiting the water absorbed by the surface of the concrete.

2. Generally, the ISA values decreased with the exposure time for all concrete specimens

3. Tar: epoxy ratio of 1:1 gave zero ISA values at all exposure times

4. acrylic coatings, and tar epoxy had positive effect on the splitting tensile and flexural strengths but with varying degrees, This was due to the excellent tensile strength and high ductility of the these materials

REFERENCE

– Neville A. M., Brooks J. J., (2010), "Concrete Technology", 2nd edition, London: Pearson.

– Richardson, M., (2002)," Fundamentals Of Durable Reinforced Concrete ", London and New York: Spon press.

– British Standards B.S. 1881: Part 5: 1970, Standards test method for determining the initial surface absorption of concrete.

– Vera, R. , Apablaza, J., Carvajal, A. and Vera, E. , "Effect of Surface Coatings in the Corrosion of Reinforced Concrete in Acid Environments", International Journal of Electrochemical Science, pp. 11832-11846, 2013.

– Orlowsky, j, Raupach , M. Baias, M. and Blümich, B., "Application of the NMR-technique to concrete-coatings" Concrete Repair, Rehabilitation and Retrofitting Taylor & Francis Group, London, ISBN 978-0-415-46850-3, 2009

- Aguiar, J., Camoes, A, and Moreira, P.,"Coating for Concrete Protection against Aggressive Environments" ,Journal of Advanced Technology Vol.6.No.1,PP. 243-250,2008.
- Iraqi Standard Specification No.45, "sieve analysis of aggregate", 1984.
- Cement Badoosh factory, Personal communication.
- American Society for Testing and Materials. ASTM C 192-98, Standard test method for curing concrete test specimens in the laboratory. ASTM Standards 2004.
- American Society for Testing and Materials. ASTM C 511-98, Standard test method for casting concrete test specimens in the laboratory. ASTM Standards 2004.
- Petrie .E, (2000), "Handbook of Adhesives and Sealants", McGraw Hill.
- American Society for Testing and Materials. ASTM C 143-98, Standard test method for slump of hydraulic-cement concrete. Standards 2004.
- British Standard B.S., "Method for Determination of compressive strength of concrete cubes", part 116, 1983.
- American Society for Testing and Materials. ASTM C 78-94, Standard test method for flexural strength of concrete (using simple beam with third-Point loading).Standards 2004.
- American Society for Testing and Materials. ASTMC 496-96, Standard test method for splitting tensile strength of cylindrical concrete specimens. Standard 2004.

SIMULATION MODELS FOR BEKHMA RESERVOIR OPERATION SYSTEM (COMPARISON STUDY)

MAHDI **D**AWOOD, **K**AMEL **A. AL-M**OHSEEN and **S**HAKER **A. J**ALIL
Dept. Of Water resource Engineering, Faculty of Engineering, University of Duhok, Kurdistan Region-Iraq
Dept. Of Dams and Water resource Engineering, College of Engineering, University of Mosul-Iraq
Dept. Of Water resource Engineering, Faculty of Engineering, University of Duhok, Kurdistan Region-Iraq

(Received: March 18, 2014; Accepted for publication: December 3, 2014)

ABSTRACT

Simulation procedures have been developed to test the performance of Bekhma reservoir system using two simulation models viz: HEC-ResSim (Model-I) and Simulink based technique (Model-II). In the present study being reported, one of the simulations modeling process requirement is to disaggregate the monthly inflow data into daily based data, and as far as the demand from Bekhma reservoir is of concern, a constant value of 332m^3/sec has been proposed based on the achievement of high reliability level in Model-I and 318 m3/sec for the same reliability in Model-II. In order to test the performance of the reservoir system in generating hydroelectric power, the same set of data have been introduced to both models , the average power generated by first model was 510.3 MW while the second was 495.9 MW which they are closed to each other . In addition the current research work is considered as an opportunity to check the capability of Simulink approach in modeling water resource systems in general and reservoir systems in particular.

1. INTRODUCTION

The optimum utilization of our limited supply of water resources is becoming the central point in planning, operation and management of all water resources projects. The ever growing population of the world and the limited resources of land and water are imposing great constraints on food production and its availability.

Reservoirs are considered the major components of any water resource system. The public perceptions and needs, objectives and numerous other factors that affect reservoir operation change over time. Consequently, operating procedures should be periodically reevaluated and modified whenever changing conditions so warrant. However, there is no standard format for specifying reservoir system operating rules applicable to all situations (AlMohseen, K. A. 2003).

Each reservoir system has its own unique set of aspects and a variety of measures may be used to define its operating rules in order to attain situations. Each reservoir system has its own unique set of aspects and a variety of measures may be used to define its operating rules in order to attain a defined goal (Al-Mohseen, 2003).Additionally, any reservoir model should be able to evaluate the quality of its solutions and compute values of explicitly defined performance measures as a function of the sought storage capacity/water release policy, (Wurbs, 1996). This can be done by means of simulation models.

2. SIMULATION MODELS

Simulation seeks to mimic the operation of a real system. It is a modeling technique that is used to approximate the behavior of a system on computer, representing all the characteristics of the system largely by a mathematical concepts based on well known hydrological equation of mass balance of reservoir inflows, outflows and storage fluctuations. There are several readily available, well-documented, generalized computer programs for reservoir system simulation. These include HEC-5, SSARR, MIT Simulation Models, and several Texas Department of Water Resources models. Other well-known simulation models were developed primarily for specific reservoir systems such as the California Central Valley Project or Tennessee Valley Authority systems (Wurbs, 1985). The earliest simulation model dealing with operational study, and developed for a system of six reservoirs on Missouri River, was made in 1953 by U.S. Army Corps of Engineers, (Hall and Dracup, 1970). According to (Wurbs, 1985), simulation, with either deterministic or synthetically generated stochastic hydrologic

inputs, will likely continue to be the "work-horse" of reservoir system analysis.

In this study, simulation models have been developed to test the performance of Bekhma reservoir system (Kurdistan Region, northern part of Iraq) which is considered as a strategic component of Iraq water resource using two simulation models viz. HEC-ResSim model (Model-I) and Simulink based technique model, (Model-II).

3. BEKHMA RESERVOIR SYSTEM

Bekhma reservoir is located on the Greater Zab River, upstream of Eski-Kelek gauging station (with coordinates 435388.85 m E and 4062517.8 m N), and about 62 km to the north west of Erbil city. The present study is an attempt toward the development of improved management strategies to operate an existing multi-purpose reservoir system. The possibility of realizing the potential for increasing the overall benefits provided by Bekhma reservoir system through improved or updated operating policies is evaluated in the study being reported. Reservoir systems operation often offers substantial increases in benefits for relatively small improvements in operating efficiency. Though Bekhma reservoir is a multi-purpose reservoir, however, its main purposes is to produce hydroelectricity, so the power generation from this system will be used as a measure of efficacy Figure (1) shows the geographic location of Bekhma reservoir the pertinent data to Bekhma reservoir are presented in section 4.3 below

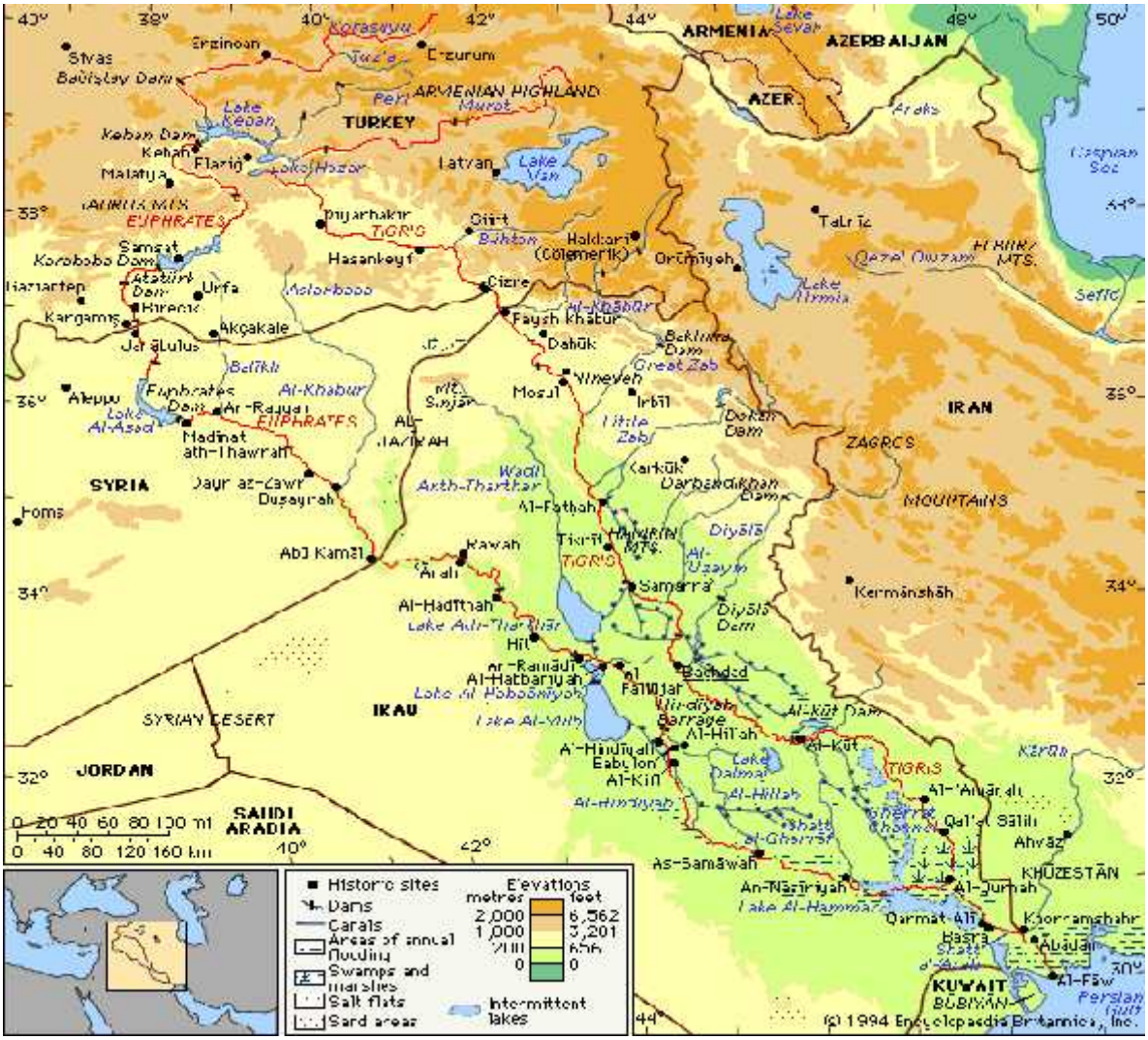

Fig. (1): Geographic Map of greater zab river and Bekhma Reservoir location.

4. DATA PREPARATION

4.1 Inflow Time Series

The means monthly flow at dam site is available over the period January 1st 1932 to December 1st 2004, i.e. (876) mean monthly flow records. But the proposed Model-I requires the inflow data to be presented on daily basis. Consequently, the monthly data has been subjected to a disaggregation procedures to convert them to daily data (26633 days) using a tool available in HEC-ResSim program. figure (2) shows part of inflow disaggregation (during year 1932), obtained from HEC-ResSim simulation program, and figure (3) depicts the daily inflow into Bekhma Reservoir for the period January 1st 1932 to December 1st 2004 after being disaggregated

1932	January	February	March	April	May	June	July	August	September	October	November	December	Mean
1	241.7	466.3	651.8	763.2	669.1	379.8	175.7	106.8	109.1	133.1	131.9	133.2	330.14
2	351.1	581.5	722	804.4	533.8	225.7	125.7	87.8	130.3	135.8	128	138.4	330.38
3	351.1	581.5	722	804.4	533.8	225.7	125.7	87.8	130.3	135.8	128	138.4	330.38
4	351.1	581.5	722	804.4	533.8	225.7	125.7	87.8	130.3	135.8	128	138.4	330.38
5	351.1	581.5	722	804.4	533.8	225.7	125.7	87.8	130.3	135.8	128	138.4	330.38
6	351.1	581.5	722	804.4	533.8	225.7	125.7	87.8	130.3	135.8	128	138.4	330.38
7	351.1	581.5	722	804.4	533.8	225.7	125.7	87.8	130.3	135.8	128	138.4	330.38
8	351.1	581.5	722	804.4	533.8	225.7	125.7	87.8	130.3	135.8	128	138.4	330.38
9	351.1	581.5	722	804.4	533.8	225.7	125.7	87.8	130.3	135.8	128	138.4	330.38
10	351.1	581.5	722	804.4	533.8	225.7	125.7	87.8	130.3	135.8	128	138.4	330.38
11	351.1	581.5	722	804.4	533.8	225.7	125.7	87.8	130.3	135.8	128	138.4	330.38
12	351.1	581.5	722	804.4	533.8	225.7	125.7	87.8	130.3	135.8	128	138.4	330.38
13	351.1	581.5	722	804.4	533.8	225.7	125.7	87.8	130.3	135.8	128	138.4	330.38
14	351.1	581.5	722	804.4	533.8	225.7	125.7	87.8	130.3	135.8	128	138.4	330.38
15	351.1	581.5	722	804.4	533.8	225.7	125.7	87.8	130.3	135.8	128	138.4	330.38
16	351.1	581.5	722	804.4	533.8	225.7	125.7	87.8	130.3	135.8	128	138.4	330.38
17	351.1	581.5	722	804.4	533.8	225.7	125.7	87.8	130.3	135.8	128	138.4	330.38
18	351.1	581.5	722	804.4	533.8	225.7	125.7	87.8	130.3	135.8	128	138.4	330.38
19	351.1	581.5	722	804.4	533.8	225.7	125.7	87.8	130.3	135.8	128	138.4	330.38
20	351.1	581.5	722	804.4	533.8	225.7	125.7	87.8	130.3	135.8	128	138.4	330.38
21	351.1	581.5	722	804.4	533.8	225.7	125.7	87.8	130.3	135.8	128	138.4	330.38
22	351.1	581.5	722	804.4	533.8	225.7	125.7	87.8	130.3	135.8	128	138.4	330.38
23	351.1	581.5	722	804.4	533.8	225.7	125.7	87.8	130.3	135.8	128	138.4	330.38
24	351.1	581.5	722	804.4	533.8	225.7	125.7	87.8	130.3	135.8	128	138.4	330.38
25	351.1	581.5	722	804.4	533.8	225.7	125.7	87.8	130.3	135.8	128	138.4	330.38
26	351.1	581.5	722	804.4	533.8	225.7	125.7	87.8	130.3	135.8	128	138.4	330.38
27	351.1	581.5	722	804.4	533.8	225.7	125.7	87.8	130.3	135.8	128	138.4	330.38
28	351.1	581.5	722	804.4	533.8	225.7	125.7	87.8	130.3	135.8	128	138.4	330.38
29	351.1	581.5	722	804.4	533.8	225.7	125.7	87.8	130.3	135.8	128	138.4	330.38
30	351.1		722	804.4	533.8	225.7	125.7	87.8	130.3	135.8	128	138.4	307.55
31	351.1		722		533.8		125.7	87.8		135.8		138.4	299.23
Sum	10774.7	16748.3	22,311.80	24,090.80	16,683.10	6,925.10	3,946.70	2,740.80	3,887.80	4,207.10	3,843.90	4,285.20	3,885.33

Fig. (2): daily Inflow into Reservoir (during year 1932) after disaggregation by HEC-ResSim program

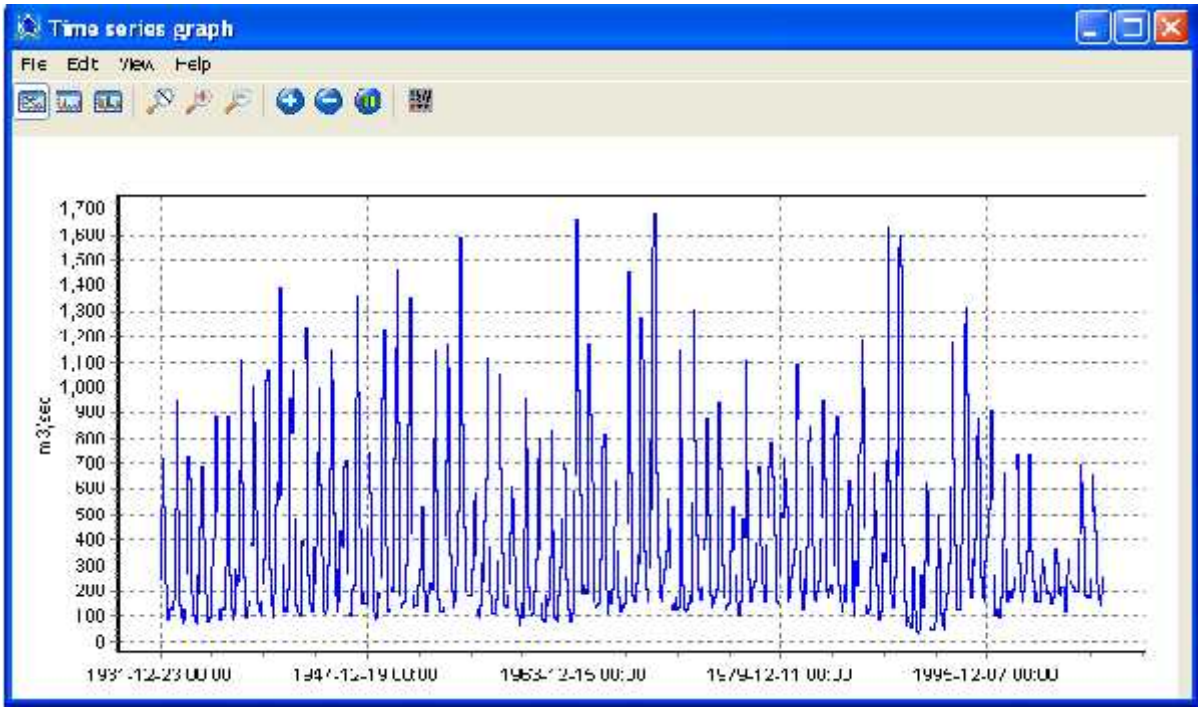

Fig. (3): daily inflow into Reservoir for the period January 1st 1932 to December 1st 2004

4.2 Releases From The Reservoir

Release target is usually not known a priori and estimation of reasonable and, presumably feasible, levels of release target is essential for a sound management of any reservoir system. In fact, there are two approaches usually used in specifying the release from the reservoir. The first approach is achieved by assigning a constant release target to the used simulation models and measuring the performance of the system under this conditional state, this paper will focus on this approach, the release target is assigned a specified fixed level for simulation purposes; real world management makes it imperative for a Water Resources System Manager to be able to objectively fix, a priori, reasonable release targets for any reservoir system. Consequently, the process of fixing the release target a priori has required trial and error procedures. This procedures based on reliability level in which trails values of release have been assumed then the simulation model was run for each value presumed release until a reasonable level of reliability is achieved (in this case 100% reliability was sought, i.e. there is no failure either beyond the minimum elevation or maximum elevation of storage in the reservoir over all simulation time using the whole set of daily inflows). Since a value of 311 m3/sec of release is meeting all the demands including the environment requirements, therefore for trial and error process for finding the target release have started with this value until which reservoir would not get empty, consequently value of 332m3/sec and 318m3/sec which achieved the satisfactory reliabilities have been used in the two models respectively in the consequent simulation process

The differences in the release targets for two models are due to the calculation methods used, i.e. Model-I adopted linear interpolation to calculate the head as a function of storage, while model-II has used a fourth degree polynomial approximation technique to calculate the head from storage values.

4.3 Bekhma Reservoir Physical Data

A power plant with a capability of generating (1526 MW) has been proposed for Bekhma Dam with estimated maximum reservoir capacity of around 17.07 Billion cubic meters. While the minimum storage is 12.72 Billion cubic meters

The Elevation-Surface Area- Storage of the reservoir are shown in Figure (4) below in which they appear as per required by Model-I's GUI. Also Table (1) lists the mean monthly depth of pan evaporation in (mm)

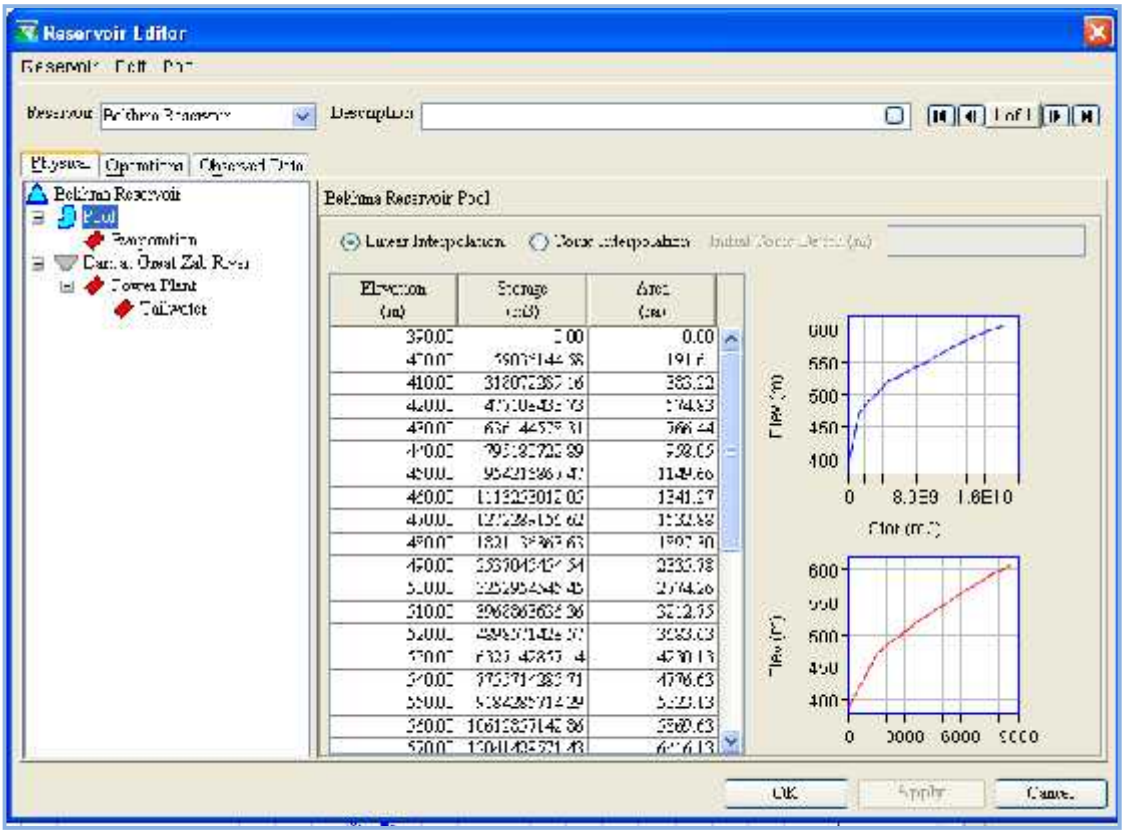

Fig. (4): volume- surface area - elevation curves for Bekhma reservoir.

Table (1): Mean Monthly Evaporation at Bekhma Reservoir Site

Time (months)	Jan.	Feb.	Mar.	Apr.	May	Jun.	Jul.	Aug.	Sep.	Oct.	Nov.	Dec.
Evaporation (mm)	20	20	20	40	100	240	390	420	290	150	80	20

5. HEC-ResSim (MODEL-I)

The Hydrologic Engineering Center (HEC) of the U.S. Army Corps of Engineers has developed a new reservoir simulation model, HEC-ResSim, as the successor to the well-known HEC-5.

HEC-ResSim uses an original rule-based approach to mimic the actual decision-making process that reservoir operators must use to meet operating requirements for flood control, power generation, water supply, and environmental quality. The graphical user interface makes HEC-ResSim easy to use and the customizable plotting and reporting tools facilitate output analysis. The basic input data requirements for program consist of reservoir pool capacity and surface area of the reservoir, evaporation data, seepage quantities, power plant characteristics, pumps, controlled and uncontrolled structures parameters, rule curves of operation and hydrologic time series data (Loucks D. and Eelco van Beek, 2005).

6. SIMULINK MODEL (MODEL-II)

Another simulation model was designed using Simulink based technique in MATLAB environment. Simulink is a software package for modeling, simulating, and analyzing dynamical systems. It supports both linear as well as nonlinear systems, modeled in continuous time, sampled time or a hybrid of the two. For

modeling, Simulink provides a graphical user interface (GUI) for building models as block diagrams, using click-and-drag mouse operations. This is a far cry from previous simulation packages that required a formulation of mathematical expressions and equations in a language or a program. Simulink includes a comprehensive block library of sinks, and sources in the form of linear and nonlinear components and connectors. A key feature of Simulink is that it is built on MATLAB platform and as a result, provides direct access to the wide range of MATLAB-based computational and analytical tools (The Math Works, 1999).

This study is an opportunity to test the capability of this modern technique to simulate a complex system like Bekhma reservoir. Simulink model based on continuity (storage equation) has been built for Bekhma reservoir and is shown in Figure (5).

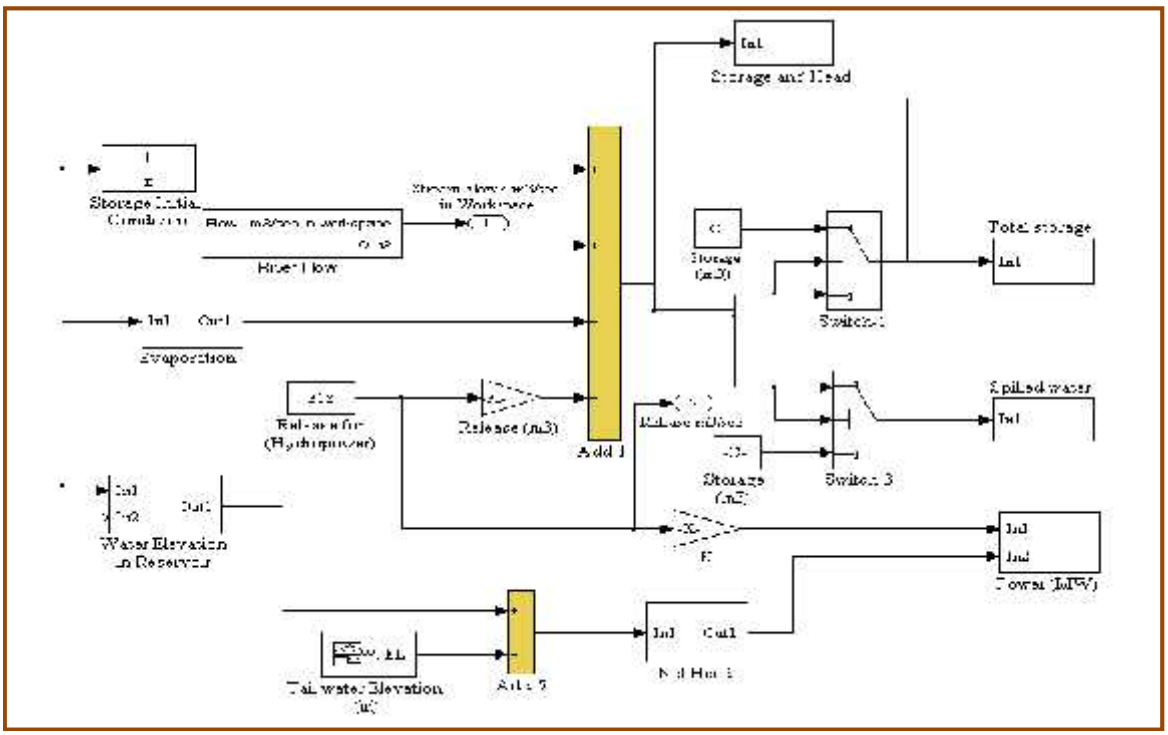

Fig. (5): Simulink layout model for Bekhma reservoir system

7. MODELS APPLICATION

7.1 Model-I

After feeding Model-I with the required data and simulates the reservoir over the period January 1st 1932 to December 1st 2004 for hydropower generation with constant release of 332 m3/sec (aforementioned in section 4.2), the obtained results are given in Figures (6) and (7). Figure (6) shows the elevation of the reservoir over the simulated period, note that the elevation was kept within the permissible trajectory and the reservoir did not get empty at any time. While Figure (7) depicts the electrical power generated by the turbines during the period of simulation

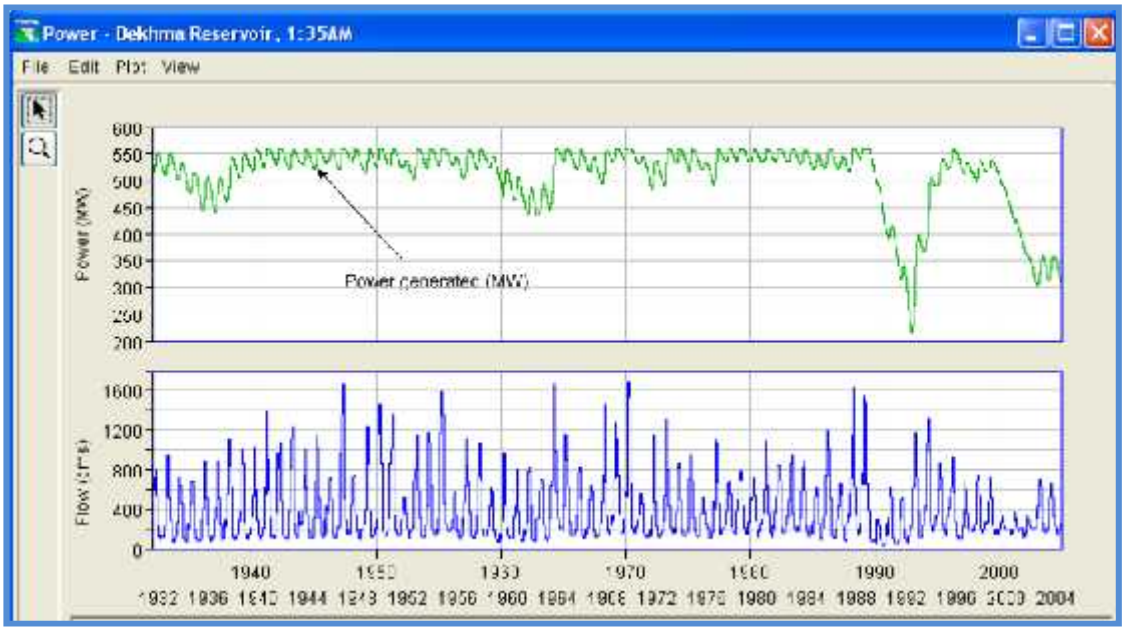

Fig. (6): The Operating Policy of Bekhma Reservoir over the period of simulation using Model-I

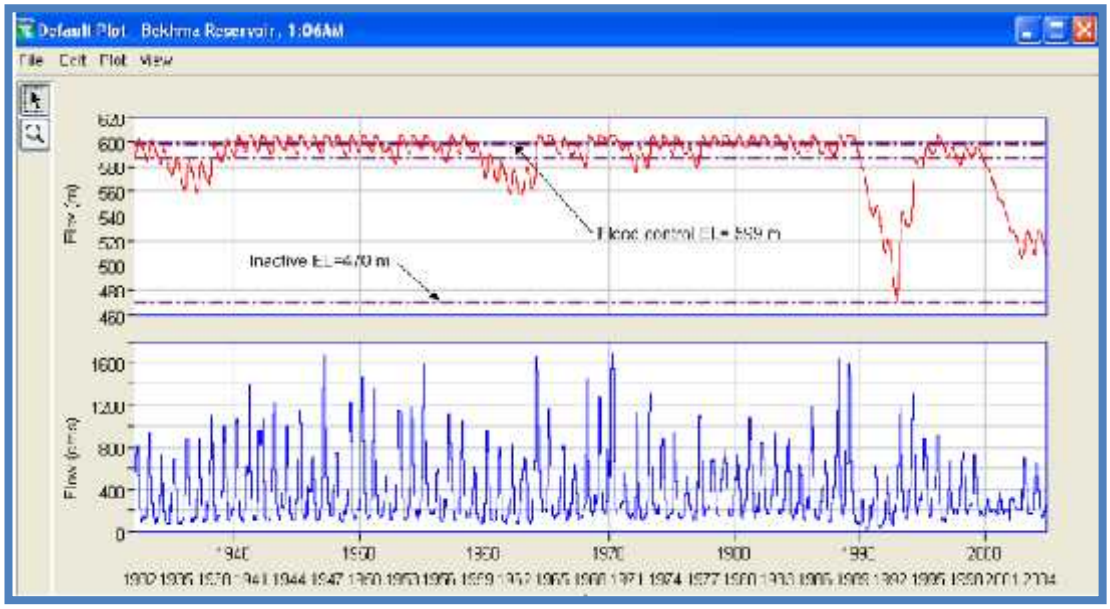

Fig. (7): generated power in (MW) from Bekhma reservoir over the period of simulation using Model-I.

7.2 MODEL-II

In order to find a basis of comparison, the same set of data has been introduced to Model-II. The simulation process was carried out for the same period as in Model-I. Figure (8) shows the operating policy in terms of elevation of water in the reservoir while Figure (9) gives the generated energy during the simulation period

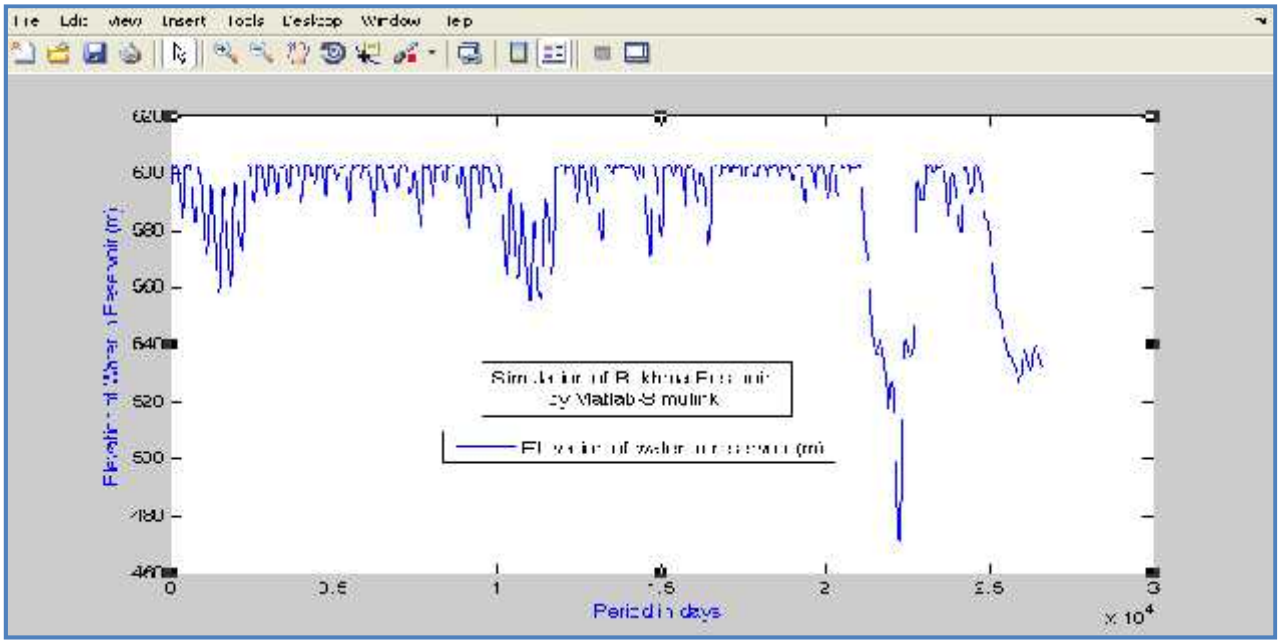

.**Fig. (8):** the Operating Policy of Bekhma reservoir over the period of simulation using Model-II

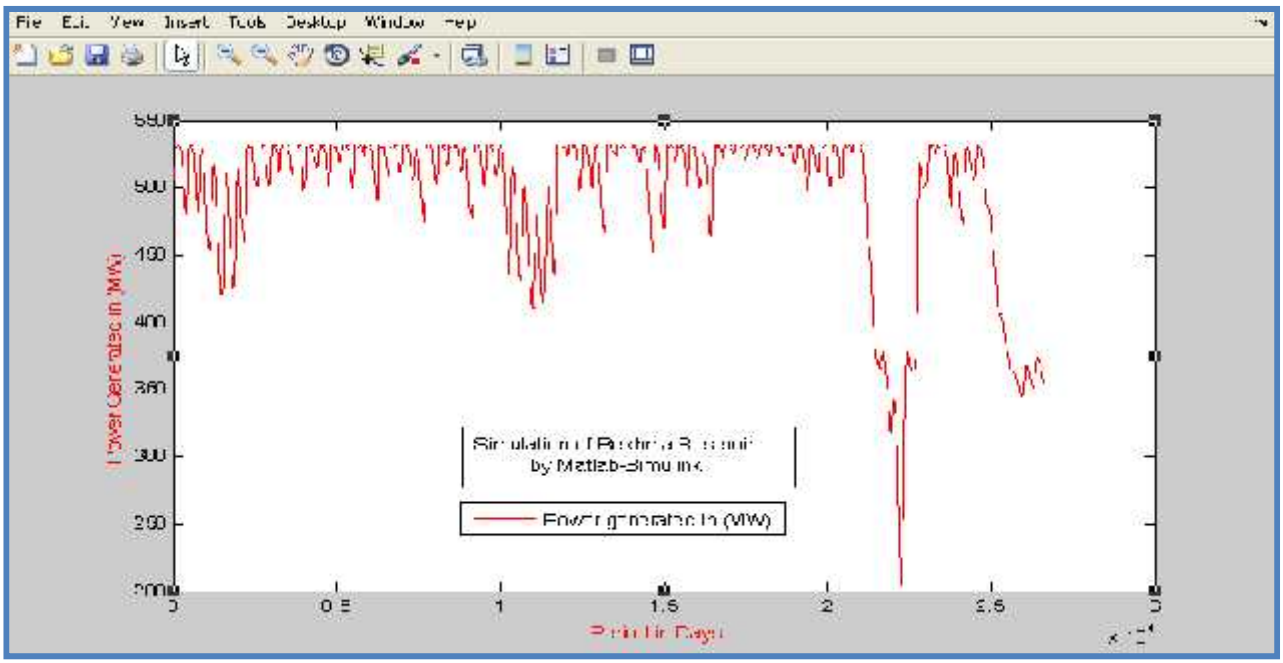

Fig. (9): generated power in (MW) over the period of simulation using Model-II.

8. RESULTS AND DISCUSSIONS

Optimal controlled water release and hydropower generated characteristics in Daily produced from both models simulations are present in Table(2),while Figure (10), graph showing results of the power (MW) produced from simulations of the reservoir during the period from (01 January 1932 to 01 December 2004).

Table(2): hydropower generation characteristics results from both simulation models.

Models	Average Power Generated in (Mw)	Max. Power Generated in (Mw)	Min. Power Capacity in (Mw)
HEC-ResSim (Model- I)	510.3	556.13	213.4
Matlab -Simulink Technique (Model- II)	495.9	532.00	203.5

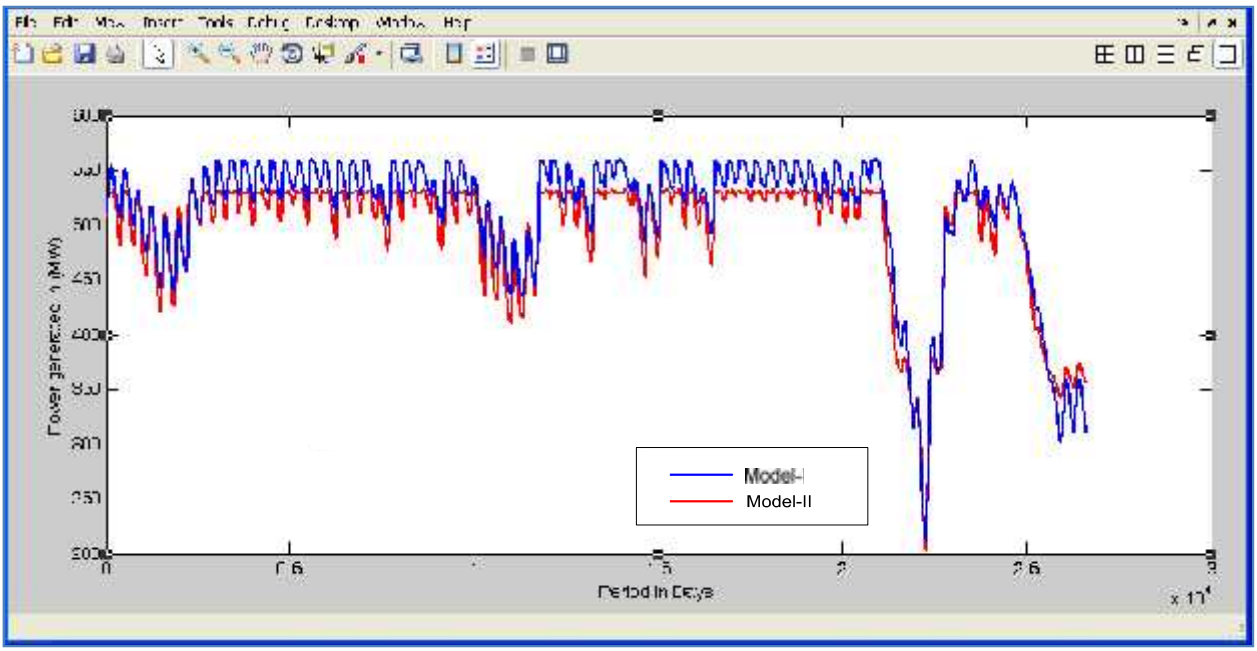

Fig.(10): generated power produced by both simulation models from Bekhma rreservoir during the period (01 January 1932 to 01 December 2004).

The daily (26633 days) operation rule curves (policy operation) obtained from both models are presented in figures (6 through 8) above, these data is relatively large and difficult to be analyzed , consequently, hard work has been devoted to extract the average monthly operation policy for Bekhma Reservoir. The monthly operation rule curves (operating polices) obtained from both models are calculated and presented in figure (11) based on water elevation in the reservoir. Note that close operating policies have been result from both models.

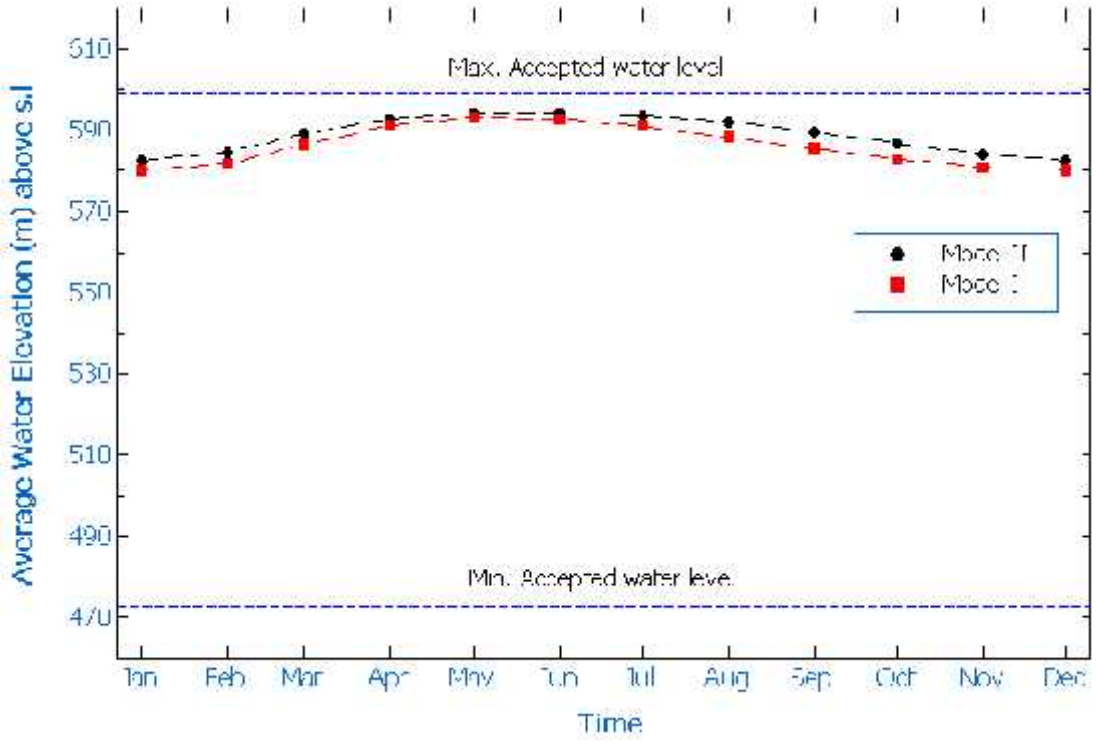

Fig. (11) monthly operating policies of Bekhma reservoir using Model-I and Model-II

9. CONCLUSIONS

A comparison study has been conducted to study the performance of Bekhma Reservoir system in generating hydroelectric power by means of two simulation models. The study required to disaggregate the monthly flow time series into daily series as per required by HEC-ResSim model. Additionally, the current research work is considered an opportunity to check the ability of Simulink approach in modeling water resource system in general and reservoir system in particular. The authors believe that this technique would open the door widely for those who work in this area to be able to model more complex systems by making use of the high capabilities of Matlab software which is very rich in terms of built in functions and tools and can be used easily through Simulink technique. The study reveals that Both models have given close results in terms of power generation using the same scenarios of daily inflow for a given fixed target of release, i.e. with an average daily power generation of 510.3 MW/day obtained from Model-I and 495.9 MW/day from Model-II. Moreover good agreement was also notice in the monthly operating rules.

10. REFERENCES

- AlMohseen, K. A (2003) "Optimal Operation of multi-purpose multi-reservoir water resources system", PhD Thesis, Department of Civil Engineering, IIT,Delhi, India.
- Vedula & Majumdar, S Vedula P P Mujumdar (2005). Water Resources Systems, .V,New Delhi, Tata McGraw-Hill Education.
- Hydrologic Engineering Center (1991). Optimization of Multiple-Purpose Reservoir System Operations: A Review of Modeling and Analysis Approaches, U.S. Army Corps of Engineers ,609 Second Street, Davis, CA 95616,(916) 756-1104 .
- Loucks D.and Eelco van Beek (2005). Water Resources Systems Planning and Management, An Introduction to Methods, Models and Applications, Netherland ,UESCO 2005 and WL /Delft Hydraulics .

- Klipsch, D. J (2009). Reservoir operations modeling with HEC-ResSim , Hydrologic Engineering Center, U.S. Army Corps of Engineers Davis, CA. 530-756-1104 .
- Joan D.Klipsch.Mariln B. Hurst (2007). HEC-ReSim,Reservoir System Simulation User Manual ,version 3.0 U.S. Army Corps of Engineers ,609 Second Street, Davis, CA 95616-4687.
- S.K. JAIN and V.P. SINGH.(2003). Water Resources Systems Planning and Management, Elsevier Science B.V. Amsterdam, the Netherlands.
- AlMohseen, K. A(2008). "Operation of Alaziziya Evaporation Pond Using Simulink Trechnique", Alrafiden Engineering Journal, College of Engineering, Mosul University, Vol.16, No.3, Iraq.
- Steven T. Karris (2008). Introduction to Simulink with Engineering Applications Second Edition Orchard Publications.
- The Math Works, Simulink® Control Design™ (2011). User's Guide, The Math Works, Inc.3 Apple Hill Drive Natick, MA 01760-2098.
- The Math Works. (1999). Simulink ,Dynamic System Simulation for Matlab, Using Simulink Version 3, The MathWorks, Inc. 24 Prime Park Way Natick, MA 01760-1500.
- Mohammad Karamouz,Ferenc Szidarovszky,Banafsheh Zahraie (2003) Water Resources Systems Analysis ,United States of America, TC409.K37 2003 333.91—dc21, A CRC Press Company, Lewis publishers.
- Ladislav Votruba, Vojtech broza(1989). water management in reservoirs, Elsevier Science Publishers B.V. Sara Burgerhartstraat 25, P.O. Box 211, 1000 AE Aamsterdam, the Netherlands.
- Slobodan P. Simonovic (2008). Managing Water Resources ,Methods and Tools for a Systems Approach, UNESCO Publishing 7, place de Fontenoy, 75352 Paris 07 SP, France.
- Thomas A, McMahon& Russel G.Mein (1978). Reservoir capacity And Yield, Elsevier Science B.V. 335 Jan van Galenstraat, Amsterdam, the Netherlands.
- B. Roffel· B. H. Betlem (2004). Advanced Practical Process Control, Springer-Veriag Berlin Heidelberg.
- Qibo Mao • Stanislaw Pietrzko(2013). Control of Noise and Structural Vibration, A ATLAB®-Based Approach, Springer-Verlag London .